ARCHIVES
MASSACHUSETTS INSTITUTE OF TECHNOLOLGY
APR 14 2015
LIBRARIES

Designing nanoparticles for highly efficient endothelial siRNA delivery

by

James E. Dahlman

B.S. Biomedical Engineering, Wright State University (2009)

Submitted to the Harvard-MIT Program in Health Sciences and Technology (HST)
in Partial Fulfillment of the Requirements for the Degree of

Doctor of Philosophy

at the

Massachusetts Institute of Technology

February 2015

© Massachusetts Institute of Technology. All rights reserved.
2015

Author Signature _____ Signature redacted
Harvard-MIT Program in Health Sciences and Technology
November 13, 2014

Certified by _____ Signature redacted
Daniel G. Anderson, PhD
Professor of Chemical Engineering
Thesis Supervisor

Certified by _____ Signature redacted
Robert Langer, PhD
David H. Koch Institute Professor
Thesis Supervisor

Accepted by _____ Signature redacted
Emery N. Brown, MD/PhD
Director, Harvard-MIT Program in Health Sciences and Technology
Professor of Computational Neuroscience and Health Sciences and Technology

Designing nanoparticles for highly efficient endothelial siRNA delivery

by

James E. Dahlman

Submitted to the Harvard-MIT Program in Health Sciences and Technology on November 13, 2014 in Partial Fulfillment of the Requirements for the Degree of Doctor of Philosophy in Medical Engineering and Medical Physics.

Abstract
RNA potently regulates gene expression. However, the utility of RNA has been limited by the ability to efficiently deliver it to specific cells *in vivo*. *In vivo* RNA delivery is challenging; vehicles must avoid phagocytosis in the bloodstream, reach the target tissue, and get into, and out of, an endosome, all without setting off an unwanted immune response. Despite these challenges, nanoparticles have delivered siRNA to hepatocytes after intravenous injections as low as 0.001 mg/kg. By contrast, efficient, durable, and robust silencing in other cell types has remained challenging.

Herein we describe 7C1, a low molecular weight polymeric nanoparticle that delivers siRNA to endothelial cells *in vivo* at doses as low as 0.017 mg/kg. 7C1 nanoparticles reduced target mRNA expression for more than three weeks after a single injection, and delivered five siRNAs concurrently *in vivo*. Notably, 7C1 transfects endothelial cells at low doses without significantly reducing gene expression in hepatocytes or immune cells. 7C1 was optimized for stability and consistency, and used to study inflammation, cardiovascular disease, emphysema, primary tumor growth, and metastasis in labs across the United States. These data demonstrate that 7C1 can be used to potently modify the expression of multiple endothelial genes *in vivo*.

Thesis Supervisors: Daniel G. Anderson and Robert Langer
Titles: Professor of Chemical Engineering and David H. Koch Institute Professor, respectively

Biographical Notes and Acknowledgements

I have always been, and will most likely remain, atypically interested in understanding how scientific systems interact. This is particularly true of engineering and biology; I believe that by properly combining these disciplines, we will transform how disease is treated. As a result, I look to the future with great optimism.

I owe a great many people thanks for impacting my life in a way that has led me to MIT. First and foremost, I cannot overstate how thankful I am for my mother, father, and sister. They are the source of my curiosity, persistence, and happiness.

My parents prepared me well for the classroom, where I received tremendous assistance from my scientific mentors, most notably Jeff McManus, Dan Miracle, and Avi Schroeder. Jeff McManus ignited my interest in science. Dan Miracle taught me how to research and gave me opportunities to design experiments and think for myself, even as an undergraduate student. And Avi showed me how innovative, creative, and considerate a great scientist could be.

Working in the Langer Lab has been an incredible experience. The mentorship I received from Robert Langer and Dan Anderson has fundamentally changed the way I approach science. Their impact been buttressed by many people including, but not limited to, Mark Kalinich, Apeksha Dave, Yiping Xing, Lauren Lo, Kevin Kauffman, Victor Koteliansky, Dipak Panigrahy, Tyler Jacks, Phil Sharp, Sangeeta Bhatia, Kevin Love, Chris Alabi, Chris Levins, Carmen Barnes, Aude Thiriot, Wen Xue, Tuomas Tammela, Hendrik Sager, and Sid Jhunjhunwala.

I would like to thank Will Taylor, Tim O'Shea, and Jordan Cattie. Despite their different backgrounds, all three of them share one important characteristic: they improve the lives of those around them. I am proud to be a friend to all three. Will Taylor has been my best friend since we were kids in Kettering, Ohio. He has grown into a definition of doggedness and humility. Tim O'Shea has been my best friend at MIT. He and I both came to Boston from different parts of the world. Through a series of shared experiences, we reshaped this city into a second home. Finally, I would like to thank Jordan Cattie. She is supportive, caring, compassionate, and brilliant. Moreover, she has an incredible talent for helping people who need it. I know she appreciates brevity, so I'll keep this succinct: she is the best person I have ever known.

Finally, I would like to thank Taylor Shaw. She is an inspiration to all who know her.

Table of Contents **Page**

Abstract..... 2
Biographical Notes and Acknowledgements..... 3
List of Figures..... 6
List of Tables..... 7

Chapter 1. RNAs have tremendous potential that is limited by *inv vivo* delivery..... 8
1.1 *In vivo* RNA delivery is challenging..... 8
1.2 RNA targeting strategies..... 9
1.3 Liver physiology can promote siRNA delivery..... 12
1.4 Strategies to develop highly efficient liver targeting nanoparticles.....13
1.5 Alleviating disease *in vivo* with optimized liver targeting nanoparticles.....18
1.6 Lessons from lipidoids can be applied to non-liver delivery vehicles.....21
1.7 Conjugate systems for hepatic siRNA delivery.....21
1.8 Tumor physiology can promote or inhibit siRNA delivery.....24
1.9 Endothelial cell targeting 26
1.10 Figures.....28
1.11 References.....30

Chapter 2. The nanoparticle 7C1 efficiently delivers siRNA to endothelial cells *in vivo*.....37
2.1 Introduction.....37
2.2 Efficient siRNA delivery to endothelium *in vitro* and *in vivo*.....38
2.3 Endothelial RNAi affects multiple animal models.....41
2.4 7C1 *in vivo* tolerability.....42
2.5 Conclusions.....43
2.6 Materials and Methods.....43
2.7 Figures.....50
2.8 References.....66

Chapter 3. 7C1 enables targeted 5-siRNA therapy for ischemic heart disease.....69
3.1 Introduction.....69
3.2 7C1 nanoparticles deliver siRNA to aortic endothelial cells.....70
3.3 siCAM^5 treatment suppresses leukocyte recruitment to atherosclerotic plaques....70
3.4 siCAM^5 reduces myocardial inflammation after ischemia reperfusion injury.....71
3.5 Discussion.....72
3.6 Materials and Methods.....73
3.7 Figures.....77
3.8 References.....83

Chapter 4. 7C1-mediated delivery of a small RNA combination therapy for lung cancer.....85
4.1 miRNA therapies have clinical potential.....85
4.2 Delivery of siRNA to lung adenocarcinoma cells *in vitro*.....87
4.3 Delivery of siRNA to lung adenocarcinoma *in vivo*.....87
4.4 Systemic miR-34a delivery delays lung tumor progression.....88
4.5 Systemic siKras delivery elicits anti-tumor effects.....89

4.6 Concurrent delivery of miR-34a and siKras improves therapeutic responses.....90
4.7 7C1-siKras has a therapeutic effect on *KRAS* mutant human NSCLC.....91
4.8 Discussion.....91
4.9 Materials and Methods.....93
4.10 Figures.....95
4.11 References.....104

Chapter 5. Future work – treating metastatic cancer with nanotechnology.....108
5.1 Nanotechnology for metastasis.....108
5.2 Therapeutic mechanisms.....109
5.3 Targeting metastasis – primary targeting.....109
5.4 Targeting metastasis – secondary targeting.....112
5.5 Therapeutic nanocarriers.....114
5.6 Diagnostic nanomaterials.....116
5.7 Unmet needs in metastatic therapies.....117
5.8 Figures.....119
5.9 References.....122

Chapter 6. Future work – Improved RNA delivery vehicles.....135

List of Figures

1.1 Chemical reactions used to synthesize siRNA conjugates.....28
1.2 The efficacy of hepatocyte-targeting delivery vehicles has improved.....28
1.3 Chemistry schemes for the synthesis of lipidoids.....29
1.4 Designing iterative libraries.....30
2.1 7C1 synthesis, characterization, and *in vivo* biodistribution.....50
2.2 7C1 delivers siRNA to endothelial cells.....51
2.3 7C1 preferentially delivers siRNA to pulmonary endothelial cells *in vivo*.....52
2.4 7C1 mediated mRNA silencing modifies endothelial function *in vivo*.....53
2S.1 Selection of 7C1 from a structurally diverse library of PEI analogs, 7C1 *in vitro* gene silencing, and characterization of 7C1 stability and size.....55
2S.2 7C1 enables multigene mRNA silencing in multiple vascular beds.....57
2S.3 Lung weight, a correlate of lung metastases, in Lewis Lung Carcinoma model of metastasis.....58
2S.4 7C1 is well tolerated in acute and chronic models of toxicity.....59
2S.5 Chemical characterization of 7C1.....60
2S.6 Selection of siRNA.....61
2S.7 Purification and optimization of 7C1.....62
2S.8 Batch-to-batch repeatability of 7C1.....64
3.1 7C1 delivers siRNA to aortic endothelial cells *in vivo*.....77
3.2 siRNA-mediated knockdown in aortic endothelial cells.....78
3.3 siRNA treatment impedes recruitment of myeloid cells to atherosclerotic plaques and reduces inflammation.....79
3.4 siRNA treatment leads to less inflammation in atherosclerotic aortae.....80
3.5 siRNA treatment impedes recruitment of myeloid cells to the heart three days following after an acute MI.....81
3S.1 Identifying aortic endothelial cells by flow cytometry.....82
4.1 Efficient delivery of siRNAs to murine adenocarcinoma *in vivo*.....95
4.2 Systemic miR-34a delivery delays tumor progression.....96
4.3 Systemic siKras delivery elicits anti-tumor responses.....97
4.4 Concurrent delivery of miR-34a and siKras improves therapeutic response.....98
4S.1 7C1 nanoparticles efficiently deliver siRNAs to murine lung adenocarcinoma cells *in vitro*.....99
4S.2 7C1 nanoparticles carrying luciferase siRNA efficiently knockdown luciferase in murine lung adenocarcinoma *in vivo*.....100
4S.3 Biodistribution of 7C1 nanoparticles.....100
4S.4 miR-34a and miR-34c are relatively under-expressed in $Kras^{LSL\text{-}G12D\ wt}$;$p53^{flox\ flox}$ lung tumors compared to normal lung.....101
4S.5 Comparing miR-34a delivery efficiency using three injection methods.....101
4S.6 Body weight in mice dosed with 7C1 nanoparticles carrying single siRNA/miRNA

or combinations.....102
4S.7 Screening effective siRNA targeting mouse Kras.....102
4S.8 7C1 nanoparticles deliver siKras.1212 in the KP model.....103
4S.9 Detecting *miR-34a* mimic and siKras in lung tumors dosed with 7C1 nanoparticles simultaneously complexed to siKras and miR-34a.....103
4S.10 7C1 nanoparticles carrying miRNA/siRNA do not induce an immune response.....104
5.1 Metastasis requires several steps, each of which presents an opportunity for new therapies.....119
5.2 The ability to target nanoparticles to cancer cells and to influence their uptake into specific cellular compartments is now feasible.....119
5.3 Blood flow patterns can predict the specific regions of metastases in approximately two-thirds of cancers.....120
5.4 The EPR effect enables nanomaterials to accumulate and be retained by a tumour.....120

List of Tables

2.1 The percent of compounds reducing firefly luciferase more than 70%, while not reducing Renilla luciferase more than 25%, ...64
2.2 Intravenous dose required to reduce target mRNA expression by 50% *in vivo*.....64
2.3 Target gene expression in cardiovascular, renal, and hepatic endothelial cells.....65
5.1 Primary targeting — general considerations for nanoparticle delivery.....121
5.2 Nanoparticulate building blocks and their uses.....121

Chapter 1. RNAs have tremendous clinical potential that is limited by insufficient delivery

Chapter 1.1 *In vivo* RNA delivery is challenging

Once primarily viewed as an intermediary between DNA and protein, RNA is now known to actively regulate gene expression by interacting with DNA, other RNAs, and proteins[1,2]. Because many of these regulatory functions are dictated by sequence-specific interactions between the RNA sequence and its target, RNAs can precisely modify gene expression and downstream cellular behavior. One well-known example of RNA-mediated gene regulation is RNA interference (RNAi), an endogenous mechanism that reduces protein expression by inhibiting translation of mRNA[3]. RNAi is induced by short interfering RNAs (siRNAs) and microRNAs (miRNAs). These small RNAs, which can be introduced into the cytoplasm endogenously by transcription or exogenously through transfection, discourage translation by guiding a protein complex called RISC (RNA-induced silencing complex) to a complementary sequence on the target mRNA[4]. While the RNAi pathway has been studied closely for over ten years, more recent evidence suggests that RNA-RNA interactions can regulate genes through non-RNAi mechanisms. For example, circular RNAs (circRNAs) can sequester miRNAs by binding to them in the cytoplasm[5].

RNAs can also interact directly with DNA and protein; as a result, RNA-mediated gene regulation does not require RNA-RNA interactions[2]. Long non-coding (lncRNAs) can affect genomic stability by interacting with DNA and protein complexes that modify the epigenetic state of the cell[2]. Similarly, RNAs derived from bacterial clustered regularly interspaced palindromic repeats (CRISPRs) can bind to Cas9, a nuclease that induces a double stranded cut in DNA[6]. Once bound to Cas9, the RNA guides the nuclease to a complementary DNA sequence. The result is targeted genomic modification mediated by the DNA-RNA-protein complex. More simply, RNAs can simultaneously bind two separate proteins and bring them together to activate downstream signaling. These, and other mechanisms reviewed elsewhere, provide strong evidence that RNAs play a fundamental role in cellular function[1,2,5].

As biologists continue to uncover RNAs that promote health and disease, the number of clinical applications requiring therapeutic RNA delivery will expand. However, to date, effective therapeutic RNA delivery has been limited to siRNAs targeted to hepatocytes of the liver[7]. Therapeutic siRNA delivery has reduced pathological protein in patients with liver diseases including TTR amyloidosis and familial hypercholesterolemia[8,9]. One study showed that nanoparticle-mediated delivery of siRNA targeting TTR reduced serum TTR in humans by nearly 90% after a systemic injection[8]. A related formulation reduced low density lipoprotein (LDL) by 57% for one individual in the trial after silencing PCSK9, a gene involved in lipid transport[9]. Additional clinical trials that use the same delivery vehicles are planned for other liver diseases, since the biophysical characteristics of the nanoparticles used in these studies do not change with the siRNA sequence. This effect is also illustrated by broad application of the liver-targeting nanoparticle C12-200, which is currently being evaluated for clinical use[10].

While these nanoparticles convincingly demonstrate that siRNA can affect liver disease in mice, nonhuman primates, and humans, significant needs in the RNA delivery field remain unmet. Most notably, highly efficient delivery to cells outside the liver, and the delivery of longer RNAs to any tissue has remained challenging[7]. Highly efficient *in vivo* delivery requires the material to perform several difficult functions. Without eliciting an unwanted immune response, the material must locate and transfect the target cell in a highly complex and heterogeneous microenvironment[11,12]. This requires that the material maximize interactions with the cell of interest while minimizing similar interactions with non-target cells and the reticuloendothelial system. A substantial amount of material is typically lost through these unwanted interactions, most notably those interactions with the kidney, liver, and immune system. If the RNA avoids these tissues and reaches the cell of interest, it must get both into and out of an endosome. Even this endocytotic process is inefficient; only 1-2% of siRNA endocytosed by hepatocytes *in vivo* eventually reached the cytoplasm[13]. The rest of the material was degraded or recycled out of the cell.

The potential for targeted drug delivery vehicles to address important clinical problems has inspired many labs to design nanomaterials for targeted siRNA delivery. For the remainder of this publication, we define targeted delivery systems as those that preferentially transfect certain cells after administration *in vivo.* Delivery can be achieved by active mechanisms (e.g. targeting ligands) or passive mechanisms (e.g. modifying biophysical nanoparticle characteristics like size and charge). As described below, specific strategies within these subsets, each with their own advantages and disadvantages, can be applied to improve siRNA delivery *in vivo.*

Chapter 1.2 RNA Targeting strategies

As soon as a nanoparticle is injected *in vivo*, it interacts with its environment. If a particle is injected intravenously, the system is initially exposed to blood and endothelial cells that line the vasculature. By contrast, subcutaneous injection exposes the material to the local microenvironment, lymphatic system, and capillary beds near the injection site. These immediate local interactions, and those experienced by the particle as it is transported around the body, can influence where the material delivered, how well it is delivered, and whether the system induces a unwanted immune response. Put more directly, there is increasing evidence that interactions between particles and the natural physiology of the body can have a substantial effect on the pharmacokinetic profile of the delivery system[14].

Enabling natural physiology to passively target siRNA *in vivo* is a promising therapeutic strategy for two reasons. First, passive targeting systems do not contain extraneous active targeting ligands like antibodies, aptamers, or small molecules. This may simplify the synthesis, formulation, and characterization of the delivery system, and thereby reduce batch-to-batch variability. Second, there are many well-characterized differences in physiology that can be exploited for RNA delivery. One such example is the differential structure and function of endothelial cells that line blood vessels throughout the body[15,16]. Endothelial cells were once considered passive conduits for oxygen and nutrients, but are now known to actively modify

metabolism, the immune response, endocytosis, and inflammation by secreting factors and expressing cell-surface receptors[17,18]. In addition to playing a critical role in health and disease, endothelial cells are functionally heterogeneous. The structure, function, and gene expression of these cells vary across different tissues, and within a given tissue[15,16]. These differences can promote delivery to specific tissues; for instance, delivery to hepatocytes is enhanced by regions of endothelial cells which contain gaps, while delivery to neurons and glial cells in the brain is limited by the tight and continuous barrier of endothelial cells lining the blood brain barrier (BBB). In this same way, natural routes of clearance that increase blood flow to the liver can promote delivery to hepatocytes. The same mechanisms designed to remove and concentrate toxins from the blood can be exploited to concentrate nanoparticles in cells of interest[19].

Active targeting systems utilize ligands like proteins or small molecules to bind specific receptors on a target cell surface. The binding can either stabilize the particle on the outside of the cell or trigger receptor-mediated endocytosis and internalization. While many different targeting ligands can be used for targeted siRNA delivery, most scientists have utilized three types of ligands: small molecules, peptides, and proteins. Small molecule targeting ligands are molecules with a distinct chemical structure and a molecular weight generally less than 1 kiloDalton (kDa). These compounds can mimic natural biomolecules, and are synthesized by traditional organic chemistry techniques. Peptide and protein targeting ligands are made of amino acids; peptides consist of less than approximately 50 amino acids while proteins are composed of many more, up to tens of thousands of amino acids. Peptide- and protein-mediated targeting requires precise three-dimensional folding that results from secondary and tertiary protein structures. Other targeting ligands, like aptamers for example, are also currently being studied but have not yet realized the same success as small molecules, peptides, and proteins. Aptamers are short (generally less than 60 bases) synthetic oligonucleotides that bind to receptors after forming complex nucleic acid secondary and tertiary structures. A library of random sequences are passed over immobilized target receptors and washed off; those that bind strongly are left over, and tested again in a process termed Systematic Evolution of Ligands by Exponential Enrichment (SELEX).

Targeting molecules can be attached to the siRNA directly, however, the synthesis of these siRNA conjugates is challenging. Effective synthesis of siRNA conjugates requires chemical synthesis schemes that meet three criteria. First, reaction conditions that degrade or denature the siRNA or ligand must be avoided. Second, conjugating the siRNA and targeting ligand together can not reduce the efficacy of either component: the siRNA must still be incorporated into RISC and the ligand must still have specificity for its target receptor. Third, the reaction should generate the highest yield possible so that expensive and inefficient purification is minimized.

One limiting factor in the synthesis of siRNA conjugates is the stability of the siRNA in different chemical reactions. The siRNA must not be denatured during the reaction, since siRNA must remain as a duplex to be properly loaded into RISC and subsequently silence genes[3]. To maintain RNA integrity, siRNA conjugation reactions should be run in conditions that avoid high

temperatures, harsh solvents, and high concentrations of reactive intermediates. One method to avoid denaturing the double stranded RNA during synthesis is to perform conjugation chemistry on the sense strand and then duplex with the antisense strand later. Sense strand modifications have been made to both the 3' and 5' end of the siRNA. However, further work is required to understand whether the location of the targeting ligand on the sense strand affects RISC loading and mRNA silencing. Conjugations to the antisense strand should be avoided, since the antisense strand should not have steric hindrances which prevent hybridization with the target mRNA in the RNAi pathway. It is also very important to chemically modify the RNA nucleotides and phosphodiester bonds, as unmodified siRNAs can both induce an immune response and be easily degraded by endogenous ribonucleases. It is common to replace the 2'-hydoxy group on some riboses in the sequence with a 2'-O-methyl group or 2'-fluoro and/or to replace one or several phosphodiester bonds with phosphorothioate bonds, although many more modifications have been reported with varying degrees of success[11]. These internal modifications are crucial for *in vivo* experiments as they can dramatically both decrease immunogenicity and increase serum stability of the siRNA.

Selecting the right solvent to ligate small molecules to the siRNA can be a particularly import decision. siRNA is soluble in aqueous conditions and precipitates in solutions with too much organic solvent. At the same time, many small molecules commonly linked to siRNA, like cholesterol and folate, are hydrophobic, and therefore require an organic solvent to solubilize. Researchers have overcome this problem using two strategies: first, small molecules and siRNA have been solubilized and reacted in a mixture of water and organic solvent like dimethylsulfoxide (DMSO) or acetonitrile. Second, researchers have attached small molecules during the oligonucleotide synthesis process. For example, cholesterol was conjugated to siRNA by initiating the siRNA synthesis on a controlled-pore glass solid support carrying a cholesterol-aminocaproic acid-pyrrolidine linker; this linker placed a cholesterol on the 3' end of the sense strand[20]. However, these techniques are limited by the fact that only certain small molecules are soluble in solvents with aqueous and organic components, many labs do not have access to oligonucleotide synthesis machines, and the solid support method requires optimization for each desired targeting ligand. Reaction conditions that do not affect double stranded siRNA still might denature small molecules, proteins, or oligonucleotides. For example, solvents with aqueous and organic components may differentially attract hydrophobic and hydrophilic regions of a protein, resulting in protein denaturing and loss of function. It is also critical that any modifications to the targeting ligand do not change its ability to bind its receptor. As a result, the active site of the ligand should be identified and conjugations should be performed as far away from this area as possible. Because conjugation reactions change for each targeting ligand, reactions that universally promote conjugation remain an important unmet need.

Despite the strict criteria associated with these reactions, several schemes that successfully conjugate biomolecules have been described (Fig. 1). Many of these reactions utilize common biological functional groups, including amines, carboxylic acids, and thiols. Importantly, siRNAs with these functional groups on the 3' or 5' of the sense strand can be

purchased from commercial vendors. A bifunctional crosslinker is then used to connect the functional group on the RNA to a different functional group on the targeting ligand. In one example, primary amines are reacted with N-hydroxysuccinimide (NHS) esters to form an amide bond that is stable in physiological pH for several hours. The NHS esters can be generated from carboxylic acids using 1-Ethyl-3-(3-dimethylaminopropyl)carbodiimide (EDC) chemistry. Another reaction that is commonly used takes place between thiols and maleimide groups; the reaction forms thioether bonds that are stable in physiological pH. Conjugates can also be formed using the highly efficient reaction that takes place bewteen streptavidin and biotin conjugation. This reaction may not be appropriate for smaller targeting ligands, however, because the size of the 53 kDa streptavidin protein can sterically interfere with the targeting ligand. These bioconjugation techniques have been complemented by new approaches that rely on highly efficient and mild 'click chemistry.' One type of promising click reaction used for siRNA-small molecule conjugation links an azide group with an alkyne using a copper catalyst[21]. This reaction generates a stable and biologically inert triazole linkage, and can be even performed without the need for a toxic copper catalyst if the alkyne is replaced with a strained cyclooctyne group[22]. The reaction is rapid and robust, bioorthogonal, and can take place in an aqueous solvent at room temperature.

Chapter 1.3 Liver physiology can promote siRNA delivery

Dysfunction of the liver can negatively affect metabolism, glycogen storage, hormone secretion, and serum lipid concentrations. As result, this tissue contributes to a myriad of common diseases that may be amenable to genetic therapies, including cancer, diabetes, clotting disorders, and heart disease. To date, the most clinically advanced siRNA therapies have targeted aberrant gene expression in hepatocytes[7]. The relative ease with which hepatocytes have been targeted can be partially attributed to distinct physiological characteristics that promote hepatocyte delivery. The liver is perfused with the hepatic portal vein, which directs blood gastrointestinal tract to the liver. As a result, delivery systems circulating in the blood have excellent access to the liver. Circulating drugs that flow by the liver can extravasate out of the bloodstream into surrounding liver tissue through nanoscale holes (fenestrae) in sinusoidal endothelial cells[7]. The average diameter of these fenestrae, roughly 100-150 nm depending on the animal species, make fenestrated endothelial cells ideal as a way for nanoscale drug delivery systems designed to reach hepatocytes[23]. Finally, liver delivery mediated by lipid nanoparticles (LNPs) and other hydrophobic systems may be enhanced by the natural mechanisms the liver uses to remove circulating lipids from the bloodstream[19].

The most advanced clinical siRNA delivery systems utilize LNPs which passively target hepatocytes. One disease that has been treated with LNP formulations is familial hypercholesterolemia, an autosomal dominant genetic disorder characterized by elevated low density lipoprotein (LDL) cholesterol. This disease, which greatly increases the risk for cardiovascular disease and sudden death, is driven by overactive PCSK9, a gene whose protein binds to and degrades LDL receptors. A Phase I clinical trial studied the tolerability and efficacy

of an LNP developed by Alnylam Pharmaceuticals that was formulated with siRNA targeting the PCSK9 gene[9]. This formulation, termed ALN-PCS02, was tolerated at all tested doses. Moreover, at the highest dose (0.4 mg/kg siRNA) an average of 70% reduction in PCSK9 protein and 40% reduction in LDL cholesterol from baseline was reported. Using another LNP formulation, Alnylam made nanoparticles targeting transthyretin (TTR), a gene whose gain of function mutations cause TTR-amyloidosis, a debilitating and fatal genetic disease characterized by extracellular deposits of insoluble, misfolded proteins. This formulation was well tolerated in Phase I clinical trials, with no drug related serious adverse events reported. The formulation, called ALN-TTR02, was also effective, reducing TTR levels by over 80% with doses between 0.15 and 0.3 mg/kg in humans[8]. Robust and durable protein reduction was also observed with this LNP: TTR serum protein decreased between 57% and 67% 28 days after treatment. ALN-TTR02 has completed Phase II clinical trials and is currently enrolling patients for a Phase III clinical trial.

Incredibly, *in vivo* LNP efficiency with hepatocytes has increased by more than 10,000x within the last ten years, as shown in Figure 2. This rapid improvement has been catalyzed by high throughput screening and rational design techniques that generate lipids and lipid-like materials that promote delivery (Fig. 2). These LNPs are typically formulated with three components: (1) cationic or ionizable lipids containing a hydrophilic amine group, a hydrophobic carbon tail, and a chemical linker that binds them, (2) lipid-anchored polyethylene glycol (PEG), which "shields" the LNP against non-specific uptake by macrophages, increases the circulation time *in vivo* and reduces particle aggregation, and (3) cholesterol or other sterol-like molecules, which increase LNP stability. These formulation parameters affect physical properties of the LNP, including size, surface charge, and siRNA loading. Moreover, a growing body of work suggests that the ratio of lipid : PEG : cholesterol : siRNA needs to be tuned to optimize RNA delivery[24].

Chapter 1.4 Strategies to develop highly efficient liver targeting nanoparticles

Originally reported in 2008, lipidoids were designed to deliver siRNA efficiently to hepatocytes. These materials were inspired by lipids, which can facilitate siRNA transfection through direct conjugation to the payload or through physical entrapment[25,26]. Though these early successes hinted at what types of materials might effectively deliver siRNA, the investigation of new materials was limited by difficult chemical syntheses that required multiple steps and purifications. The engineering community had faced similar issues related to the delivery of DNA, which shares many of the physical properties of RNA.

To overcome these difficulties, a simple hypothesis – that biodegradable, cationic compounds might facilitate safe delivery – was used as rationale for the synthesis of a structurally-diverse library of poly(ß-amino esters)[27]. To produce a large library without time-consuming protection and purification steps, diacrylates were reacted with amines via the Michael addition. This efficient scheme produced more than 2,000 distinct compounds, enough to justify relationships between chemical structure, particle size, and gene transfection

efficiency[27]. The structure-function relationships from this library were used to design a second library[28], which in turn led to the identification of a potent compound that was fine-tuned to optimize delivery[29]. These studies illustrated that a broad structural class of molecules could be screened to enable the isolation of a specific, robust compound through iterative libraries derived from efficient chemistry[27-29].

Inspired by the success of iterative rational libraries for DNA delivery, first-generation lipidoids were designed to deliver small RNAs. Cationic lipid-like structures were chosen for three reasons. First, cationic lipids had previously been shown to deliver siRNA[25]. Second, we hypothesized that smaller cationic compounds would bind to highly anionic siRNA tightly enough to prevent dissociation in the bloodstream, but loosely enough to release the RNA once it was inside the cytoplasm. Finally, we proposed that lipid tails – which facilitate interaction with membranes, enhancing uptake by the plasma membrane and destabilizing endosomal membranes[30] – might work in concert with amines – which condense nucleic acids and have been suggested to induce endosomal rupture.

Alkyl-acrylamide or alkyl-acrylate lipid tails were conjugated to amine backbones via the Michael addition, generating more than 700 first-generation lipidoids[31] (Fig. 3). Four structural parameters were modulated. First, alkyl-acrylamides and alkyl-acrylate tail length was varied between nine and 18 fully saturated carbons. Second, sundry amine backbones were chosen in order to maximize structural diversity, thus increasing the probability of identifying critical structural motifs; the chemical space explored was, however, focused by knowledge obtained from analysis of previous libraries. Third, the bond linking the amine backbone to the alkyl tail was comprised of either a biodegradable ester or a stable amide. Finally, the impact of backbone charge was investigated by quaternizing amines with methyl iodide[32]. This alkylating agent imparted a permanent positive charge on the amine.

Once the library was synthesized, an efficient *in vitro* assay was required to screen the large number of structures. An ideal assay would measure target and control gene expression concurrently, so that potent silencing would not be confused with cytotoxicity. To achieve this, human cervical cancer (HeLa) cells were made to express stably both firefly and renilla luciferases (termed dual HeLa cells). Lipidoids were complexed with firefly luciferase-targeting siRNA (siFire) before the activities of both luciferases – which have different substrates – were measured by luminescence the following day. Measuring target and control gene expression concurrently with luminescence is efficient, permitting the rapid identification of effective compounds and structure function relationships. In this case, lipidoids with at least two amines per backbone, two long lipid tails, or many shorter lipid tails potently silenced the target gene without influencing control gene expression.

These structure-function relationships were used to inform the synthesis of a second-generation lipidoid library, consisting of more than 500 new molecules. Of the 1,200 total structures, ~5% silenced target gene expression at least as efficiently as the positive control, Lipofectamine 2000, a commercially-available transfection reagent. The second-generation library led to the insights that compounds with amide linkages, more than two alkyl tails between

8 and 12 carbons, and one alkyl tail less than saturating substitution delivered siRNA to dual HeLa cells most efficiently. After identifying effective candidates in HeLa cells, the ability of compounds to silence genes in human hepatocellular carcinoma (HepG2) cells and primary bone marrow-derived murine macrophages was investigated. These additional *in vitro* assays were performed because transfection efficiencies can vary dramatically between different cell lines. Lipidoids were less proficient than Lipofectamine 2000 when silencing endogenous genes in HepG2 cells but more efficient when silencing endogenous genes in macrophages, with 50% target gene reduction at siRNA doses as low as 1 nM. By contrast, Lipofectamine did not silence macrophages even at 10 nM, suggesting lipidoids might be useful for transfecting cell lines that were previously refractory to treatment[31].

Based on the results of *in vitro* screens in multiple cell lines, 17 compounds were chosen for *in vivo* evaluation. The *in vivo* screen for hepatocyte delivery measured the serum concentration of Factor 7 (F7), a target produced specifically by hepatocytes. Hepatocytes were chosen as a target cell because they play an important role in cancer, hepatitis, hypercholesterolemia, malaria and many other pathologies[33]. Since F7 is produced specifically by hepatocytes, the assay measured hepatocyte delivery independent of delivery to kupffer cells, immune cells that reside in the liver[31].

Lipidoids were mixed with cholesterol and PEG-lipid conjugates prior to intravenous injection. These excipients had been shown to increase serum stability, resistance to aggregation, and *in vivo* tolerability[34,35]. After administering a dose of 5 mg/kg, five of the seventeen compounds silenced target protein expression by over 50%, with one (termed $98N_{12}$) silencing F7 by more than 90% relative to saline control. Before continuing with additional *in vivo* models, we discerned the active isomer of $98N_{12}$, whose reaction yields multiple products. The chemical mixture was separated into constituents that were distinguished by the number of tails attached to the amine backbone. A structure with five tails ($98N_{12}$-5), one less than saturating substitution, was identified as the active component, while the other variants were found to be relatively ineffective. Purified $98N_{12}$-5 was tested to determine how much siRNA was required to silence a target gene by 50%, how long silencing persisted, whether F7 silencing resulted in the expected physiological effect, and whether it could mediate the silencing of another liver-specific gene, Apolipoprotein B (ApoB). $98N_{12}$-5 was shown to result in dose-dependent silencing that lasted more than two weeks. The silencing of F7 and ApoB both led to increased clotting time and decreased LDL levels. Finally, the compound was evaluated in rats, which are used for pre-clinical immunological assays, and in non-human primates. It potently silenced endogenous target genes in both species.

During the original investigation of $98N_{12}$-5, delivery was enhanced by purifying a chemical mixture into constituents differentiated by the number of tails attached to the amine backbone[31]. However, this chemical optimization neglected the effect of both PEG-lipid and cholesterol on delivery. Since these components are known to influence the stability, half-life, and distribution of nanoparticles, the effect of lipidoid: siRNA mass ratio, type of PEG-lipid, and particle size on delivery was investgated[24].

The first variable modified was the lipidoid: siRNA mass ratio. High mass ratios increase the amount of lipid injected into the animal, which could cause toxic effects. Conversely, lowering the mass ratio could reduce the amount of siRNA entrapped by the particle, since fewer positive amines would be available to interact with the anionic RNA backbone. Non-entrapped siRNA would remain free in solution, effectively wasted. Consequently, siRNA entrapment was measured at mass ratios between 5 and 30. Entrapment was almost 100% at mass ratios between 10 and 30 but decreased dramatically at a mass ratio equal to 5. Consequently, efficacy and toxicity were tested at ratios of 7.5, 10, 15, 20, and 30. At a mass ratio of 7.5, compounds were well tolerated at all doses, while larger ratios resulted in weight loss at 10 mg/kg. Since efficacy decreased modestly, a mass ratio of 7.5 was selected for additional studies.

After optimizing the lipidoid: siRNA mass ratio, efficacy and tolerability as a function of the PEG-lipid tail length was evaluated at 2.5 and 25 mg/kg. PEG-lipids are anchored into the nanoparticle membrane via hydrophobic interactions. Consequently, adjusting the PEG tail length influences how securely PEG inserts into the particle. PEG-lipid length was varied between ten and 16 carbons. At 2.5 mg/kg, mouse weight loss remained constant as lipid length changed, but differed dramatically at 25 mg/kg. At 25 mg/kg, lipids with 14, 15, or 16 carbons were better tolerated than chains between ten and 13 carbons. At the same time, efficacy was maximized for tails 13 to 15 carbons in length. These studies demonstrated that alkyl tails with 14 or 15 carbons were optimal. Since even-numbered carbon tails are less expensive, C14 was chosen for subsequent studies, which sought to correlate particle size and efficacy.

To control particle size, $98N_{12}$-5 particles were made with identical molar ratios and extruded through membranes with different pore sizes. This produced particles with diameters of 150, 85, 60, and 50 nm, respectively. F7 levels measured 48 hours after intravenous injection at a siRNA dose of 3 mg/kg clearly showed improved silencing as size decreased. These results were expected, since smaller particles enter into liver parenchyma through fenestrated hepatic vasculature more easily. Liver distribution was later verified using radioactively labeled $98N_{12}$-5. Following intravenous injection, particles were observed predominantly in the liver (92% of injected dose), with a small percentage found in the spleen, another fenestrated organ.

First-generation lipidoids were optimized so that 50% reduction of a hepatic target gene was achieved when siRNA was injected intravenously at 1 mg/kg. Lipidoid synthesis revealed that new lipid delivery agents could be produced without time-consuming and expensive chemical synthesis. Consequently, second generation compounds designed to facilitate delivery at doses less than 1 mg/kg were synthesized. The original lipidoid library demonstrated that fully-saturated alkyl tails were more effective than non-alkyl tails and that lipids attached to amines through stable amide bonds were more effective than those connected by ester linkages[31]. To this end, the second-generation lipidoid library was based on stable chemical bonds between fully saturated alkyl tails and amines generated by an epoxide ring-opening reaction[10]. Alkyl tail length was varied between nine and 18 carbons, and amines were selected if they were effective in previous studies or if they possessed an interesting structural element not yet analyzed. Similar

to the Michael addition, the epoxide ring-opening reaction did not require purification or protection steps and can be performed in open air.

More than one hundred second-generation lipidoids were evaluated *in vitro* using the Dual HeLa assay. Several compounds conferred 90% silencing at an siRNA dose of 33 nM. Negligible off-target effects initially measured by constant Renilla expression were later confirmed using an MTS cell viability assay. Subsequent dose response studies in HeLa cells demonstrated that three compounds (C14-113, C12-113, and C14-120) silenced the target gene by 70% at 3.3 nM. Based on these studies, 12 promising candidates were tested for their ability to silence F7 *in vivo* at a dose of 3 mg/kg. Three compounds (C12-200, C16-96, and C14-110) silenced F7 completely. Reduced doses revealed that C12-200 inhibited F7 expression by 50% at a dose of 0.01 mg/kg, increasing efficiency by two orders or magnitude compared to $98N_{12}$-5 and stable nucleic acid lipid particles (SNALP)[25] formulations. After efficient silencing was achieved in mice, the authors examined hepatocyte silencing in non-human primates. Transthyretin (TTR) was chosen as a target gene since mutated forms cause familial cardiomyopathy and neuropathy and can be treated only by liver transplant[36]. C12-200 reduced mRNA expression by 90%, 85%, and 75% after doses of 0.3, 0.1 and 0.03 mg/kg, respectively.

C12-200's sizable therapeutic window also enables several genes to be silenced concurrently. The potential to silence many genes at once is one of the most salient advantages siRNA has over traditional small therapeutics. Most pathologies are driven by an assortment of genes acting in concert[33]. For example, viral infections like Hepatitis C evade therapies by rapidly changing gene expression[37]. Similarly, multiple mutations in hepatocellular carcinoma and other cancers are responsible for aggressive growth, metastasis, and drug resistance[38]. Since a single delivery vehicle can transport all of the therapeutic RNAs together, each treated cell would receive an integrated effect. In contrast, small molecule drugs have different pharmacokinetic properties, so some cells might experience the effects of one drug but not another. Accordingly, the authors investigated whether they could silence five hepatic genes related to cholesterol homeostasis. C12-200 was formulated with equal amounts of siRNAs targeting F7, ApoB, proprotein convertase subtilisin/kexin type 9 (PCKS9), sortillin 1 (SORT1) or x-box binding protein (Xpb1). The dose of an individual siRNA was varied between 0.005 and 0.2 mg/kg, leading to a cumulative dose between 0.025 and 1.0 mg/kg. At the highest dose, all five genes were silenced 65-90%. Although this combination was not tested for its potential to treat cholesterol-based pathologies, it did demonstrate that five genes could be knocked down simultaneously.

The therapeutic window also enabled us to investigate whether higher siRNA doses resulted in extended silencing. F7 was measured as a function of time after intravenous dosing of mice at 0.1 and 1.0 mg/kg. Serum levels returned to baseline after 20 and 35 days at these respective doses. These results illustrate that siRNA therapies can be tailored to diseases as they evolve over time. For example, as inflammatory responses advance from acute to chronic, the expression levels of the genes responsible for driving disease progression change[17]. A low dose of siRNA targeting innate cell recruitment (important in acute inflammation) could be given in

concert with a high dose targeting adaptive cytokine signaling, which is important in both acute and chronic stages[39]. Similarly, cancer cells often upregulate drug efflux pumps and different metabolic genes in response to treatment with chemotherapy[40]. Increased expression of these "contingency" genes allows cells to survive, leading to disease remission. siRNAs targeting traditional oncogenes could be combined with siRNAs targeting such contingency genes, thereby enhancing the efficacy of co-administered small molecule drugs.

Chapter 1.5 Alleviating disease *in vivo* with optimized liver targeting nanoparticles

One noteworthy advantage to RNAi therapeutics is that effective delivery does not depend on RNA sequence. Consequently, the same delivery vehicle can deliver siRNAs targeting different genes, and can be leveraged to treat many diseases. For example, $98N_{12}$-5 delivered therapeutic siRNA to mouse models of three dissimilar diseases: hypercholesterolemia, malaria, and metastatic prostate cancer. Both hypercholesterolemia and malaria are impacted by hepatocytes, but in disparate ways. Hepatocytes both produce and remove cholesterol from the bloodstream, making them critical in cholesterol homeostasis. Malaria, on the other hand, is a multi-stage disease in which small parasites, termed sporozites, mature in the liver before rapidly infecting red blood cells.

$98N_{12}$-5 reduced serum cholesterol levels by silencing PCKS9, a gene whose product binds and degrades low-density lipoprotein receptors (LDLRs) in the liver[41]. LDLRs reduce serum concentrations of harmful cholesterol by removing it from the bloodstream. This mechanism, which has been confirmed in mice and humans, is made pathological by somatic or familial mutations that lead to PCKS9 overexpression[42,43]. The combination of a well-defined pathway and pathology dependent on a gain of function mutation made PCKS9 an excellent candidate for an RNAi therapy. As a result, the effect of silencing PCKS9 in normal mice, transgenic mice, rats, and non-human primates was investigated[41]. The use of multiple animal models was critical since rodents transport most of their cholesterol as high-density lipoproteins (HDL), whereas primates transport the majority of the cholesterol as LDL.

In addition to testing multiple animal models, it is important to confirm that therapeutic responses are due to RNAi rather than off-target or immunostimulatory effects[11]. Although there is no formal standard procedure to demonstrate this, the case for an on-target RNAi-mediated effect is strengthened by (a) modifying siRNA with non-immunostimulatory 2'-O-methyl groups, (b) testing siRNA for cytokine induction in whole blood or *in vivo*, (c) using a scrambled RNA control, and (d) confirming that knockdown is dose responsive. While investigating PCKS9 silencing, all of these controls were used. The levels of PCKS9 mRNA, PCKS9 protein, and serum cholesterol were also measured as a function of time. $98N_{12}$-5 reduced PCKS9 and/or serum cholesterol in all four animal models using modified siRNA that did not elicit a cytokine response. In wild-type mice, PCKS9 mRNA was reduced for 28 days after intravenous injections of 7.5 mg/kg, while PCKS9 protein levels were reduced to the limit of detection for three days in transgenic mice after injecting 5 mg/kg siRNA. Serum cholesterol levels remained lowered for 30 days in rats. Target mRNA cleavage was also confirmed by 5'-RACE. Delivery of off-target

siRNA did not reduce target gene expression, while PCSK9 was silenced in a dose-dependent fashion.

$98N_{12}$-5 was then used to reduce infectious disease. Malaria is a multi-stage infection that begins when a mosquito deposits sporozites under the skin of a human host. Sporozites migrate to hepatocytes, attracted by their highly-sulfated heparan sulfate proteoglycans[44]. After maturing in the liver, sporozites rupture the hepatocytes, enter the bloodstream, and infect red blood cells. Malaria continues to devastate parts of the developing world, particularly in Africa and Asia. Disturbingly, it was recently reported that mosquitoes may be acquiring resistance to Artemisinin[45], the most potent anti-malarial drug produced to date. If true, it is projected that the 250 million cases and one million deaths each year caused by malaria will rise dramatically[45].

To this end, $98N_{12}$-5 was used to silence a hepatic gene that promoted malaria infection, Heme Oxygenase-1 (HO-1)[46]. HO-1, which plays a critical role in the metabolism of heme, is normally expressed at low levels. Expression increases in response to several stimuli, including heavy metals, hypoxia, heat shock, and sporozite infection[46]. HO-1 upregulation is known to inhibit cerebral malaria, a dangerous stage of the disease that comes after sporozites relocate from hepatocytes to red blood cells[47]. However, the role of HO-1 in the liver (pre-erythrocytic) stage of malaria remained unclear. To study how HO-1 expression influenced susceptibility to sporozite liver infection, Plasmodium levels were measured in mice expressing HO-1 ($Hmox^{+/+}$) and in mice genetically modified not to express HO-1 ($Hmox^{-/-}$). In contrast to the anti-malarial role it plays in the red blood cell stage of the disease, HO-1 expression was found to increase susceptibility to liver infection. To address this hepatic role of HO-1 therapeutically, siRNA-targeting HO-1 was complexed with $98N_{12}$-5 and administered intravenously to $Hmox^{+/+}$ mice at a dose of 5 mg/kg. The resultant 60% silencing of HO-1 achieved through systemic siRNA treatment conferred the same effect as genomic deletion of the gene, namely prevention of blood-stage infection[46].

This investigation illustrates that genetically modified mice can serve as an important control in siRNA studies. Conversely, in the case that modified mice are not readily available, siRNA-mediated silencing might be used in place of genetic models. In this way, systemic gene silencing can be used to answer interesting biological questions. For example, $98N_{12}$-5 was also used to answer a question critical to the field of RNAi: whether exogenous siRNAs disrupted endogenous microRNA (miRNA) pathways *in vivo*[48]. miRNAs are small RNAs produced in the nucleus and exported to the cytoplasm, where they regulate genes controlling critical cell processes, including proliferation and survival[4,49]. Previously, it was reported that genomically-integrated short hairpin RNA (shRNA) disrupted miRNA pathways, leading to acute and non-specific toxicity[50]. To investigate whether the introduction of exogenous small RNAs downstream of exportin-5 – which had been saturated in the shRNA experiments, resulting in the observed toxicity – would mitigate this deleterious effect, $98N_{12}$-5 was complexed with siRNA targeting F7 or ApoB and injected intravenously into mice at a dose of either 2 or 5 mg/kg. After confirming target gene silencing, the levels of miRNAs miR-122, miR-16, and let-7 were found

to be unaltered relative to saline control, demonstrating that siRNA delivery did not disrupt miRNA production[48].

After demonstrating that intravenously-injected lipidoids could efficiently silence hepatic genes, we investigated whether they could be used to silence genes in monocytes[51]. Monocytes are precursors to the phagocytotic macrophages of the innate immune system, mediating inflammatory responses to a variety of diseases, including cancer, myocardial infarction, and diabetes[52]. Although paramount to the initial immune response, one subset termed "inflammatory monocytes" often supports disease by promoting chronic inflammation. Such inflammatory monocytes are thus an attractive therapeutic target; however, inactivating them without disrupting other immune functions remained challenging[53]. To inhibit the function of this particular subset, C12-200 was complexed with siRNA targeting chemokine receptor 2 (CCR2), a protein critical in their recruitment[51]. CCR2 mediates inflammatory monocyte behavior but does not have a functional role in noninflammatory monocytes[51].

Because the spleen, bone marrow, and blood are rich in monocytes, members of our lab quantified real-time biodistribution of C12-200 in multiple organs. After complexation with fluorescently-tagged siRNA, particles were tracked using fluorescence molecular tomography and computed tomography (FMT-CT) imaging[54]. siRNA concentration was highest in the monocyte-rich spleen and bone marrow for the first 24 hours following intravenous injection of 1 mg/kg siRNA. Subsequent histological staining and FACS analyses demonstrated that C12-200 transfected inflammatory monocytes more efficiently than other immune cell types. Once delivery to inflammatory monocytes was confirmed, 50% mRNA silencing and reduced protein expression was measured following intravenous injection of 0.5 mg/kg CCR2 siRNA.

By inhibiting inflammatory monocyte recruitment, C12-200 was used to mitigate inflammatory responses in myocardial infarctions, pancreatic islet transplant rejection, and lymphoma. Since activated macrophages and other inflammatory cells lead both to plaque rupture and increase infarct size once a heart attack occurs, the authors sought to reduce their accumulation in plaques[55,56]. Both macrophage accumulation and infarct size were measured after control or CCR2 siRNA was injected intravenously into mice at a dose of 0.5 mg/kg. Excitingly, both parameters were markedly reduced relative to controls. They also investigated whether CCR2 silencing would promote islet transplantation. Although islet transplantation has been successful in treating diabetes, grafts are often rejected by the host immune system[57]. After intravenous injection of lipidoids containing CCR2 siRNA at a dose of 0.5 mg/kg, graft survival was enhanced, leading to improved glycemic performance.

Finally, the effects of CCR2 on tumor-associated macrophage (TAM) recruitment were measured. TAMs promote tumor growth and metastasis via the release of matrix metalloproteinases (MMPs) and other molecules that degrade extracelluar matrix, releasing growth factors and clearing a path for cells to migrate[58]. Accordingly, the presence of TAMs correlates with poor prognosis in lymphoma[59]. CCR2 silencing reduced TAM accumulation, tumor volume, and tumor vascularization after lymphoma cell implantation.

Chapter 1.6 Lessons from lipidoids can be applied to non-liver delivery vehicles

RNAi has fundamentally changed the way biologists study gene expression. Excitingly, the role of RNA continues to broaden. Specific gene silencing via siRNA has been augmented by miRNA-mediated regulation of gene networks and, more recently, regulation by non-coding RNAs[49,60]. The non-linear and dynamic behavior of gene networks has recently been a focus of biologists working in concert with advanced mathematics. This line of investigation has led to the identification of genes that, despite being upregulated only by a small amount, act as potent nodes in complicated genomic networks[61]. Such advances will likely reveal a plethora of genetic targets in many cell types.

The roles these new targets will play in biology and medicine may be diverse, but they will share an important commonality: our ability to utilize them will be limited by our ability to deliver them. High throughput *in vitro* and *in vivo* assays designed to test for delivery to hepatocytes enabled iterative studies, through which two potent compounds, $98N_{12}$-5 and C12-200, were discovered (Fig. 4).

These iterative studies identified variables that impact delivery *in vivo*. Combining small amines – which electrostatically condense nucleic acids and facilitate endosomal escape – with lipid tails that enhance delivery by interacting with the plasma and endosomal membranes, improves delivery[10,30-32]. To this end, new libraries consisting of combinations of materials that work through disparate mechanisms could lead to effective vehicles. Prospective studies could also evaluate combinations of endogenous compounds, combining molecules that are naturally endocytosed[62] with cell-penetrating peptides[63]. Once an effective structure is identified, the systematic study of material: siRNA ratios and the effect of excipients can improve the therapeutic window. This is critical since a large therapeutic window permits concurrent silencing of multiple genes simultaneously[10]. Because pathology-inducing genes can vary between patients, RNAi treatments might one day be tailored to patient-specific mutations. This flexibility could be extended to diseases that evolve over time, since high doses of siRNA silence for longer periods (temporal targeting).

Because delivery does not depend on RNA sequence, a successful delivery vehicle can be used to treat sundry diseases driven by upregulation of gene expression in a given cell type. Such versatility was demonstrated with $98N_{12}$-5, which delivered siRNAs to address pathologies as diverse as cancer[64], malaria[46], and hypercholesterolemia[65]. While potent and durable gene silencing has been established upon delivery of siRNA to hepatocytes, realizing the full potential of RNAi will require the synthesis of materials and development of appropriate *in vivo* screening assays to facilitate the identification of new compounds confer silencing in other cell types at low doses. Improved *in vivo* assays will help uncover structure-function relationships governing the important objective of non-liver delivery. The iterative, combinatorial approach described herein represents one rigorous approach to achieve this aim.

Chapter 1.7 Conjugate systems for hepatic siRNA delivery

Complementing LNPs which passively target the liver are systems that have been designed to actively target hepatocytes by binding to the asialoglycoprotein receptor (ASGPR). This receptor, which is constitutively and specifically expressed on the surface of hepatocytes, has a carbohydrate recognition domain (CRD) that binds to the monosaccharide galactose, and plays an important role in glycoprotein homeostasis[66]. Binding between galactose and ASGPR is well characterized: alcohol groups at the 3- and 4- positions of the galactose bind to ASGPR by interacting with a calcium ion in the ASGPR and forming hydrogen bonds with neighboring amino acids[67]. This binding changes the configuration of the receptor and triggers receptor-mediated endocytosis. Because this receptor is expressed primarily on hepatocytes, several labs have developed galactose-analog conjugates for the delivery of siRNAs and other therapeutics[67]. This interest has grown as evidence suggests that these analogs can effectively deliver therapeutics to hepatocytes without significantly transfecting Kupffer cells *in vivo*.

Hepatocyte-targeting with galactose and its analogs has improved with our understanding of the mechanisms that govern the interaction between the ligand and its receptor. Early work relied on a cationic polymer polyethyleneimine (PEI) that was conjugated to galactose and complexed with DNA[68]. This compound improved DNA delivery to hepatocytes *in vivo,* but was limited by the inherent toxicity associated with high molecular weight PEI. To improve selectivity and tolerability, groups utilized the ligand N-Acetylgalactosamine (GalNAc), a simple derivative of galactose with an acetylamino group replacing the hydroxyl at the 2-position of the sugar, that binds to the ASGPR receptor with higher selectivity than unmodified galactose[69]. This engineering approach was used to study whether additional chemical modifications made to the 2- and 6- positions of GalNAc increased the binding affinity to ASGPR. Indeed, when trifluoroacetyl modifications were made to the 2- postion GalNAc, the binding affinity for ASGPR increased by more than fifty fold (dissociation constant K_d = 0.7 vs 40 uM, respectively)[69]. Because this binding study was performed without RNA, it will be important to understand whether increased affinity is still observed with conjugated siRNA.

The binding of GalNAc to ASGPR has also been improved by increasing the valency of the GalNAc ligand. It has been shown that binding affinity increases when clusters of glycoside receptors are simultaneously bound with an optimal spacing of at least 15 Å between sugar residues[70]. To take advantage of this clustering effect, triantennary GalNAc was synthesized; its ASGPR dissociation constant was 2 nM, 2000 fold lower that than the single GalNAc system[57]. Triantennary GalNAc conjugated directly to the 3' end of the sense strand of siRNA has been used by Alnylam Pharmaceutics in clinical trials. The most clinically advanced triantennary GalNAc siRNA conjugate is ALN-TTRsc, a subcutaneously-administered therapeutic for treatment of TTR-mediated amyloidosis. No significant adverse effects were observed in Phase I clinical trials, and TTR serum protein was reduced in patients treated with 2.5 mg/kg dose. Increasing the dose to 10 mg/kg resulted in more potent TTR protein reduction; up to 94% protein reduction was measured after a single dose. Although these siRNA doses are much higher than Alnylam's lipid nanoparticle TTR formulation (ALN-TTR02), the direct GalNAc-siRNA conjugates were well-tolerated at doses well above those needed for potent silencing.

Moreover, these targeted conjugates did not require PEG or cholesterol, and were administered subcutaneously instead of intravenously. This makes patients more likely to tolerate the injection, and in turn, increases the number of clinical indications to which these systems can be applied. Alnylam is currently utilizing the GalNAc conjugates to reduce PCSK9 and antithrombin (AT) to treat familial hypercholesterolemia and hemophilia, respectively.

GalNAc targeting ligands have also been used by the Dynamic Polyconjugate (DPC) system[71,72]. First-generation DPCs used an amphipathic polymer made of butyl and amino vinyl ethers (PBAVE) as a reactive backbone to which siRNA, the GalNAc targeting ligand, PEG were attached via acid-labile linkages[71]. While the exact mechanism of action remains unclear, it is hypothesized that these linkages break in the acidic environment of the endosome, allowing the newly "unmasked" amine groups on the PBAVE to help destabilize the membrane and facilitate endosomal escape. First generation DPCs administered intravenously to mice at a 2.5 mg/kg siRNA dose reduced ApoB by 80-90%. This potent silencing was accompanied by a phenotypic reduction in serum cholesterol[71]. Slight but non-significant increases of liver enzymes and cytokines were observed during the study; however, the authors concluded DPC was well-tolerated. Based on the hypothesis that a biodegradable polymer would decrease toxicity, Merck synthesized a bioreducible variant of the DPC system by incorporating disulfide bonds in the polymer. This compound reduced ApoB mRNA expression by 80% in mice after a 3 mg/kg injection[73].

Recently, it was reported that the PBAVE polymer need not be covalently bound to the siRNA for efficient hepatocyte gene silencing[72]. When authors co-injected PBAVE and a cholesterol-siRNA conjugate, they found that both systems co-localized to mouse hepatocytes and silenced genes, even when the polymer and siRNA were injected two hours apart. Injecting the endosomolytic agent and cholesterol-siRNA improved the efficiency by 500-fold compared to cholesterol-siRNA alone and greatly simplified the formulation process. A second-generation delivery system utilizing a GalNAc conjugated to a small peptide called melittin, a small biodegradable peptide component of bee venom which is thought to disrupt the endosome and enhance endosomal escape[74]. This system delivered siRNA that reduced chronic Hepatitis B virus (HBV) infection in mice. These results demonstrated that melittin promoted delivery without generating anti-melittin antibodies. The successful mouse and non-human primate results of this study led to a Phase I clinical study studying the safety and tolerability of a co-injection of GalNAc/masked-melittin conjugates with siRNA-cholesterol conjugates (called ARC-520) to treat chronic hepatitis B infection in humans. In March 2014, a Phase IIa clinical trial of ARC-520 was started in patients with chronic HBV.

GalNAc ligands have also been used to actively target nanoparticles to hepatocytes. Triantennary GalNAc was incorporated into DLin-KC2-DMA nanoparticles and injected *in vivo*[19]. This conjugation significantly improved siRNA delivery compared to unmodified DLin-KC2-DMA nanoparticles in $ApoE^{-/-}$ mice, which could not use the endogenous ApoE-depedent endocytosis mechanism and thus forced ASGPR-mediated endocytosis.

Chapter 1.8 Tumor physiology can promote or inhibit delivery of siRNA

The term cancer encompasses hundreds of complicated diseases with distinct presentations, available treatments, and prognoses. At the most basic level, cancers are characterized by aberrant and uncontrolled cell growth. As mutated cells continue to grow more rapidly and die less often than normal cells, the physiology of the resulting primary tumor becomes unstable and heterogeneous. The complicated genetic and phenotypic landscape of primary tumors (and their metastases) often creates an environment that can either promote or prevent the delivery of nanotherapeutics. Tumor vasculature, for instance, can be discontinuous, twisted, and leaky[75]. This occurs because the synthesis of normal functional blood vessels requires an intricate cascade of molecular signals that occur in specific order both in space and time[76]. Abnormal signaling that takes place in the tumor prevents the normal signaling cascade from being completed, leading to the rapid generation of dysfunctional, tortuous vessels. While leakiness may enhance the delivery of some drug delivery systems in certain animal models, there is also strong evidence that suggests just the opposite: because the tumor vessels had been leaky for some time and new cells were being generated rapidly in the tumor, hydrostatic pressure builds up in the tumor microenvironment[77]. As a result, nanoparticles are not able to exit tumor vessels. Delivery may also be affected by the immunological state of the tumor. Tumor physiology is pro-inflammatory; as a result, tumors are often filled with immune cells, which can endocytose nanoparticles[78]. Finally, the cancer cells and co-opted cells of the tumor microenvironment are often mutated, leading to abnormal cellular function. Cells can undergo mutations that can either promote or inhibit endocytosis and cytoplasmic delivery. Taken together, these factors suggest that the relationship between drug delivery and tumor physiology will remain contentious, and will likely depend on the specific tumor and type and *in vivo* model.

Primary tumors can also shed cells into the circulation. A small fraction of these cells can spread to distant organs through a process called metastasis. This process has been difficult to treat therapeutically because surgical resection and localized radiation are often not viable options when the disease has spread. As a result, over 90% of cancer deaths result from metastasis. Metastasis is a relatively complicated, and therefore inefficient, biological process that requires cells to clear a path to the vasculature, enter the circulation, exit the circulation, and proliferate in the secondary site[79]. Metastasis is initially promoted by primary tumor growth. Rapid growth leads to the formation of dysfunctional and inefficient blood vessels; poor perfusion in the tumor prompts cancer cells to express genes that induce cell motility and anaerobic metabolism[79]. In some cases, cancer cells can actively degrade extracellular matrix and epithelial cell-cell junctions in their surrounding microenvironment to clear a path towards nutrient-rich vasculature[80]. Once at the vasculature, the cells can enter the bloodstream by degrading endothelial cell-cell junctions or increasing endothelial cell permeability by releasing molecules like vascular endothelial growth factor (VEGF). Metastatic cells in the bloodstream can bind circulating platelets and leukocytes to increase survival before they reach their secondary site. At the secondary site, the cells must extravasate out of the circulation, survive in an unfamiliar microenvironment, and proliferate. Cancer cells exit the circulation in a process

akin to the one they use to enter it; they release molecules that induce endothelial cell death and degrade the surrounding extracellular matrix. At that point, the metastatic cells can co-opt natural growth signals in the microenvironment to enhance their own survival and growth. For example, metastatic breast cancer cells embedded in bone marrow express CXCR4 receptors that bind to nearby CXCL12 ligands, leading to metastatic progression[81].

Aberrant gene expression in tumors can result in the overexpression of cell surface receptors that can be actively targeted. One such receptor used active targeted tumor delivery is the folate receptor. This receptor is expressed in low levels on healthy cells, but is overexpressed in epithelial cancers (including those of the ovary, colon, lung, prostate, nose, throat, and brain) and hematopoietic malignancies of myeloid origin (including myelogenous leukemias)[82]. Binding between the folate receptor and its ligand (folate, also termed folic acid) initiates downstream signaling that promotes cell survival and proliferation. The utility of folate as a ligand is enhanced by its γ-carboxylic acid. This carboxylic acid has been directly conjugated to nanoparticles, siRNA, and even DNA origami structures that were simultaneously bound to siRNA[83]. In all cases, delivery to cells with folate receptors was greater than delivery to cells without the receptor. For example, one study found that mesoporous silica nanoparticles conjugated with folate delivered drugs more effectively to pancreatic xenograft tumors in mice than nanoparticles than without folate[83]. Similarly, siRNA that was directly conjugated to folate via a low molecular weight PEG spacer showed increased RNA delivery compared to non-conjugated siRNA[84].

In addition to the 441 Da folate molecule, the 78 kDa glycoprotein transferrin can also be used in cancer-targeting RNA therapies. The transferrin receptor, which affects ion transportation and cell growth, is overexpressed on malignant cells[85]. Transferrin was used to target a linear, cationic cyclodextrin polymer that has been formulated into nanoparticles which preferentially deliver siRNA to tumors *in vivo*[86]. In one example, the nanoparticles delivered an siRNA targeting the M2 subunit of ribonucleotide reductase (RRM2), an enzyme whose inhibition reduces cancer cell proliferation both *in vitro* and *in vivo* for humans and other species[82]. The transferrin targeting ligand is crucial for potency: at 2.5 mg/kg dosing in mice, RRM2-siRNA loaded cyclodextrin nanoparticles formulated with the transferrin ligand slowed tumor growth, while identical particles formulated without the transferrin ligand did not[81]. A study was performed in non-human primates to determine the tolerability of these cyclodextrin-based nanoparticles with siRNA[87,88]. Doses up to 9 mg/kg appeared to be well-tolerated with no detectable toxicity, whereas doses at 27 mg/kg produced a mild immune response, an unsurprising result considering the authors used siRNA which contained no chemical modifications to reduce immunogenicity.

The transferrin-targeted, cyclodextrin-based nanoparticles with RRM2-siRNA (called CALAA-01) were used in clinical trials, and produced the first direct evidence of RNA interference in humans[87]. The nanoparticles were injected IV into patients with solid cancers refractory to standard-of-care therapies at mg/kg on days 1, 3, 8 and 10 of a 21-day cycle.

Preliminary results from the Phase I clinical trials showed that the treatment reduced RRM2 mRNA and protein levels and induced mRNA cleavage, as measured by 5'-RLM-RACE.
Active siRNA delivery to ovarian cancer cells has been achieved with siRNA conjugated to tumor-targeting peptides. More specifically, the cyclic nonapeptide LyP-1, found through an *in vivo* screen of random peptides displayed on phage surfaces, targeted lymphatic endothelial cells in tumors and by selectively binding to HABP1, a mitochondrial protein overexpressed in ovarian and other tumors[89]. Lyp-1 has also been modified to increase functionality: dual peptides with Lyp-1 domains and transportin domains were synthesized to promote tumor penetration and membrane transport, respectively. The tandem peptide was complexed with siRNA targeting ID4, an oncogene that was found to be essential for proliferation in many ovarian cancers[90]. The conjugates were then formulated into nanoplexes and injected in the peritoneal cavity or intravenously with ovarian tumor-bearing mice. The particles penetrated deeply into tumor parenchyma, reduced tumor ID4 mRNA expression by 80%, and significantly reduced tumor growth. These delivery systems also distributed to the liver, spleen, and lung. Although intraperitoneal injection showed better accumulation in the ovarian tumor, there was not a significant difference in ID4 knockdown between the two routes of administration.

Chapter 1.9 Endothelial cell targeting

Endothelial cells, which line the blood vessels that penetrate nearly every tissue in the body, actively influence blood pressure, inflammation, metabolism, angiogenesis, and microenvironmental regulation. As a result, these cells contribute to more disease than any other tissue in the body, including cardiovascular ischemia, cerebrovascular ischemia (e.g. stroke), primary tumor growth, metastasis, diabetes, and chronic inflammation[33]. Because there are many diseases that would benefit from highly efficient endothelial siRNA delivery, a number of delivery systems have been designed to deliver siRNA to endothelial cells *in vivo*[91]. LNPs made from a cationic lipid, a helper lipid, and PEG were injected intravenously at a dose of 1.88 mg/kg on four consecutive days. Following this total dose of 7.52 mg/kg siRNA, pulmonary and hepatic endothelial cell mRNA and protein decreased significantly[92,93]. Second-generation lipid nanoparticles were then shown to reduce pulmonary endothelial cell mRNA expression after a total dose of 2.8 mg/kg siRNA[94]. While these delivery systems effectively targeted pulmonary endothelial cells *in vivo*, they required doses much higher than those required for potent hepatocyte silencing (0.01 mg/kg) (Fig. 2).

Inspired by the highly efficient hepatocyte delivery a library of low molecular lipid-polymer materials was developed for endothelial delivery. Formulations were first screened them for their ability to reduce target mRNA expression in multiple cell lines, including two endothelial cell lines. Lead candidates were screened *in vivo,* leading to selection of a compound termed 7C1, a low molecular weight compound made by conjugating C_{15} epoxide-terminated lipids and extremely low molecular weight (M_N = 600 Da) branched PEI[95]. 7C1 nanoparticle formulation was optimized to ensure particles were small, stable, and repeatedly silenced target mRNA *in vivo*. For example, seven batches of 7C1 nanoparticles were made with either

extrusion or microfluidic mixing, and injected intravenously. Particles made with microfluidic mixing silenced mRNA expression much more consistently than those made with extrusion. The 7C1 formulation was then made with different 7C1: cholesterol: PEG molar ratios; unlike liver-targeting compounds, 7C1 did not require cholesterol to maximize mRNA silencing. The optimized 7C1 formulations potently reduced target mRNA expression in pulmonary, cardiovascular, and renal endothelial cells *in vivo* after injections of 0.017, 0.04, and 0.08 mg/kg, respectively (Fig. 2). These compounds did not reduce target mRNA expression in pulmonary immune cells, systemic immune cells, or hepatocytes *in vivo*. The precise mechanism governing the preferential targeting of 7C1 particles to endothelial cells is currently unclear, but may be related to interactions with serum proteins. 7C1 delivery also reduced target mRNA expression for over 21 days following one injection, and to simultaneously deliver siRNAs targeting five different genes concurrently *in vivo.*

The functional effect of 7C1-mediated endothelial siRNA delivery was confirmed in animal models of vascular permeability, emphysema, primary tumor growth, and metastasis[12]. However, in all these cases, a single siRNA was used to elicit a desired phenotype. Because multiple small RNAs can be formulated into a single 7C1 nanoparticle, we investigated whether targeted combination therapy could reduce disease progression and extend survival in a genetically engineered mouse model of non-small cell lung cancer (NSCLC). A clinically-relevant spontaneous tumor model in which lung epithelial cells simultaneously express tumorigenic $Kras^{G12D}$ was investigated. These so-called KP tumors are extremely aggressive, and mimic both human lung cancer progression and response to therapeutics. 7C1 was first formulated with a therapeutic miRNA called miR-34a that is downregulated in NSCLC. miR-34a replacement significantly reduced tumor growth without inducing measurable increases in serum cytokine expression. 7C1 nanoparticles were then formulated with siRNA targeting Kras, an oncogene that drives tumor progression and metastasis. siKras therapy significantly slowed tumor growth, and increased tumor apoptosis. The combination therapy with both miR-34a and siKras resulted in tumor regression and significantly extended survival on its own and when used in concert with cisplatin, a first-line NSCLC therapy[96].

1.10 Figures

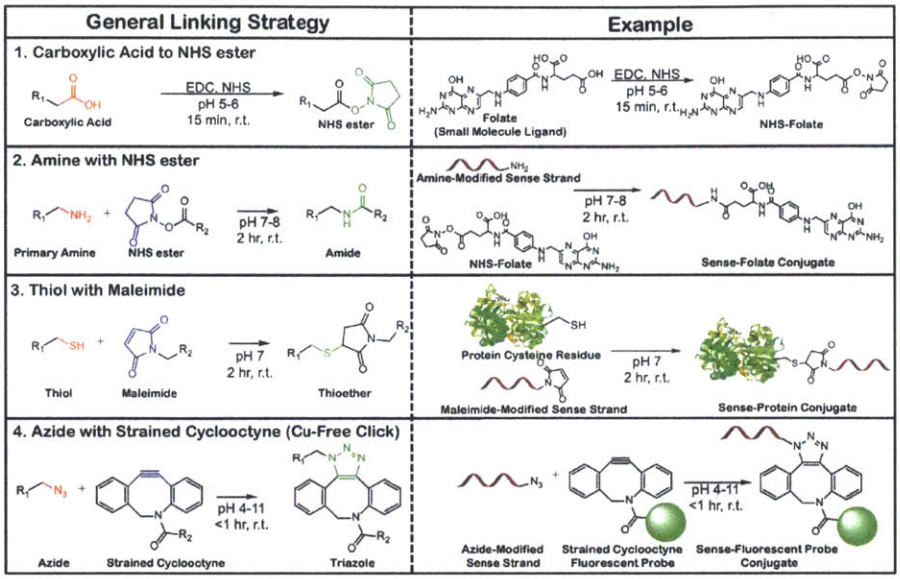

Figure 1.1. Chemical reactions used to synthesize siRNA conjugates. Conjugation reactions must not denature the targeting ligand, affect siRNA stability, or prevent siRNA loading into RISC. Notably, many synthetic schemes in use today require modification for every new targeting ligand.

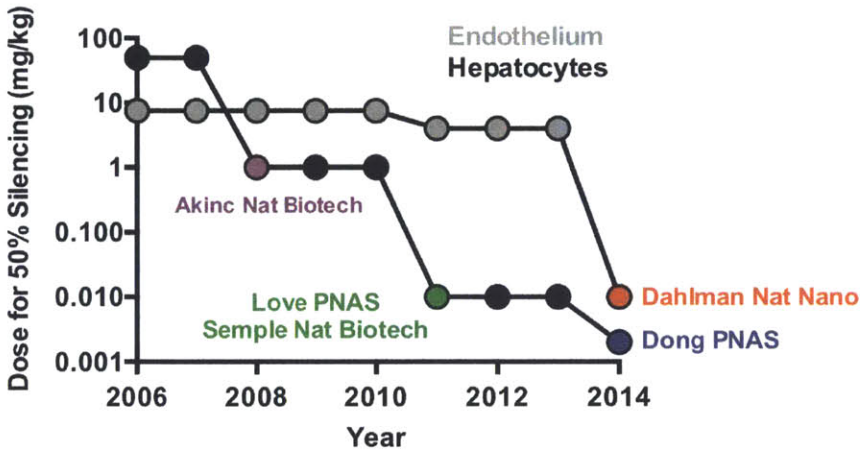

Figure 1.2. The efficacy of hepatocyte-targeting vehicles has improved dramiatically over time. The dose required to reduce target gene expression in hepatocytes by 50% *in vivo* has decreased more than 10,000x since 2006. siRNA delivery to other cell types, notably endothelial cells, has remained challenging.

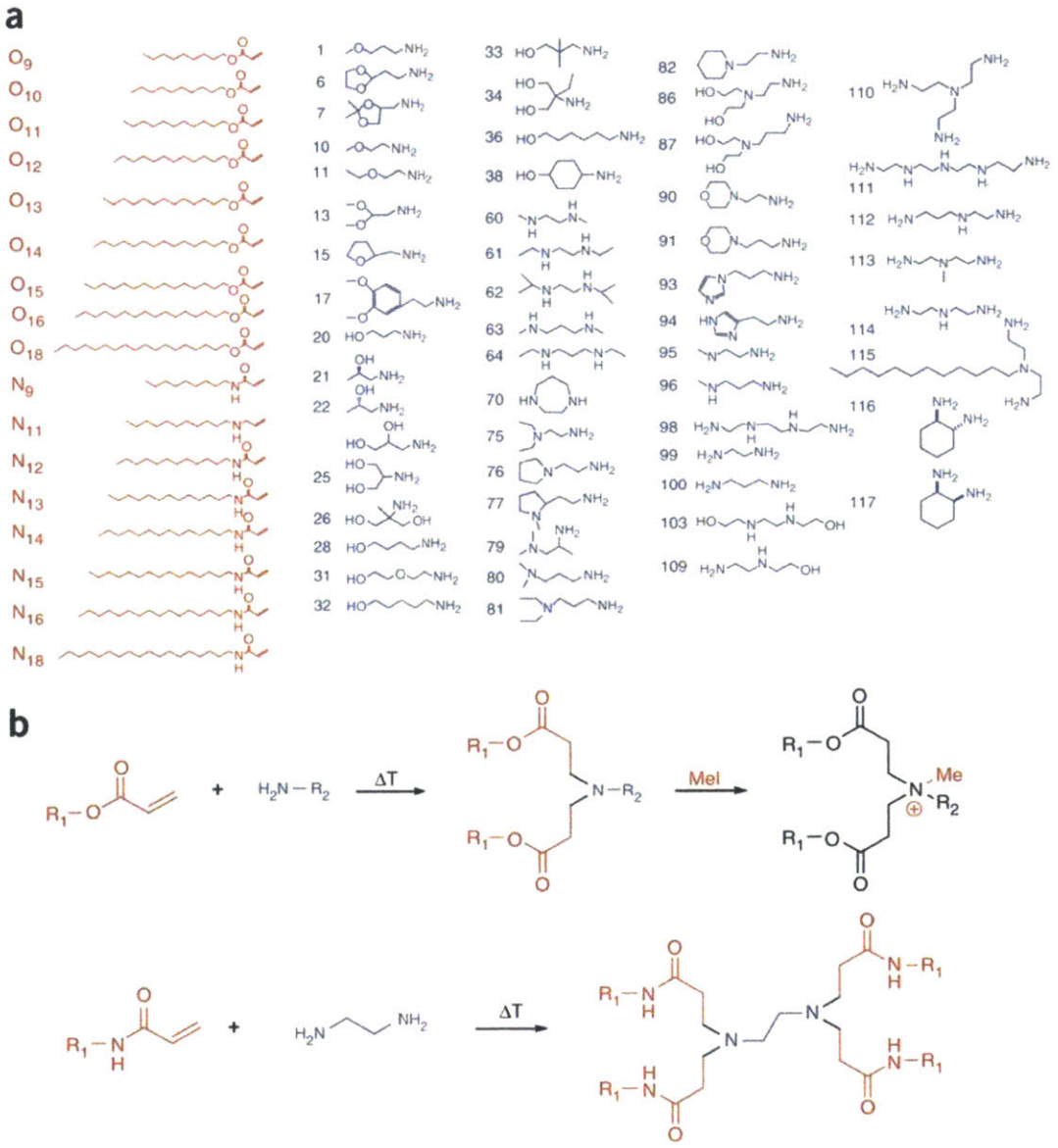

Figure 1.3. Chemical schemes for the synthesis of lipidoids. (**a**) Alkyl-acrylate, alkyl-acrylamide and amino molecules were used to synthesize a combinatorial library of lipidoids. (**b**) Synthesis occurs through the conjugate addition of amines to an acrylate or acrylamide. Depending on the number of addition sites in the amino monomer, lipidoids can be formed with anywhere from 1 to 7 tails. Amino groups in the lipidoid can be quaternized by treatment with methyl iodide. For ease of nomenclature, lipidoids are named as follows: (amine number)(acrylate or acrylamide name)-(number of tails)("+" if quaternized).

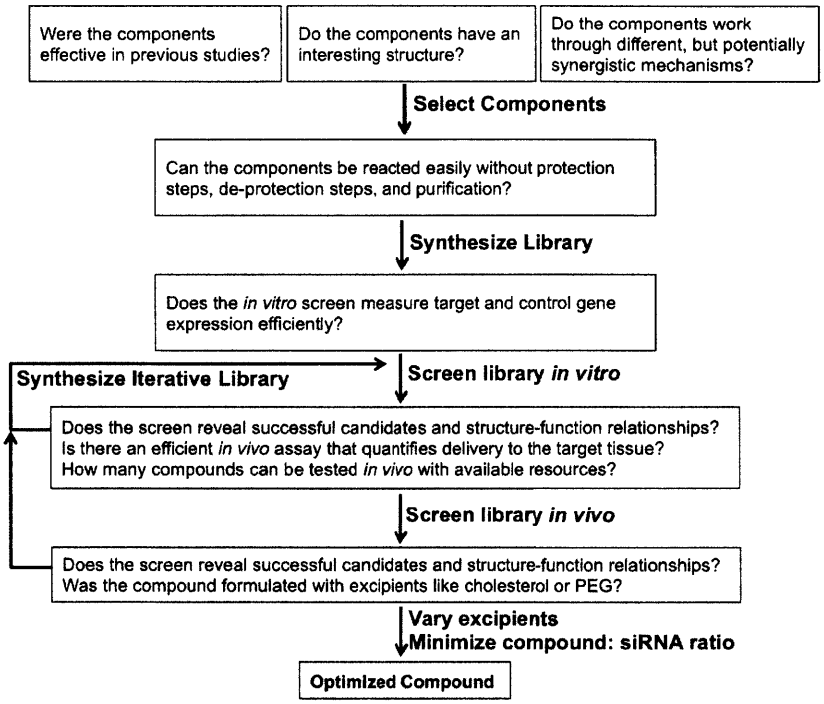

Figure 1.4. Iterative library design. Starting components should be selected rationally, based on previous studies or interesting chemical structure. After ensuring the components can be conjugated using efficient chemistry, efficient *in vitro* screens should be used to identify successful candidates. The top-performing materials can be analyzed to determine structure-function relationships. These results should inform the synthesis of iterative libraries and the selection of compounds screened *in vivo*. Once a potent *in vivo* compound is identified, any excipients used in its formulation should be systematically varied, and the minimum carrier:siRNA mass ratio can be determined.

1.11 References

1. Rinn, J.L. & Chang, H.Y. Genome regulation by long noncoding RNAs. *Annu Rev Biochem* **81**, 145-166 (2012).
2. Sabin, L.R., Delas, M.J. & Hannon, G.J. Dogma derailed: the many influences of RNA on the genome. *Mol Cell* **49**, 783-794 (2013).
3. Bumcrot, D., Manoharan, M., Koteliansky, V. & Sah, D.W.Y. RNAi therapeutics: a potential new class of pharmaceutical drugs. in *Nat Chem Biol*, Vol. 2 711-719 (2006).
4. Rana, T.M. Illuminating the silence: understanding the structure and function of small RNAs. in *Nat Rev Mol Cell Biol*, Vol. 8 23-36 (2007).
5. Jeck, W.R. & Sharpless, N.E. Detecting and characterizing circular RNAs. *Nat Biotechnol* **32**, 453-461 (2014).

6. Sander, J.D. & Joung, J.K. CRISPR-Cas systems for editing, regulating and targeting genomes. *Nat Biotechnol* **32**, 347-355 (2014).
7. Kanasty, R., Dorkin, J.R., Vegas, A. & Anderson, D. Delivery materials for siRNA therapeutics. *Nat Mater* **12**, 967-977 (2013).
8. Coelho, T., *et al.* Safety and efficacy of RNAi therapy for transthyretin amyloidosis. *N Engl J Med* **369**, 819-829 (2013).
9. Fitzgerald, K., *et al.* Effect of an RNA interference drug on the synthesis of proprotein convertase subtilisin/kexin type 9 (PCSK9) and the concentration of serum LDL cholesterol in healthy volunteers: a randomised, single-blind, placebo-controlled, phase 1 trial. *Lancet* **383**, 60-68 (2014).
10. Love, K.T., *et al.* Lipid-like materials for low-dose, in vivo gene silencing. in *Proc Natl Acad Sci USA*, Vol. 107 1864-1869 (2010).
11. Whitehead, K., Dahlman, J.E., Langer, R.S. & Anderson, D.G. Silencing or Stimulation? siRNA Delivery and the Immune System. *Annual Review of Chemical and Biomolecular Engineering* (2010).
12. Whitehead, K.A., Langer, R. & Anderson, D.G. Knocking down barriers: advances in siRNA delivery. in *Nature Reviews Drug Discovery*, Vol. 8 129-138 (2009).
13. Querbes, W., *et al.* Treatment of erythropoietin deficiency in mice with systemically administered siRNA. *Blood* **120**, 1916-1922 (2012).
14. Monopoli, M.P., Aberg, C., Salvati, A. & Dawson, K.A. Biomolecular coronas provide the biological identity of nanosized materials. *Nat Nanotechnol* 7, 779-786 (2012).
15. Aird, W. Phenotypic Heterogeneity of the Endothelium: II. Representative Vascular Beds. *Circulation Research* **100**, 174-190 (2007).
16. Aird, W. Mechanisms of Endothelial Cell Heterogeneity in Health and Disease. *Circulation Research* **98**, 159-162 (2006).
17. Pober, J.S. & Sessa, W.C. Evolving functions of endothelial cells in inflammation. *Nat Rev Immunol* 7, 803-815 (2007).
18. Hagberg, C.E., *et al.* Vascular endothelial growth factor B controls endothelial fatty acid uptake. *Nature* **464**, 917-921 (2010).
19. Akinc, A., *et al.* Targeted delivery of RNAi therapeutics with endogenous and exogenous ligand-based mechanisms. *Mol Ther* **18**, 1357-1364 (2010).
20. Soutschek, J., *et al.* Therapeutic silencing of an endogenous gene by systemic administration of modified siRNAs. in *Nature*, Vol. 432 173-178 (2004).
21. Yamada, T., *et al.* Versatile site-specific conjugation of small molecules to siRNA using click chemistry. *J Org Chem* **76**, 1198-1211 (2011).
22. Chang, P.V., *et al.* Copper-free click chemistry in living animals. *Proc Natl Acad Sci U S A* **107**, 1821-1826 (2010).
23. Wisse, E., Jacobs, F., Topal, B., Frederik, P. & De Geest, B. The size of endothelial fenestrae in human liver sinusoids: implications for hepatocyte-directed gene transfer. *Gene Ther* **15**, 1193-1199 (2008).

24. Akinc, A., *et al.* Development of Lipidoid-siRNA Formulations for Systemic Delivery to the Liver. *Mol Ther* **17**, 872-879 (2009).
25. Zimmermann, T.S., *et al.* RNAi-mediated gene silencing in non-human primates. in *Nature*, Vol. 441 111-114 (2006).
26. Morrissey, D.V., *et al.* Potent and persistent in vivo anti-HBV activity of chemically modified siRNAs. in *Nat Biotechnol*, Vol. 23 1002-1007 (2005).
27. Anderson, D.G., Lynn, D.M. & Langer, R. Semi-Automated Synthesis and Screening of a Large Library of Degradable Cationic Polymers for Gene Delivery. *Angewandte Chemie International Edition* **42**, 3153-3158 (2003).
28. Anderson, D., Akinc, A., Hossain, N. & Langer, R. Structure/property studies of polymeric gene delivery using a library of poly(Œ≤-amino esters). *Molecular Therapy* **11**, 426-434 (2005).
29. Zugates, G.T., *et al.* Rapid Optimization of Gene Delivery by Parallel End-modification of Poly(Œ≤-amino ester)s. *Molecular Therapy* **15**, 1306-1312 (2007).
30. Hafez, I.M., Maurer, N. & Cullis, P.R. On the mechanism whereby cationic lipids promote intracellular delivery of polynucleic acids. *Gene therapy* **8**, 1188-1196 (2001).
31. Akinc, A., *et al.* A combinatorial library of lipid-like materials for delivery of RNAi therapeutics. *Nat Biotechnol* **26**, 561-569 (2008).
32. Akinc, A., Thomas, M., Klibanov, A.M. & Langer, R. Exploring polyethylenimine-mediated DNA transfection and the proton sponge hypothesis. in *J Gene Med*, Vol. 7 657-663 (2005).
33. Kumar, V., Abbas, A., Fausto, N. & Aster, J. Robbins and Cotran Pathologic Basis of Disease, Eighth Edition. (2009).
34. Klibanov, A.L., Maruyama, K., Torchilin, V.P. & Huang, L. Amphipathic polyethyleneglycols effectively prolong the circulation time of liposomes. *FEBS Letters* **268**, 235-237 (1990).
35. Senior, J. & Gregoriadis, G. Stability of small unilamellar liposomes in serum and clearance from the circulation: The effect of the phospholipid and cholesterol components. *Life Sciences* **30**, 2123-2136 (1982).
36. Sekijima, Y., Kelly, J.W. & Ikeda, S. Pathogenesis of and therapeutic strategies to ameliorate the transthyretin amyloidoses. *Curr Pharm Des* **14**, 3219-3230 (2008).
37. Kronke, J., *et al.* Alternative approaches for efficient inhibition of hepatitis C virus RNA replication by small interfering RNAs. *J Virol* **78**, 3436-3446 (2004).
38. El-Serag, H.B. Hepatocellular carcinoma. *N Engl J Med* **365**, 1118-1127 (2011).
39. Kopf, M., Bachmann, M. & Marsland, B. Averting inflammation by targeting the cytokine environment. *Nature Reviews Drug Discovery* **9**, 703-718 (2010).
40. Fletcher, J.I., Haber, M., Henderson, M.J. & Norris, M.D. ABC transporters in cancer: more than just drug efflux pumps. *Nat Rev Cancer* **10**, 147-156 (2010).

41. Frank-Kamenetsky, M., *et al.* Therapeutic RNAi targeting PCSK9 acutely lowers plasma cholesterol in rodents and LDL cholesterol in nonhuman primates. *Proceedings of the National Academy of Sciences* **105**, 11915-11920 (2008).
42. Abifadel, M., *et al.* Mutations in PCSK9 cause autosomal dominant hypercholesterolemia. *Nat Genet* **34**, 154-156 (2003).
43. Horton, J.D., Cohen, J.C. & Hobbs, H.H. Molecular biology of PCSK9: its role in LDL metabolism. *Trends Biochem Sci* **32**, 71-77 (2007).
44. Coppi, A., *et al.* Heparan sulfate proteoglycans provide a signal to Plasmodium sporozoites to stop migrating and productively invade host cells. *Cell Host Microbe* **2**, 316-327 (2007).
45. Noedl, H., Socheat, D. & Satimai, W. Artemisinin-Resistant Malaria in Asia. *New England Journal of Medicine* **361**, 540-541 (2009).
46. Epiphanio, S., *et al.* Heme Oxygenase-1 Is an Anti-Inflammatory Host Factor that Promotes Murine Plasmodium Liver Infection. *Cell Host & Microbe* **3**, 331-338 (2008).
47. Pamplona, A., *et al.* Heme oxygenase-1 and carbon monoxide suppress the pathogenesis of experimental cerebral malaria. *Nat Med* **13**, 703-710 (2007).
48. John, M., *et al.* Effective RNAi-mediated gene silencing without interruption of the endogenous microRNA pathway. *Nature* **449**, 745-747 (2007).
49. Carthew, R.W. & Sontheimer, E.J. Origins and Mechanisms of miRNAs and siRNAs. *Cell* **136**, 642-655 (2010).
50. Grimm, D., *et al.* Fatality in mice due to oversaturation of cellular microRNA/short hairpin RNA pathways. *Nature* **441**, 537-541 (2006).
51. Leuschner, F., *et al.* Therapeutic siRNA silencing in inflammatory monocytes in mice. *Nat Biotechnol* **9**(2011).
52. Gordon, S. & Taylor, P.R. Monocyte and macrophage heterogeneity. *Nat Rev Immunol* **5**, 953-964 (2005).
53. Charo, I.F. & Ransohoff, R.M. The many roles of chemokines and chemokine receptors in inflammation. *N Engl J Med* **354**, 610-621 (2006).
54. Nahrendorf, M., *et al.* Hybrid PET-optical imaging using targeted probes. *Proc Natl Acad Sci U S A* **107**, 7910-7915 (2010).
55. Swirski, F.K., *et al.* Identification of splenic reservoir monocytes and their deployment to inflammatory sites. *Science* **325**, 612-616 (2009).
56. Nahrendorf, M., Pittet, M.J. & Swirski, F.K. Monocytes: protagonists of infarct inflammation and repair after myocardial infarction. *Circulation* **121**, 2437-2445 (2010).
57. Robertson, R.P. Islet transplantation as a treatment for diabetes - a work in progress. *N Engl J Med* **350**, 694-705 (2004).
58. de Visser, K.E., Eichten, A. & Coussens, L.M. Paradoxical roles of the immune system during cancer development. *Nat Rev Cancer* **6**, 24-37 (2006).
59. Steidl, C., *et al.* Tumor-associated macrophages and survival in classic Hodgkin's lymphoma. *N Engl J Med* **362**, 875-885 (2010).

60. Mercer, T.R., Dinger, M.E. & Mattick, J.S. Long non-coding RNAs: insights into functions. *Nat Rev Genet* **10**, 155-159 (2009).
61. Carro, M.S., *et al.* The transcriptional network for mesenchymal transformation of brain tumours. *Nature* **463**, 318-325 (2010).
62. Rajendran, L., Knölker, H.-J. & Simons, K. Subcellular targeting strategies for drug design and delivery. in *Nature Reviews Drug Discovery*, Vol. 9 29-42 (2010).
63. Morris, M.C., Deshayes, S., Heitz, F. & Divita, G. Cell-penetrating peptides: from molecular mechanisms to therapeutics. *Biology of the cell / under the auspices of the European Cell Biology Organization* **100**, 201-217 (2008).
64. Huang, Y.-H., *et al.* Claudin-3 gene silencing with siRNA suppresses ovarian tumor growth and metastasis. *Proceedings of the National Academy of Sciences* **106**, 3426-3430 (2009).
65. Frank-Kamenetsky, M., *et al.* Therapeutic RNAi targeting PCSK9 acutely lowers plasma cholesterol in rodents and LDL cholesterol in nonhuman primates. in *Proceedings of the National Academy of Sciences*, Vol. 105 11915-11920 (2008).
66. Meier, M., Bider, M.D., Malashkevich, V.N., Spiess, M. & Burkhard, P. Crystal structure of the carbohydrate recognition domain of the H1 subunit of the asialoglycoprotein receptor. *J Mol Biol* **300**, 857-865 (2000).
67. Jain, K., Kesharwani, P., Gupta, U. & Jain, N.K. A review of glycosylated carriers for drug delivery. *Biomaterials* **33**, 4166-4186 (2012).
68. Kim, E.M., *et al.* Asialoglycoprotein receptor targeted gene delivery using galactosylated polyethylenimine-graft-poly(ethylene glycol): in vitro and in vivo studies. *J Control Release* **108**, 557-567 (2005).
69. Iobst, S.T. & Drickamer, K. Selective sugar binding to the carbohydrate recognition domains of the rat hepatic and macrophage asialoglycoprotein receptors. *J Biol Chem* **271**, 6686-6693 (1996).
70. Rensen, P.C., *et al.* Determination of the upper size limit for uptake and processing of ligands by the asialoglycoprotein receptor on hepatocytes in vitro and in vivo. *J Biol Chem* **276**, 37577-37584 (2001).
71. Rozema, D.B., *et al.* Dynamic PolyConjugates for targeted in vivo delivery of siRNA to hepatocytes. *Proc Natl Acad Sci U S A* **104**, 12982-12987 (2007).
72. Wong, S.C., *et al.* Co-injection of a targeted, reversibly masked endosomolytic polymer dramatically improves the efficacy of cholesterol-conjugated small interfering RNAs in vivo. *Nucleic Acid Ther* **22**, 380-390 (2012).
73. Parmar, R.G., *et al.* Endosomolytic bioreducible poly(amido amine disulfide) polymer conjugates for the in vivo systemic delivery of siRNA therapeutics. *Bioconjug Chem* **24**, 640-647 (2013).
74. Wooddell, C.I., *et al.* Hepatocyte-targeted RNAi therapeutics for the treatment of chronic hepatitis B virus infection. *Mol Ther* **21**, 973-985 (2013).

75. Carmeliet, P. & Jain, R.K. Molecular mechanisms and clinical applications of angiogenesis. *Nature* **473**, 298-307 (2011).
76. Herbert, S.P. & Stainier, D.Y. Molecular control of endothelial cell behaviour during blood vessel morphogenesis. *Nat Rev Mol Cell Biol* **12**, 551-564 (2011).
77. Jain, R.K. Barriers to drug delivery in solid tumors. *Sci Am* **271**, 58-65 (1994).
78. Joyce, J.A. & Pollard, J.W. Microenvironmental regulation of metastasis. *Nat Rev Cancer* **9**, 239-252 (2009).
79. Chiang, A.C. & Massague, J. Molecular basis of metastasis. *N Engl J Med* **359**, 2814-2823 (2008).
80. Gray, J. Genomics of Metastasis. *Nature* **464**(2008).
81. Wang, J., Loberg, R. & Taichman, R.S. The pivotal role of CXCL12 (SDF-1)/CXCR4 axis in bone metastasis. *Cancer Metastasis Rev* **25**, 573-587 (2006).
82. Hilgenbrink, A.R. & Low, P.S. Folate receptor-mediated drug targeting: from therapeutics to diagnostics. *J Pharm Sci* **94**, 2135-2146 (2005).
83. Lee, H., *et al.* Molecularly self-assembled nucleic acid nanoparticles for targeted in vivo siRNA delivery. *Nat Nanotechnol* **7**, 389-393 (2012).
84. Dohmen, C., *et al.* Defined Folate-PEG-siRNA Conjugates for Receptor-specific Gene Silencing. *Mol Ther Nucleic Acids* **1**, e7 (2012).
85. Tortorella, S. & Karagiannis, T.C. Transferrin receptor-mediated endocytosis: a useful target for cancer therapy. *J Membr Biol* **247**, 291-307 (2014).
86. Gonzalez, H., Hwang, S.J. & Davis, M.E. New class of polymers for the delivery of macromolecular therapeutics. *Bioconjug Chem* **10**, 1068-1074 (1999).
87. Davis, M.E., *et al.* Evidence of RNAi in humans from systemically administered siRNA via targeted nanoparticles. *Nature*, 1-8 (2010).
88. Heidel, J.D., *et al.* Administration in non-human primates of escalating intravenous doses of targeted nanoparticles containing ribonucleotide reductase subunit M2 siRNA. *Proc Natl Acad Sci U S A* **104**, 5715-5721 (2007).
89. Fogal, V., Zhang, L., Krajewski, S. & Ruoslahti, E. Mitochondrial/cell-surface protein p32/gC1qR as a molecular target in tumor cells and tumor stroma. *Cancer Res* **68**, 7210-7218 (2008).
90. Ren, Y., *et al.* Targeted tumor-penetrating siRNA nanocomplexes for credentialing the ovarian cancer oncogene ID4. *Sci Transl Med* **4**, 147ra112 (2012).
91. Kaufmann, J., Ahrens, K. & Santel, A. RNA interference for therapy in the vascular endothelium. *Microvascular Research* **80**, 286-293 (2010).
92. Santel, A., *et al.* RNA interference in the mouse vascular endothelium by systemic administration of siRNA-lipoplexes for cancer therapy. *Gene Ther* **13**, 1360-1370 (2006).
93. Santel, A., *et al.* A novel siRNA-lipoplex technology for RNA interference in the mouse vascular endothelium. *Gene therapy* **13**, 1222-1234 (2006).
94. Aleku, M., *et al.* Atu027, a Liposomal Small Interfering RNA Formulation Targeting Protein Kinase N3, Inhibits Cancer Progression. *Cancer research* **68**, 9788-9798 (2008).

95. Dahlman, J.E., *et al.* In vivo endothelial siRNA delivery using polymeric nanoparticles with low molecular weight. *Nat Nanotechnol* **11**, 84 (2014).
96. Meylan, E., *et al.* Requirement for NF-kappaB signalling in a mouse model of lung adenocarcinoma. (2009).

Chapter 2. The nanoparticle 7C1 efficiently delivers siRNA to endothelial cells *in vivo*

Chapter 2.1 Introduction

Dysfunctional endothelium contributes to more disease than any other tissue in the body. Small interfering RNAs (siRNAs) have the potential to help study and treat endothelial cells *in vivo* by durably silencing multiple genes simultaneously, but efficient siRNA delivery has so far remained challenging. Here we show that polymeric nanoparticles made of low molecular weight polyamines and lipids can deliver siRNA to endothelial cells with high efficiency, thereby facilitating the simultaneous silencing of multiple endothelial genes *in vivo.* Unlike lipid or lipid-like nanoparticles, this formulation does not significantly reduce gene expression in hepatocytes or immune cells even at the dosage necessary for endothelial gene silencing. It mediates the most durable non-liver silencing reported to date, and facilitates the delivery of siRNAs that modify endothelial function in mouse models of vascular permeability, emphysema, primary tumour growth, and metastasis. We believe these nanoparticles improve the ability to study endothelial gene function *in vivo*, and may be used to treat diseases caused by vascular dysfunction.

The vascular system releases factors into the bloodstream, changes the expression of specific receptors, modifies intercellular junctions, and regulates the immune response[1]. Endothelial cells also mediate biological functions including endocytosis and metabolism[2]. Because these processes relate fundamentally to physiology, dysfunctional endothelium promotes more disease than any other tissue in the body[3]. Yet modulating the behavior of endothelial cells *in vivo* remains challenging, particularly in cases which require inhibition of multiple endothelial genes.

RNAi-mediated modification of gene expression has the potential to improve disease treatment and *in vivo* studies of complex biological processes. However its utility is limited by inefficient systemic delivery, with the exception of ionizable lipids and lipid-like compounds termed lipidoids, which reduce hepatic gene expression by 50% after injections of 0.01 mg/kg siRNA[4-7]. By contrast, efficient endothelial gene silencing without the transfection of hepatocytes has remained challenging. While cationic lipids have been reported to deliver siRNA to endothelial cells, these endothelial delivery systems require cumulative doses of up to 7.5 mg/kg to achieve robust gene silencing[8-13].

Nanoformulations based on polymeric materials have delivered siRNA to hepatocytes and melanoma[14,15]. Unlike lipid-based nanoparticles, polymer-nucleic acid nanoparticles condense via multivalent interactions, leading to significantly different physical stability. One polymer class that has been investigated as a gene delivery material is polyethyleneimine (PEI)[16]. Although nanoparticles made from high molecular weight PEI (M_w~25,000 Da) have delivered nucleic acids, they are associated with off-target effects[17]. In contrast, nanoformualtions from low molecular weight PEI (M_w~600 Da) are relatively well tolerated but cannot facilitate siRNA delivery[17,18].

Here we report an siRNA-nanoparticle formulation that reduces endothelial gene expression by over 90% at a dose of 0.10 mg/kg, and by 50% at doses as low as 0.02 mg/kg. This

formulation, termed 7C1, differs from traditional lipid-based nanoparticle formulations by delivering siRNA to lung endothelial cells without substantially reducing gene expression in pulmonary immune cells, hepatocytes, or peritoneal immune cells, at low doses. To demonstrate that 7C1-mediated endothelial gene silencing affected function *in vivo*, it was used to modify models of vascular permeability, emphysema, lung tumour growth, and lung metastasis. To our knowledge, these results describe the first highly efficient endothelial RNA delivery system, as well as the first description of *in vivo* endothelial multigene silencing, and suggest that 7C1 may have utility for the study and treatment of vascular disease *in vivo*.

Chapter 2.2 Efficient siRNA delivery to endothelium *in vitro* and *in vivo*

A diverse library of epoxide-modified lipid-polymer hybrids was synthesized (Supplementary Information, Fig. 1a, Supplementary Fig. 1a). Compounds were tested for their ability to reduce gene expression in HeLa cells at four different lipid: siRNA mass ratios (2.5:1, 5:1, 10:1, 15:1) (Supplementary Fig. 1b). HeLa cells expressing Firefly and Renilla luciferase were chosen as a first-pass screen for these 2,000 nanoparticles formulated with siLuciferase because of the cost-effectiveness of the assay[5]. We defined a successful nanoparticle as one that silenced Firefly luminescence more than 70%, but decreased Renilla luminescence less than 25%. While only 0.9% percent of the library was successful at a mass ratio equal to 2.5, 6.5% were successful when the mass ratio equaled 15 (Table 1). We then measured Firefly luminescence as a function of lipids bound to successful PEI_{600} compounds. Luminescence decreased with the number of lipids bound (Supplementary Fig. 1c). A subset of formulations tested in HeLa cells were tested for their ability to deliver siRNA to human (HMVEC) and murine (bEnd.3) endothelial cells *in vitro*. The most effective compound, termed 7C1 based on its composition, reduced target mRNA expression by more than 85% in HeLa, HMVECs, and bEnd.3 cells at a dose of 30 nM (Fig. 1b). Interestingly, 7C1 efficacy did not change with mass ratio in HeLa cells (Supplementary Fig. 1d). Only 2 nM was required to reduce target gene expression in bEnd.3 cells by 50%, and 7C1 did not affect bEnd.3 cell morphology or induce apoptosis *in vitro* at doses as high as 133 nM (Supplementary Fig. 1e-f).

7C1 was synthesized by reacting C_{15} epoxide-terminated lipids with PEI_{600} at a 14:1 molar ratio, and was formulated with $C_{14}PEG_{2000}$ to produce nanoparticles with a diameter between 35 and 60 nm that were stable in PBS solution for at least 40 days (Fig. 1c-e, Supplementary Fig. 1g-i). Particles formed multilamellar vesicles rather than periodic aqueous compartments containing siRNA that make up stable nucleic acid lipid particle formulations[19] (Fig. 1d, Supplementary Fig. 1j). Because particle charge at different pH can affect delivery by modifying interactions with serum proteins, the zeta potential of 7C1 formulated with siRNA at blood physiological pH (7.4) and pKa were measured[6] (Fig. 1f). While 7C1 formed electrically neutral particles at pH 7.4, its pKa was 5.0. Interestingly, this value contrasts the pKa of particles optimized for hepatocyte delivery[20].

We investigated the serum kinetics and biodistribution of 7C1 siRNA nanoparticles *in vivo*. 7C1 was complexed with Alexa647-tagged siRNA and injected intravenously. After one

hour, skin tissue whole-mounted for confocal microscopy showed colocalization between 7C1 and endothelial cells, suggesting endothelial cells endocytosed 7C1 *in vivo* (Fig 1g). Endothelial cell uptake was confirmed by an increase in Alexa647 mean fluorescence intensity in endothelial cells sorted from pulmonary tissue one hour after injection with 7C1 formulated with Alexa647-tagged siRNA (Fig. 2g). 7C1 serum kinetics was then measured. 7C1 serum concentration decreased by 50% within 20 minutes after intravenous injection, indicating the formulation was rapidly cleared or endocytosed (Fig. 1h). To investigate 7C1 biodistribution, Cy5.5 fluorescence was quantified 4 and 24 hours after injection (when 7C1 serum concentrations were negligible) (Fig. 1i). Renal fluorescence was high, indicating that the kidneys aid in the clearance of siRNA delivered by 7C1. *In vitro*, HMVECs take up 7C1 via caveolae- and clathrin-mediated endocytosis (Supplementary Information, Fig. 2a).

To confirm endothelial localization resulted in functional siRNA delivery, gene silencing was measured after 7C1 was formulated with siRNAs targeting genes expressed primarily by endothelial cells. 7C1 was formulated with siRNA targeting the gene ICAM-2 and injected with a dose of 0.6 mg/kg on day one and four. Five days later, skin was analyzed with confocal microscopy and flow cytometry (Supplementary Fig. 2a-b). ICAM-2 expression on lymph node and omentum endothelial cells was also measured with flow cytometry (Supplementary Fig. 2b). ICAM-2 expression decreased compared to PBS- and siLuciferase- (termed siCntrol) treated mice. 7C1 was then formulated with 0.60, 0.05, 0.02, or 0.007 mg/kg si-ICAM2 and injected once (Fig. 2b). Because ICAM-2 is principally expressed by endothelial cells in all major tissue beds, this assay detect endothelial gene silencing in any organ[21]. 7C1 reduced ICAM-2 mRNA expression in the pulmonary, cardiovascular, and renal endothelium by 50% after a dose of 0.02, 0.08, and 0.08 mg/kg, respectively (Fig. 2b). To ensure efficient delivery was not limited to siICAM-2, we measured gene silencing in mice treated with siRNA targeting VE-cadherin (VEcad), a junctional protein whose expression is limited to endothelium. Cardiovascular, renal, and pulmonary VEcad mRNA decreased by 50% at doses of 0.04, 0.08, and less than 0.02 mg/kg, respectively (Fig. 2c). 7C1-siVEcad also reduced VEcad protein levels in whole lung homogenates at 0.03 mg/kg (Fig. 2d). We then investigated whether reduced VEcad protein levels increased vascular permeability. Compared to mice treated with PBS or siCntrol, the extravasation of Evans Blue Dye out of the pulmonary vasculature increased 2.5 fold seven and fourteen days after a single 0.6 mg/kg injection of siVEcad (Fig. 2e). These data demonstrate that 7C1 facilitates the most efficient non-liver siRNA delivery reported to date.

Because *in vivo* multigene silencing requires highly efficient delivery, it has been limited to hepatocytes[5]. 7C1 silenced five endothelial genes (Tie1, Tie2, VEcad, VEGFR-2, and ICAM2) concurrently. Three days following an intravenous injection with a total dose of 0.25 mg/kg, target mRNA of all five genes decreased between 60% and 80% in pulmonary vasculature (Fig. 2f, Supplementary Fig. 2c-e). Target gene expression remained constant after siCntrol was injected with a total dose of 2.0 mg/kg, suggesting reduced mRNA levels were due to RNAi. To our knowledge, this is the first demonstration of multi-gene silencing in endothelial cells *in vivo*.

Efficient delivery also facilitates durable gene silencing, since the duration of gene silencing is generally dose dependent[5]. mRNA silencing was measured as a function of time after a 0.6 mg/kg injection of siICAM-2 (Fig. 2g). Pulmonary ICAM-2 mRNA expression initially decreased by 92% and remained suppressed between 73% and 85% for twenty-one days. By contrast, cardiovascular and renal endothelial ICAM-2 expression continually increased over the first twenty-eight days, reaching 50% of initial expression after day ten, again suggesting less efficient endothelial cell delivery in these vascular beds compared to lung endothelium (Fig. 2g). We then measured gene silencing in different organs after modifying particle size and 7C1: siRNA mass ratio (Supplementary Information, Supplementary Fig. 2f-i). 7C1 was complexed siRNA targeting the endothelial specific gene Tie2[21]. In all cases, the most potent delivery was measured in pulmonary endothelial cells (Supplementary Fig. 2f-i).

While others have reported siRNA delivery to the lung, functional gene silencing required doses much higher than 0.02 mg/kg. Since the relative silencing in different cell types informs the type of *in vivo* models nanoparticles can be used to study, we studied 7C1 biodistribution and silencing in pulmonary epithelial cells, hematopoietic cells, T cells, and B cells (Fig. 3a-c). We also measured gene silencing in hepatocytes and peritoneal immune cells, two cell types that have been preferentially transfected by lipid nanoparticles (Fig. 3d-f).

We quantified uptake of Alexa647 labeled siRNA delivered by 7C1. One hour after a 1.0 mg/kg injection, lungs were digested into a single cell suspension and labeled with antibodies. Flow cytometry revealed that Alexa647 median fluorescent intensity was significantly higher in endothelial cells than pulmonary epithelial cells, hematopoietic cells, T cells, and B cells (Fig. 3a). Twenty-four hours after injection, endothelial cell uptake decreased. While the significance of the decreased signal is unknown, it could result from fluorophore cleavage. We then used flow cytometry to simultaneously quantify ICAM-2 protein expression in pulmonary endothelial cells, hematopoietic cells, T cells, and B cells. Three days following injection of 0.30, 0.20, 0.10, or 0.05 mg/kg, pulmonary endothelial cell ICAM-2 median fluorescent intensity decreased between 60% and 68% compared to cells from siCntrol treated mice (Fig. 3b). ICAM-2 median fluorescent intensity did not decrease in pulmonary hematopoietic cells, T cells, or B cells. The relative delivery to lung endothelium and epithelium was then quantified with siRNA targeting Integrinß1 (Fig. 3c). Two days after injection, lungs were digested before epithelial and endothelial cells were sorted into separate tubes with fluorescence activated cell sorting. The purity of the sorted cells was confirmed by measuring cell-specific markers using RT-PCR (Supplementary Fig. 2j). Compared to siCntrol-treated cells, endothelial cell Integrinß1 mRNA decreased between 70% and 82%, while epithelial cell mRNA did not change substantially (Fig. 3c). These data indicate that at these doses, 7C1 preferentially delivers siRNA to pulmonary endothelial cells.

We then analyzed whether 7C1 delivered siRNA to hepatocytes, which are preferentially targeted by many lipid nanoparticle formulations (Fig. 3d). We measured the expression of a hepatocyte-specific gene Factor 7 (F7) after injection with the highly potent siF7[5]. While F7 serum concentration remained constant after siF7 was injected at a dose of 1.5 mg/kg, and was

only reduced by 35% after an injection of 2.0 mg/kg, the positive control lipid nanoparticle Hepat01 decreased F7 expression by 95% after a 0.30 mg/kg dose (Fig. 3d). To confirm that 7C1 reduced endothelial gene silencing without silencing hepatocyte gene expression, 7C1 was simultaneously complexed with siF7 and siTie2 (Fig. 3e). Since efficacy can vary with the molar ratio of PEG and cholesterol, we performed this two-gene experiment with particles formulated with different 7C1: Cholesterol: $C_{14}PEG_{2000}$ molar ratios. Two formulations reduced lung Tie2 mRNA by nearly 90% after a single 0.15 mg/kg dose, but did not reduce F7 expression (Fig. 3e).

Intravenously injected particles may also transfect peritoneal immune cells, especially $CD11b^{+}$ monocytes and macrophages[22]. CD45 median fluorescent intensity was quantified in immune cells isolated from the peritoneal cavity following intravenous injection of 2.0 mg/kg 7C1 formulated with an siRNA targeting CD45 (siCD45)[22] (Fig. 3f). CD45 protein expression remained constant in macrophages, B cells, T cells, and dendritic cells following treatment with 7C1 (Fig. 3f). By contrast, CD45 expression decreased in macrophages cells following treatment with the positive control lipid nanoparticle C12-200. Taken together, these data indicate that 7C1 does not deliver siRNA to hepatocytes or peritoneal immune cells in healthy BL\6 mice at any dose tested.

Chapter 2.3 Endothelial RNAi affects multiple animal models

Whether RNA delivery could change endothelial function was then investigated in mouse models of emphysema, primary tumour growth, and lung metastasis. Emphysema is characterized by decreased pulmonary surface area, which reduces gas transport, causing dyspnea and cough[23,24]. Along with macrophage-mediated protease imbalance, decreased VEGF and VEGFR-2 expression has been documented in lungs of patients with chronic obstructive pulmonary disease; moreover, genetic Cre-lox mediated deletion of VEGF causes emphysema in mice[24]. VEGF receptor blockade with SU5416 promotes emphysema in rodents, leading to decreased alveolar surface to volume ratios, increased lung volume, and increased distance between alveolar walls (termed the mean linear intercept)[23]. Because SU5416 simultaneously inhibits VEGFR-1 and VEGFR-2, we characterized pulmonary phenotype following VEGFR-2 specific silencing. VEGFR-2 silencing induced emphysema-like changes, indicated by decreased alveolar surface to volume ratios and increases in lung volume and mean linear intercept compared to siCntrol treated mice (Fig. 3g-i, Fig. 3k). These changes were not due to infiltration of myeloid cells (Fig. 3j). These results suggest VEGFR-2 specific silencing is sufficient to induce emphysema-like phenotypes in mice, and that systemic endothelial cell RNAi can be used to investigate the role of endothelial gene function *in vivo*.

The therapeutic effect of endothelial RNAi on primary tumour growth was then investigated in a Lewis lung carcinoma model. Previous work demonstrated antibodies targeting VEGFR-1 and Dll4 can reduce primary tumour growth through disrupted or non-productive angiogenesis, respectively[25,26]. In particular, targeting VEGFR-1, which is expressed on endothelial cells and pro-angiogenic myeloid cells, reduced tumour progression, metastasis, and formation of a pre-metastatic niche[27,28]. However, monoclonal antibodies may function

differently than RNAi-based methods, which inhibit both extracellular and intracellular signaling[29]. To investigate whether therapeutic deletion of VEGFR-1 and Dll4, both of which have intracellular signaling components, would have similar effects as therapeutic antibodies, 7C1 was complexed with siCntrol, siVEGFR-1, or siDll4. Compared to siCntrol, siVEGFR-1 and siDll4 formulations had a significant therapeutic effect, reducing primary tumour growth by 40% and 70%, respectively, and increasing tumour necrosis (Fig. 4a-c). While some tumours treated with siVEGFR-1 exhibited high levels of cell death, others showed low levels[30]. These data suggest targeted deletion of both the intracellular and extracellular portion of VEGFR-1 or Dll4 may reduce primary tumour growth.

While the role of VEGFR-1 and Dll4 in primary tumour growth has been extensively studied, the role of these genes, particularly Dll4, in metastasis is less clearly understood[31,32]. Consequently, the effect of VEGFR-1 and Dll4 deletion on lung tumour metastases was studied in a metastatic Lewis lung carcinoma model (Fig. 4d-e, Supplementary Fig. 3). siVEGFR-1 reduced surface metastases by 52%, while siDll4 reduced surface metastases by 63% compared to siCntrol treated mice (Fig. 4d-e). Lung weight, which correlates to the growth of lung metastases, decreased by 50% after siVEGFR-1 therapy and 60% after siDll4 therapy (Supplementary Fig. 3).

Chapter 2.4 7C1 *in vivo* tolerability

7C1 nanoformulations were well tolerated in animal models of toxicity following acute and chronic high-dose treatment (Supplementary Fig. 4). We measured serum concentration of markers associated with toxicity after four 0.6 mg/kg intravenous injections in highly immunoactive $CD1^+$ mice, a mouse model used for pre-clinical toxicology studies. Mice were injected with a 0.6 mg/kg dose of siCntrol or siICAM-2 once per week for four weeks. Forty-eight hours after the last injection, serum concentration of markers for hepatic, cardiovascular, and renal injury were quantified. Importantly, we observed no evidence of kidney damage (Supplementary Fig. 4a).

7C1 tolerability was also investigated in BL\6 mice at doses much higher than those required for functional gene silencing (2 mg/kg) in acute and chronic models. Over twenty-eight days, mice were injected eight times with PBS solution or 2 mg/kg 7C1. Murine weight gain equaled that of mice injected with PBS (Supplementary Fig. 4b). Four hours after the final injection, mice were sacrificed and lungs were removed before mRNA expression of cytokines (IL-6, TNF-α), markers of endothelial dysfunction (ICAM-2, E-selectin), and immune cell infiltration (CD45) were quantified (Supplementary Fig. 4c). Serum concentration of 30 cytokines was also quantified. mRNA expression and cytokine concentration did not increase significantly when compared to PBS treated mice (Supplementary Fig. 4d).

We then measured serum cytokine concentration two, four, six, and twenty-four hours following a 2.0 mg/kg injection. While the serum concentration of five factors did increase between two and six hours, only one factor (CXCL2) equaled the concentration of mice treated with a low dose LPS control, and all five returned to baseline twenty-four hours after injection

(Supplementary Fig. 4e). These data suggest that while 7C1 likely interacts with cells to produce a transient response at doses much higher than those required for gene silencing, the formulation appears to be well tolerated in multiple mouse models *in vivo.*

Chapter 2.5 Conclusions

Motivated by the utility of hepatocyte-targeting vehicles and the role of vasculature in pathologies ranging from heart disease to cancer, we identified a nanoparticle that efficiently delivers siRNA to endothelial cells. Unlike previously reported lipid and lipidoid-based nanoparticles, 7C1 transfected endothelial cells *in vivo* at low doses, without significantly reducing gene expression in hepatocytes, peritoneal immune cells, pulmonary epithelial cells, or pulmonary immune cells. While the molecular mechanism governing this effect remains under investigation, it may be due to interactions with serum proteins, which can promote delivery to certain cell types[33]. As a result, 7C1 may be an interesting system to study how physiochemical interactions between nanomaterials and serum proteins direct nanoparticles to endothelial cells *in vivo*[34].

The potency of this nanoformulation allowed for the simultaneous silencing of multiple endothelial genes. While some immune cells are known to express Tie1, Tie2, and ICAM-2, the lack of significant pulmonary immune cell gene silencing mediated by 7C1 indicates that this multigene silencing occurred primarily in endothelial cells. We anticipate that 7C1 may have utility in the study of gene combinations in complex biological pathways *in vivo*, a strategy termed *in vivo genomics*.

7C1 reduced primary tumour growth and lung metastases in a model of lung cancer. While this study examined targets whose extracellular activity can also be inhibited by antibodies, future therapies may be designed to target combinations of proteins currently considered 'undruggable'. Similarly, future RNA therapies may enhance the effects of non-RNA drugs. For example, modifying the expression of gene involved in the exocytosis of a small molecule might enhance its delivery.

7C1 durably reduced target gene expression in multiple animal models. This ability to extend a therapeutic effect may increase the utility of *in vivo* endothelial RNAi. Because 7C1 is well tolerated at doses far higher than those required for gene silencing, we believe this technology will be used to manipulate gene expression *in vivo*. Our results demonstrate that 7C1 nanoformulations facilitate highly efficient endothelial RNA delivery, providing biologists and engineers with a new tool to deliver siRNA to endothelium.

Chapter 2.6 Materials and Methods

7C1 Synthesis, characterization, and formulation

C_{15} lipids and PEI_{600} were combined and heated to 90°C in 100% ethanol for 48-72 hours. Products were characterized with MALDI-TOF and ^{1}H-NMR (Supplementary Fig. 5a-b). To formulate particles, 7C1 was combined with $C_{14}PEG_{2000}$ and mixed with siRNA in a microfluidic

device as previously described[35]. Particles were dialyzed against 1X PBS before sterile filtration through a 0.22 um membrane. Particle size and structure was analyzed by dynamic light scattering (DLS) (Zetapals, Brookhaven Instruments), TEM, or cryo-TEM. DLS samples were measured in PBS at an approximate siRNA concentration of 1.0-3.0 ug/mL. TEM samples were prepared on carbon film-coated grid to which 1% sodium phosphotungstate was added for negative staining before images were obtained (JEOL 200CX EM, 120 kV). Cryo-TEM specimens were prepared in the controlled environment vitrification system at 25 °C and ~ 100% relative humidity. Vitrified samples were examined with a Tecnai 12 G^2 TEM (FEI), and images were recorded on an UltraScan 1000 CCD camera (Gatan) at low dose conditions as previously described. siRNA concentration was measured using Quant-iT™ RiboGreen (Invitrogen), HPLC absorbance against a known standard.

TNS pKa assay

TNS, a molecule whose fluorescence is quenched in aqueous solution, was added to particles and buffer solution at variable pH. As pH decreased, 7C1 charge increased; this increased charge promoted interactions with TNS, thereby increasing its fluorescence. Fluorescence was measured in a black plate (excitation 322 nm, emission 431 nm).

siRNA synthesis and *in vitro* siRNA selection

siRNAs were synthesized and modified to at the 2' position to avoid off-target effects and immunostimulation (Alnylam Pharmaceuticals)[36]. siRNAs to the same gene target were screened *in vitro* to maximize potency (Supplementary Fig. 6a-b). siRNAs to CD45, Luciferase (siCntrol), and Factor 7, and Alexa 647-tagged-GFP have been previously described, while all others are listed in Supplementary Table 1[5,22]. Sequences were selected after measuring target mRNA expression in Bend.3 (ATCC) following Lipofectamine RNAiMAX transfection (Invitrogen).

Gene	Sense	Antisense
CD45	cuGGcuGAAuuucAGAGcATdT	UGCUCUGAAAUUcAGCcAGTdT
Dll4	uccuGuAuGGGAcAucuuudTsdT	AAAGAUGUCCcAuAcAGGAdTsdT
FVII	GGAUfCfAUfCfUfCfAAGUfCfUfUfACfdTsdT	GUfAAGACfUfUfGAGAUfGAUfCfCfdTsdT
Icam2	AGGAcGGucucAAcuuuucdTsdT	GAAAAGUuGAGACCGUCCUdTsdT
Luc	cuuAcGcuGAGuAcuucGAdTsdT	UCGAAGuACUcAGCGuAAGdTsdT
Tie1	GuGAGAAuGuGAcAuuAAudTsdT	AUuAAUGUcAcAUUCUcACdTsdT
Tie2	GAAGAuGcAGuGAuuuAcAdTsdT	UGuAAAUcACUGcAUCUUCdTsdT
VE-Cadherin	ccAAAAGAGAGAcuGGAuudTsdT	AAUCcAGUCUCUCUUUUGGdTsdT
Vegfr1	cAGAAGuucucGuuAGAGAdTsdT	UCUCuAACGAGAACUUCUGdTsdT
Vegfr2	cAAccAGAGAcccucGuuudTsdT	AAACGAGGGUCUCUGGUUGdTsdT
Vegfr3	GuGuuGAGAAGAAccGuuudTsdT	AAACGGUUCUUCUcAAcACdTsdT

Supplementary Table 1. siRNA sequences used in this publication. All sequences were optimized using the process outlined in Supplementary Fig. 6. Lowercase letter correspond to nucleotides modified with 2-O-Methyl modifications, which decrease immunostimulation and promote antisense strand selection in the RISC complex.

7C1 *in vitro* delivery

7C1 was selected from an *in vitro* screen of 500 compounds. 500 structurally diverse PEI analogs were synthesized by conjugating small polyamines to alkyl tails. Amines reacted with epoxide-terminated alkyl tails in 100% EtOH at 90°C for 48-72 hours (Supplementary Fig. 1a). 7C1-mediated mRNA silencing in HeLa, murine endothelioma cells (bEnd.3, ATCC), and pooled human dermal microvascular endothelial (HMVECs, Clonetics, Lonza) was measured (Fig. 1b). HeLa cells (cultured with 10% heat inactivated FBS) expressing Firefly and Renilla Luciferase were transfected with 7C1 complexed to siRNA targeting firefly (siFire) at a dose of 30 nM[5]. HeLa cells were seeded in a 96 well plate at a density of 15,000 cells/well. 24 hours later, cells were treated with 30 nM of siRNA before luminescence was measured 24 hours after transfection.

bEnd.3 and HMVEC were transfected with siTie2. Endothelial cells were seeded at density of 15,000 cells/well in a 96 well plate. 24 hours after seeding, 7C1 complexed with siTie2 was added before cells were analyzed 24 hours later. bEnd.3 cells were cultured under their suggested conditions (10% heat inactivated FBS). HMVEC cells were cultured under their suggested conditions (EGM-2 MV) and used within the first six passages.

7C1 endothelial cell uptake

The role of clathrin- and caveolae-mediated endocytosis in the uptake of 7C1 by HMVEC cells was studied. HMVEC cells were incubated with 7C1 complexed to fluorescent siRNA. Cells were seeded at 15,000 cells/well in black 96-well plates (Greiner Bio-one) and pre-incubated with inhibitors of endocytosis: chlorpromazine 10μM (clathrin mediated endocytosis), Fillipin 5μM (caveolae mediated endocytosis) and dynasore 100μM (clathrin and caveolae mediated endocytosis) for 30 minutes. These non-toxic concentrations did not affect cell viability, confirmed by constant cell number (data not shown). Cells were transfected with 50nM of 7C1 encapsulated with Alexa 647 labeled siRNA for 60 min in the presence or absence of the endocytic inhibitors. Cells were washed, fixed and counterstained in PBS containing Hoechst (2 μg/ml) for nuclei identification. The cells were imaged using an automated spinning disk confocal microscope (OPERA, Perkin Elmer) with a 40X objective. The same defined pattern of 20 fields from each well was acquired to eliminate bias and provide a statistically significant number of cells for analysis. After identification of cell location and perimeter, intracellular siRNA signal intensity over single field was calculated using Acapella software. Data represents intracellular intensity from 20 different fields. All experiments were done in triplicates and errors are reported as the Standard Error Mean (S.E.M).

Mouse experiments

All animal procedures were approved by the Institutional Animal Care and Use Committee and were in accordance with local, state, and federal regulations. All experiments were tested in 6 to 8 week-old C57BL/6 female mice (Charles River Laboratories). All experiments used 4-5 mice per group unless noted otherwise.

7C1 serum concentration and biodistribution

BL\6 mice were injected with 1.5 mg/kg 7C1 formulated with Cy5.5-tagged siRNA. Mice were immediately bled following injection to obtain an individual baseline serum Cy5.5 value. Mice were then bled at the appropriate time point. Blood was centrifuged at 13,000 rpm for 10 minutes to retrieve serum. 12.5 uL of serum was placed in a black 96 well plate and diluted with 37.5 uL 1X PBS before Cy5.5 fluorescence (excitation 695 nm, emission 720 nm) was quantified against a standard curve.

Biodistribution in tissues associated with clearance (liver, spleen, and kidney) as well as lung and heart were measured 4 and 24 hours after injection with 1.5 mg/kg 7C1 formulated with Cy5.5-tagged siRNA. Cy5.5 fluorescence was quantified (IVIS imaging) and normalized by individual tissue weight.

7C1 purification

Since PEI_{600} is not monodisperse (M_n=600, PDI = 0.33), 7C1 was purified using high performance liquid chromatography (HPLC). More specifically, 7C1 ran on a silica column with DCM. Over 45 minutes, MeOH and NH_4OH were added to the solvent, decreasing its polarity. In this way, the HPLC separated 7C1 into fractions related to the hydrophobic C_{15}: hydrophilic PEI ratio. The mixture was split into five fractions, which were tested for their ability to reduce gene expression *in vivo.* Fractions that were less potent were discarded, leaving the most potent fraction (Supplementary Fig. 7a).

Confocal imaging

One hour after intravenous injection with Alexa647-tagged siRNA formulated with 7C1, mice were sacrificed. Ear or omentum tissues were harvested and fixed with PLP solution. Whole mount tissues were stained with anti-CD31 (clone 390) and anti-ICAM2 (clone 3C4).

Flow cytometry and fluorescent activated cell sorting analysis of pulmonary tissue

Mice were sacrificed, and perfused with sterile 1X PBS. Lungs were digested with DNAse, collagenase XI, and collagenase I for 30 minutes at 37°C. Endothelial cells ($CD31^+CD45^-$), hematopoietic cells ($CD31^-CD45^+$), epithelial cells ($CD31^-CD45^-CD326^+$), T cells ($CD31^-CD45^+TCR\beta^+$), and B cells ($CD31^-CD45^+CD19^+$) were isolated using the following antibodies: CD31 (clone 390), CD45 (clone 104), CD326 (clone G8.8), TCRß (clone H57-597), and CD19 (clone 6D5).

Flow cytometry in skin, lymph node, and adipose tissue

Mice were injected with 0.6 mg/kg si-ICAM2, siCntrol, or PBS on day 1 and 4. Three days after the final injection, mice were sacrificed and $CD31^+CD45^-CD11b^-Ter119^-$ endothelial cells were isolated from skin, lymph node and adipose tissue (Supplementary Fig. 2). Data is representative of two experiments (n = 4 mice / group / experiment).

7C1 biophysical optimization

We characterized gene silencing in thirteen separate formulations; six made by extrusion, and seven by microfluidic mixing (N=4 to 5 mice per group, per formulation). Particles made with microfluidic devices were more potent and consistent (Supplementary Fig. 7b). Target gene silencing after varying 7C1: siRNA ratio and size was measured. Particle size varied from 135 nm to 40 nm while the formulation process was optimized (Supplementary Fig. 2f). All formulations had a mass ratio of 15:1 and a 7C1: Cholesterol: PEG molar ratio equal to 62: 22: 16 or 80: 0: 20, two ratios with equal potency (Supplementary Fig. 7c). Smaller particles were obtained with $C_{14}PEG_{2000}$, while larger particles were formulated with $C_{16}PEG_{2000}$.

Pulmonary, renal, and cardiovascular Tie2 expression was also measured after formulating nanoparticles with 7C1: siRNA mass ratio between 15:1 and 3:1 and injecting intravenously with a dose of 0.15 mg/kg (Supplementary Fig. 2g).

***In vivo* mRNA and protein measurements**

All endothelial gene silencing (siTie2, siTie1, siICAM2, siVE-Cadherin, siVEGFR-2) experiments were conducted 48-72 hours after injection, unless otherwise specified. Hepatocyte silencing (Factor 7) was examined 24 hours after injection as previously described[5]. Blood was collected from mice and centrifuged at 13,000 rpm for 10 minutes to isolate serum before F7 concentration was measured according to manufacturer instructions (Aniara). CD45 median fluorescent intensity was measured 72 hours after injection[22]. Cells from the peritoneal cavity were harvested using PBS and stained following red blood-cell lysis. The following clones were used: CD45 (clone 30-F11), CD11b (clone M1/70), TCRβ (clone H57-597); CD19 (clone 1D3), CD11c (clone N418); and propidium iodide (Sigma-Aldrich). Cells were analyzed with flow cytometry (LSR-Fortessa, BD Biosciences, and FloJo).

mRNA silencing was measured as target gene/GAPDH levels. The target gene/GapDH ratio was measured in mice treated with 7C1, and compared to the ratio in mice treated with siCntrol or PBS. For multi-gene silencing, five endothelial-specific siRNAs were simultaneously formulated in the same particle. The concentrations for each siRNA was based on its potency so that 1 mg of total siRNA contained 0.075 mg of siVEcad, 0.125 mg of siICAM2, 0.3 mg of siTie1, 0.25 mg of siTie2, and 0.25 mg of siVEGFR-2.

Western blots lysates were prepared with RIPA Lysis and ExtractionBuffer, as well as Halt Protease and Phosphatase Inhibitor Cocktail (Pierce Biotechnology). Total protein concentration was determined by the Pierce BCA protein assay kit (Thermo Scientific, Rockford, IL). Each lane of the pre-cast Mini-PROTEAN TGX 4-15% polyacrylamide gradient gels was loaded with equal amounts of total protein. Equal total protein loading was confirmed by Ponceau S staining. Blots were probed with goat anti-mouse IgG polyclonal VE-cadherin (R&D Systems) and donkey anti-goat IgG-HRP (Santa Cruz Biotechnology, Inc.) antibodies, and developed with Amersham ECL Prime Western blotting detection reagents (GE-Healthcare Life Sciences). Blots were imaged and densitometry was performed with a GE ImageQuant LAS 400 luminescent image analyzer and software (GE-Healthcare Life Sciences).

Batch-to-batch repeatability
We measured particle size and *in vivo* gene silencing with 7C1 synthesized with different PEI_{600} lots. Each batch was purified independently before being formulated with siRNA targeting ICAM-2 and injected intravenously at a dose of 0.15 mg/kg. There was no significant difference in particle size or ICAM-2 mRNA silencing across batches (Supplementary Fig. 8a-b).

Permeability Study
Mice were treated with 0.6 mg/kg of 7C1-siVEcad, 7C1-siCntrol, or PBS control (5-7 mice per group). After seven or fourteen days, mice were injected intravenously with an Evans Blue dye solution (200 uL of 0.5% in 0.9% NaCl, filtered). After 30 min, mice were sedated and perfused with PBS. Lungs were dried overnight at 55°C. Evans blue dye was extracted in formamide (10 uL/mg of dried tissue, 55C, 24h), and 620 nm absorbance was measured.

Emphysema Model
7C1 was formulated with siVEGFR-2 or siCntrol. Mice (N=7 per group) were injected on days one and eight before lungs were removed on day 22 for analysis[23].

Lewis lung carcinoma Primary Tumour Study. C57BL/6 mice (N=7-10 per group) were injected subcutaneously with Lewis lung carcinoma cells as described[37]. Mice received 1.0 mg/kg doses of siCntrol, siVEGFR-1, or siDll4 ten, fifteen, and nineteen days after primary tumour cell injection before mice were sacrificed three days following the last injection. Tumour growth was measured by calipers[37]. At sacrifice, mice were perfused with 3.6% paraformaldehye (PFA) through the left ventricle. Tumour tissue was placed in 3.6% PFA at 4°C for 8 hours. After rinsing with PBS, the sample was placed in 70% EtOH at 4°C before fixation and CC3 staining (Rabbit anti-mouse 1° antibody, Cell Signaling).

Lewis lung carcinoma Metastasis Study
C57BL/6 mice (N=4-6 per group) were injected subcutaneously with Lewis lung carcinoma cells. The primary tumour was allowed to grow for twenty days before cells were resected as previously described[37]. Following resection, lung metastases grow aggressively. Two, six, ten, and twelve days after resection, mice were injected intravenously with 1 mg/kg siCntrol, siVEGFR-1, or siDll4. Three days after the final injection, mice were sacrificed and analysis of metastases was performed as previously described[37].

***In vitro* cell live dead study**
The effect of 7C1 on cell viability was assessed using the bEnd.3 endothelial cell line (ATCC). Cells were plated at 30,000/well in a 48 well plate, and cultured for 24 hours in DMEM containing 10%FBS and 1% penicillin/streptomycin/amphotericin-B. One day following treatment with 7C1, cells were assessed by live/dead viability staining (Invitrogen Life

Technologies) and imaged using an EVOS fluorescent microscope (Advanced Microscopy Group). Calcein AM indicates live cells by green fluorescence of the cytosol and ethidium homodimer indicates dead cells by red fluorescence of the nucleus.

Statistics

Unless noted otherwise, all error bars are standard deviations. Statistical significance was measured by student T test.

Chapter 2.7 Figures

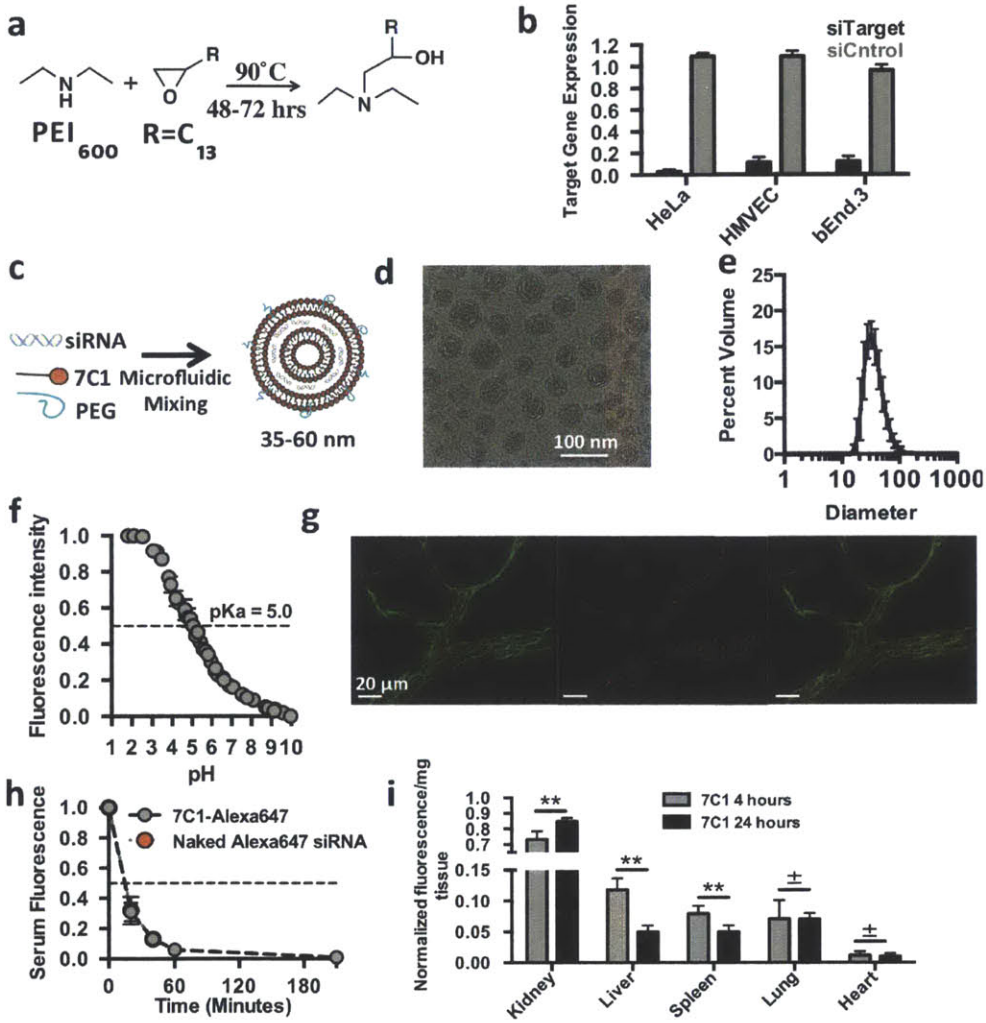

Figure 2.1. 7C1 synthesis, characterization, and *in vivo* biodistribution. (A) 7C1 synthesis scheme. (B) Target gene expression 24 hours following 30 nM treatment with siRNA in human cervical carcinoma (HeLa), human primary endothelial (HMVEC), and murine endothelial (bEnd.3) cells. HeLa target gene expression was measured as Firefly luminescence in HeLa cells expressing Luciferase that were treated with siRNA targeting luciferase. bEnd.3 and HMVEC target gene expression was measured as Tie2 mRNA levels following treatment with siRNA targeting Tie2. (C) 7C1 formulation scheme. 7C1 nanoparticles were mixed with $C_{14}PEG_{2000}$ and siRNA in a high throughput microfluidic chamber as previously described[30]. (D) 7C1 internal structure characterized by cryo-TEM. Dark bands indicate lipid layers and light bands indicate regions with siRNA. (E) Average 7C1 hydrodynamic diameter, measured by dynamic light scattering, and weighted by volume (N=20 formulations). (F) TNS fluorescence of formulated 7C1 nanoparticles as a function of pH (used to measure 7C1 pKa). (G) Representative confocal image of Alexa647-tagged siRNA complexed to 7C1 one hour after intravenous injection. CD31 is a ubiquitous marker for endothelium (Scale bar = 20 um). (H) Serum Cy5.5 concentration following with 7C1-Cy5.5 siRNA or naked Cy5.5 siRNA (I) Cy5.5 fluorescence/mg tissue after injection with 7C1-Cy5.5 siRNA. Tissues were removed after injection and weighed individually. Cy5.5 intensity was normalized to each individual tissue. Timepoints were selected to measure systemic siRNA accumulation after Cy5.5 was cleared from serum. N=4-5 mice/group. In all cases, data shown as mean +/- std. *p<0.05, **p<0.005, ***p<0.0008, ±p>0.75.

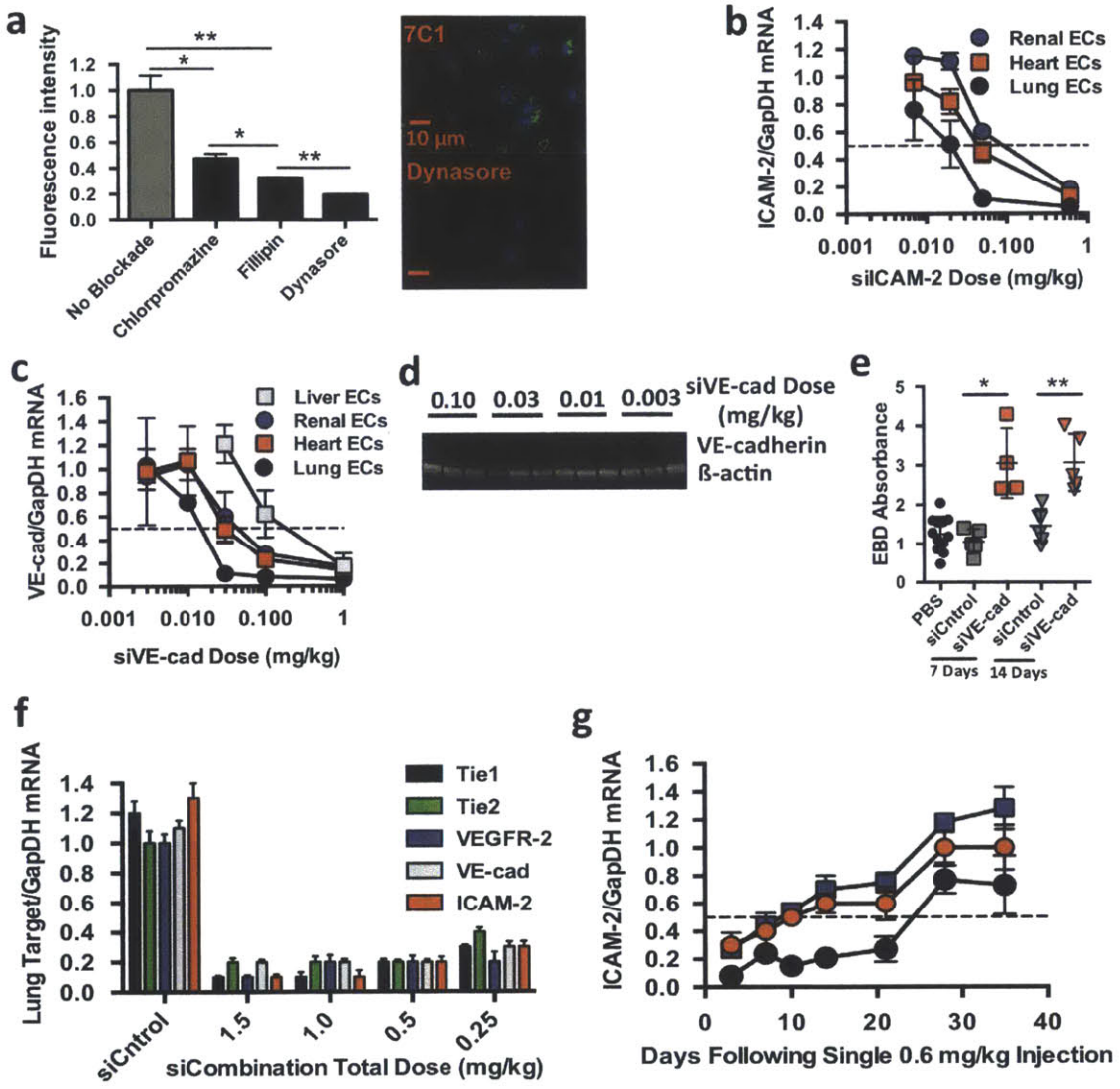

Figure 2.2. 7C1 delivers siRNA to endothelial cells. **(A)** Alexa647 fluorescence uptake in HMVEC cells following 7C1-Alexa647 siRNA treatments and administration of small molecules blockading clathrin (Chlorpromazine), caveolin (Fillipin), and both endocytotic pathways (Dynasore). **(B)** ICAM-2/GapDH mRNA ratios (normalized to PBS-treated mice) following intravenous injection of 7C1-siICAM-2. **(C)** VE-cadherin/GapDH mRNA ratios (normalized to PBS-treated mice) following intravenous injection of 7C1-siVEcad. **(D)** VE-cadherin and ß-actin protein expression following treatment with 7C1-siVEcad. **(E)** Evans Blue Dye pulmonary absorbance seven and fourteen days following a 0.6 mg/kg injection of 7C1-siVEcad. **(F)** Target/GapDH mRNA ratios (normalized to PBS-treated mice) following injection of 7C1 formulated with siCntrol or five siRNAs targeting ICAM-2, Tie2, VE-cadherin, VEGFR2, or Tie1, respectively (siCombination). **(G)** ICAM-2/GapDH mRNA levels as a function of time following a 0.6 mg/kg injection of siICAM-2. Data shown as mean +/- std. N=4 to 5 mice per group, *p< 0.05, **p< 0.005.

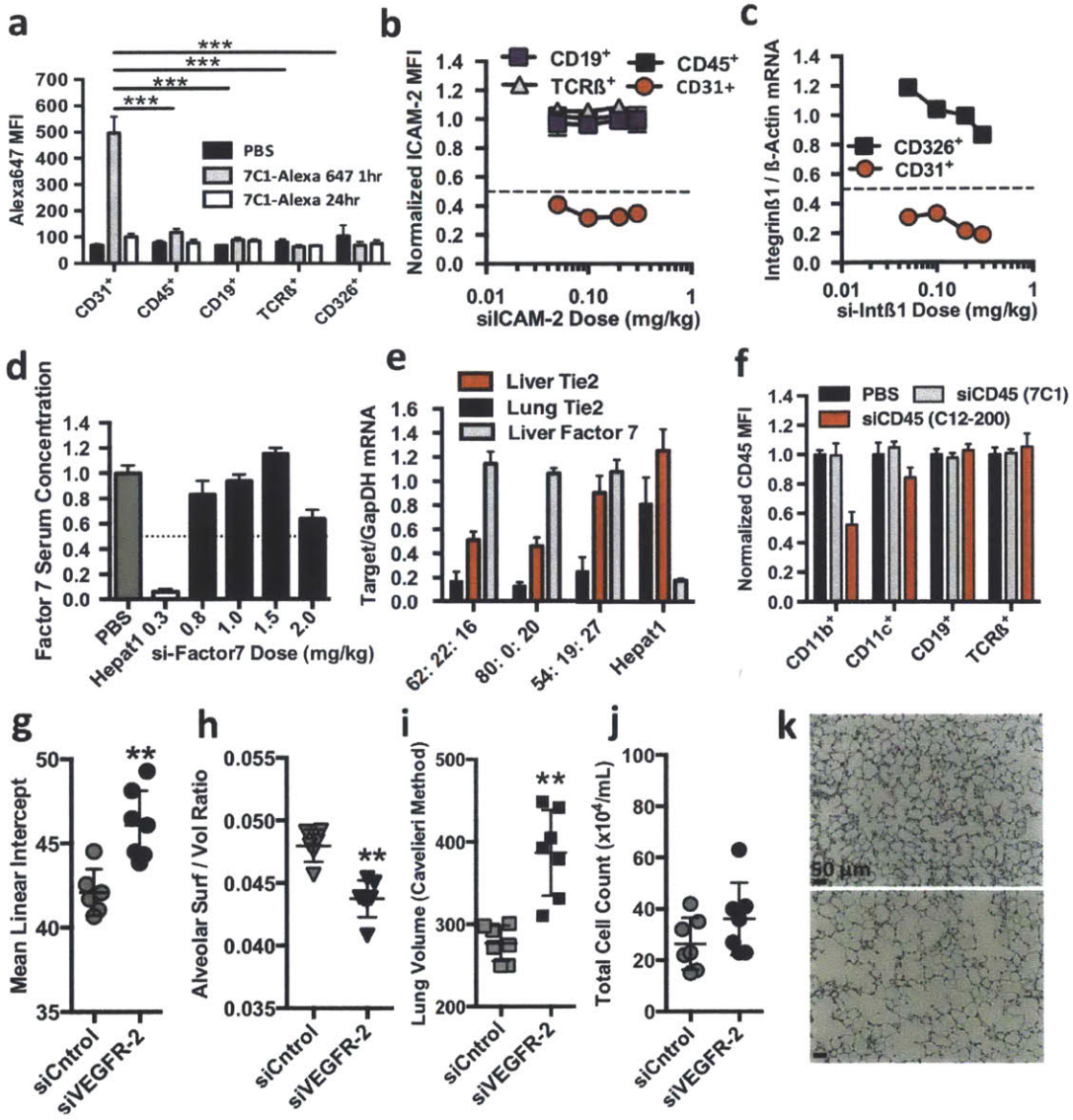

Figure 2.3. 7C1 preferentially delivers siRNA to pulmonary endothelial cells *in vivo*. **(A)** Alexa647 median fluorescent intensity in pulmonary endothelial ($CD31^+$), hematopoietic ($CD45^+$), epithelial ($CD326^+$), B ($CD19^+$), or T ($TCR\beta^+$) cells isolated from mice after treatment with 7C1 formulated with Alexa647-tagged siRNA. Statistical significance calculated between endothelial cells and other pulmonary cell types one hour after injection. **(B)** ICAM-2 median fluorescent intensity in pulmonary cells (normalized to siCntrol-treated mice) isolated from mice three days followings treatment with 7C1-siICAM-2. **(C)** Integrinß1/ß-actin mRNA ratios (normalized to siCntrol-treated mice) in pulmonary endothelial and epithelial cells isolated from mice two days after treatment with siIntegrinß1. **(D)** Factor 7 serum concentration (normalized to PBS-treated animals) two days following treatment with liver targeting molecule Hepat01-siFactor7 or 7C1-siFactor7 **(E)** Tie2 and Factor7/GapDH mRNA expression following a 0.15 mg/kg injection of 7C1 concurrently formulated with siTie2 and siFactor7. Particles were formulated with different 7C1: Cholesterol: $C_{14}PEG_{2000}$ molar ratios. 7C1 decreased Tie2 mRNA expression in pulmonary, renal, and hepatic endothelium without reducing F7 mRNA expression. **(F)** CD45 median fluorescent intensity following treatment with 7C1-siCD45 or positive control C12-200-siCD45. **(G-K)** Mean Linear Intercept (MLI) between alveoli, pulmonary surface/volume ratio, total volume, and pulmonary histology following two 0.5 mg/kg injections of siCntrol or siVEGFR2. Increased MLI, alveolar volume, decreased surface/volume ratios, and constant infiltrating myeloid cells are consistent with an induced emphysema-like phenotype (N=6 to 7 animals / group, data shown as average +/- std, scale bar = 50 um) *$p < 0.05$, **$p<0.002$, ***$p<0.001$.

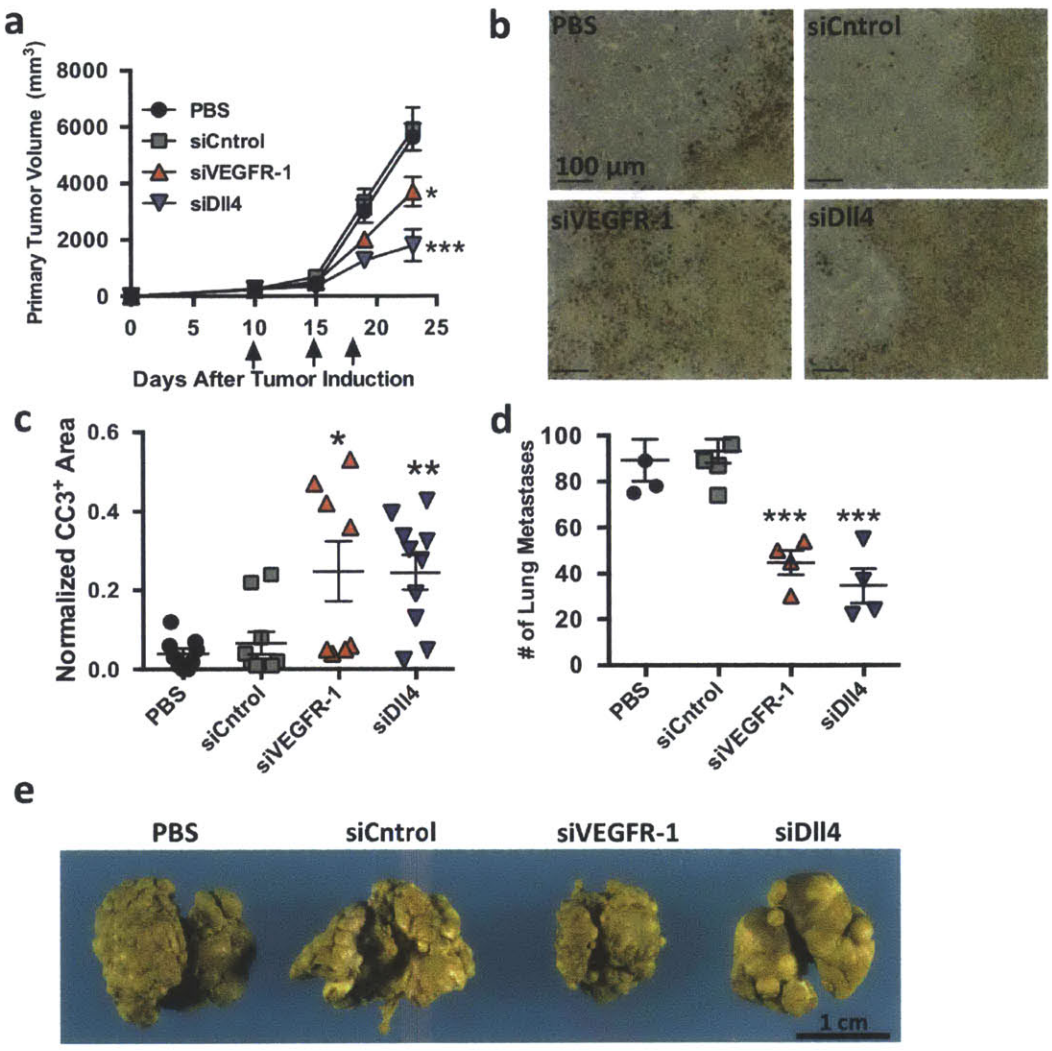

Figure 2.4. 7C1 mediated mRNA silencing modifies endothelial function *in vivo*. (A) Primary Lewis Lung Carcinoma (LLC) growth following three 1.0 mg/kg treatments with PBS, siCntrol, siVEGFR-1, or siDll4 (N=7 to 10 animals per group, data shown as average +/- SEM). (B,C) Representative image and quantification of cleaved caspase 3 (CC3) staining, a marker for apoptosis, following treatment with PBS, siCntrol, siVEGFR-1, siDll4. Normalized $CC3^+$ area defined as the total $CC3^+$ surface area divided by the tumor surface area. Scale bar = 100 um. (D) Number of pulmonary surface metastases following four 1.0 mg/kg injections with PBS, siCntrol, siVEGFR-1, or siDll4 (N=4 to 6 per group, data shown as average +/- SEM). To measure effects independent of primary tumor growth, animals were not treated until after primary tumor resection. (E) Murine lungs with metastatic lesion removed after treatment with PBS, siLuc, siVEGFR-1, or siDll4. *$p < 0.05$, **$p<0.002$, ***$p<0.001$.

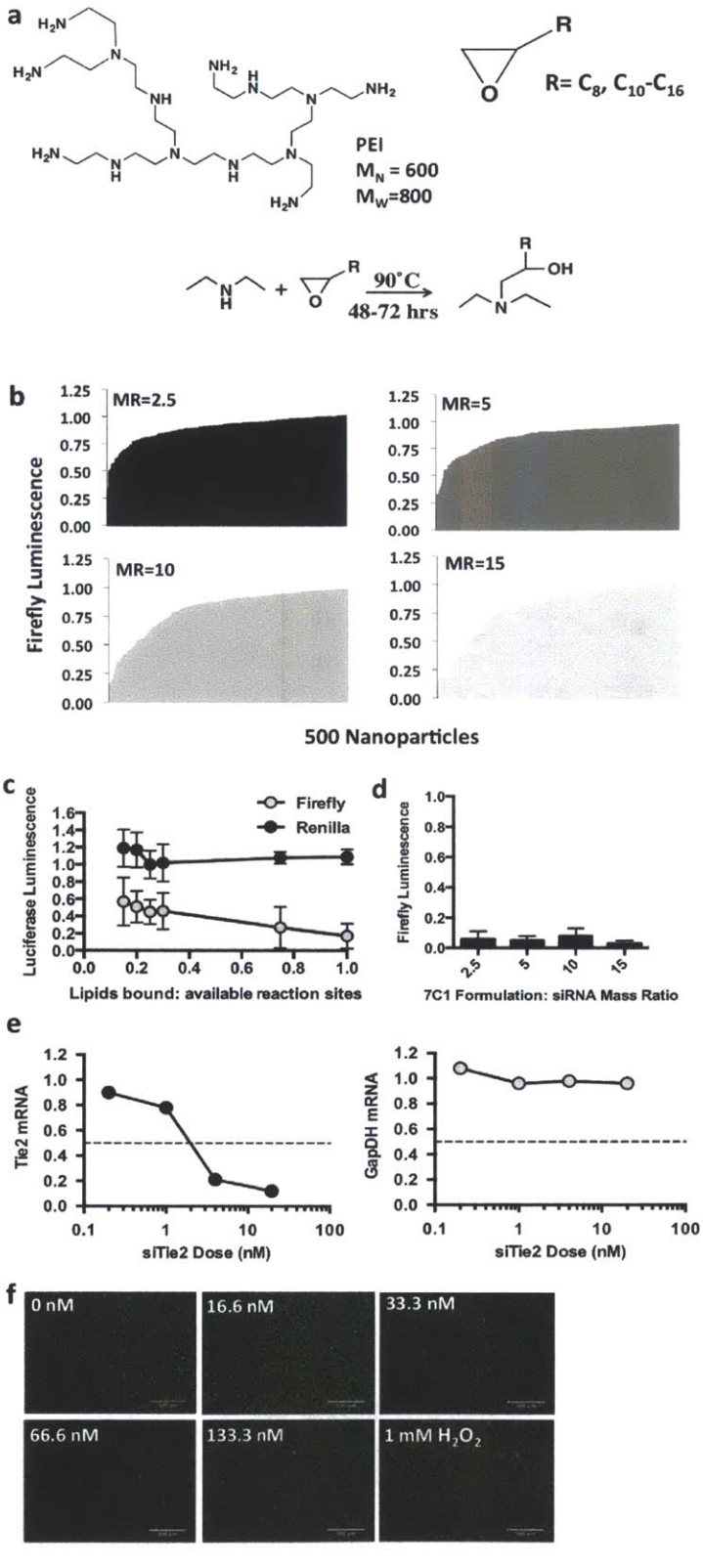
a
PEI
M_N = 600
M_W=800
R= C_8, C_{10}-C_{16}
90°C
48-72 hrs
b
MR=2.5
MR=5
MR=10
MR=15
Firefly Luminescence
500 Nanoparticles
c
Firefly
Renilla
Luciferase Luminescence
Lipids bound: available reaction sites
d
Firefly Luminescence
7C1 Formulation: siRNA Mass Ratio
e
Tie2 mRNA
siTie2 Dose (nM)
GapDH mRNA
siTie2 Dose (nM)
f
0 nM
16.6 nM
33.3 nM
66.6 nM
133.3 nM
1 mM H_2O_2

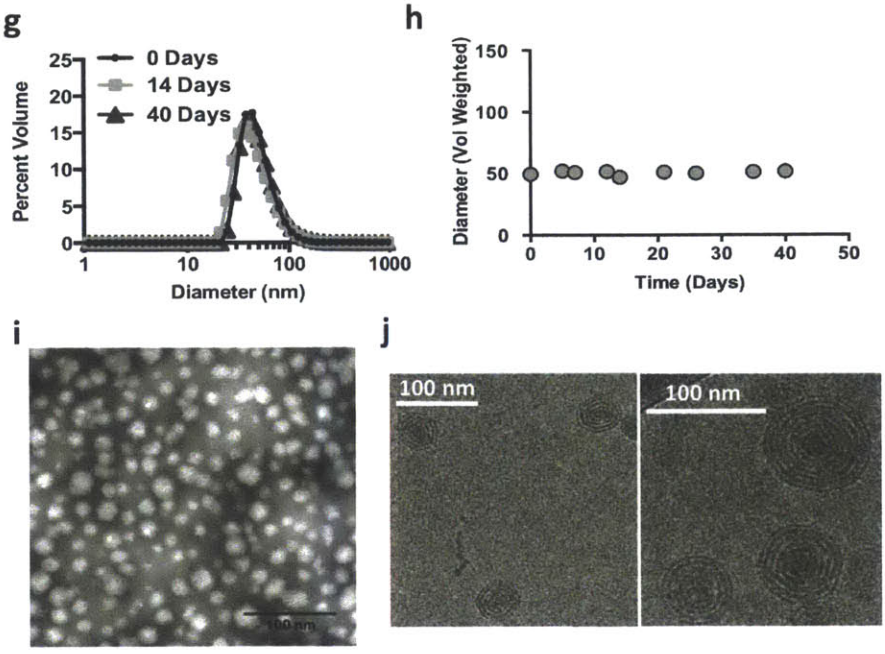

Figure 2S.1. Selection of 7C1 from a structurally diverse library of PEI analogs, 7C1 *in vitro* gene silencing, and characterization of 7C1 stability and size. **(A)** Reaction scheme for 500 nanoparticle library. Small polyamines were conjugated to alkyl tails via an epoxide ring-opening reaction. Variation of amine backbone, lipid length, and the molar ratio of lipids: amines generated a structurally diverse library. **(B)** Firefly luciferase luminescence 24 hours following a 30 nM treatment of siRNA targeting Firefly luciferase complexed to a different nanoparticles[2]. MR refers to the lipid: siRNA mass ratio used in the formulations. **(C)** Firefly and Renilla luminescence as a function of the number of lipids bounds to $BPEI_{600}$ 24 hours following a 30 nM dose of siRNA targeting Firefly. **(D)** Firefly luminescence 24 hours after treatment with 30 nM 7C1 at four mass ratios. 7C1 silencing was potent at all four mass ratios. **(E)** Tie2 and GapDH mRNA expression in bEnd.3 cells following treatment with 7C1-siTie2. **(F)** Live/dead staining in bEnd.3 cells 24 hours following treatment with 7C1-siCntrol. **(G)** Particle size 1, 14, or 40 days after formulation and storage in 1X PBS at 4˚C. **(H)** Average diameter (weighted by volume) measured over time for formulated 7C1 stored at 4˚C. **(I)** Transmission electron microscopy (TEM) image of formulated 7C1. Scale bar = 100 nm. **(J)** Cryo-TEM images of 7C1 after formulation. Dark bands indicate lipid layers and light bands indicate regions with siRNA.

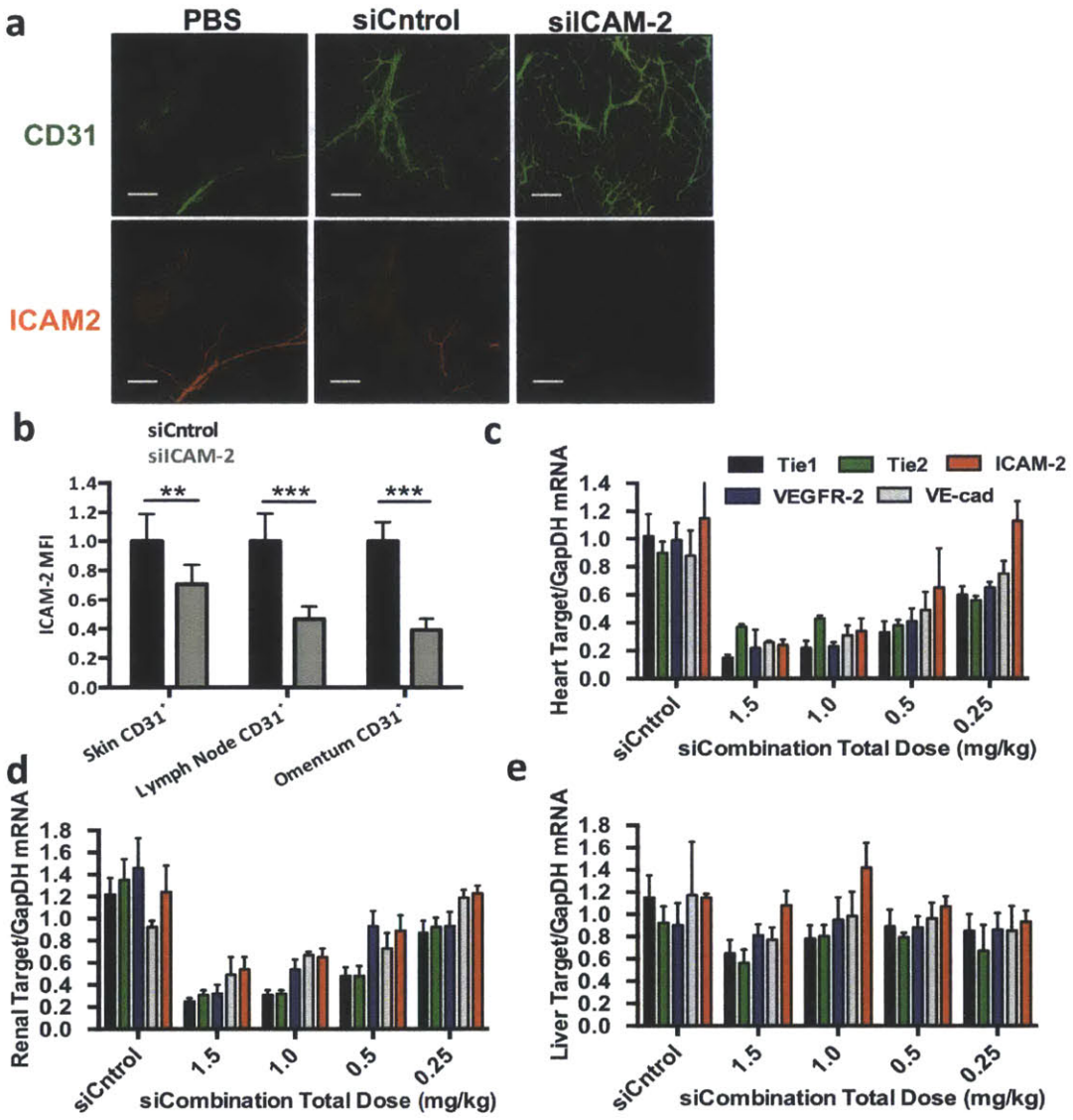
a
PBS
siCntrol
siICAM-2
CD31
ICAM2
b
siCntrol
siICAM-2
ICAM-2 MFI
**
***
***
Skin CD31+
Lymph Node CD31+
Omentum CD31+
c
Tie1
Tie2
ICAM-2
VEGFR-2
VE-cad
Heart Target/GapDH mRNA
siCntrol
1.5
1.0
0.5
0.25
siCombination Total Dose (mg/kg)
d
Renal Target/GapDH mRNA
siCntrol
1.5
1.0
0.5
0.25
siCombination Total Dose (mg/kg)
e
Liver Target/GapDH mRNA
siCntrol
1.5
1.0
0.5
0.25
siCombination Total Dose (mg/kg)

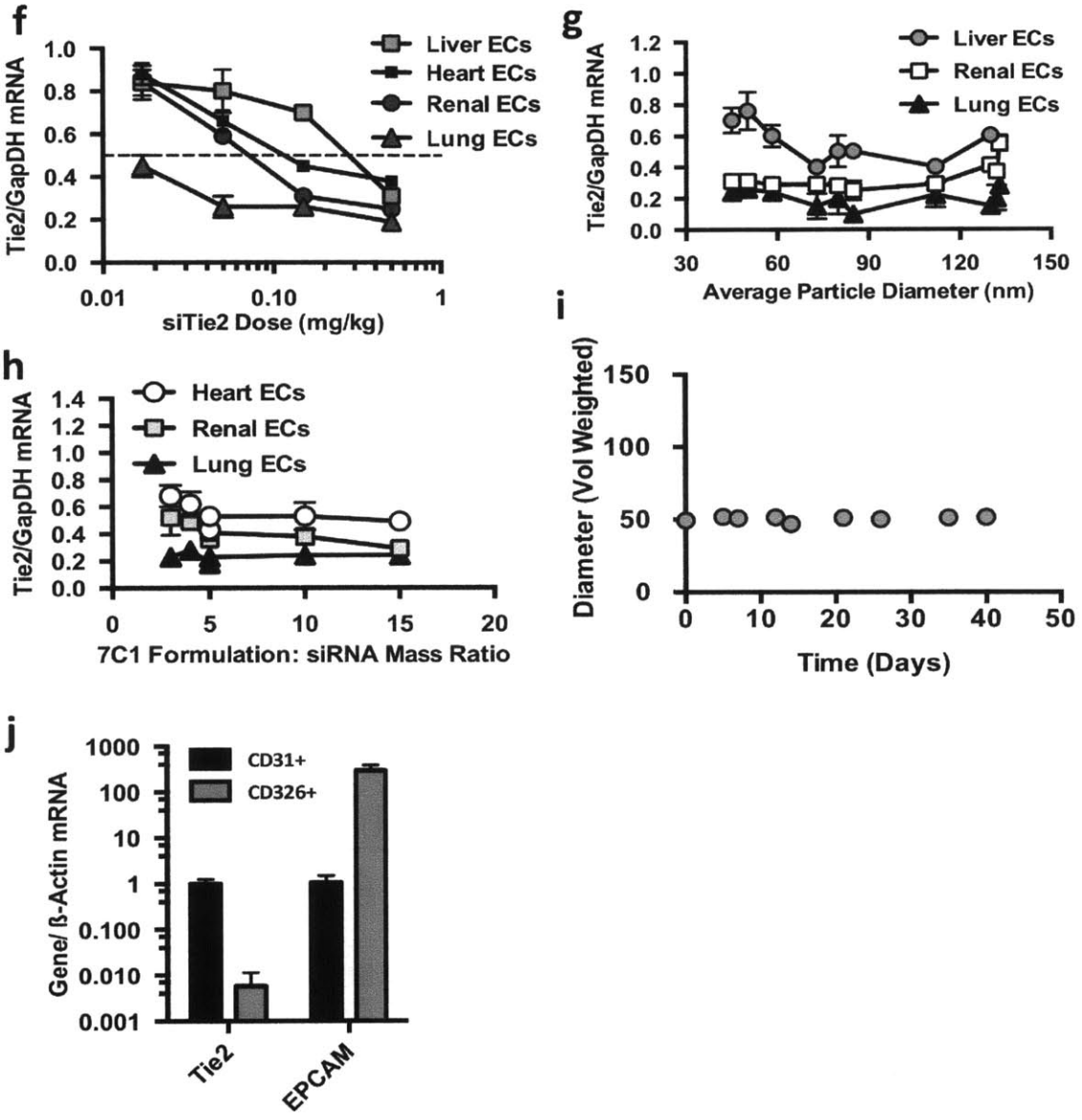

Figure 2.S2. (A) ICAM-2 and CD31 expression in skin endothelial cells following two injections of 7C1-siICAM2. **(B)** ICAM-2 median fluorescent intensity in skin, lymphatic, and omentum endothelial cells following two injections of 7C1-siICAM2 (N=2 experiments, 4 mice per group per experiment). **(C-E)** Target gene expression in **(C)** cardiovascular, **(D)** renal, and **(E)** hepatic vasculature following injection of 7C1 complexed with siRNA targeting Luc or Tie1, Tie2, VE-cad, VEGFR-2, and ICAM2. A 1 mg/kg total dose consisted of 0.075 mg/kg siVE-cad, 0.125 mg/kg siICAM2, 0.25 mg/kg siVEGFR-2, 0.25 mg/kg siTie2, and 0.30 mg/kg siTie1. **(F)** Tie2/GapDH mRNA ratios (normalized to PBS-treated mice) two to three days following treatment with 7C1-siTie2. **(G)** Tie2/GapDH mRNA ratios (normalized to PBS- or siCntrol-treated mice) two to three days after treatment with 7C1-siTie2 particles of varying size. N=4 to 5 mice/group. **(H)** Tie2/GapDH mRNA ratios (normalized to PBS- or siCntrol-treated mice) two to three days after treatment with 7C1-siTie2 particles formulated with differing lipid: siRNA mass ratios. N=4 to 5 mice/group. **(I)** Particle size associated with **(H).** 7C1 endothelial delivery was most potent in pulmonary tissue independent of particle size or mass ratio. **(J)** Tie2/ß-actin and EPCAM/ß-actin mRNA ratios for $CD31^{+}CD326^{-}$ and $CD31^{-}CD326^{+}$ cells isolated from lungs of mice treated with siIntegrinß1 (N=19 mice/group). All data shown as average +/- std. **p< 0.005, ***p<0.0001.

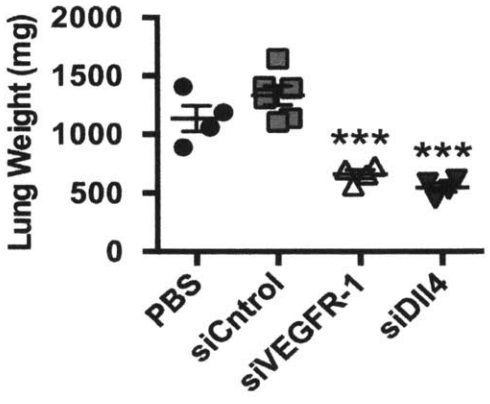

Figure 2.S3. Lung weight, a correlate of lung metastases, in Lewis Lung Carcinoma model of metastasis. N=4 to 6 mice per group, Data shown as average +/- SEM. ***p < 0.0003.

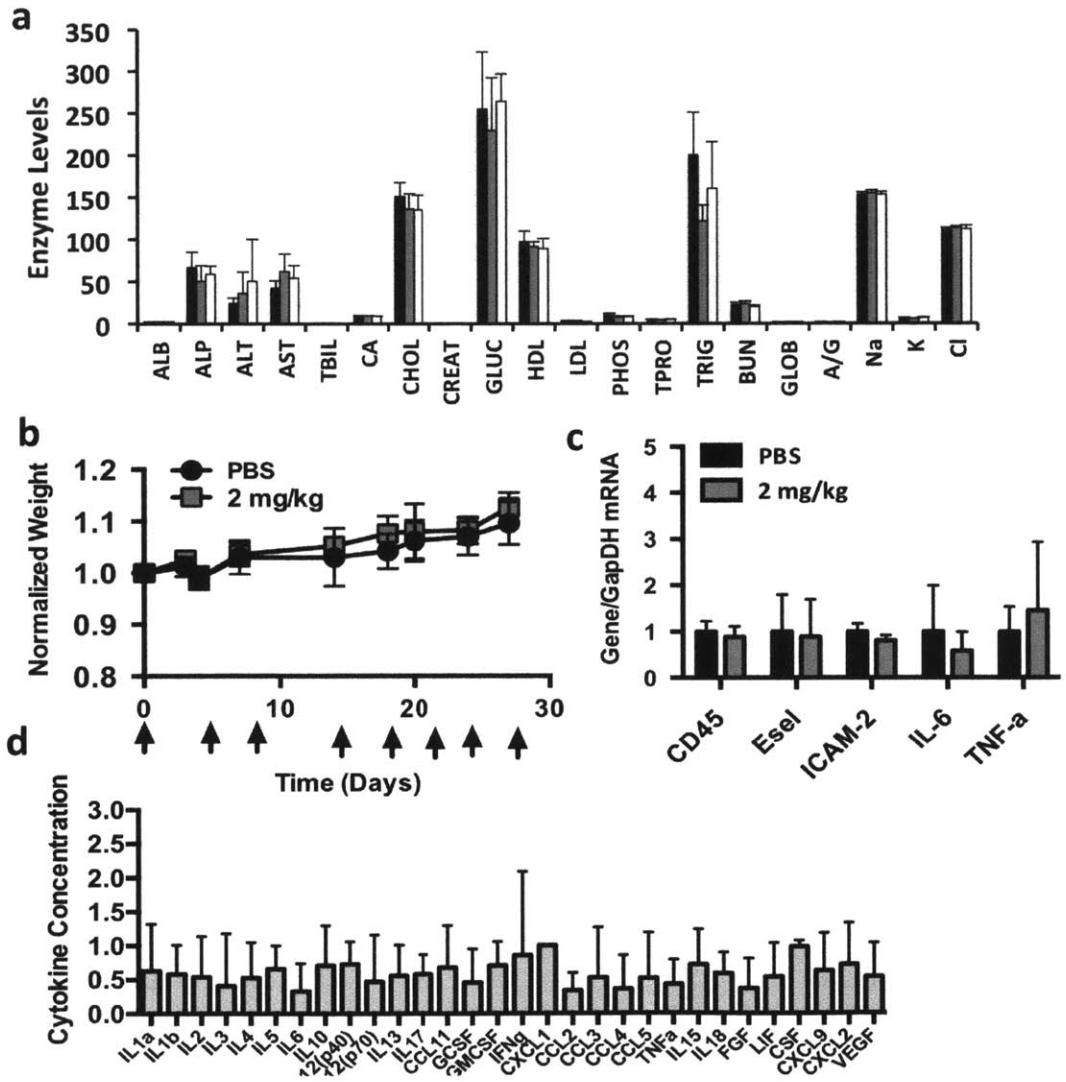

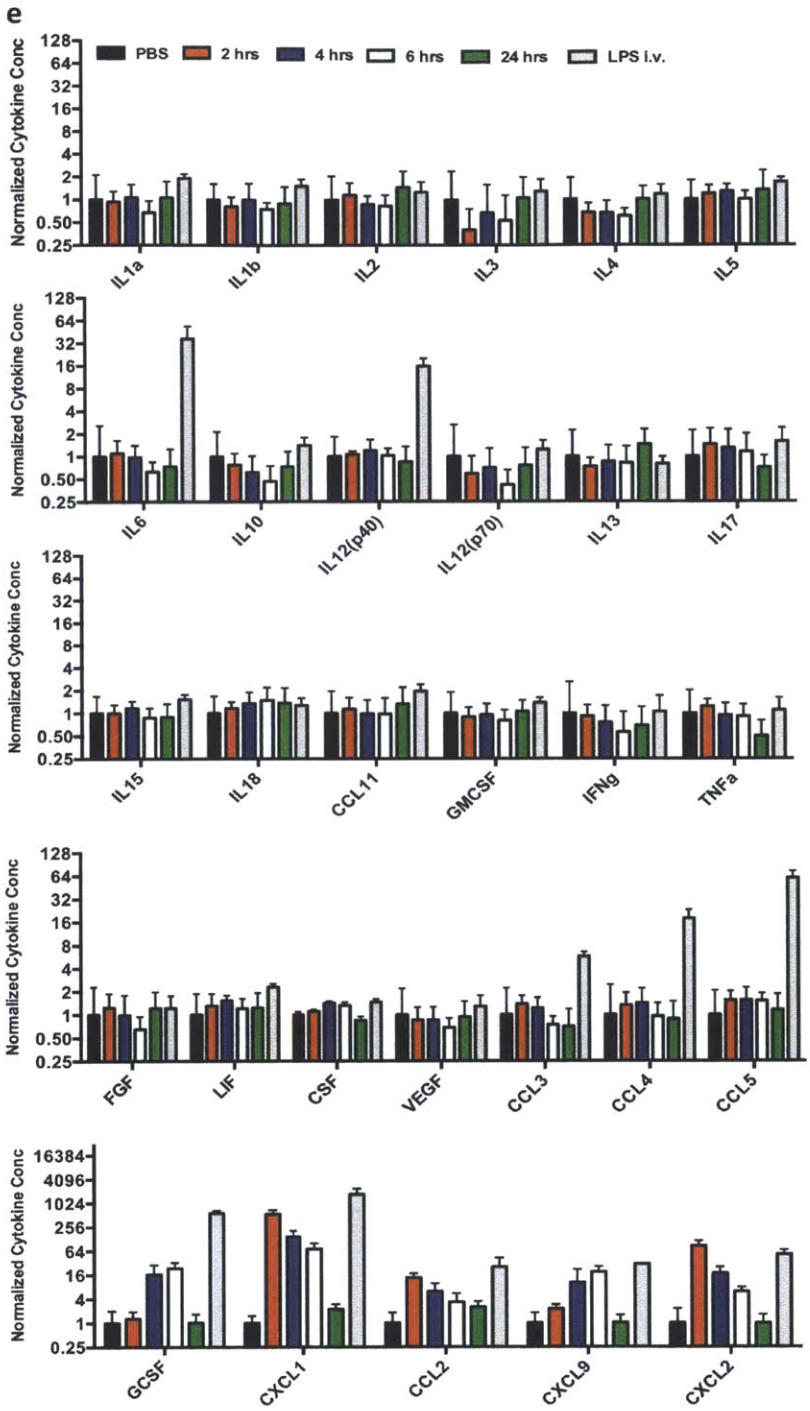

Figure 2.S4. 7C1 is well tolerated in acute and chronic models of toxicity. **(A)** Liver, kidney, and cardiovascular damage enzymes 48 hours after the fourth 0.6 mg/kg 7C1 injection in highly immunoactive $CD1^+$ mice. **(B)** Normalized murine weight following eight injections of PBS or 2 mg/kg 7C1 over a period of four weeks. **(C)** Cytokine and endothelial dysfunction marker mRNA expression 4 hours following the final injection of **(B)**. E-selectin and ICAM-2, two markers of endothelial dysfunction did not increase after chronic treatment. CD45, a marker for increased immune cell infiltration did not increase following chronic treatment. Finally, IL-6 and TNF-a, two markers for cationic particle-induced immunostimulation did not increase. **(D)** Serum cytokine expression (normalized to PBS-treated mice) 4 hours following the final injection of **(B)**. None of the 30 markers changed substantially after chronic treatment. **(E)** Serum cytokine expression profile 2, 4, 6, and 24 hours following a 2 mg/kg injection of 7C1. Low dose LPS (0.25 mg/kg) serves as a positive control. N=5 mice/group. Data shown as average +/- std.

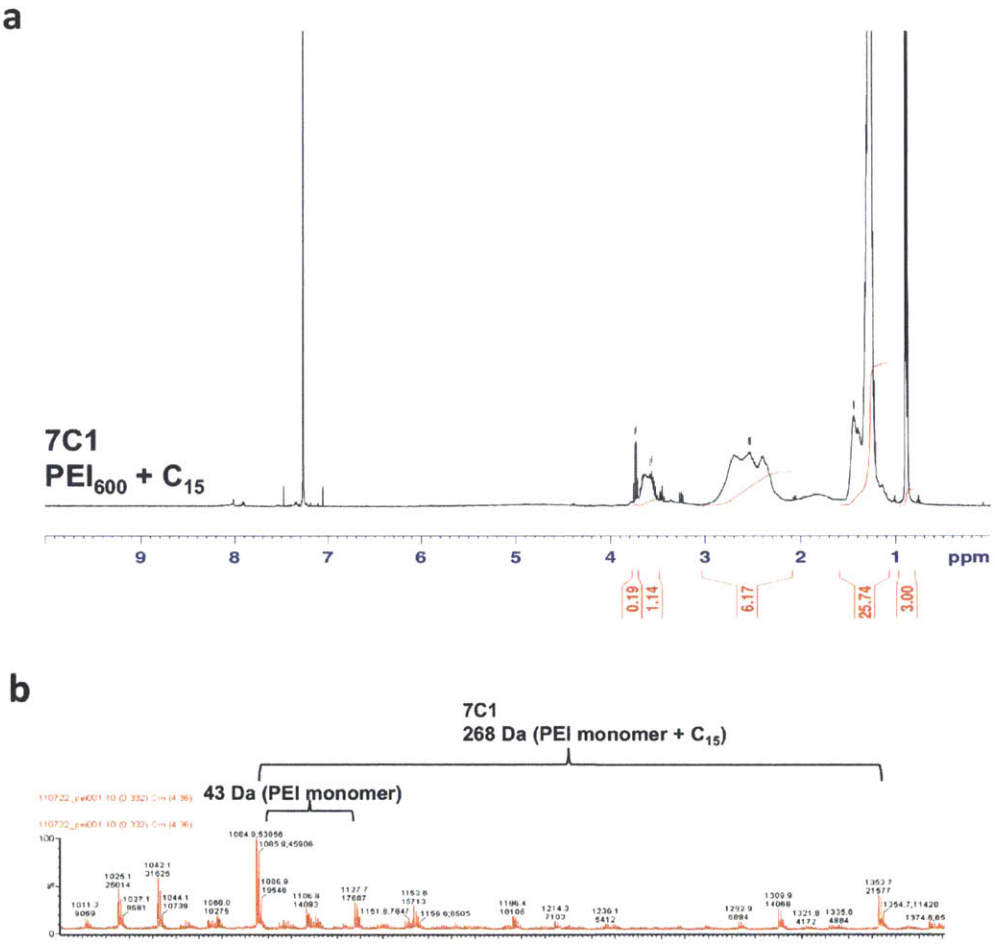

Figure 2.S5. Chemical characterization of 7C1. 7C1 was synthesized by mixing molecular weight PEI_{600} and an epoxide-terminated alkyl tail with 15 carbons together at 1:14 molar ratio for 72 hours in 100% EtOH at 90˚C. **(A)** ^{1}H-NMR spectroscopy, and **(B)** Maldi-TOF analysis.

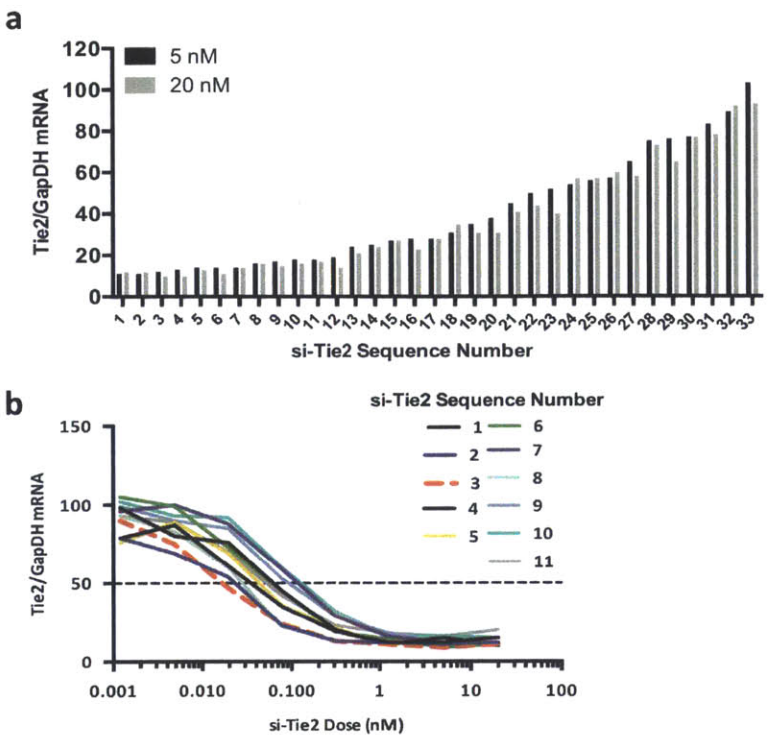

Figure 2.S6. Selection of siRNA. **(A)** Tie2/GapDH mRNA ratios in bEnd.3 cells 24 hours following treatment with 20 nM or 5 nM siRNA targeting Tie2. 31 sequences were designed against Tie2. **(B)** Tie2/GapDH dose response of 11 most potent sequences from **(A)** in bEnd.3 cells. Sequence 3 was the most potent, and was used for *in vivo* studies (Table 4).

a

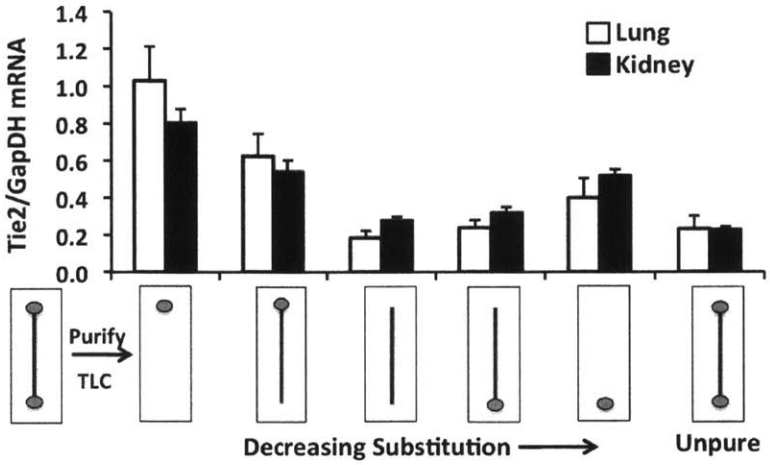

b

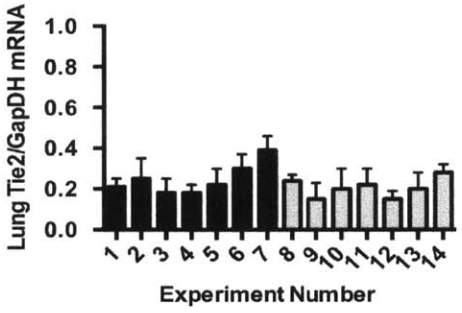

Renal ECs	Avg	Std Dev
Extrusion	0.60	0.34
Inline	0.36	0.09

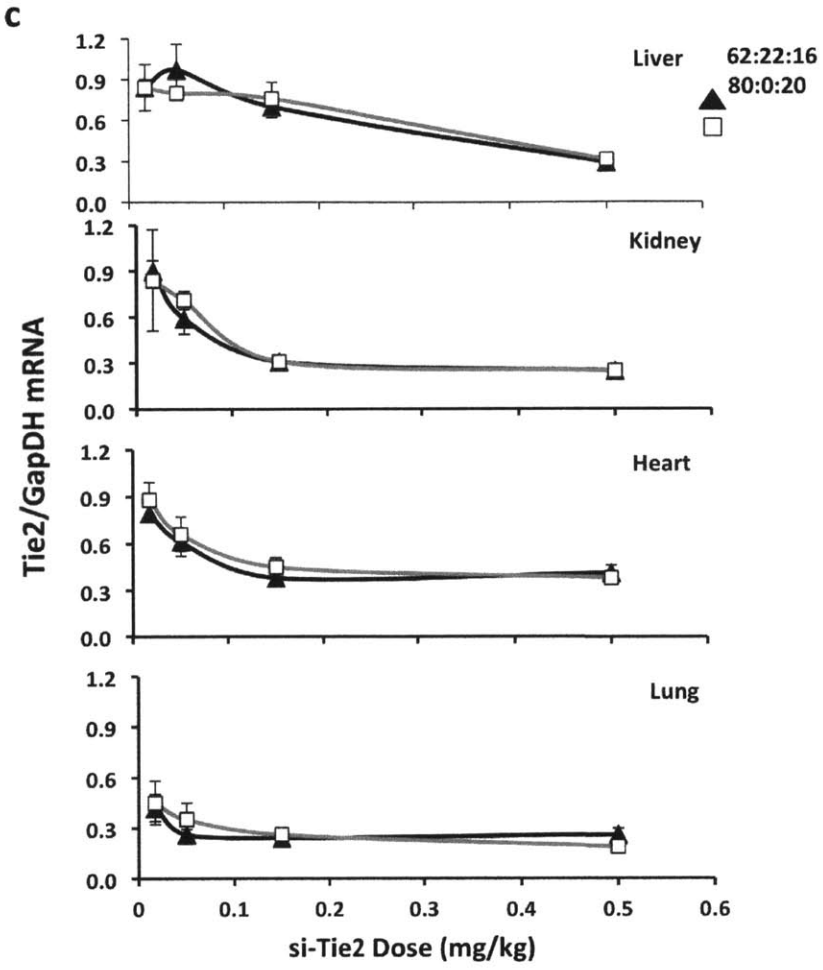

Figure 2.S7. Purification and optimization of 7C1, which is not a monodisperse molecule. **(A)** Tie2/GapDH mRNA levels two to three days after a 0.15 mg/kg injection of 7C1 with differing hydrophobic/hydrophilic ratios, as illustrated in the representative schematic of a thin layer chromatography (TLC) plate. Compounds with a more hydrophobic character are located at the top of the TLC plate. 7C1 was purified by high performance liquid chromatography (HPLC) before different fractions were injected. **(B)** Tie2/GapDH mRNA levels for six separate formulations made by extrusion and seven formulations made by microfluidic mixing. Microfluidic mixing produced more potent and consistent mRNA silencing. **(C)** Tie2/GapDH mRNA levels following injection with nanoparticles formulated with two different 7C1: cholesterol: $C_{14}PEG_{2000}$ molar ratios (62:22:16 or 80:0:20). There was no difference between formulations, suggesting 7C1 requires 7C1 and PEG, and does not require cholesterol. Data shown as average +/- std, N=4-5 animals/group.

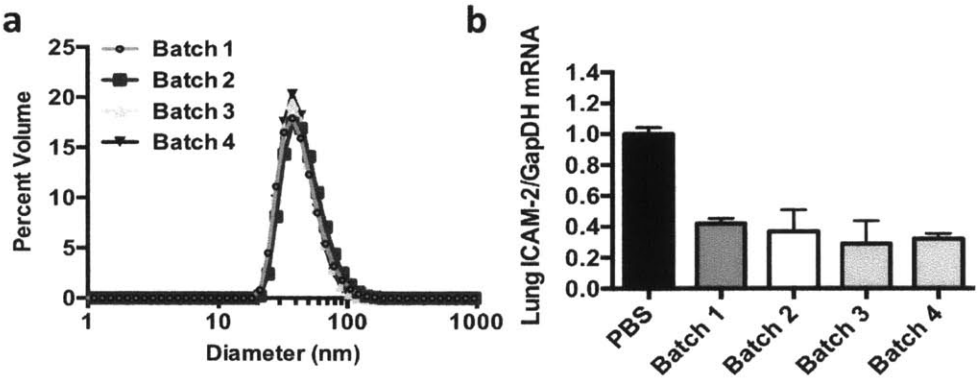

Figure 2.S8. Batch-to-batch repeatability of 7C1, which is not a monodisperse molecule. (A) Particle diameter (weighted by volume) and (B) pulmonary ICAM-2/GapDH mRNA expression three days after a 0.15 mg/kg intravenous injection of PBS or si-ICAM2. Four independent batches of 7C1, synthesized with different lots of PEI_{600} (Sigma Aldrich) are shown. Data shown are average +/- std, N=4-5 mice/group.

Compound: siFire Mass Ratio	Successful nanoparticles (%)
2.5	0.9
5	0.7
10	3.5
15	6.5

Table 1. The percent of compounds reducing Firefly luminescence more than 70% while not reducing Renilla luminescence more than 25% as a function of lipid: siFire mass ratio.

Gene	Lung	Heart	Kidney
VEcad	0.02	0.04	0.08
ICAM2	0.02	0.08	0.15
Tie2	0.04	0.12	0.12
VEGFR-2*	0.05	0.10	0.25
Tie1*	0.05	0.10	0.15

Table 2. Intravenous dose required to reduce target gene mRNA expression by 50% *in vivo* (mg/kg), termed the ED_{50}. *ED_{50} value calculated from multigene silencing experiment (Fig. 2d).

a

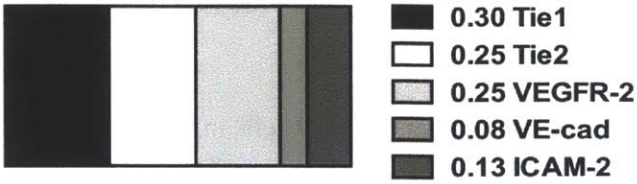

b

Total Dose (mg/kg)	2.0 siLuc	1.5 si 5 genes	1.0 si 5 genes	0.5 si 5 genes	0.25 si 5 genes
Tie1	1.02 ± 0.16	0.15 ± 0.02	0.22 ± 0.05	0.33 ± 0.08	0.60 ± 0.06
Tie2	0.90 ± 0.08	0.37 ± 0.02	0.43 ± 0.02	0.38 ± 0.04	0.56 ± 0.03
VE-cad	0.88 ± 0.18	0.26 ± 0.01	0.31 ± 0.07	0.49 ± 0.13	0.75 ± 0.09
VEGFR-2	0.99 ± 0.13	0.22 ± 0.03	0.23 ± 0.03	0.41 ± 0.09	0.65 ± 0.04
ICAM2	1.15 ± 0.26	0.24 ± 0.04	0.34 ± 0.09	0.65 ± 0.28	1.13 ± 0.14

c

Tie1	1.22 ± 0.15	0.25 ± 0.03	0.31 ± 0.04	0.48 ± 0.08	0.87 ± 0.11
Tie2	1.35 ± 0.19	0.31 ± 0.04	0.32 ± 0.03	0.48 ± 0.09	0.92 ± 0.09
VE-cad	0.92 ± 0.06	0.49 ± 0.16	0.67 ± 0.03	0.73 ± 0.14	1.19 ± 0.07
VEGFR-2	1.46 ± 0.27	0.32 ± 0.08	0.54 ± 0.09	0.93 ± 0.14	0.93 ± 0.13
ICAM2	1.24 ± 0.24	0.54 ± 0.11	0.65 ± 0.08	0.89 ± 0.14	1.23 ± 0.07

d

Tie1	1.15 ± 0.20	0.65 ± 0.12	0.78 ± 0.12	0.89 ± 0.15	0.84 ± 0.15
Tie2	0.92 ± 0.15	0.56 ± 0.12	0.80 ± 0.10	0.79 ± 0.04	0.67 ± 0.23
VE-cad	1.17 ± 0.48	0.77 ± 0.11	0.98 ± 0.22	0.96 ± 0.14	0.85 ± 0.22
VEGFR-2	0.90 ± 0.20	0.81 ± 0.10	0.95 ± 0.20	0.88 ± 0.10	0.86 ± 0.15
ICAM2	1.15 ± 0.33	1.08 ± 0.13	1.42 ± 0.22	1.07 ± 0.09	0.93 ± 0.10

Table 3. Target gene expression in (B) cardiovascular, (C) renal, and (D) hepatic vasculature following injection of 7C1 complexed with siRNA targeting Luc or Tie1, Tie2, VE-cad, VEGFR-2, and ICAM2. (A) Importantly, a 1 mg/kg total dose consisted of 0.075 mg/kg siVE-cad, 0.125 mg/kg siICAM2, 0.25 mg/kg siVEGFR-2, 0.25 mg/kg siTie2, and 0.30 mg/kg siTie1.

Chapter 2.8 References

1. Pober, J.S. & Sessa, W.C. Evolving functions of endothelial cells in inflammation. *Nat Rev Immunol* **7**, 803-815 (2007).
2. Hagberg, C.E., *et al.* Targeting VEGF-B as a novel treatment for insulin resistance and type 2 diabetes. *Nature* **490**, 426-430 (2012).
3. Kumar, V., Abbas, A., Fausto, N. & Aster, J. Robbins and Cotran Pathologic Basis of Disease, Eighth Edition. (2009).
4. Kanasty, R., Dorkin, J.R., Vegas, A. & Anderson, D. Delivery materials for siRNA therapeutics. *Nat Mater* **12**, 967-977 (2013).
5. Love, K.T., *et al.* Lipid-like materials for low-dose, in vivo gene silencing. in *Proc Natl Acad Sci USA*, Vol. 107 1864-1869 (2010).
6. Semple, S., *et al.* Rational design of cationic lipids for siRNA delivery. *Nature biotechnology* **28**, 172-176 (2010).
7. Whitehead, K.A., Langer, R. & Anderson, D.G. Knocking down barriers: advances in siRNA delivery. in *Nature Reviews Drug Discovery*, Vol. 8 129-138 (2009).
8. Aleku, M., *et al.* Atu027, a Liposomal Small Interfering RNA Formulation Targeting Protein Kinase N3, Inhibits Cancer Progression. *Cancer research* **68**, 9788-9798 (2008).
9. Aleku, M., *et al.* Intracellular localization of lipoplexed siRNA in vascular endothelial cells of different mouse tissues. *Microvascular Research* **76**, 31-41 (2008).
10. Santel, A., *et al.* RNA interference in the mouse vascular endothelium by systemic administration of siRNA-lipoplexes for cancer therapy. *Gene Ther* **13**, 1360-1370 (2006).
11. Santel, A., *et al.* A novel siRNA-lipoplex technology for RNA interference in the mouse vascular endothelium. *Gene therapy* **13**, 1222-1234 (2006).
12. Polach, K.J., *et al.* Delivery of siRNA to the Mouse Lung via a Functionalized Lipopolyamine. *Mol Ther* **11**, 210 (2011).
13. Kaufmann, J., Ahrens, K. & Santel, A. RNA interference for therapy in the vascular endothelium. *Microvascular Research* **80**, 286-293 (2010).
14. Davis, M.E., *et al.* Evidence of RNAi in humans from systemically administered siRNA via targeted nanoparticles. *Nature*, 1-8 (2010).
15. Rozema, D.B., *et al.* Dynamic PolyConjugates for targeted in vivo delivery of siRNA to hepatocytes. *Proc Natl Acad Sci U S A* **104**, 12982-12987 (2007).
16. Godbey, W.T., Wu, K.K. & Mikos, A.G. Poly(ethylenimine) and its role in gene delivery. *Journal of Controlled Release* **60**, 149-160 (1999).
17. Breunig, M., Lungwitz, U., Liebl, R. & Goepferich, A. Breaking up the correlation between efficacy and toxicity for nonviral gene delivery. *Proc Natl Acad Sci U S A* **104**, 14454-14459 (2007).
18. Richards Grayson, A.C., Doody, A.M. & Putnam, D. Biophysical and structural characterization of polyethylenimine-mediated siRNA delivery in vitro. *Pharmaceutical research* (2006).

19. Crawford, R., *et al.* Analysis of lipid nanoparticles by Cryo-EM for characterizing siRNA delivery vehicles. *Int J Pharm* **403**, 237-244 (2011).
20. Jayaraman, M., *et al.* Maximizing the potency of siRNA lipid nanoparticles for hepatic gene silencing in vivo. *Angew Chem Int Ed Engl* **51**, 8529-8533 (2012).
21. Huang, H., Bhat, A., Woodnutt, G. & Lappe, R. Targeting the ANGPT-TIE2 pathway in malignancy. *Nat Rev Cancer* **10**, 575-585 (2010).
22. Novobrantseva, T.I., *et al.* Systemic RNAi-mediated Gene Silencing in Nonhuman Primate and Rodent Myeloid Cells. *Molecular Therapy - Nucleic Acids* (2012).
23. Kasahara, Y., *et al.* Inhibition of VEGF receptors causes lung cell apoptosis and emphysema. *J Clin Invest* **106**, 1311-1319 (2000).
24. Tuder, R.M. & Yun, J.H. Vascular endothelial growth factor of the lung: friend or foe. *Curr Opin Pharmacol* **8**, 255-260 (2008).
25. Thurston, G., Noguera-Troise, I. & Yancopoulos, G.D. The Delta paradox: DLL4 blockade leads to more tumour vessels but less tumour growth. *Nat Rev Cancer* **7**, 327-331 (2007).
26. Fischer, C., Mazzone, M., Jonckx, B. & Carmeliet, P. FLT1 and its ligands VEGFB and PlGF: drug targets for anti-angiogenic therapy? *Nat Rev Cancer* **8**, 942-956 (2008).
27. Lyden, D., *et al.* Impaired recruitment of bone-marrow-derived endothelial and hematopoietic precursor cells blocks tumor angiogenesis and growth. *Nat Med* **7**, 1194-1201 (2001).
28. Kaplan, R.N., *et al.* VEGFR1-positive haematopoietic bone marrow progenitors initiate the pre-metastatic niche. *Nature* **438**, 820-827 (2005).
29. Tammela, T., *et al.* VEGFR-3 controls tip to stalk conversion at vessel fusion sites by reinforcing Notch signalling. *Nat Cell Biol* **13**, 1202-1213 (2011).
30. Stevens, J.B., *et al.* Heterogeneity of cell death. *Cytogenet Genome Res* **139**, 164-173 (2013).
31. Kuramoto, T., *et al.* Dll4-Fc, an Inhibitor of Dll4-Notch Signaling, Suppresses Liver Metastasis of Small Cell Lung Cancer Cells through the Downregulation of the NF-kappaB Activity. *Mol Cancer Ther* **11**, 2578-2587 (2012).
32. Garcia, A. & Kandel, J.J. Notch: a key regulator of tumor angiogenesis and metastasis. *Histol Histopathol* **27**, 151-156 (2012).
33. Akinc, A., *et al.* Targeted delivery of RNAi therapeutics with endogenous and exogenous ligand-based mechanisms. *Mol Ther* **18**, 1357-1364 (2010).
34. Monopoli, M.P., Aberg, C., Salvati, A. & Dawson, K.A. Biomolecular coronas provide the biological identity of nanosized materials. *Nat Nanotechnol* **7**, 779-786 (2012).
35. Chen, D., *et al.* Rapid discovery of potent siRNA-containing lipid nanoparticles enabled by controlled microfluidic formulation. *J Am Chem Soc* **134**, 6948-6951 (2012).
36. Whitehead, K., Dahlman, J.E., Langer, R.S. & Anderson, D.G. Silencing or Stimulation? siRNA Delivery and the Immune System. *Annual Review of Chemical and Biomolecular Engineering* (2010).

37. Panigrahy, D., *et al.* Epoxyeicosanoids stimulate multiorgan metastasis and tumor dormancy escape in mice. *J Clin Invest* **122**, 178-191 (2012).

Chapter 3. 7C1 enables targeted 5-siRNA therapy for ischemic heart disease

Chapter 3.1 Introduction

Leukocytes are key cellular components of atherosclerotic plaque inflammation[1]. Myeloid cells drive disease progression and complication by delivering inflammatory mediators and tissue-destabilizing proteases to the arterial wall[2]. While we are on the brink of identifying vulnerable patients and with vulnerable plaques with advanced risk assessment and imaging, we currently lack clinical means of rapid and efficient systemic interventions once rupture prone plaque(s) are identified[3].

Recent insight points to rapid turn-over of macrophages in growing arterial lesions. In the early stage of atherosclerosis, monocyte recruitment from the blood contributes to macrophages accumulation[4]. In addition to several chemokines, endothelial cell adhesion molecules play a significant role in leukocyte recruitment[5]. Leukocyte recruitment is a multistep process that involves rolling (mediated by endothelial E- and P-Selectins), firm arrest and adhesion (mediated by endothelial VCAM-1 and ICAM-1) and transmigration (partially mediated by endothelial ICAM-2)[5]. These five leukocyte adhesion molecules are expressed at high levels in atherosclerotic plaque endothelial cells[5]. Interestingly, experiments in mice deficient for two adhesion molecules suggest that synergistic effects can be achieved by inhibiting more than one adhesion molecule[6]. We thus reasoned that parallel inhibition of all five adhesion molecules would impede leukocyte recruitment, reduce arterial inflammation and stabilize atherosclerotic plaques.

Because small interfering RNA (siRNA) inhibits gene expression by mediating mRNA cleavage in a sequence-specific manner, the concurrent delivery of five distinct siRNAs is an attractive strategy to simultaneously reduce the translation of multiple targets with high specificity. However, combination therapies require highly efficient delivery vehicles, which historically have been limited to those targeting hepatocytes[7]. Lipid-like compounds termed 'lipidoids' reduce hepatocyte expression at low doses in mice, and have generated promising data in non-human primates and humans[8-10]. By contrast, 100-fold higher doses were required for the robust reduction of a single mRNA in endothelial cells[11]. We recently developed a nanoformulation that delivers siRNA to endothelial cells at doses as low as 0.02 mg/kg[12]. The delivery material was synthesized by conjugating a fully saturated epoxide-terminated C_{15} lipid with a small (MW=600) branched poly(ethyeleneimine) (PEI). This conjugate was then mixed with polyethylene glycol and siRNA to form 30-60 nm particles that were well tolerated *in vivo.*

Here we employ these novel endothelial-avid nanoparticles to simultaneously reduce the expression of five cell adhesion molecules in ApoE-/- mice with atherosclerosis. The combination therapy, termed siCAM5, substantially decreased leukocyte recruitment and plaque inflammation, thereby rapidly improving plaque stability. Similarly, siCAM5 treatment decreased immune cell infiltration into acutely ischemic myocardium. Taken together, the data constitute a proof-of-principle that targeted multi-gene therapies may be an interesting therapeutic avenue to rapidly reverse atherosclerotic disease progression.

In addition to control siRNA with an irrelevant sequence, we used five siRNA sequences targeting the major adhesion molecules expressed by endothelial cells lining atherosclerotic plaques. For each protein, reduced expression had shown effects on leukocyte recruitment to atherosclerotic lesions and impact on plaque size and phenotype, thus informing our target choice[6,13,14]. The specific siRNA sequences were identified by *in vitro* screening of respective in silico predicted candidate sequences. The best duplexes were selected for scale up, formulation and nanoparticle formulation (Table 1). All siRNAs used in the study were modified to minimize immunostimulation and off-target silencing[15].

Chapter 3.2 7C1 nanoparticles deliver siRNAs to aortic endothelial cells.

We delivered siRNA with a nanoparticle optimized for delivery to endothelial cells *in vivo*[12]. The low molecular weight polymer 7C1 was combined in a glass syringe with $C_{14}PEG_{2000}$ at a molar ratio of 80:20 before particles were formed by mixing with siRNAs in a microfluidic channel[16]. Particles were formulated with siRNAs targeting luciferase (termed siCntrol) or a combination of five siRNAs targeting the leukocyte adhesion molecules ICAM-1, ICAM-2, VCAM-1, E-Selectin, and P-Selectin (termed siCAM5). The five siRNAs were mixed together in a molar ratio of 1: 0.35: 1: 1: 1, based on their *in vitro* potency (Fig. 1a). After formulation with siCntrol or siCAM5, particle size was characterized with dynamic light scattering (DLS), and internal structure was characterized with cryoTEM (Fig. 1b). Nanoparticles formulated with one siRNA or five siRNAs exhibited consistent structural properties; both formed multilamellar structures of siRNA and lipid that had an average of 45 +/- 16 nm (Fig. 1c). We examined the efficacy with which 7C1 delivered siRNA to arterial endothelial cells in $ApoE^{-/-}$ mice with atherosclerosis. Cy3- conjugated siRNA was formulated in nanoparticles and injected intravenously at a dose of 1.0 mg/kg siRNA. Two hours later, Cy3 signal was detected by fluorescent histology in $CD31^+$ (PECAM-1, an endothelial cell marker) cells located in the tunica intima of atherosclerotic plaques in the aortic root and arch (Fig. 1d). To further validate siRNA delivery, we employed a method to process and stain aortic endothelial cells for flow cytometry (Fig. S1*)*. Two hours after a 1.0 mg/kg injection with nanoparticle- encapsulated Alexa647-tagged siRNA, Alexa647 signal increased more than 50-fold in $CD45^-CD31^+CD107^+$ cells isolated from digested aortae (Fig. 1e).

We next measured mRNA and protein levels of target genes in aortic endothelial cells from $ApoE^{-/-}$ mice treated with siCntrol or siCAM5. Mice were injected with either 3.0 mg/kg siCntrol or siCAM5 seven and four days before $CD45^-CD31^+CD107^+$ cells were FACS-sorted from $ApoE^{-/-}$ aortae. Compared to siCntrol-treated mice, target gene mRNA and protein levels decreased significantly after siCAM5-treatment (Fig. 2a-c). Taken together, these data demonstrate that 7C1 nanoparticle efficiently deliver siRNA to arterial endothelial cells in $ApoE^{-/-}$ mice, and that it is feasible to simultaneously reduce expression of five proteins in vivo.

Chapter 3.3 siCAM[5] treatment suppresses leukocyte recruitment to atherosclerotic plaque.

To determine whether siCAM5 treatment would curtail recruitment of circulating leukocytes to atherosclerotic plaques, we treated ApoE-/- mice with either siCntrol or siCAM5 over a period of two weeks (three intravenous injections of 3 mg/kg cumulative siRNA dose each over a 2 week

time period) before adoptive transfer of two million GFP^+ neutrophils together with two million $GFP^+/Ly6C^+$ monocytes. These myeloid cells, which rely on adhesion molecules for their recruitment, are the main instigators of plaque growth and destabilization[1]. Two days after adoptive transfer, the number of $CD11b^+/GFP^+$ cells recruited into the aortae of siCAM5 treated mice was 50% lower compared to mice treated with siCntrol, while the number of $CD11b^+/GFP^+$ cells circulating in the blood remained unchanged (Fig. 3a,b, Fig. S2).

We then assessed the effect of siCntrol or siCAM5 (cumulative dose of 9.0 mg/kg siRNA dose) on plaque phenotype in $ApoE^{-/-}$ mice which were treated for two weeks. On day fourteen, the aortae were isolated and digested before the number of neutrophils, Ly-$6C^+$ monocytes, and macrophages were quantified using flow cytometry. While the number of neutrophils and Ly-$6C^+$ monocytes in the blood remained constant, their numbers decreased in the aortae by at least one third (Fig. 3b-d). The number of plaque macrophages also decreased (Fig. 3b,c), while circulating myeloid cells remained constant (Fig. 3c). These flow cytometry-based data, which suggest that siCAM5 treatment reduced leukocyte recruitment, were substantiated by immunohistochemistry and qRT-PCR studies. Specifically, a reduction of at least 40% in myeloid cells and neutrophils was observed in aortic root sections stained with antibodies against CD11b and Ly6G (Fig. 3d,e). Expression of myeloperoxidase (MPO), which is produced by neutrophils and inflammatory monocytes, and F4/80, a marker for macrophages, decreased in aortic plaques isolated from siCAM5-treated mice by at least 75%, relative to those treated by siCntrol (Fig. 4a). Because decreased leukocyte content could mitigate inflammatory signaling in atherosclerotic lesions, we quantified the mRNA levels of inflammatory cytokines and matrix metalloproteinases (MMPs) with qRT-PCR. Atherosclerotic plaques isolated from $ApoE^{-/-}$ mice treated with siCAM5 expressed less TNFa, IL-6, IL-1b and IL-12 than those treated with siCntrol (Fig. 4a). MMPs released by inflammatory cells promote extracellular matrix degradation, vessel remodeling, and may render the fibrous cap unstable. MMP2, MMP3 and MMP9 mRNA decreased in mice treated with siCAM5 (Fig. 4a) by up to 85%. To investigate whether siCAM5 treatment lowered protease activity and thus improved plaque stability, we imaged activation of an *in vivo* protease sensor in the aortic root using Fluorescence Molecular Tomography-Computed Tomography (FMT-CT). Protease activity was significantly lower in mice treated with siCAM5 compared to mice treated with siCntrol (Fig. 4b). In mice treated with siCAM5 we further observed smaller necrotic cores and thicker fibrous caps (Fig. 4c), in line with the lower protease activity. The size of the aortic root plaque was not changed by 2two weeks of treatment (Fig. 4d). Together, these data demonstrate that parallel *in vivo* silencing of adhesion molecule expression reduced the number of leukocytes recruited to atherosclerotic plaques, leading to a less inflammatory atherosclerotic lesion phenotype.

Chapter 3.4 siCAM[5] reduces myocardial inflammation after ischemia reperfusion injury. We then investigated whether siCAM5 affected leukocyte recruitment in a model of acute myocardial ischemia, an injury that is enhanced by an overzealous immune response[1]. Here, we injected a single dose of either 3.0 mg/kg siCntrol or siCAM5 immediately after the induction of coronary ligation and enumerated leukocytes within the infarct and the border zone three days

later. The treatment reduced neutrophil and Ly-6Chigh monocyte numbers by more than 50% (Fig. 5a). In contrast, the number of cells circulating in the blood was similar in both groups (Fig. 5b).

Chapter 3.5 Discussion

Ischemic organ injury leading to stroke and myocardial infarction remains the most frequent cause of death[17]. The events in arterial plaques leading up to tissue hypoxia are dominated by leukocytes; however, state of the art clinical therapy does not specifically target these cells. Rather, in addition to mechanical vessel reopening and intervention aimed at the coagulation system, we treat risk factors such as hyperlipidemia and hypertension. Commonly, the clinical benefits of modulating these risk factors come about slowly. Our increased ability to identify vulnerable patients and even individual plaques at high risk of complication, however, warrants therapeutic options that allow rapid and decisive systemic interventions preventing ischemic events. Improved risk prediction algorithms in conjunction with advanced imaging approaches currently entering the clinical arena, will further enhance the need for intervention options beyond what is currently clinically available[18]. Therapeutic targeting of leukocyte supply appears particularly attractive because these cells turn over rapidly in atherosclerotic plaque, fueled by bone marrow derived monocytes and neutrophils circulating in the blood stream[4]. The correlation of leukocytosis with outcome in cardiovascular patients, as well as numerous preclinical studies that genetically targeted leukocyte supply in mice with atherosclerosis support this concept[14].

Recruitment of circulating neutrophils and monocytes to sites of inflammation is a tightly regulated process[5]. Chemokines receptors like CCR2, CCR2, and CX3CR1 together with vascular adhesion molecules conduct pivotal roles in that leukocyte recruitment cascade[19]. There are three major steps involved in that process: tethering and rolling, adhesion and transmigration[14]. The selectins are mainly involved in tethering and rolling. P- and E- selectins are expressed on activated endothelial cells and bind to the leukocyte ligand PSGL-1. Leukocyte accumulation is associated with an increase in plaque vulnerability which in turn makes the plaque more likely to ruptur leading to thrombus formation, vascular occlusion and either myocardial infarction or stroke[20]. Among the leukocytes, macrophages have emerged as the key players in atherosclerosis. They accumulate in lesions, become foam cells after lipid digestion and drive disease by producing a myriad of pro-inflammtory mediators. Macrophage originate predominately from circulation inflammatory monocytes[4]. The role of neutrophils in atherosclerosis is less well investigated. Neutrophils also accumulate in the vessel wall at early stages of atherosclerosis and plaque size was reduced after neutrophil depletion[21].

In the ischemic heart neutrophils are the first leukocyte population that arrives at the site of inflammation[4]. These phagocytic cells fuel a pro-inflammatory environment by producing numerous inflammatory cytokines and also applying oxidative stress to the infarct tissue[1]. The next prominent population that dominates the infarct tissue are classical or inflammatory monocytes (Ly-6C$^+$ monocytes) whereas macrophages start to accumulate from day 4 after MI on. Both cell types phagocyte infarct debris, which is then replaced with granulation tissue

during scar formation[1].

Based on these data, the field has pursued blocking of chemokine/chemokine receptor interaction and the function of adhesion molecules, mostly relying on small molecule inhibitors or antibodies[22]. While promising, single-target strategies may suffer from low efficacy rooted in the redundancies of the leukocyte recruitment cascade. The methodology described here takes a novel approach by simultaneously suppressing the expression of the five major adhesion molecules in endothelial cells lining inflamed atherosclerotic plaque. Enabled by a novel, high-efficiency delivery nanoparticle with avidity for endothelial cells, the siRNA doses necessary for significant knock down were low enough to allow the combination of five duplexes into one nanoparticle. Similar advances in siRNA delivery technology, together with siRNA modification reducing off-target effects, initiated a resurgence of activities in clinical translation of systemic RNAi[9,23]. We believe that these data, which clearly demonstrate that targeted multiplex siRNA is feasible, constitute a proof of concept that will further increase interest in RNAi-based therapies.

Chapter 3.6 Materials and Methods

siRNA formulation into 7C1 nanoparticles. Purified 7C1 nanoparticles were synthesized and formulated as previously described {Dahlman, #72157}. Specifically, polyethyleneimine with a number molecular weight of 600 (PEI600, Sigma Aldrich) was combined with 200 proof ethanol and an epoxide-terminated C15 lipid at a lipid:PEI molar ratio equal to 14:1. The mixture was heated at 90℃ for 48 hours before purification was performed with a silica column as previously described[12]. To formulate nanoparticles, purified 7C1 was combined with 200 proof ethanol and $C_{14}PEG_{2000}$ (Alnylam Pharmaceuticals) at a 7C1:$C_{14}PEG_{2000}$ molar ratio equal to 4:1 in a glass syringe. siRNA was dissolved in pH 3 10 mM citrate solution in a separate syringe. The two syringes were connected to a syringe pump and the fluid was pushed through a microfluidic device as previously described[16]. The resulting nanoparticles were dialyzed in 1x PBS and filtered through a 0.22 um sieve before their size was characterized. Particle size was characterized with dynamic light scattering (Malvern Zetasizer).

Mice. Female C57BL/6J mice (WT), female ubiquitous GFP mice (C57BL/6-Tg (UBC- GFP) 30Scha/J) and female apolipoprotein E–deficient mice ($ApoE^{-/-}$; B6.129P2- Apoetm1Unc/J) were purchased from The Jackson Laboratories (Bar Harbor, Maine). At 12 weeks of age, $ApoE^{-/-}$ mice were placed on high cholesterol diet (HCD, 21.2% fat by weight and 0.2% cholesterol; Harlan Teklad, Madison, WI) for the durations of 4-6 weeks. All procedures were approved by the Institutional Animal Care and Use Committee (IACUC) Subcommittee on Research Animal Care (SRAC), Massachusetts General Hospital, Charlestown, MA.

Cells. Blood for flow cytometric analysis was collected by cardiac puncture using a 50 mM EDTA (Ethyinene Diamine Tetra Acitic Acid) solution (Sigma Aldrich, St. Louis, MO) as an anticoagulant. Erythrocytes were lysed using a red blood cell lysis buffer (Biolegend, San Diego, CA). After organ harvest, single-cell suspensions were obtained as follows. Aortae were

extensively flushed with PBS and then excised from aortic root to iliac bifurcation using a microscope, minced with scissors and digested in either collagenase I (450 U/ml), collagenase XI (125 U/ml), DNase I (60 U/ml) and hyaluronidase (60 U/ml) (Sigma-Aldrich, St. Louis, MO) at 37o C at 750 rpm for 1 hour {Swirski et al., 2007, #74879} for a myeloid cell staining or in collagenase IV (Worthington, Lakewood, NJ) and DNase I (20 U/ml) (Sigma-Aldrich, St. Louis, MO) at 37o C at 750 rpm for 40 min for an endothelial cell staining. Aortae were then homogenized through a 40-μm nylon mesh. Total viable cell numbers were obtained using Trypan blue (Cellgro, Mediatech, Inc., VA).

Nanoparticle and siRNA dosing. Particles were injected intravenously via a tail vein in a volume of 300 μl. For a one-week study we injected particles on the 1st and 3rd day and for a two-weeks period we did an additional third injection on the 10th day. Particles contained either 3.0 mg/kg of siRNA targeting luciferase (termed siCntrol) or 3.0 mg/kg of a combination of five siRNAs encapsulated in the same particle targeting the leukocyte adhesion molecules ICAM-1, ICAM-2, VCAM-1, E-Selectin, and P-Selectin (termed siCAM5). The five siRNAs were mixed together in a molar ratio of 1: 0.35: 1: 1: 1 with 0.69 mg/kg of ICAM-1, VCAM-1, E-Selectin, and P-Selectin and 0.24 mg/kg of ICAM-2.

Flow cytometry: leukocyte staining. For staining myeloid cells, cells were first stained with mouse hematopoietic lineage markers including phycoerythrin (PE) anti-mouse antibodies directed against B220 (BD Biosciences, clone RA3-6B2), CD90 (Biolegend, clone 53-2.1), CD49b (BD Biosciences, clone DX5), Ly-6G (BD Biosciences, clone 1A8), NK1.1 (Biolegend, clone PK136) and Ter-119 (BD Biosciences, clone TER-119). This was followed by a second staining covering CD45.2 (BD Biosciences, clone 104), CD11b (BD Biosciences, clone M1/70), CD115 (Biolegend, AFS98), CD11c (BD Biosciences, clone HL3), F4/80 (Biolegend, clone BM8), MHCII (Biolegend, clone M5/114.15.2) and Ly6C (BD Biosciences, clone AL-21). Neutrophils were identified as (CD90/B220/CD49b/NK1.1/Ter119)low, (CD45.2/CD11b)high, CD115low, Ly6Ghigh. Monocytes were identified as (CD90/B220/CD49b/NK1.1/Ter119)low, CD11bhigh, (F4/80/ CD11c)low, Ly-6Chigh/low or (CD45.2/CD11b)high, Ly6Glow, CD115high, Ly-6Chigh/low. Macrophages were identified as (CD90/B220/CD49b/NK1.1/Ter119)$^{-}$, CD11b^{+}, Ly6Clow/int, Ly6G^{-},F4/80^{+}.

Flow cytometry: endothelial cell staining. For staining endothelial cells we used: ICAM-1-APC (Biolegend, clone Yn1/1.7.4), ICAM-2-biotin (Biolegend, clone 3C4), VCAM-1-PE-Cy 7 (Biolegend, clone 429), E-Selectin (CD62E)-PE (BD Biosciences, clone 10E9.6), P-Selectin (CD62P)-FITC (BD Biosciences, clone RB40.34), CD31- Pacific Blue (Biolegend, clone 390), CD107a (LAMP-1)-APC-Cy7 (Biolegend, clone 1D4B) and CD45.2-Alexa 700 (Biolegend, clone 104). Streptavidin-Pacific Orange was used to label biotinylated antibodies. Endothelial cells were identified as CD45.2low, CD31high and CD107aint/high. Data were acquired on an LSR II flow cytometer (BD Biosciences) and analyzed with FlowJo version 8.8.6 (Tree Star, Inc.).

Cell sorting. For sorting of GFPhigh neutrophils and GFPhigh/Ly6Chigh monocytes, bone marrow cells were collected from individual mice by crushing bones from both femurs, tibias, humeri, from the pelvis and the spine using mortar and pestle, then re-suspended in PBS buffer supplemented with 2 mM EDTA and 2% fetal bovine serum (FBS). To purify neutrophils and monocytes from other lineage-committed cells, we used MACS (magnetic-activated cell sorting) depletion columns (LD columns, Miltenyi) after incubation with a cocktail of PE-labeled antibodies including B220 (BD Biosciences, clone RA3-6B2), CD90 (Biolegend, clone 53-2.1), CD49b (BD Biosciences, clone DX5), NK1.1 (Biolegend, clone PK136) and Ter-119 (BD Biosciences, clone TER-119) followed by incubation with PE-coated microbeads (Miltenyi). Then cells were subsequently stained as described above. GFP^+ neutrophils and $GFP^+/Ly6C^+$ monocytes were FACS-sorted using a FACSAria II cell sorter (BD Biosystems). For sorting of endothelial cells, aortae were excised, processed and stained as described above. Endothelial cells were identified as $CD45.2^-$, $CD31^+$ and $CD107^+$ and FACS (Fluorescence Activated Cell Sorting)-sorted using a FACSAria II cell sorter (BD Biosystems).

Adoptive transfer. Neutrophils and Ly-$6C^+$ monocytes were FACS sorted from UBC- GFP mice as described above. $ApoE^{-/-}$ mice receiving either siCntrol or siCAM5 treatment were injected i.v. two days prior to the end of the two weeks treatment period with 2x106 neutrophils together with 2x106 Ly-$6C^+$ monocytes each and aortae were harvested 48h later. The number of $CD11b^+/GFP^+$ cells within the vessel wall and the blood was quantified by using flow cytometry.

Quantitative real-time PCR. RNA was extracted from either aortic arches using the RNeasy Mini Kit (Qiagen, Hilden, Germany) or from FACS-sorted endothelial cells using the Arcturus PicoPure RNA Isolation Kit (Applied Biosystems, NY, USA) according to the manufacturers' protocol. One microgram of mRNA was transcribed to complimentary DNA (cDNA) with the high capacity RNA to cDNA kit (Applied Biosystems, NY, USA). As for the quantitative PCR we exclusively used Taqman probes (Applied Biosystems, NY, USA). Results were expressed by Ct values normalized to the housekeeping gene Gapdh with the control set as one.

Fluorescence Molecular Tomography-Computed Tomography (FMT/CT). To non-invasively investigate changes of the protease activity in atherosclerotic plaques of $ApoE^{-/-}$ mice, which is a marker of the inflammatory activity in the plaque, fluorescence molecular tomography (FMT) was used in a combined approach with computed tomography (CT). After two weeks of either siCntrol or siCAM5 treatment, FMT/CT imaging was performed on $ApoE^{-/-}$ animals. Pan-cathepsin protease sensor (Prosense-680, 5 nmol per mouse, PerkinElmer, MA, USA) was injected intravenously 24 hours prior to the imaging. On the day of the imaging, the mouse was shaved and placed in a custom designed plexiglas mouse holder which allowed continuous supply of anesthesia. To identify anatomic regions a CT angiography (exposure time: 370-400 ms, operated at 80 kVp and 500 μA, Inveon PET-CT, Siemens) was used. Isovue-370 (at 55 μL/min through vein catheter) was infused to obtain vascular contrast. Then the mouse holder was transferred into the FMT (680/700 nm excitation/emission) and a 3D dataset was acquired

on an FMT2500 system (PerkinElmer), and reconstructed to express fluorescence per voxel in nM. Osirix software (The Osirix Foundation, Geneva) and fiducial markers were used for FMT/CT image fusion.

Histology. Aortic roots were harvested and embedded in OCT compound (Sakura Finetek). Embedded tissues were snap-frozen in a 2-methylbutane bath cooled with dry ice. Sections of 5μm thickness were then stained using an anti-CD11b (BD Biosciences, clone M1/70,) or anti-Ly6G (Biolegend, clone 18A) antibody. Staining was followed with a biotinylated secondary antibody. For color development we used the VECTA STAIN ABC kit (Vector Laboratories, Inc.) and AEC substrate (DakoCytomation). Necrotic core and fibrous cap thickness were assessed using Masson trichrome staining. Necrotic core was evaluated measuring the total acellular area within each plaque. For fibrous cap thickness three to five measurements representing the thinnest part of the fibrous cap were averaged for each plaque as previously described {Seimon et al., 2009, #40064}. Sections were scanned with NanoZoomer 2.0-RS (Hamamatsu) in 40x magnification and analyzed using IPLab (version 3.9.3; Scanalytics, Inc.).

Statistics. Statistical analyses were performed using GraphPad Prism software (GraphPad Software, Inc.). Results are depicted as mean±standard error of mean if not stated otherwise. For a two-group comparison, a t-test was applied if the pre-test for normality (D'Agostino-Pearson normality test) and equality of variances (Bartlett's test) was not rejected at 0.05 significance level, otherwise a Mann-Whitney U test for nonparametric data was used. For a comparison of more than two groups an ANOVA, followed by a Bonferroni test for multiple comparison, was applied. P values of <0.05 indicate statistical significance.

Chapter 3.7 Figures

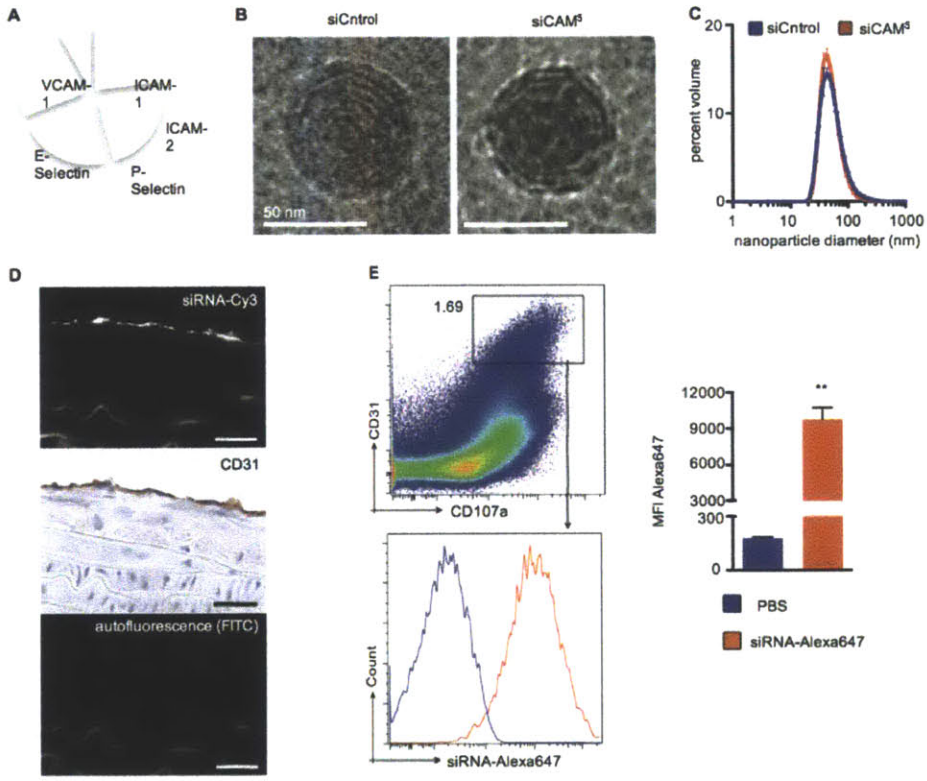

Figure 3.1. 7C1 delivers siRNA to aortic endothelial cells *in vivo*. **(A)** Distribution of five siRNAs delivered concurrently. **(B)** CryoTEM image of 7C1 cross sectional structure. Dark bands are indicative of 7C1 lipid and PEG, and light bands are indicative of siRNA. **(C)** Nanoparticle diameter (nm), measured by dynamic light scattering (DLS) after dialysis into PBS and filtration. Particle size remained constant, whether one siRNA was encapsulated (siCntrol) or five siRNAs were encapsulated (siCAM5) (mean +/- SEM, N=8 formulations). **(D)** Immunofluorescence evaluation of aortic arches 2h after injection of Cy3-tagged siRNAs. The middle image shows an immunohistochemical staining of the same section for CD31, an endothelial cell marker. Scale bar, 10 μm. (n=2 $ApoE^{-/-}$ mice fed a high cholesterol diet for 6 weeks) **(E)** Flow cytometric gating on aortic endothelial cells ($CD45^{-}CD31^{+}CD107^{+}$) and quantification of the mean fluorescence intensity (MFI) of Alexa647 in these cells 2 h after injection of Alexa647-tagged siRNAs (n=6 BL/6 mice per group, mean±SEM, **p<0.01).

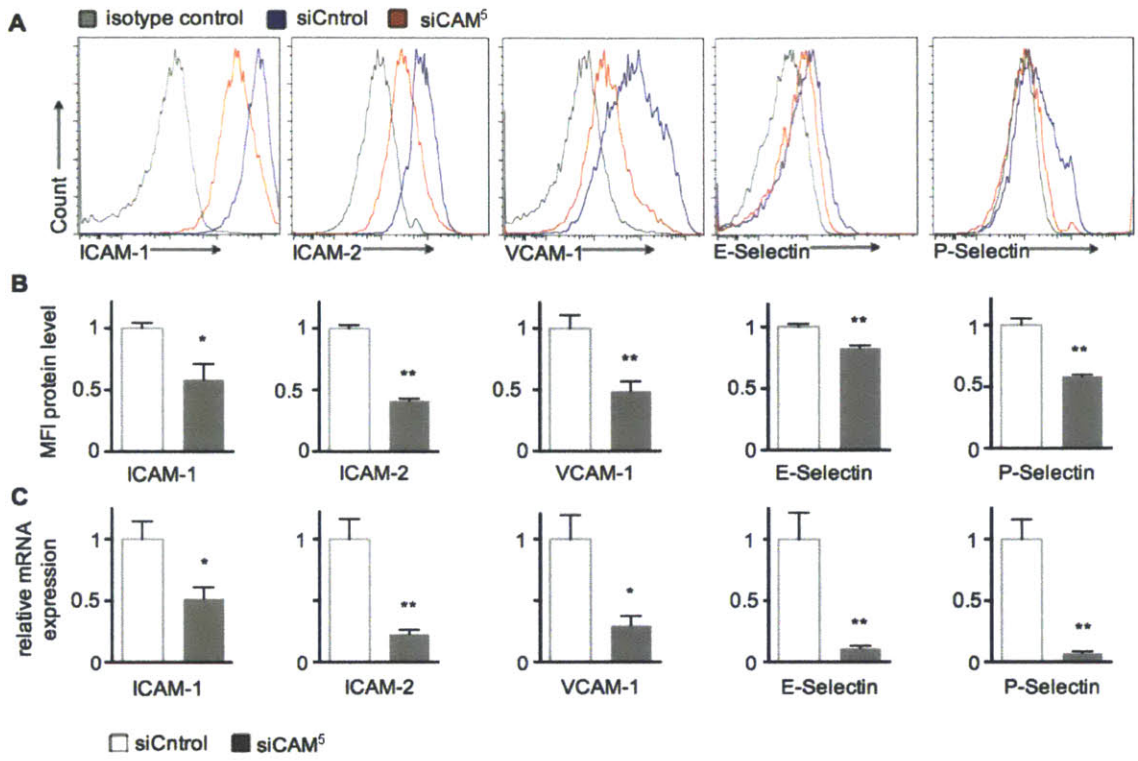

Figure 3.2. siRNA mediated knockdown in aortic endothelial cells. **(A)** Representative histograms showing levels of the target proteins in aortic endothelial cells (grey curve: isotype control, blue: siCntrol and red: siCAM5 group). **(B)** Protein levels on aortic endothelial cells, quantified as mean fluorescence intensity. **(C)** mRNA levels of sorted aortic endothelial cells isolated from siCntrol- or siCAM5-treated mice, (n=6-7 $ApoE^{-/-}$ mice/group fed a high cholesterol diet for 6 weeks, mean +/- SEM, *$p<0.05$, **$p<0.01$).

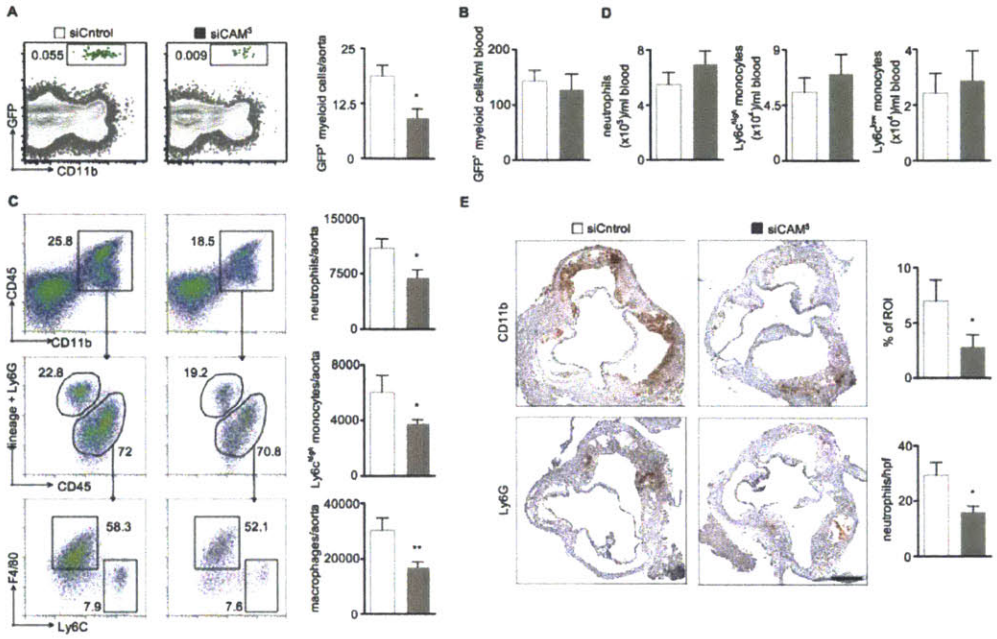

Figure 3.3. siRNA treatment impedes recruitment of myeloid cells to atherosclerotic plaques and reduces inflammation. (A,B) Flow cytometric gating and quantification of GFP^+ myeloid cells (A) in plaques (B) and in the blood after adoptive transfer of two million GFP^+ $Ly6C^+$ monocytes and two million GFP^+ neutrophils (n=6 $ApoE^{-/-}$ mice/group fed with a high cholesterol diet for 6 weeks, mean±SEM, *p<0.05). (C) Flow cytometric gating and quantification of neutrophils, $Ly6C^+$ monocytes and macrophages from atherosclerotic aortae (n=6-9 $ApoE^{-/-}$ mice/group fed a HCD for 6 weeks, mean±SEM, *p<0.05, **p<0.01). (D) Quantification of blood neutrophils and $Ly6C^{+/-}$ monocytes (n=6-9 $ApoE^{-/-}$ mice/group fed a HCD for 6 weeks, mean±SEM). (E) Immunohistochemical evaluation of myeloid cells and neutrophils in aortic roots after two weeks of treatment with siCntrol or siCAM5. Bar graphs show percentage of positive staining per region of interest (ROI) or number of cells per high power field (hpf), (n=5-6 $ApoE^{-/-}$ mice/group fed a HCD for 6 weeks, mean±SEM, *p<0.05). Scale bar, 250 μm.

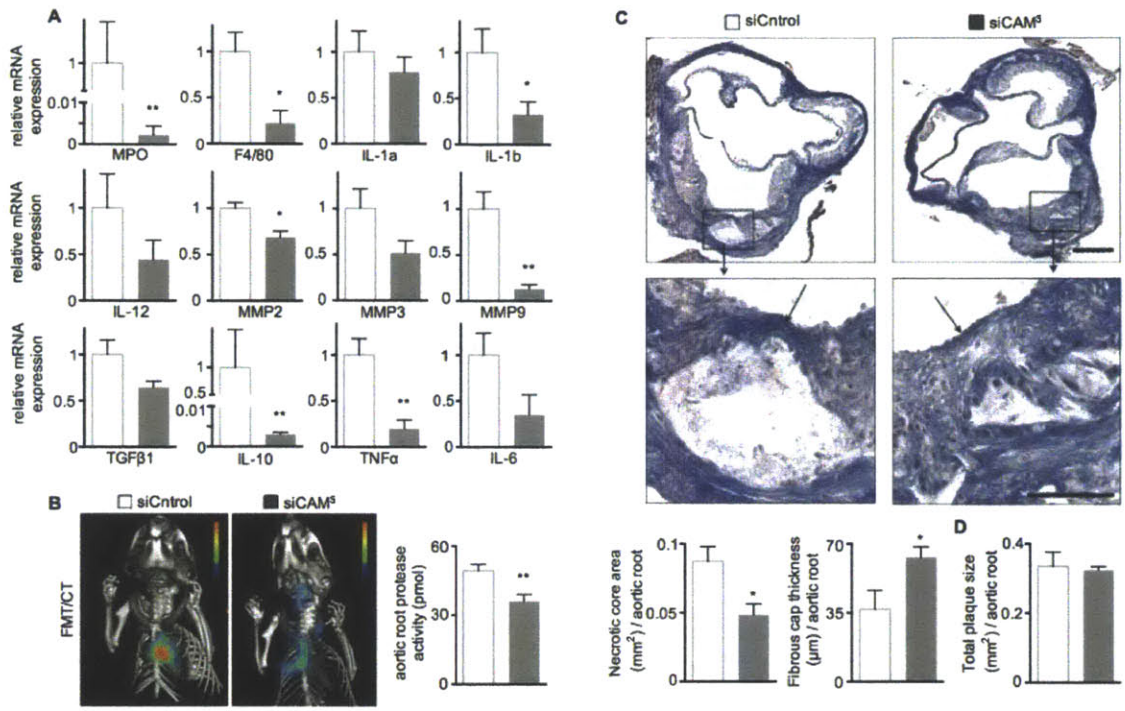

Figure 3.4. siRNA treatment leads to less inflammation in atherosclerotic aortae. (A) Ratios of target gene/GapDH mRNA for pro-/anti-inflammatory genes in aortic arches following treatment with siCntrol or siCAM5 (n=5-6 ApoE$^{-/-}$ mice/group fed a HCD for 6 weeks, mean±SEM, *p<0.05, **p<0.01). (B) Aortic root protease activity after treatment with either siCntrol or siCAM5, measured by FMT/CT (n=5-6 ApoE$^{-/-}$ mice/group fed a HCD for 6 weeks, mean±SEM, **p<0.01). (C,D) Masson staining of aortic roots after treatment siCntrol or siCAM5. Bar graphs show (C) fibrous cap thickness and necrotic core area and (D) total plaque size per section (n=5-6 ApoE$^{-/-}$ mice/group fed a HCD for 6 weeks, mean±SEM, *p<0.05). Scale bars, 250 µm or 100 µm, respectively. Arrows point at exemplary fibrous caps covering a necrotic core.

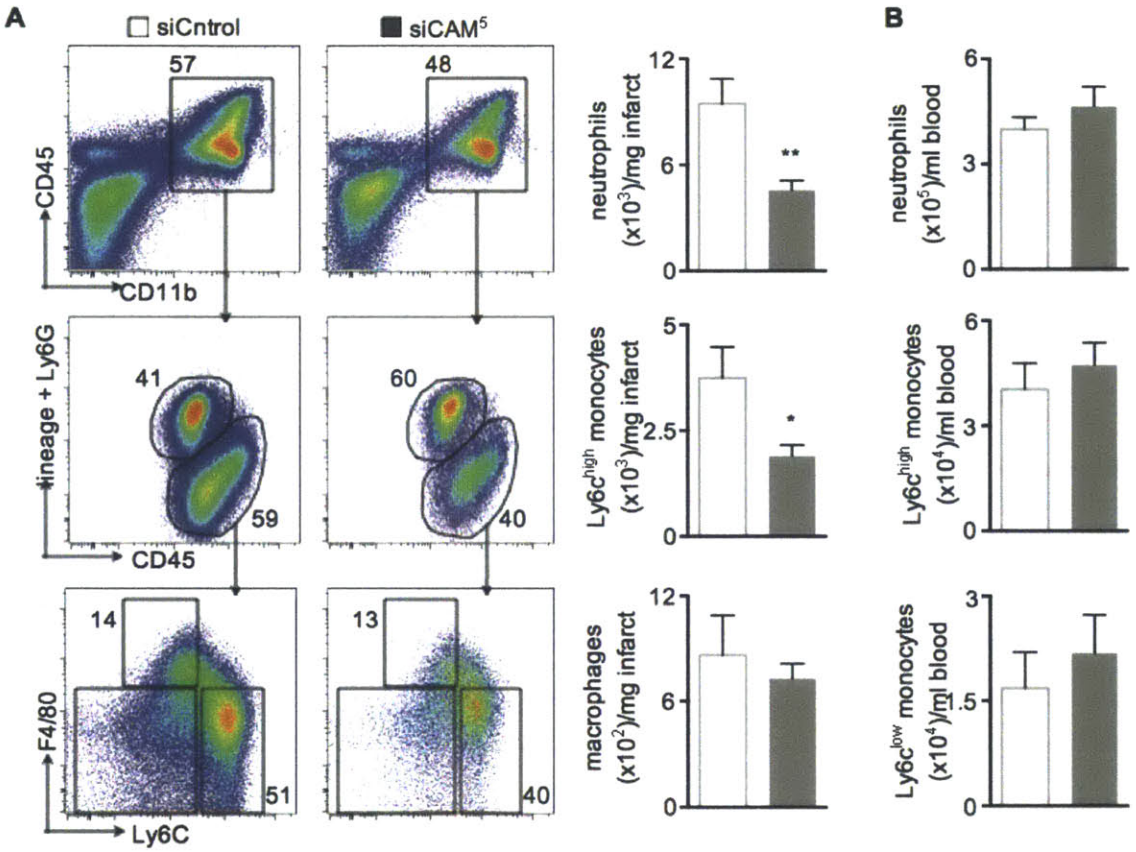

Figure 3.5. siRNA treatment impedes recruitment of myeloid cells to the heart three days after acute MI. (A) Flow cytometric gating and quantification of neutrophils, Ly6C$^{+/-}$ monocytes, and macrophages from three day old infarcts (n=6 BL/6 mice/group treated with either siCntrol or siCAM5 immediately following the induction of a MI, mean±SEM, *$p<0.05$, **$p<0.01$). (B) Quantification of blood neutrophils and Ly6C$^{+/-}$ monocytes three days after inducing a MI (n=6 BL/6 mice/group treated with either 3 mg/kg siCntrol or 3 mg/kg siCAM5 immediately following the induction of a MI, mean±SEM).

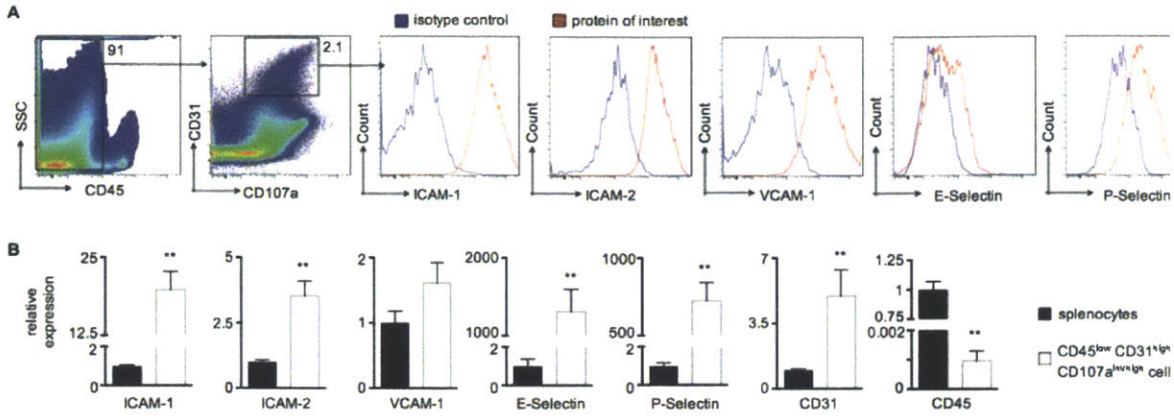

Figure 3S.1. Identifying aortic EC by flow cytometry. FACS-sorted CD45$^-$CD31+CD107+ cells from digested aortae. To provide evidence that these are cells indeed represent endothelial cells, we (A) compared mean fluorescence intensities (MFI) for additional endothelial cell specific proteins (ICAM-1, ICAM-2, VCAM-1, E-Selectin, and P-Selectin) to isotype controls in these cells and (B) compared respective mRNA levels in FACS sorted aortic endothelial cells to the ones in splenocytes by qRT-PCR (n=7 ApoE$^{-/-}$ mice/group fed a HCD for 6 weeks, mean±SEM, **p<0.01).

Chapter 3.8 References

1. Swirski, F.K. & Nahrendorf, M. Leukocyte behavior in atherosclerosis, myocardial infarction, and heart failure. *Science* **339**, 161-166 (2013).
2. Silvestre-Roig, C., *et al.* Atherosclerotic plaque destabilization: mechanisms, models, and therapeutic strategies. *Circ Res* **114**, 214-226 (2014).
3. Waxman, S., Ishibashi, F. & Muller, J.E. Detection and treatment of vulnerable plaques and vulnerable patients: novel approaches to prevention of coronary events. *Circulation* **114**, 2390-2411 (2006).
4. Robbins, C.S., *et al.* Local proliferation dominates lesional macrophage accumulation in atherosclerosis. *Nat Med* **19**, 1166-1172 (2013).
5. Pober, J.S. & Sessa, W.C. Evolving functions of endothelial cells in inflammation. *Nat Rev Immunol* **7**, 803-815 (2007).
6. Dong, Z.M., *et al.* The combined role of P- and E-selectins in atherosclerosis. *J Clin Invest* **102**, 145-152 (1998).
7. Kanasty, R., Dorkin, J.R., Vegas, A. & Anderson, D. Delivery materials for siRNA therapeutics. *Nat Mater* **12**, 967-977 (2013).
8. Semple, S., *et al.* Rational design of cationic lipids for siRNA delivery. *Nature biotechnology* **28**, 172-176 (2010).
9. Coelho, T., *et al.* Safety and efficacy of RNAi therapy for transthyretin amyloidosis. *N Engl J Med* **369**, 819-829 (2013).
10. Love, K.T., *et al.* Lipid-like materials for low-dose, in vivo gene silencing. in *Proc Natl Acad Sci USA*, Vol. 107 1864-1869 (2010).
11. Kaufmann, J., Ahrens, K. & Santel, A. RNA interference for therapy in the vascular endothelium. *Microvascular Research* **80**, 286-293 (2010).
12. Dahlman, J.E., *et al.* In vivo endothelial siRNA delivery using polymeric nanoparticles with low molecular weight. *Nat Nanotechnol* **11**, 84 (2014).
13. Collins, R.G., *et al.* P-Selectin or intercellular adhesion molecule (ICAM)-1 deficiency substantially protects against atherosclerosis in apolipoprotein E-deficient mice. *J Exp Med* **191**, 189-194 (2000).
14. Mestas, J. & Ley, K. Monocyte-endothelial cell interactions in the development of atherosclerosis. *Trends Cardiovasc Med* **18**, 228-232 (2008).
15. Whitehead, K., Dahlman, J.E., Langer, R.S. & Anderson, D.G. Silencing or Stimulation? siRNA Delivery and the Immune System. *Annual Review of Chemical and Biomolecular Engineering* (2010).
16. Chen, D., *et al.* Rapid discovery of potent siRNA-containing lipid nanoparticles enabled by controlled microfluidic formulation. *J Am Chem Soc* **134**, 6948-6951 (2012).
17. Kumar, V., Abbas, A., Fausto, N. & Aster, J. Robbins and Cotran Pathologic Basis of Disease, Eighth Edition. (2009).
18. Lloyd-Jones, D.M. Cardiovascular risk prediction: basic concepts, current status, and future directions. *Circulation* **121**, 1768-1777 (2010).

19. Tacke, F., *et al.* Monocyte subsets differentially employ CCR2, CCR5, and CX3CR1 to accumulate within atherosclerotic plaques. *J Clin Invest* **117**, 185-194 (2007).
20. Woollard, K.J. & Geissmann, F. Monocytes in atherosclerosis: subsets and functions. *Nat Rev Cardiol* **7**, 77-86 (2010).
21. Drechsler, M., Megens, R.T., van Zandvoort, M., Weber, C. & Soehnlein, O. Hyperlipidemia-triggered neutrophilia promotes early atherosclerosis. *Circulation* **122**, 1837-1845 (2010).
22. Leuschner, F., *et al.* Therapeutic siRNA silencing in inflammatory monocytes in mice. *Nat Biotechnol* **29**, 1005-1010 (2011).
23. Fitzgerald, K., *et al.* Effect of an RNA interference drug on the synthesis of proprotein convertase subtilisin/kexin type 9 (PCSK9) and the concentration of serum LDL cholesterol in healthy volunteers: a randomised, single-blind, placebo-controlled, phase 1 trial. *Lancet* **383**, 60-68 (2014).

Chapter 4. 7C1-mediated delivery of a small RNA combination therapy slows lung cancer

Chapter 4.1 miRNAs therapies have clinical potential

microRNAs (miRNAs) mediate multiple biological processes, and alterations in miRNA function have been associated with different diseases, including cancer[1-4]. In model systems, the over-expression of tumor suppressor miRNAs or inhibition of oncogenic miRNAs has shown therapeutic potential [5]. Moreover, short interfering RNAs (siRNAs) hold great promise as therapeutic agents for cancer through RNA interference (RNAi) of oncogene expression[6-9]. While numerous studies have evaluated small RNA therapy mediated by delivery vehicles in xenograft models of cancer [5,6,9,10], the relevance of these results is limited by the fact that tumors are implanted in ectopic sites. Similarly, while viral-mediated small RNA delivery has led to promising anti-tumor responses in genetically-engineered mouse models of cancer[11,12], the utility of viral delivery systems may be limited by pre-existing immunity, toxicity, concerns about mutational genomic insertions, and insufficient delivery efficiency. To overcome these barriers, many non-viral small RNA delivery vehicles have been designed. While most of these have been tested in xenograft models[13,14], some have been evaluated in autochthonous mouse models as well[15,16].

Lung cancer is an attractive cancer type for local or systemic small RNA delivery treatment[7]. It is the leading cause of cancer death worldwide, with non-small cell lung cancers (NSCLC) accounting for 85% of all lung cancer cases[17]. The most common NSCLC subtype, adenocarcinoma, is associated with frequent mutations in *KRAS* (~20-30%) and *TP53* (~50%)[17]. Targeted mutations of these two genes in the adult murine lung epithelium results in lung adenocarcinomas that mimic the histopathological progression of the human disease[18]. The so-called "KP" model of lung adenocarcinoma involves activation of an oncogenic *Kras* allele ($Kras^{G12D}$) and inactivation of two conditional (floxed) alleles of *p53* following intranasal or intratracheal administration of recombinant virus particles expressing Cre recombinase[18]. Although lung cancers in the KP model respond to certain chemotherapeutics, durable responses have not been observed[19-24]. Of note, despite recent progress in the treatment of human lung cancer carrying activating mutations in *EGFR* and translocations involving *ALK* with targeted anti-cancer agents[17,25], advanced *KRAS*-mutant lung cancers are treated with conventional therapy, most often with limited success.

Because lung adenocarcinoma is so often associated with mutations in *KRAS* and *TP53*, targeted inhibition of KRAS expression and stimulation of TP53 effector functions are attractive therapeutic strategies for this disease. However, direct and specific KRAS inhibition by small molecule compounds has been elusive[25,26]. As a result, KRAS is a promising candidate for RNAi-based therapy, which can inhibit traditionally undruggable targets by directly reducing mRNA expression. Importantly, mouse models utilizing conditional expression of oncogenic *Ras* alleles have demonstrated that withdrawal of RAS signaling results in rapid tumor regression in established tumors[27-29]. These data provide proof of principle that oncogenic RAS can play a

critical role in tumor maintenance and suggest that inhibiting oncogenic *RAS* with siRNA might be an effective therapy.

The *p53* tumor suppressor gene (also known as *TP53*, *Trp53*) is among the most frequently mutated genes in human cancer[30,31]; multiple tumor types exhibit high frequency mutation or loss of this key tumor suppressor. Restoring p53 function induces anti-tumor effects in multiple tumor types (reviewed in [31]), including lung cancer [30,32]. Despite its high frequency involvement in human cancer, loss-of-function mutations in p53 are a challenging therapeutic target, with the possible exception of drugs that convert mutant p53 proteins to a functional state[31]. The miR-34 family of miRNAs are direct transcriptional targets of p53 and can mediate certain effects of the p53 response[33,34]. The three members of this family, miR-34a, b, and c, have been shown to inhibit genes involved in controlling cell cycle, progression, metabolism and apoptosis[35-37]. miR-34 overexpression has been shown to limit cancer cell growth and tumor progression in subcutaneous models and an autochthonous model of NSCLC, in which oncogenic *Kras* is activated without the concurrent deletion of p53[12,16,34,38]. These data suggest that systematic delivery of miR-34 might be an effective strategy to stimulate the tumor suppressor pathway downstream of p53.

While the therapeutic potential of RNA therapies is substantial, the biggest challenge in small RNA therapy remains the efficient and specific delivery to the desired target tissues [7]. *in vivo* RNA delivery is limited by several factors, including reticuloendothelial system clearance and nuclease degradation. Nanomaterials formed with gold, silver, protein, cholesterol, DNA origami, lipids, and cationic polymers have all been investigated as potential vehicles for small RNA delivery *in vivo*[39]. Yet despite the diverse chemical and physical structures examined to date, highly efficient non-viral delivery has been largely limited to hepatocytes. For example, lipids and lipid-like materials termed lipidoids have reduced hepatocyte target gene expression at doses as low as 0.01 mg/kg[40,41].

Small RNA cancer therapies are beginning to be tested in human clinical trials. Lipid nanoparticles (LNP) carrying VEGF and KSP siRNA have been tested in phase I clinical trials in cancer patients with liver metastasis[42] and cyclodextrin polymer-based nanoparticles carrying RRM2 siRNA have been tested in patients with solid tumors[43]. These studies have shown promising pharmacodynamics and tolerability, indicating that nanoparticle-mediated siRNA delivery may be effective in patients. However, to extend small RNA therapy to other major cancer types, including lung cancer, delivery vehicles that target non-liver tissues are urgently needed.

Recently, we reported a new class of nanoparticle-forming compounds that were generated by combinatorial chemical synthesis[44]. The compounds were synthesized by conjugating epoxide-terminated lipids to low molecular weight polyamines with an epoxide ring-opening reaction. The resulting structures were tested for their ability to complex siRNA and reduce gene expression *in vitro*; the most effective candidates were then tested *in vivo*. We identified one compound from a library of over 500 candidate delivery materials that delivered siRNA to lung endothelium *in vivo*, silencing target genes in pulmonary vasculature at doses

several hundred-fold lower than previously reported vehicles. This compound, named 7C1, preferentially targeted lung vasculature without significantly transfecting immune cells or hepatocytes at low doses[44]. These observations suggested that 7C1 might also deliver therapeutic RNA to lung cancer cells, at higher doses. Here we describe the treatment of KP lung tumors by systemic delivery of a miR-34 mimic and siRNAs targeting Kras using 7C1 nanoparticles. Delivery of either one of these small RNAs modulated biological function in tumors and elicited anti-tumor effects. The concurrent delivery of both caused measurable regression of established tumors and prolonged survival of chemotherapy-treated mice. These results demonstrate that effective delivery of therapeutic small RNAs is possible in an autochthonous solid tumor model in the mouse and provide further impetus to develop small RNA-based treatment strategies for human lung cancer patients.

Chapter 4.2 Delivery of siRNA to lung adenocarcinoma cells *in vitro*

7C1 was discovered using a combinatorial chemical engineering approach followed by cell-based and whole-animal screening[44]. 7C1 was synthesized by reacting 600 molecular weight polyethyleneimine with a 15-carbon lipid tail in ethanol for 48-72 hours. This chemical reaction generated a compound that, when mixed with $C_{14}PEG_{2000}$ at a 7C1: PEG molar ratio equal to 80:20, formed nanoparticles with a multilamellar structure, a diameter of 50 nm, and a zeta potential equal to zero at physiological pH (Fig. 1A).

Because 7C1 allows for delivery of siRNA to pulmonary endothelial cells *in vivo,* we examined whether it could deliver small RNAs to lung tumor cell lines and lung tumors. We first tested 7C1-mediated siRNA delivery to KP-derived lung adenocarcinoma lines (KP cells) *in vitro* using fluorescence and confocal microscopy. 7C1 nanoparticles complexed with Cy5.5 fluorophore-labeled siRNA substantially increased the intracellular Cy5.5 signal in KP cells (Fig. 1B). Using KP cells stably expressing firefly luciferase, we observed that 7C1 nanoparticles carrying siRNA targeting luciferase (siLuc) also reduced luminescence in a dose-dependent fashion, while nanoparticles carrying siGFP had no effect (Fig. 1C-D). Conversely, in KP cells stably expressing GFP, 7C1 nanoparticles carrying Cy5.5-siGFP simultaneously reduced GFP expression and increased Cy5.5 fluorescence (Fig. S1). Taken together, these data demonstrate 7C1 nanoparticles can deliver siRNA in cultured murine lung cancer cells.

Chapter 4.3 Delivery of siRNA to lung adenocarcinomas *in vivo*

Previous analysis has demonstrated that 7C1 is well-tolerated in mice and does not induce liver enzymes (45). In order to assess the ability of 7C1 nanoparticles to deliver small RNAs in lung adenocarcinomas *in vivo*, KP mice were crossed with two strains carrying Lox-STOP-Lox reporter alleles, $R26^{LSL\text{-}tdTomato}$ and $R26^{LSL\text{-}Luciferase}$ [45,46], to generate $Kras^{LSL\text{-}G12D/wt}$;$p53^{flox/flox}$;$R26^{LSL\text{-}Luciferase/LSL\text{-}tdTomato}$ mice. In this model, intranasal inhalation of adeno-Cre causes deletion of p53 and activation of $Kras^{G12D}$ as well as the reporters Luciferase and tdTomato in developing lung tumors (Fig. S2A). Ten weeks after tumor initiation, mice were intravenously injected with a single 1.5 mg/kg dose of 7C1 nanoparticles formulated with Cy5.5-siLuc. Animals were sacrificed at different time points and lung tissue was isolated for confocal

image analysis. To measure the luciferase signal at the single cell level, we performed immunofluoresent staining on lung tumor sections using a luciferase antibody. Tumor luciferase staining diminished 24 hours after dosing while tdTomato fluorescence remained constant over time, indicating that siLuc selectively silenced gene expression in tumors *in vivo* following intravenous injection (Fig. 1E, Fig. S2B). 7C1 carrying siLuc also transiently reduced the luciferase signal in the lung by whole-body luciferase imaging (Fig. S2C). Biodistribution studies confirmed siRNA delivery to KP tumors *in vivo;* lung tumors isolated from mice injected with Cy5.5 labeled siRNA showed Cy5.5 fluorescence (Fig. S3, N=3 mice/group). Cy5.5 signal also distributed to kidney and other organs (Fig. S3).

Chapter 4.4 Systemic miR-34a delivery delays lung tumor progression

We next examined whether miRNA delivery might cause therapeutic responses by restoring an effector arm of the p53 pathway to these p53-deficient tumors. As predicted by the known regulation of the miR-34 family by p53, RT-Q-PCR analysis showed that mature miR-34a and miR-34c were relatively under-expressed in isolated KP lung tumors compared to normal lung samples (Fig. S4). A 22-nucleotide double-stranded RNA, 2-O-methyl modified to reduce immunostimulation and nuclease degradation, with the mature miR-34a antisense strand sequence and a complementary sense strand was used as the miR-34a mimic (Fig. S5A)[47,48]. Groups of three KP mice with established lung tumors were injected intravenously with a single 1.5 mg/kg dose of 7C1 nanoparticles complexed with siLuc, which served as a control siRNA, or the miR-34a mimic (Fig. 2A). Lung tumors were isolated 48 and 68 hours following injection, and miR-34a and miR-34c mature microRNAs were measured by RT-QPCR probes recognizing both endogenous miR-34 as well as the microRNA mimic. miR-34a increased in tumors isolated from miR-34a-treated animals compared to tumors isolated from mice treated with siLuc, while miR-34c levels remained constant (Fig. 2B). Importantly, miR-34a treatment reduced the mRNA expression of *Ccnd1, Sirt1, Cdk6* and *Ccne2*[33], demonstrating that delivery of miR-34a achieved functional inhibition of canonical miR-34a targets *in vivo* (Fig. 2C). To optimize nanoparticle administration, groups of four KP mice were injected with the miR-34a nanoparticle formulation intravenously, intranasally or intraperitoneally (Fig. S5B). Intravenous injection increased miR-34a levels in lung tumors the most, resulting in a 27-fold increase relative to mice treated with siLuc (Fig. S5C).

We next investigated the effects of miR-34a delivery on lung tumor development. Ten weeks post infection with Adeno-Cre, KP mice were scanned by micro-computed tomography (microCT) to measure individual tumor volumes. Tumor-bearing KP mice were intravenously injected with PBS, nanoparticles carrying siLuc, or nanoparticles carrying miR-34a at a dose of 1.5mg/kg twice each week for 4 weeks (N=6 mice/group). miR-34a treatment significantly delayed tumor progression compared to siLuc and PBS controls, which grew rapidly over this time period (Fig. 2D). To explore the mechanism of miR-34a in tumor suppression, lung tumors were harvested 72 hours after a single intravenous injection of 1.5 mg/kg miR-34a. Consistent with the function of miR-34a in inducing cell cycle arrest[33,34], tumors treated with miR-34a

showed reduced levels of proliferation as measured by Ki67 or phospho-histone H3 staining (pHH3) compared to PBS- or siLuc-treated mice (Fig. 2E-F). Cleaved caspase 3 (CC3) staining, a marker for apoptosis, did not significantly increase between the three groups (Fig. 2F). Despite the fact that miR-34a was increased in normal lung tissue in these animals as well (Fig. S5B), animals treated with miR-34a showed negligible weight loss over the treatment period (Fig. S6A). These results provide compelling evidence that delivery of exogenous miR-34a can suppress lung tumor development in an aggressively growing autochthonous solid tumor model.

Chapter 4.5 Systemic siKras delivery elicited anti-lung tumor effects

In addition to lacking p53 function, the tumors in KP mice carry an activated *Kras* oncogene, and oncogenic *Kras* is an attractive target for small RNA therapy. We screened nine siRNAs (2-O-methyl modified) for efficient knockdown of mouse *Kras* in KP cells (Fig. S7A). One siRNA, si923 (hereafter termed siKras), reduced total *Kras* mRNA expression by 87% 48 hours after transfection at a 10nM concentration compared to siLuc siRNA (Fig. S7A). This siKras sequence targets the 3' untranslated region (3' UTR) of *Kras* mRNA and, therefore, inhibits both the oncogenic and wild-type *Kras*. As shown in Figure 3A, incubation of KP cells with 7C1 nanoparticles carrying siKras resulted in a dose-dependent decrease in cell number and reduced phospho-Erk (p42/p44 MAPK) levels, a biomarker of Kras activity[26]. To examine whether these effects were due to on-target inhibition of *Kras*, a $Kras^{G12D}$ cDNA was cloned lacking the 3' UTR ($Kras^{G12D}$*), thus rendering it insensitive to silencing. KP cells expressing the $Kras^{G12D}$* cDNA maintained phospho-Erk levels and showed no growth defects following exposure to siKras (Fig. 3B, Fig. S7B).

To test the effects of siKras *in vivo*, tumor-bearing KP mice were treated with different doses of 7C1 nanoparticle formulated with siKras or siLuc (N=4 mice/group). Following two injections of 2 mg/kg, siKras treatment reduced *Kras* mRNA in isolated tumors by 63% compared to tumors treated with siLuc (Fig. 3C). To monitor lung tumor progression following siKras treatment, we initiated lung tumors in a cohort of KP mice. Ten weeks later, groups of six mice were injected intravenously with nanoparticles carrying 1.5 mg/kg siKras or siLuc every other day for 4 doses. Individual lung tumor volumes were measured by microCT imaging over a 2.5 week period. As shown in Figure 3D, siKras-treated tumor growth was significantly inhibited compared to tumors treated with siLuc. Moreover, a modest regression was observed in some tumors (Fig. 3D, Fig. S7C). In high-grade lung tumors from siKras-treated mice, levels of phospho-Erk were markedly lower compared to control tumors (Fig. 3E-F, Fig. S7D), suggesting that Kras knockdown inhibits downstream MAP kinase signaling. Because low grade KP tumors do not stain positively for pErk, we were not able to measure the pErk levels in low grade tumors by IHC. To further investigate mechanisms of tumor regression, we stained lung tumor sections with an antibody specific for cleaved caspase 3 (CC3), a marker of apoptosis. siKras-treated tumors had increased numbers of apoptotic cells compared to tumors treated with siLuc (Fig. 3E, Fig. 3G). These data suggest that systemic siRNA delivery reduced oncogenic Kras mRNA *in vivo* and that such treatment led to anti-tumor responses. To confirm that these effects were due

to Kras inhibition rather than off-target effects, we tested a second siRNA against *Kras* (siKras.1212). Once again, we observed downregulation of Kras expression *in vitro* and anti-tumor effects *in vivo* (Fig. 3D, Fig. S7A, Fig. S8).

Chapter 4.6 Concurrent delivery of miR-34a and siKras improves therapeutic responses

RNAi-based therapeutics can potentially inhibit multiple target genes and pathways via concurrent delivery of distinct small RNAs. We hypothesized that targeting activated *Kras* by siRNA and stimulating p53-related responses with miR-34a would increase anti-tumor activity in the KP mouse model. Thus, we formulated 7C1 nanoparticles with the miR-34a mimic and siKras in an equal molar ratio. Incubation of KP cells *in vitro* with the miR-34a/siKras combination nanoparticles led to an additive inhibition of cell proliferation compared to miR-34a or siKras alone plus siLuc (Fig. 4A). To determine the therapeutic effects of combined miR-34a and siKras delivery *in vivo*, KP mice in which tumors were initiated ten weeks earlier were randomized into four nanoparticle treatment groups (N=8 mice/group): (1) siLuc, (2) miR-34a/siLuc, (3) siKras/siLuc, and (4) miR-34a/siKras. Mice were intravenously injected with a total small RNA dose of 2.0 mg/kg every other day four times. In isolated lung tumors, small RNA QPCR revealed increased miR-34a levels and detectable siKras antisense-strand levels in miR-34a/siKras combination treated tumors (Fig. S9), demonstrating that nanoparticles successfully delivered both small RNAs into lung tumors. Moreover, microCT imaging revealed that miR-34a/siKras combination therapy induced measurable lung tumor regression, shrinking tumors to an average of 63% of the original volume in two weeks (Fig. 4B). Combination treated tumors also showed increased numbers of cleaved caspase 3-positive cells compared to miR-34a or siKras alone (Fig. 4C). These data suggest that effective delivery of two therapeutic small RNAs is possible in autochthonous lung tumors.

All animals tolerated small RNA therapy well, with only mild weight loss observed after siKras or miR-34a/siKras combination therapies (Fig. S6). Weight loss was not observed after injection of nanoparticles formulated with siLuc or miR-34a mimic (Fig. S6), suggesting that this effect was likely due to modulation of Kras levels in normal tissue. To examine whether tumor regression was due to a non-specific immune response, we collected peripheral blood from animals treated with siLuc or miR-34a/siKras nanoparticles 4 and 24 hours after the first injection, and 4 hours after the fourth injection to monitor both acute and long-term immune responses (Fig. S10A)[47,48]. The dosing regimen of nanoparticles was identical with that used for tumor treatment studies (Fig. 4B). As measured by enzyme-linked immunosorbent assays (ELISA), levels of interleukin 6 (IL6) and interferon alpha (INF-α), indicators of non-specific immune responses, were statistically indistinguishable in PBS, control siRNA or miR-34a/siKras treated animals at all time points (Fig. S10B,C). Histopathological analysis showed absence of general tissue toxicity after 7C1 miR-34a/siKras treatment (Fig. S10D). Collectively, these data suggest that tumor regression was not caused by immunostimulatory effect of small RNA or nanoparticles.

Cisplatin is a first-line lung cancer chemotherapy whose efficacy has been investigated in KP mice[24]. To analyze the long-term effects of nanoparticle therapy in combination with conventional chemotherapy and to examine its effect on long-term survival, we investigated whether nanoparticles carrying miR-34a mimic and siKras could prolong life in mice separately or in combination with cisplatin. We treated tumor-bearing KP mice with either cisplatin, nanoparticles carrying both miR-34a mimic and siKras, or the combination of the two. Using the treatment regimen shown in Figure 4D, KP mice treated with both cisplatin and the nanoparticle formulated with a combination of miR-34a/siKras (159.9±19.5 days, N=10 mice/group, $p<0.01$ compared to single treatment) survived significantly longer than mice treated with siLuc (93.7±16.1 days, N=8 mice/group), cisplatin alone (127.4±9.0 days, N=8 mice/group) or miR-34a/siKras alone (129.2±16.2 days, N=8 mice/group). These data indicate that nanoparticle-mediated miR-34a/siKras small RNA therapy can provide additional therapeutic effects in combination with conventional chemotherapeutic strategies.

Chapter 4.7 7C1-si*KRAS* siRNA has therapeutic effect in *KRAS* mutant human NSCLC

In order to assess whether 7C1 can deliver therapeutic siRNA to human NSCLC cells, we formulated 7C1 nanoparticles with siRNAs targeting human *KRAS*. As shown in Fig. S11A and S11B, 7C1 carrying siKRAS led to marked knockdown of *KRAS* mRNA in four human NSCLC cell lines harboring *KRAS* mutations and resulted in reduced cell number. 7C1.siKRAS also reduced KRAS protein in H2009 cells (Fig. S11C). To explore whether 7C1 formulated with siRNA targeting human *KRAS* mRNA had therapeutic efficacy *in vivo,* we injected *KRAS* mutant H2009 NSCLC cells subcutaneously into nude mice and treated mice when tumors reached $100mm^3$. Consistent with our data in the autochthonous mouse model (Fig. 3), 7C1 formulated with siKRAS delayed tumor growth of H2009 xenograft (N=6 tumors/group, Fig. S11D). These data indicate that 7C1 nanoparticle are capable of delivering therapeutic siRNA in human NSCLC cells and xenograft tumors.

Chapter 4.8 Discussion

Here we have demonstrated that systemic delivery of a polymer-based nanoparticle can deliver therapeutic small RNAs in an autochthonous mouse model of lung cancer, and that targeted combination RNA therapy can elicit a potent anti-tumor response. Since a significant fraction of human lung tumors, as well as other tumor types, carry mutations in *KRAS* and *p53*, these results may have direct translational implication for human cancer treatment. Moreover, because 7C1 nanoparticles complex the anionic RNA backbone independent of nucleotide sequence, 7C1 can deliver therapeutic RNAs against additional targets in tumor cells. This clearly demonstrates that combination small-RNA therapy is a modular and flexible approach for lung cancer treatment. Targeted multigene therapy may be used for personalized therapies, as combinations can be selected against mutations identified in individual patients. As nanoparticle formulations targeted to different organs become available, synthetic siRNA or miRNA can be formulated with

vehicles to target different organs of interest, potentially targeting both primary and metastatic sites.

We show here that delivery of a miR-34a mimic modulated miR-34 target genes in lung tumors and delayed tumor progression, suggesting that systematic delivery of miR-34 might be a strategy to partially restore p53 downstream functions in *TP53* mutant tumors[36]. Delivery of miR-34a reduced cell proliferation and delayed lung tumor growth, which is consistent with a recent study in a $Kras^{G12D};p53^{R172H}$ lung cancer model[12]. Because miR-34 family microRNAs also inhibit key signaling pathways including NOTCH, WNT and MET[37], miR-34 may play other tumor suppressive functions in addition to cell cycle regulation. To date, more than 30 genes targeted by miR-34a have been reported in the literature[38]. Because microRNAs generally regulate large networks of target genes, miR-34a or other tumor suppressor microRNAs could be used to potently inhibit tumor cell proliferation and survival. Importantly, the inhibition of multiple target genes and pathways might limit the ability of tumor cells to escape via secondary mutations. Future work will address whether treated tumors acquire resistance to small RNA therapies through mechanisms including reduced nanoparticle uptake, increased nanoparticle exocytosis, or global down-regulation of RNAi pathway function, and whether combination therapies designed to simultaneously inhibit the expression of resistance-promoting genes can improve therapeutic efficacy.

While small molecule inhibition of oncogenic Kras has not been successful to date[26], our results using Kras siRNA indicate that RNAi may effectively reduce Kras activity *in vivo* and induce anti-tumor effects[49]. Because the siKras sequences in this study target the 3'-untranslated region of Kras, both the G12D and the wild-type Kras mRNA are suppressed by siKras. Future work is needed to investigate how cells respond to the knockdown of wild-type Kras, and whether mutant-specific forms of siKras can be developed.

Taking advantage of the ability to package multiple small RNAs in a single nanoparticle formulation[50], we demonstrated superior anti-tumor response with the combination of miR-34a mimic and siKras in this model system. Molecular dissection of the interaction between the miR-34a and Kras network will reveal how the miR-34a and siKras combination improves therapeutic responses. When combined with cisplatin-based chemotherapy, miR-34a/siKras delivery further extended survival, indicating RNA therapy may be combined with chemotherapy, radiation, or surgery to improve the efficacy of existing cancer therapies. More specifically, the response to chemotherapy might be improved by specifically modulating genes in chemoresistance pathways. For example, murine lung adenocarcinoma resistant to cisplatin treatment often have elevated expression of the apoptosis modulator *Pidd*[24]. Similarly, *MET* tyrosine kinase amplification has been identified in some EGFR inhibitor resistant lung cancers[51].

Given that 7C1 nanoparticles are known to target endothelial cells, additional studies are required to delineate the impact of siKras and miR-34a delivery on normal tissue and the tumor microenvironment. However, it is clear that these small RNAs had direct effects on the tumor cells as well, as evidenced by knockdown of a tumor cell-specific luciferase reporter *in vivo* (Fig. 1E).

Taken together, our findings demonstrate the feasibility of small RNA-based combination therapy in a physiologically relevant mouse model of human lung cancer. The effective delivery of small RNAs to solid tumors in the model, combined with the modulation of divergent aspects of tumors biology as well as potent therapeutic responses, provide a compelling case for the use of small RNA therapies in human lung cancer patients.

Chapter 4.9 Materials and Methods

7C1 nanoparticle formulation

7C1 was synthesized and purified as previously described[44]. Particles were formulated with a microfluidic device[52] at a 7C1:RNA mass ratio equal to 5:1, dialyzed into 1X PBS, filtered with a sterile 0.2 um filter under a sterile biohood, and stored at 4°C. Particle diameter was measured with a Malvern Zetasizer (Malvern Incorporated, United Kingdom).

Mice and 7C1 nanoparticle treatment

All animal study protocols were approved by the MIT Animal Care and Use Committee. Cohorts of KP and KP;*R26*$^{LSL\text{-}Luciferase/LSL\text{-}tdTomato}$ mice were infected with $2.5x10^7$ plaque-forming units (PFU) of Adeno-Cre (University of Iowa) by intra-nasal inhalation as described previously. Mice were injected with 7C1 nanoparticles intravenously (i.v.) and Cisplatin intraperitoneally[24] as indicated. $5x10^6$ H2009 cells were injected subcutaneously on immunocompromised mice (6-8 weeks old). Tumor volume was measured by caliper and calculated as 0.52 x length x width^2. Upon tumor formation (~100mm^3), mice were treated with PBS or 7C1 siRNA as indicated.

Immunohistochemistry

Mice were sacrificed by carbon dioxide asphyxiation. Lungs were inflated with 4% formalin (NBF), fixed overnight, and transferred to 70% ethanol. Lung lobes were embedded in paraffin, sectioned at 4 μm and stained with hematoxylin and eosin (H&E) for tumor pathology. Lung tumor sections were de-waxed, rehydrated and stained using standard immunohistochemistry protocols[21]. The following antibodies were used: anti-cleaved caspase 3 (Cell Signaling #9661, 1:200), anti-Ki67 (vector lab VP-K452, 1:100), anti-Phospho Histone H3 (Cell Signaling, #9701, 1:200) and anti-pErk Thr202/Tyr204 (Cell Signaling #4370, 1:300). The number of positive cells per tumor area was quantified. Tumor numbers and mice numbers were indicated in the figure legends.

MicroCT and bioluminescence imaging

At indicated time points, mice were scanned for 5 min under isoflurane anesthesia using a small animal micro-computed tomography (eXplore CT120 whole mouse microCT, GE Healthcare). Images were acquired and processed using GE eXplore software. One or two independent lung tumors from each mouse was quantified. Bioluminescence imaging was performed as previously described [21]. Signals in mice or cells were quantified using Living Imaging software (Xenogen).

Immunoblotting, ELISA and immunofluorescence

Cell pellets were lysed in Laemmli buffer. Equal amounts of protein (16μg) were separated on 10% SDS-polyacrylamide gels and transferred to PVDF membranes. Blots were probed with antibodies (1:1000 dilution) against Kras (sc-30), pErk (Cell Signaling #4370) or Tubulin. Serum cytokine concentrations were measured in an ELISA-based assay, according to the manufacturer's instructions (eBiosciences). Immunofluorescence was performed as previously described [53]. Goat anti-luciferase (Promega G7451) and donkey anti-goat Alexa-488 (Invitrogen) antibodies were used. Slides were counterstained with 4, 6-diamidino-2-phenylindole (DAPI, Sigma) and mounted in Vectashield anti-fade mountant (Vector Laboratories, Burlingame, CA).

Cell number measurement

Cells were split into 96-well plates (1,000 cells per well). After 24 hours, cells were co-incubated with 7C1 nanoparticles for 24 hours. After 48-72hrs, cell number was measured by Cell Titer Glo kit (Promega) in triplicates. Control siRNA treated cell values were set to 1 (100%). For Fig 1D, 3A, 4A and 5B, the data are representative of two independent experiments.

Gene expression analysis and small RNA qPCR

RNA was purified using Trizol (Invitrogen) and reverse-transcribed using a High-Capacity cDNA Reverse Transcription Kit (Applied Biosystems). Real-time PCR (qPCR) reactions were performed using Taqman probes (Applied Biosystems). mRNA levels were normalized to *Actin* mRNA. For measuring microRNA expression, 10ng total RNA were reverse-transcribed using microRNA-specific RT primer and measured by real-time PCR using microRNA-specific probes (Applied Biosystems). siKras levels were quantified similarly using a custom small RNA Taqman assay (Applied Biosystems). Data were normalized to the U6 RNA.

Sequence of Kras siRNAs (Antisense 5'-3')

4504 AUGACCAACAUUCCCUAGG 2606 UAGUUUAAAUCCCACUAUG
1442 UACUAUUUCAUACUGGGUCUG 1212 UAAAGUCUAGGACACGCUG
923 CUUAGAAAAAAGAAGGUUUCC 745 AUUCACAUAACUGUACACC
593 AAUCCCGUAACUCCUUGCU 562 UGUUUCGUGUCUACUGUUC
218 UACGCCACCAGCUCCAACC
scramble siRNA for 923 GCCUAAUAAUAAGGAAUACGU
ON-TARGET plus Human KRAS SMART pool was purchased from Dharmacon.
All siRNAs have dTdT overhang in the 3' end.

Statistics. P values were determined by Prism 5 (GraphPad) and Student's t-tests.

Fig. 1

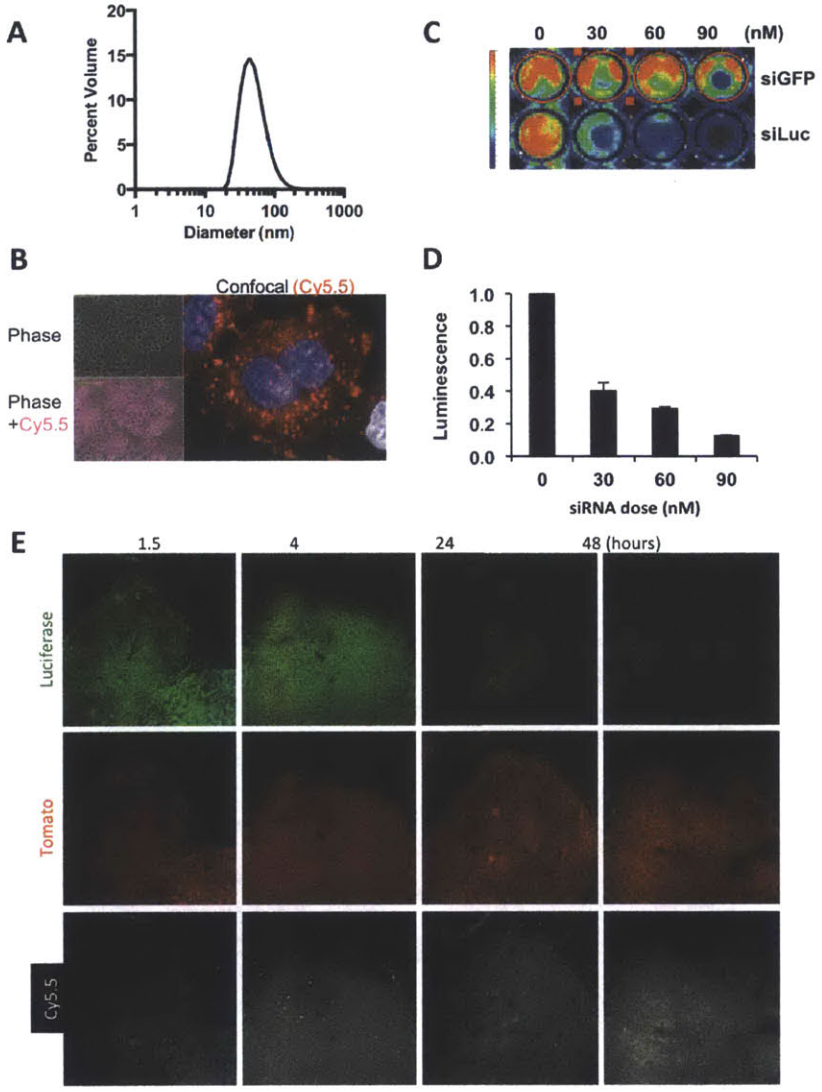

Figure 4.1. Efficient delivery of siRNAs to murine lung adenocarcinoma *in vitro* and *in vivo*. (A) 7C1-siRNA particle diameter, weighted by volume. (B) Cy5.5 fluorescence in KP (*Kras*$^{LSL\text{-}G12D/wt}$;*p53*$^{flox/flox}$) cells following incubation with 7C1 nanoparticles formulated with Cy5.5-labeled siRNA at an siRNA concentration of 30 nM. Cells were washed extensively and imaged using an epifluorescence or confocal microscope. Nuclei were stained with DAPI (blue). (C) Firefly luminescence in KP cells following incubation with 7C1 nanoparticles carrying siRNA targeting luciferase (siLuc) or siRNA targeting GFP (siGFP, acting as a control). Representative images are shown. Color bar denotes luciferase signal intensity. (D) Quantification of luciferase signal in (C). Error bars are s.d. (N=3 wells). (E) 7C1 nanoparticles carrying siLuc knock down luciferase expression in KP tumors *in vivo*. Lung tumors were initiated in *Kras*$^{LSL\text{-}G12D/wt}$;*p53*$^{flox/flox}$;*R26*$^{LSL\text{-}Luciferase/LSL\text{-}tdTomato}$ mice with Adeno-Cre. Ten weeks later, mice were dosed with 1.5mg/kg Cy5.5-siLuc formulated with 7C1, and lung tumors were harvested for luciferase immunostaining and natural fluorescence of Tomato and Cy5.5 (400x confocal images). Shown are representative images from ≥7 tumors analyzed per time point.

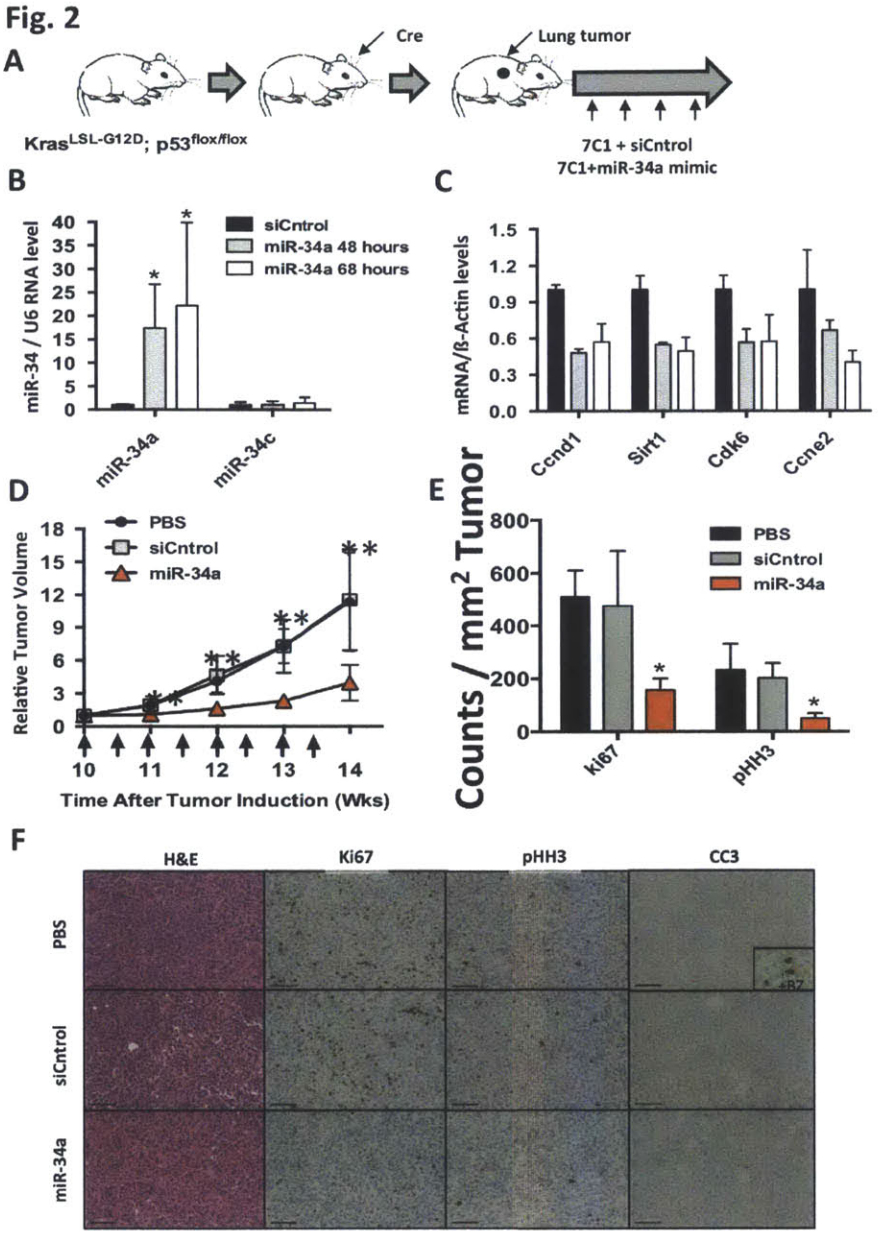

Figure 4.2. Systemic miR-34a delivery delays lung tumor progression. (A) Experimental design. (B) 7C1 nanoparticles delivers miR-34a mimics to KP lung tumors. Expression levels of mature miR-34a and miR-34c in lung tumors measured by qPCR 48 and 68 hours after a single injection of 1.5 mg/kg 7C1-siLuc or 7C1-miR-34a. Error bars are s.d. (N=4 tumors/group). (C) Expression levels of miR-34a target genes in lung tumors measured by qPCR. Error bars are s.d. (N=3 tumors/group). (D) Relative tumor volume measured by microCT shows a significant delay in lung tumor progression in KP mice treated with 7C1-miR-34a compared to 7C1-siLuc or PBS. Ten weeks after tumor initiation, mice were dosed with 1.5 mg/kg siRNA or miRNA mimic twice weekly. Error bars are s.d. (N=6 mice/group, 1 tumor/mouse). (E) Quantification of dividing cells marked by Ki67 and phospho-Histone H3 (pHH3) in treated tumors (N=10 tumors/group). (F) Representative histology and immunohistochemistry staining of lung tumors from mice treated with PBS, 7C1-siLuc or 7C1-miR-34a. Inset: Bortezomib-treated KP tumors serve as a positive control for cleaved caspase 3 (CC3) staining. Scale bar = 50um. *p<0.05, **p<0.01.

Fig. 3

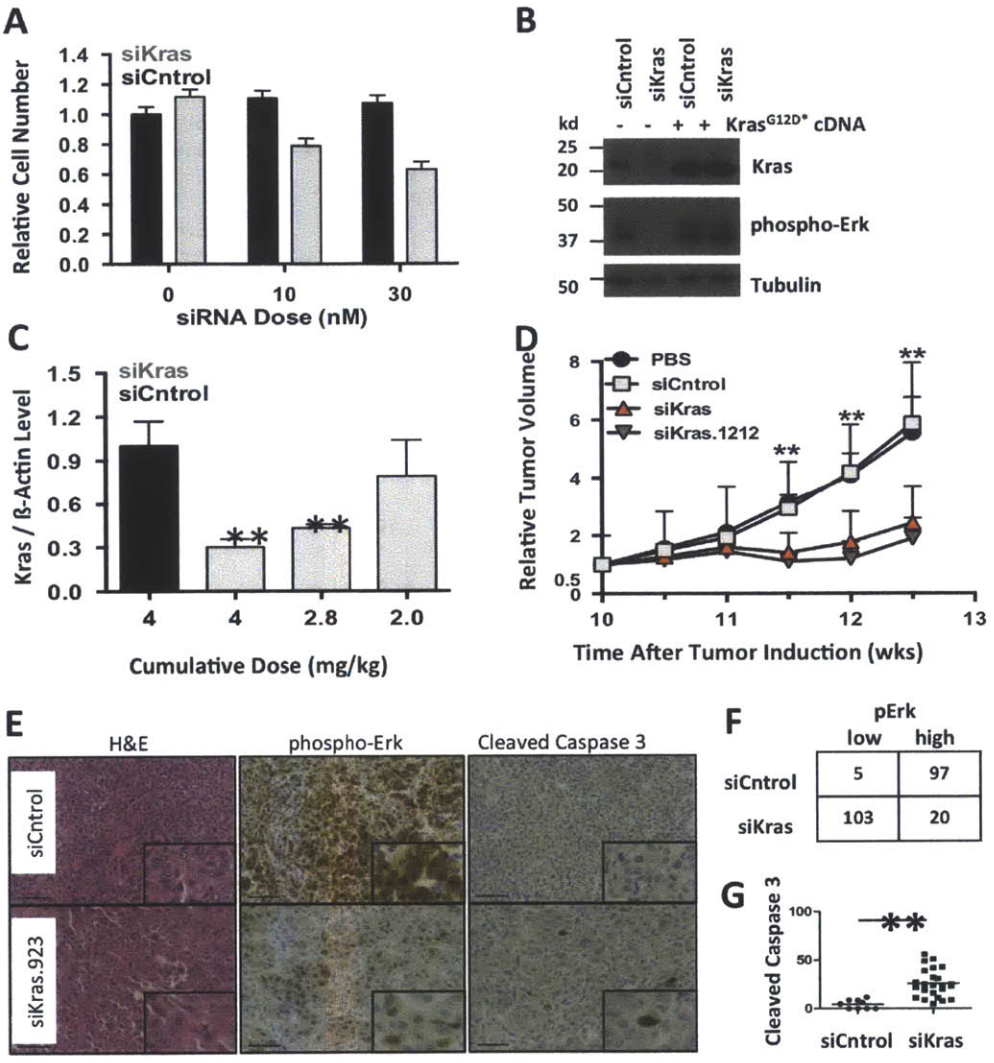

Figure 4.3. Systemic siKras delivery elicited anti-tumor effects. (A) KP cell number following incubation with 7C1-siLuc or 7C1-siKras. Error bars are s.d. (N=3 wells/group). (B) Immunoblots of protein lysates of KP cells expressing vector or a siRNA-refractory Kras cDNA ($Kras^{G12D*}$) following incubation with 7C1-siLuc or 7C1-siKras. (C) Kras mRNA expression in lung tumors isolated from KP mice following injection with 7C1-siLuc or 7C1-siKras. Mice received two i.v. injections of 7C1-siRNA and tumor RNA were harvested 72 hours after the second injection. Error bars are s.d. (N=4 mice/group, 1 tumor/mouse). (D) Relative lung tumor volume in KP mice, measured by microCT, following treatment with 7C1-siLuc or 7C1-siKras. Ten weeks after tumor initiations, mice were injected with 1.5mg/kg 7C1-siRNA every other day for four injections. Error bars are s.d. (N=6 mice/group, 2 tumors/mouse). Arrowheads indicate timepoints of nanoparticle administration. (E) Representative histology and immunohistochemistry staining of lung tumors from mice treated with 7C1-siLuc or 7C1-siKras. Scale bar=50μm. (F) Numbers of grade 3 lung tumors with low or high levels of phospho-Erk in (E). $p<10^{-6}$. (G) Quantification of cleaved caspase 3 (CC3) positive cells per mm^2 tumor area in (E). N=9 and 24 tumors analyzed. *, $p<0.05$. **, $p<0.01$.

Fig. 4

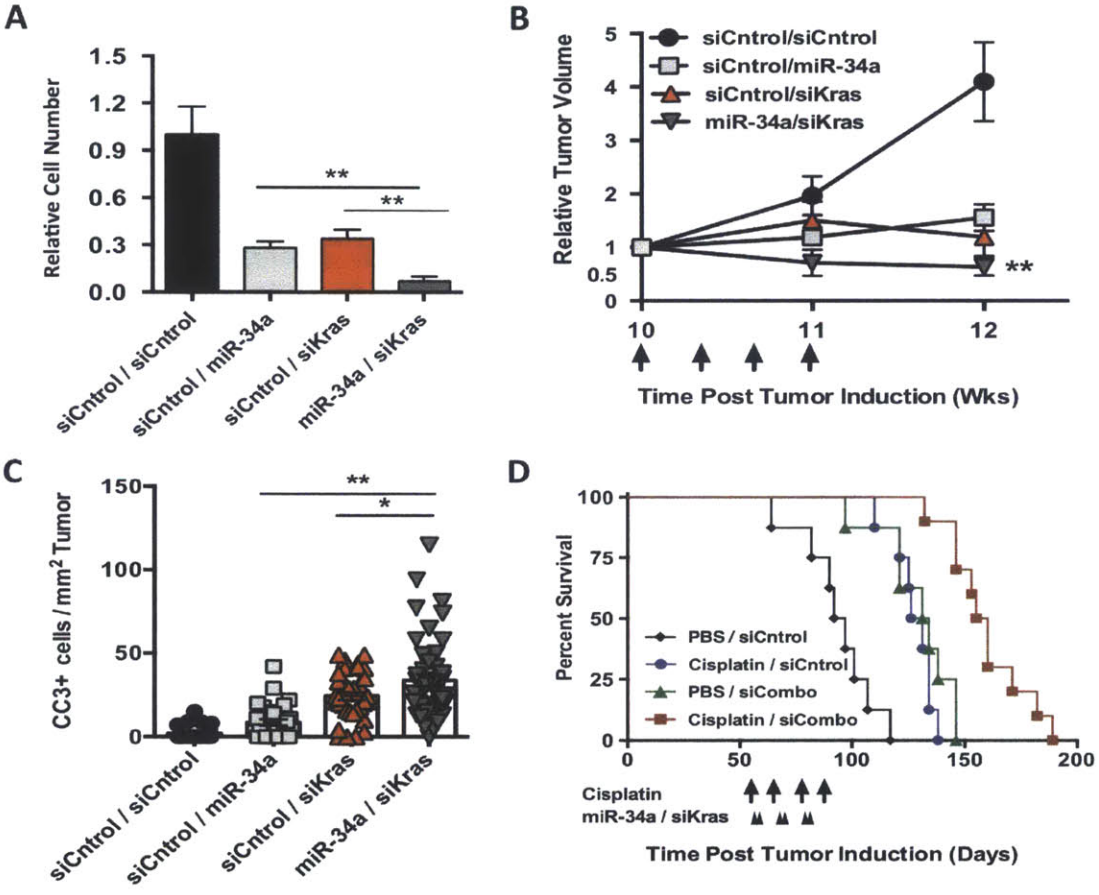

Figure 4.4. Concurrent delivery of miR-34a and siKras combination improves therapeutic response. (A) KP cell number following incubation with 7C1-siRNA combinations. Each siRNA dose is 30nM. Error bars are s.d. (N=3 wells/group). (B) Normalized lung tumor volume in KP mice following treatment with 7C1-siRNA combinations. Ten weeks after tumor initiation, mice were dosed with 2 mg/kg 7C1-siLuc or 7C1-miR-34a/siKras every other day for 4 doses. Error bars are s.d. (N=8 mice/group, 1 tumor/mouse). **, $p<0.01$ for 7C1-miR-34a/siKras compared to single treatment. (C) Quantification of apoptotic cells marked by cleaved caspase 3 (CC3) in treated tumors (N=27, 29, 36 and 46 tumors per time point, respectively). (D) Kaplan-Meier survival curve of KP mice treated with Cisplatin and 7C1 nanoparticle formulated with miR34a/siKras combination (siCombo) therapies. N=8, 8, 8 and 10 mice per group. Day 0 refers to tumor initiation. Arrows or arrowheads indicate timepoints of Cisplatin or nanoparticle administration, respectively. *$p<0.05$, **$p<0.01$.

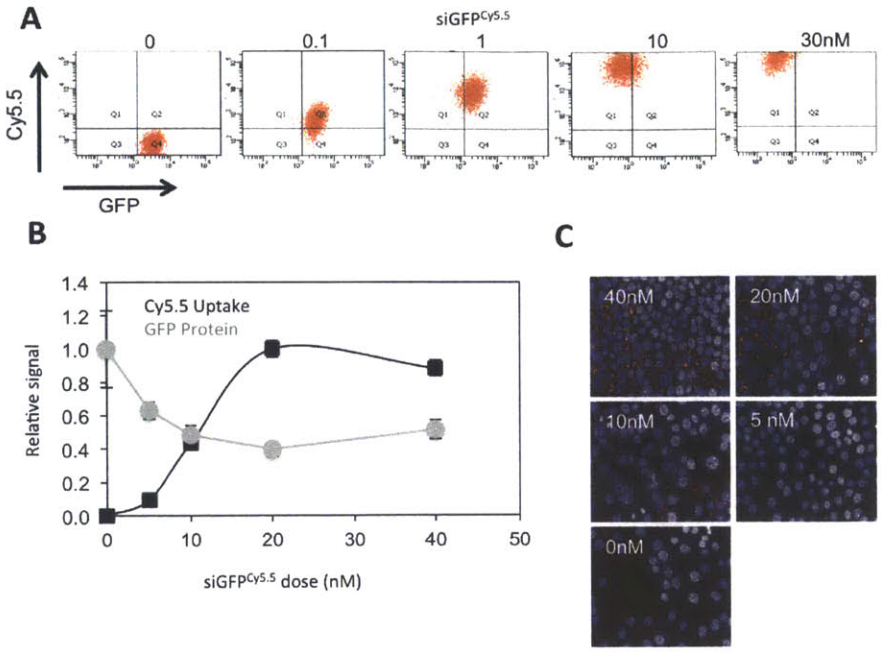

Figure 4S.1. 7C1 nanoparticles efficiently deliver siRNAs to murine lung adenocarcinoma cells *in vitro*. (A) FACS analysis of nanoparticle uptake and GFP knockdown. KP (*Kras*$^{LSL\text{-}G12D/wt}$;*p53*$^{flox/flox}$) cells expressing GFP were incubated with 7C1-siGFP (Cy5.5-labeled) at indicated concentration for 48 hours and analyzed by FACS. (B) Imaging based quantification of nanoparticle uptake and GFP knockdown. KP cells expressing GFP were incubated with 7C1-siGFP at indicated concentration for 48 hours and imaged by fluorescent microscope. GFP signal at 0nM and Cy5.5 signal at 20nM were set to 1. (**C**) Representative images from (B). Red=Cy5.5, Blue=DAPI.

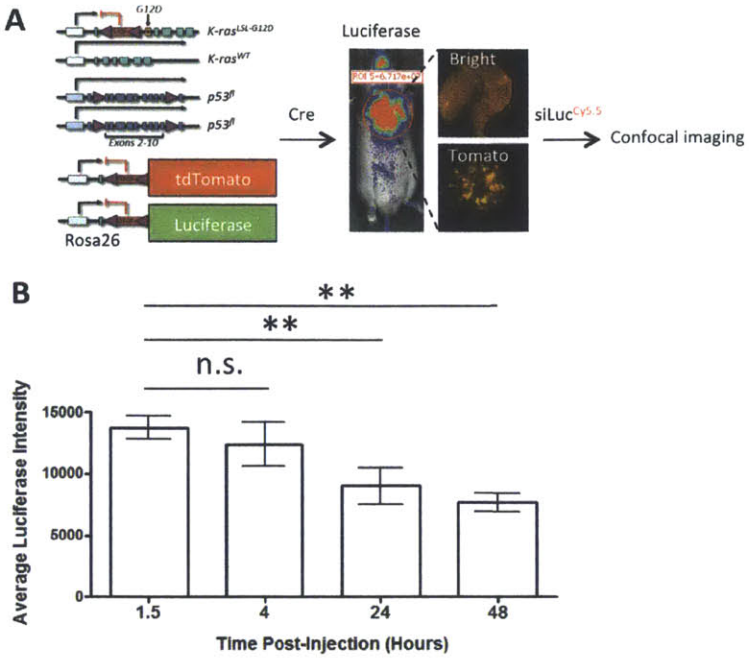

Fig. 4S.2. 7C1 nanoparticles carrying luciferase siRNA efficiently knockdown luciferase in murine lung adenocarcinoma *in vivo*. (A) Scheme of the *Kras*$^{LSL\text{-}G12D/wt}$;*p53*$^{flox/flox}$;R26$^{LSL\text{-}Luciferase/LSL\text{-}tdTomato}$ mice. Whole-body bioluminescence imaging shows luciferase signal in the lung at 10 weeks post Adeno-Cre inhalation. Explanted lung shows Tomato-positive lung tumors. Tumor bearing mice were injected with a single dose of 1.5mg/kg 7C1-siLuc$^{Cy5.5}$. Lung tumors were harvested at indicated time points for luciferase immunostaining and natural fluorescence of Tomato. (B) Quantification of luciferase immunofluorescence signal in Fig. 1E. Error bars are SEM. n=18, 13, 16 and 7 tumors analyzed. **, $p<0.01$.

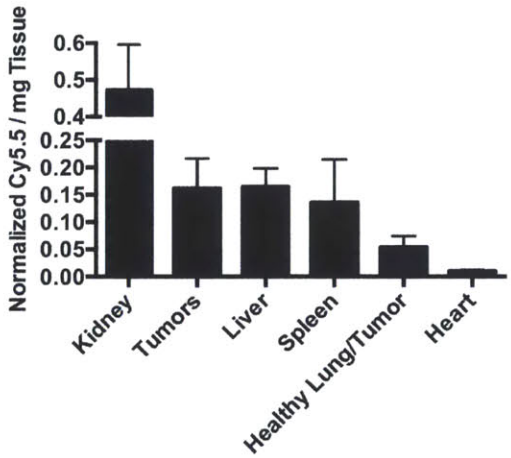

Figure 4S.3. Biodistribution of 7C1 nanoparticles. KP mice harboring lung tumors were injected with a single dose of PBS or 1.5mg/kg 7C1 nanoparticles carrying Cy5.5-labeled siRNA (three mice per group). Cy5.5 signal in microdissected lung tumors and organs were quantified using Xenogen imager at 3.5 hours after injection. Error bars are S.D. (n=3). Tumors denote autochthonous lung tumors.

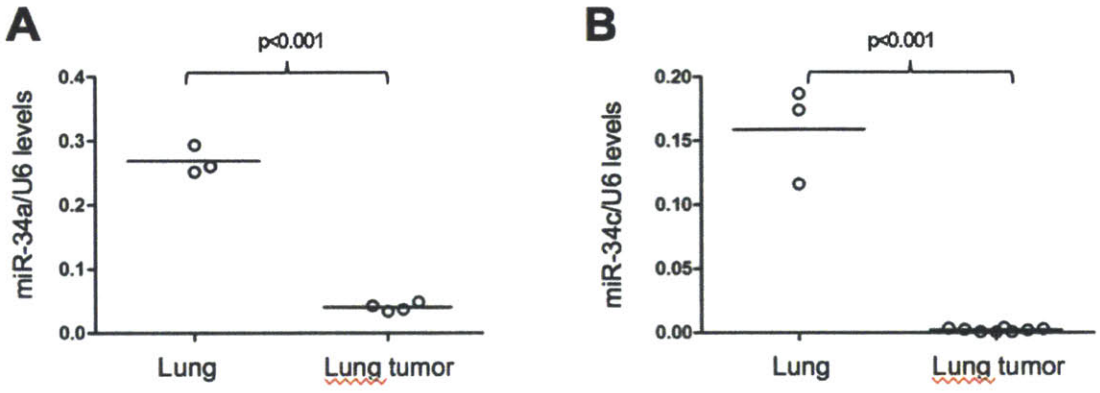

Fig. 4S.4. miR-34a and miR-34c are relatively under-expressed in *Kras*$^{LSL\text{-}G12D/wt}$;*p53*$^{flox/flox}$ lung tumors compared to normal lung. Expression levels of mature forms of miR-34a (A) and miR-34c (B) were quantified by RT-Q-PCR and normalized to U6 non-coding RNA in normal lung and KP lung tumors. Each dot represents an individual RNA sample. Lines are mean values.

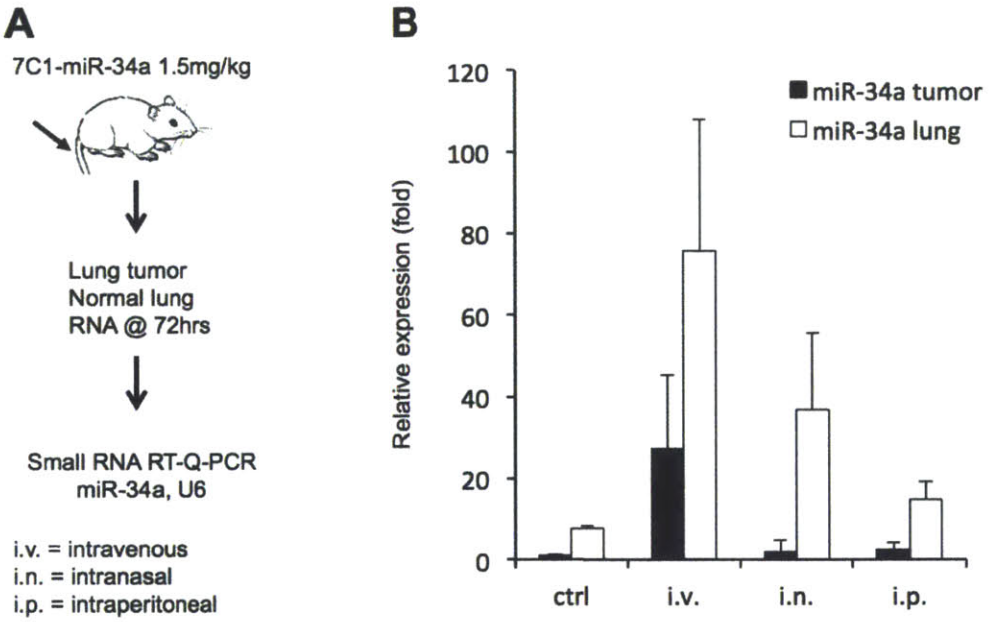

Fig. 4S.5. Comparing miR-34a delivery efficiency using three injection methods. (A) Experiment design. (B) miR-34a levels in KP lung tumors or normal lung were quantified by RT-Q-PCR and normalized to U6 non-coding RNA. Error bars are s.d. (n=4 tumors). miR-34a level in control siRNA (ctrl) treated tumors is set to 1. Intravenous injection (i.v.) delivers the highest miR-34a level in lung tumors.

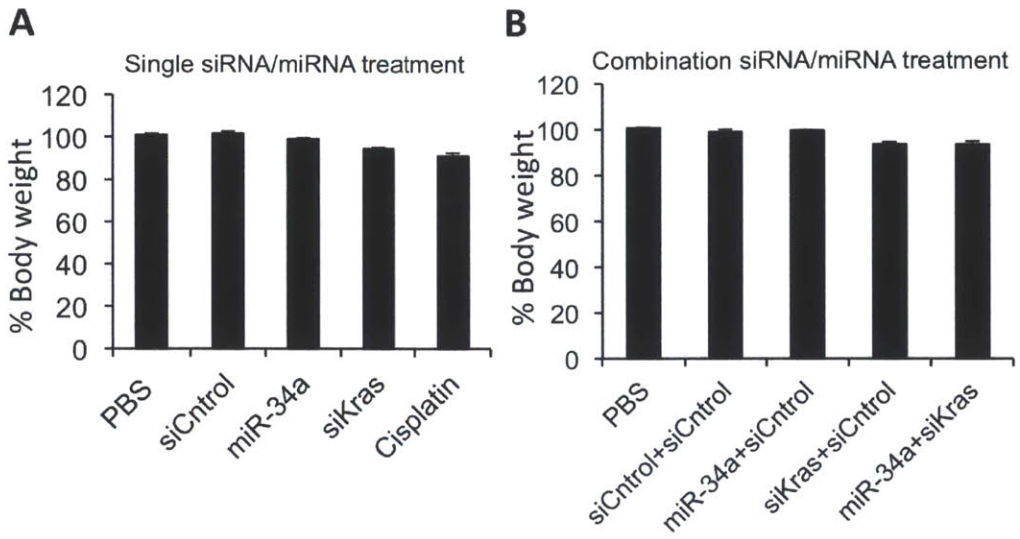

Fig. 4S.6. Body weight in mice dosed with 7C1 nanoparticles carrying single siRNA/miRNA or combinations. (A) 7C1-siCntrol, 7C1-siKras, or 7C1-miR-34a were injected at a dose of 1.5mg/kg every other day for 4 doses. Cisplatin treatment was given at a therapeutic dose (7mg/kg). Body weight was measured 7 days after injection compared to preinjection. (B) 7C1-combination siRNA/miRNA were dosed at 2mg/kg every other day for 4 doses. Error bars are s.d. (n=3 mice).

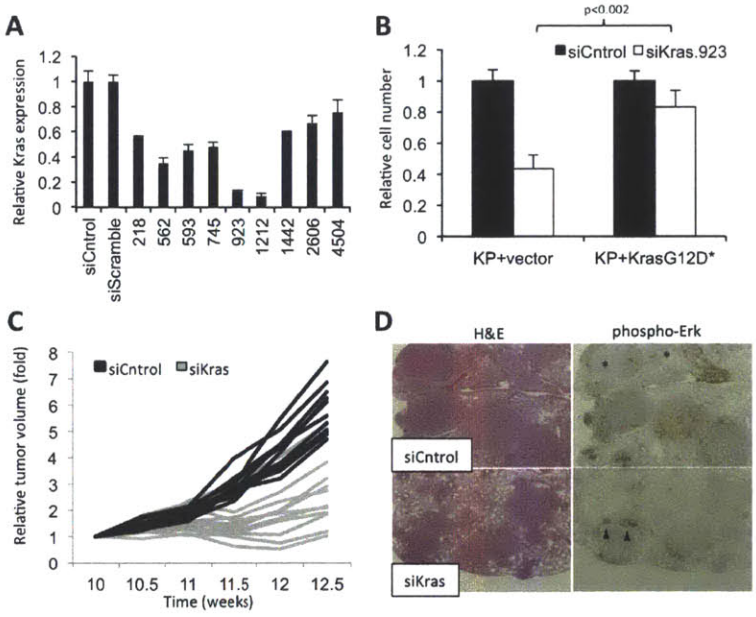

Fig 4.S7. Screening effective siRNA targeting mouse Kras. (A) KP cells were transfected with indicated Kras siRNAs or a control siRNA at 10nM. Kras expression levels were measured by RT-QPCR at 48 hours. siRNA numbers indicate positions in the Kras mRNA. Error bars are s.d. (n=3). (B) siKras effect was rescued by a non-silencible Kras cDNA ($Kras^{G12D}$*) as in Fig. 3B. KP cells stably expressing vector or $Kras^{G12D*}$ were incubated with 7C1 carrying control siRNA or siKras. Cell numbers were quantified by cell titer glo assay. (C) Individual lung tumor volume curve from Fig. 3D. (D) Representative low magnification view (20x) of Fig. 3E. Twelve weeks after tumor initiations, mice were injected with 2 doses of 1.5mg/kg 7C1-siRNA every other day and harvested 72 hours later. * indicates grade 2 tumors with low pErk in the siCntrol group. Arrowheads denote tumors retaining high pErk in the siKras group.

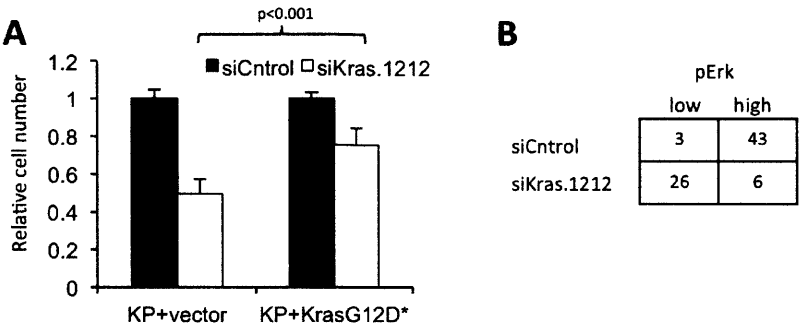

Fig. 4S.8. 7C1 nanoparticles deliver siKras.1212 in the KP model. (A) The effect of siKras.1212 on cell number was rescued by a non-silencible Kras cDNA (KrasG12D*). KP cells stably expressing vector or $Kras^{G12D*}$ were incubated with 7C1 carrying control siRNA or siKras. Cell numbers were quantified by cell titer glo assay. (B) Quantification of phospho-Erk low and high grade lung tumors. $p<10^{-12}$.

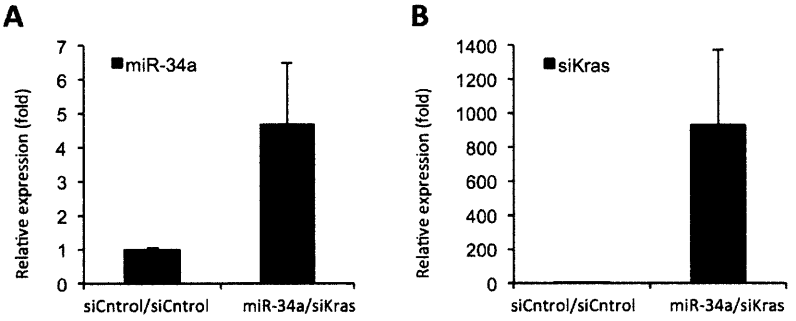

C

	siCntrol/siCntrol			miR-34a/siKras		
Tumor ID	T1	T2	T3	T1	T2	T3
miR-34a	29.1	29.0	26.8	26.1	25.2	26.2
siKras	39.0	40.0	37.2	29.1	27.9	28.9
U6	24.2	24.2	22.6	23.3	22.5	24.4

Fig. 4S.9. Detecting *miR-34a* mimic and siKras in lung tumors dosed with 7C1 nanoparticles simultaneously complexed to siKras and miR-34a. Mice were dosed with 7C1 complexed with miR-34a/siKras (2mg/kg) or 7C1 complexed with siCntrol. Small RNA in tumors were quantified by QPCR using Taqman probes specific to mature miR-34a (A) or siKras (B). Error bars are s.d. (n=3 tumors). (C) QPCR Ct numbers (cycle threshold, maximum=40 cycles) of miR-34a, siKras and U6. The miR-34a probe measures both endogenous miR-34a and delivered miR-34a mimic. The high Ct number of siKras in siCntrol/siCntrol group indicates lack of endogenous siKras in control tumors. T1-T3 denotes three individual lung tumors.

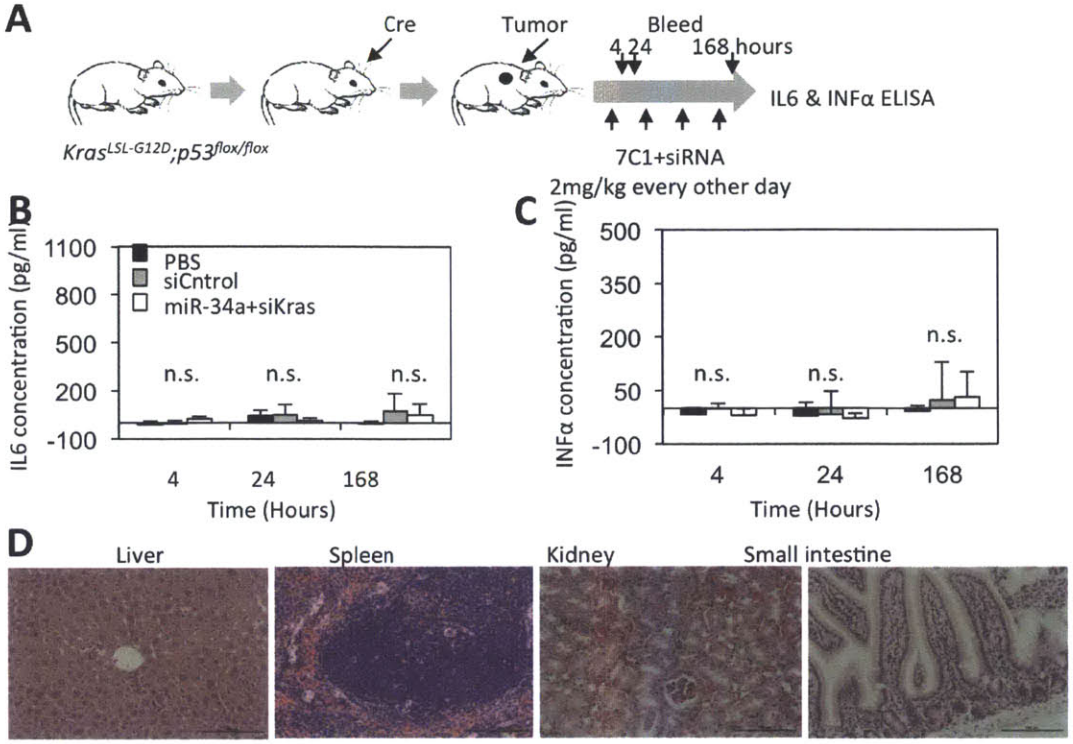

Fig. 4S.10. 7C1 nanoparticles carrying miRNA/siRNA do not induce immune response in mice. (A) Peripheral blood was collected from animals injected with 7C1 complexed to siCntrol or miR-34a/siKras combination at indicated time points. These timepoints mimicked the therapeutic regimen (Fig. 4). (B, C) IL6 and INF-α concentrations were measured by ELISA (6 mice per group). $p>0.05$ (n.s.) for 7C1-siRNA vs PBS comparison at all three time points. In the literature, siRNAs with known immuno-stimulatory effect induced >500pg/ml IL6 and >200pg/ml INF-α in the peripheral blood[1,2]. (D) Representative histology in mice treated with 7C1 miR-34a/siKras combination.

4.11 References

1. Ambros, V. The evolution of our thinking about microRNAs. *Nat Med* **14**, 1036-1040 (2008).
2. Mendell, J.T. & Olson, E.N. MicroRNAs in stress signaling and human disease. *Cell* **148**, 1172-1187 (2012).
3. Ventura, A. & Jacks, T. MicroRNAs and cancer: short RNAs go a long way. *Cell* **136**, 586-591 (2009).
4. Croce, C.M. Causes and consequences of microRNA dysregulation in cancer. *Nat Rev Genet* **10**, 704-714 (2009).
5. Kasinski, A.L. & Slack, F.J. Epigenetics and genetics. MicroRNAs en route to the clinic: progress in validating and targeting microRNAs for cancer therapy. *Nat Rev Cancer* **11**, 849-864 (2011).
6. Pecot, C.V., Calin, G.A., Coleman, R.L., Lopez-Berestein, G. & Sood, A.K. RNA interference in the clinic: challenges and future directions. *Nat Rev Cancer* **11**, 59-67 (2011).

7. Bumcrot, D., Manoharan, M., Koteliansky, V. & Sah, D.W. RNAi therapeutics: a potential new class of pharmaceutical drugs. *Nat Chem Biol* **2**, 711-719 (2006).
8. Kanasty, R.L., Whitehead, K.A., Vegas, A.J. & Anderson, D.G. Action and reaction: the biological response to siRNA and its delivery vehicles. *Mol Ther* **20**, 513-524 (2012).
9. Whitehead, K.A., Langer, R. & Anderson, D.G. Knocking down barriers: advances in siRNA delivery. *Nature Reviews Drug Discovery* **8**, 129-138 (2009).
10. Schroeder, A., *et al.* Treating metastatic cancer with nanotechnology. *Nat Rev Cancer* **12**, 39-50 (2011).
11. Kota, J., *et al.* Therapeutic microRNA delivery suppresses tumorigenesis in a murine liver cancer model. *Cell* **137**, 1005-1017 (2009).
12. Kasinski, A.L. & Slack, F.J. miRNA-34 prevents cancer initiation and progression in a therapeutically-resistant K-ras and p53-induced mouse model of lung adenocarcinoma. *Cancer Res* **10**, 10 (2012).
13. Ren, Y., *et al.* Targeted tumor-penetrating siRNA nanocomplexes for credentialing the ovarian cancer oncogene ID4. *Sci Transl Med* **4**, 147ra112 (2012).
14. Yao, Y.D., *et al.* Targeted delivery of PLK1-siRNA by ScFv suppresses Her2+ breast cancer growth and metastasis. *Sci Transl Med* **4**, 130ra148 (2012).
15. Huang, Y.H., *et al.* Claudin-3 gene silencing with siRNA suppresses ovarian tumor growth and metastasis. *Proc Natl Acad Sci U S A* **106**, 3426-3430 (2009).
16. Trang, P., *et al.* Systemic delivery of tumor suppressor microRNA mimics using a neutral lipid emulsion inhibits lung tumors in mice. *Mol Ther* **19**, 1116-1122 (2011).
17. Herbst, R.S., Heymach, J.V. & Lippman, S.M. Lung cancer. *N Engl J Med* **359**, 1367-1380 (2008).
18. DuPage, M., Dooley, A.L. & Jacks, T. Conditional mouse lung cancer models using adenoviral or lentiviral delivery of Cre recombinase. *Nat Protoc* **4**, 1064-1072 (2009).
19. Engelman, J.A., *et al.* Effective use of PI3K and MEK inhibitors to treat mutant Kras G12D and PIK3CA H1047R murine lung cancers. *Nat Med* **14**, 1351-1356 (2008).
20. Trejo, C.L., Juan, J., Vicent, S., Sweet-Cordero, A. & McMahon, M. MEK1/2 inhibition elicits regression of autochthonous lung tumors induced by KRASG12D or BRAFV600E. *Cancer Res* **72**, 3048-3059 (2012).
21. Xue, W., *et al.* Response and Resistance to NF-kappaB Inhibitors in Mouse Models of Lung Adenocarcinoma. *Cancer Discov.* **1**, 236-247 (2011).
22. De Raedt, T., *et al.* Exploiting cancer cell vulnerabilities to develop a combination therapy for ras-driven tumors. *Cancer Cell* **20**, 400-413.
23. Chen, Z., *et al.* A murine lung cancer co-clinical trial identifies genetic modifiers of therapeutic response. *Nature* **483**, 613-617 (2012).
24. Oliver, T.G., *et al.* Chronic cisplatin treatment promotes enhanced damage repair and tumor progression in a mouse model of lung cancer. *Genes & development* **24**, 837-852 (2010).
25. Heist, R.S. & Engelman, J.A. SnapShot: non-small cell lung cancer. *Cancer Cell* **21**, 448 e442 (2012).
26. Pylayeva-Gupta, Y., Grabocka, E. & Bar-Sagi, D. RAS oncogenes: weaving a tumorigenic web. *Nat Rev Cancer* **11**, 761-774 (2011).
27. Chin, L., *et al.* Essential role for oncogenic Ras in tumour maintenance. *Nature* **400**, 468-472 (1999).

28. Fisher, G.H., *et al.* Induction and apoptotic regression of lung adenocarcinomas by regulation of a K-Ras transgene in the presence and absence of tumor suppressor genes. *Genes Dev* **15**, 3249-3262 (2001).
29. Jechlinger, M., Podsypanina, K. & Varmus, H. Regulation of transgenes in three-dimensional cultures of primary mouse mammary cells demonstrates oncogene dependence and identifies cells that survive deinduction. *Genes Dev* **23**, 1677-1688 (2009).
30. Feldser, D.M., *et al.* Stage-specific sensitivity to p53 restoration during lung cancer progression. *Nature* **468**, 572-575 (2010).
31. Levine, A.J. & Oren, M. The first 30 years of p53: growing ever more complex. *Nat Rev Cancer* **9**, 749-758 (2009).
32. Junttila, M.R., *et al.* Selective activation of p53-mediated tumour suppression in high-grade tumours. *Nature* **468**, 567-571 (2010).
33. He, L., He, X., Lowe, S.W. & Hannon, G.J. microRNAs join the p53 network--another piece in the tumour-suppression puzzle. *Nat.Rev.Cancer* 7, 819-822 (2007).
34. Hermeking, H. The miR-34 family in cancer and apoptosis. *Cell Death Differ* **17**, 193-199 (2010).
35. Hermeking, H. MicroRNAs in the p53 network: micromanagement of tumour suppression. *Nat Rev Cancer* **12**, 613-626 (2012).
36. He, L., *et al.* A microRNA component of the p53 tumour suppressor network. *Nature* **447**, 1130-1134 (2007).
37. He, X., He, L. & Hannon, G.J. The guardian's little helper: microRNAs in the p53 tumor suppressor network. *Cancer Res.* **67**, 11099-11101 (2007).
38. Bader, A.G. miR-34 - a microRNA replacement therapy is headed to the clinic. *Front Genet* **3**, 120 (2012).
39. Peer, D., *et al.* Nanocarriers as an emerging platform for cancer therapy. *Nature nanotechnology* **2**, 751-760 (2007).
40. Semple, S., *et al.* Rational design of cationic lipids for siRNA delivery. *Nature biotechnology* **28**, 172-176 (2010).
41. Love, K.T., *et al.* Lipid-like materials for low-dose, in vivo gene silencing. *Proc Natl Acad Sci USA* **107**, 1864-1869 (2010).
42. Tabernero, J., *et al.* First-in-Humans Trial of an RNA Interference Therapeutic Targeting VEGF and KSP in Cancer Patients with Liver Involvement. *Cancer Discov* **3**, 406-417 (2013).
43. Davis, M.E., *et al.* Evidence of RNAi in humans from systemically administered siRNA via targeted nanoparticles. *Nature* **464**, 1067-1070 (2010).
44. Dahlman, J.E., *et al.* In vivo endothelial siRNA delivery using polymeric nanoparticles with low molecular weight. *Nat Nanotechnol* (2014).
45. Madisen, L., *et al.* A robust and high-throughput Cre reporting and characterization system for the whole mouse brain. *Nat Neurosci* **13**, 133-140 (2010).
46. Cheung, A.F., Dupage, M.J., Dong, H.K., Chen, J. & Jacks, T. Regulated expression of a tumor-associated antigen reveals multiple levels of T-cell tolerance in a mouse model of lung cancer. *Cancer Res* **68**, 9459-9468 (2008).
47. Whitehead, K., Dahlman, J.E., Langer, R.S. & Anderson, D.G. Silencing or Stimulation? siRNA Delivery and the Immune System. *Annual Review of Chemical and Biomolecular Engineering* (2010).

48. Robbins, M., Judge, A. & Maclachlan, I. siRNA and Innate Immunity. *Oligonucleotides* **19**, 89-102 (2009).
49. Zorde Khvalevsky, E., *et al.* Mutant KRAS is a druggable target for pancreatic cancer. *Proc Natl Acad Sci U S A* **110**, 20723-20728 (2013).
50. Nishimura, M., *et al.* Therapeutic synergy between microRNA and siRNA in ovarian cancer treatment. *Cancer Discov* **3**, 1302-1315 (2013).
51. Engelman, J.A., *et al.* MET amplification leads to gefitinib resistance in lung cancer by activating ERBB3 signaling. *Science* **316**, 1039-1043 (2007).
52. Chen, D., *et al.* Rapid discovery of potent siRNA-containing lipid nanoparticles enabled by controlled microfluidic formulation. *J Am Chem Soc* **134**, 6948-6951 (2012).
53. Tammela, T., *et al.* VEGFR-3 controls tip to stalk conversion at vessel fusion sites by reinforcing Notch signalling. *Nat Cell Biol* **13**, 1202-1213 (2011).

Chapter 5. Future work - treating metastatic cancer with nanotechnology

Chapter 5.1 Nanotechnology for metastasis

Metastasis, the spread of cancer cells from a primary tumor to seed secondary tumors in distant sites, is one of the greatest challenges in cancer treatment today. For many patients, by the time cancer is detected, metastasis has already occurred. Over 80% of patients diagnosed with lung cancer, for example, present with metastatic disease. Few patients with metastatic cancer are cured by surgical intervention, and other treatment modalities are limited. Across all cancer types, only one in five patients diagnosed with metastatic cancer will survive over 5 years[1].

As the biological mechanisms of metastasis (Fig. 1) are being unraveled, it is becoming clear that new approaches are needed to treat this condition. Although cancer therapies are improving, many drugs are not reaching the sites of metastases, and doubt remains over the efficacy of those that do. Methods that are effective for treating large, well-vascularized, tumors may be inadequate when dealing with small clusters of disseminated malignant cells. The expanding capabilities of nanotechnology, especially in targeting, detection, and particle trafficking, will enable novel approaches to treat cancers even after metastatic dissemination[2].

Nanotechnology has encountered hurdles in its quest towards application. However, nanotechnology is not alien to the clinic; for example, liposome-encapsulated doxorubicin (Doxil®) is widely used to treat ovarian cancer and Karposi's sarcoma (more than 300,000 patients annually) while protecting patients against the cardiotoxicity of the un-encapsulated drug[3]. Protein nanoparticles containing paclitaxel (Abraxane®), approved to treat metastatic breast cancer, have been shown to enhance tumor uptake of the drug[4]. Iron oxide nanoparticles (ferumoxytol), which are approved for treatment of iron deficiency anemia, have shown efficacy for early staging of lymph node metastasis in patients with prostate and testicular cancers[5,6]. Although the first generation of over 40 nano-therapeutics has reached the clinic, we expect that future systems will introduce new capabilities, including the simultaneous targeting of multiple metastatic sites and the earlier detection of metastases through more sensitive imaging techniques.

The purpose of this review is to outline the current state of nanotechnologies in respect to their ability to treat metastasis. It also introduces approaches for adapting nanoscale tools that were developed for treating primary tumors and other malignancies, for treating metastasis. For the purpose of this review, we define nanoparticles as synthetic constructs composed of organic or inorganic matter, where the dimensions of at least two axes are between 1 and 1000 nanometers.

There is a wide array of nanomaterial-based therapeutic approaches under development. For example, nanoparticles can be engineered to detect a stimulus, such as a molecular binding event or ionic concentration change, and respond by releasing cargo, degrading, or even performing chemical modification of drugs *in vivo*. Importantly, in addition to their potential to combine multiple therapeutic functions into a single platform, nanoparticles can be targeted to specific tissues, reach particular sub-cellular compartments or target malignant cells in

circulation (Fig. 2). As we enter an era of personalized cancer medicine, nanomaterials may potentially constitute platforms for the delivery of modular personalized therapies. However, to realize all of these goals, we need to carefully consider the biology of the metastatic process and engineer nanomaterials accordingly.

Chapter 5.2 Therapeutic mechanisms

Nanoparticle therapeutics vary from carriers of small-molecule drugs or biomacromolecules, such as proteins or small interfering RNA (siRNA),[7-16] to particles that intrinsically bear a therapeutic capacity (Fig 3). The potential benefits of loading drugs into nanoparticles, or alternatively, conjugating drugs to their surface, include: targeting drugs to the disease site, triggering drug release in specific locations in the body,[17,18] and changing a drug's pharmacokinetic profile to increase its half-life at the disease site[19]. These characteristics can potentially reduce off-target effects and lower the amount of drug that must be administered[3,20]. Nanoparticles offer more complex delivery-related capabilities, such as concomitant delivery of a drug with a molecule that modulates the vasculature,[21,22] administration of a prodrug with its activator enzyme,[23,24] or the administration of immunotherapy with a targeting ligand.[25-28] The physiological microenvironment,[29,30] or, alternatively, external stimuli, such as ultrasound,[31-33] light,[34-36] or radio-frequency (RF) electromagnetic fields,[37,38] can be used to trigger drug release locally.

Encapsulation and delivery of drugs is not the only therapeutic function of nanoparticles. Thermo-ablative therapy (the heating of tissues in order to kill tumor cells) can be enhanced by activating nanomaterials, localized in the diseased tissue, with magnetic fields, infrared light and RF ablation[39-42]. Each of these external triggers encompasses advantages and limitations, for example, electromagnetic fields can penetrate deeply (>15 cm) into tissue with minor energetic losses, but are difficult to focus[37,43]. High intensity focused ultrasound (HIFU) can penetrate deeply into tissue and can be focused to a volume of several mm^3, but its capabilities are diminished when applied within bones or gas-filled organs[44]. Infrared (IR) light, of wavelengths spanning from ~750-1300 nm, penetrates tissue to depths of up to 1 cm, after which penetration decreases substantially[45]. Therefore, IR is mostly applicable to lesions near the skin surface, during surgical procedures, or with a minimally invasive laser catheter. Recently, radiofrequency-induced heating of gold nanoparticles has generated interest, and high tissue-penetration depths are predicted[46].

Chapter 5.3 Targeting Metastasis – primary targeting

Targeting nanoparticles to sites of metastasis can be divided into two steps. Primary targeting is the act of steering nanoparticles to the specific organ or organs in which the metastases reside. Secondary targeting is the direction of these delivered materials to the cancer cells and even to a specific sub-cellular location within the cancer cell. The following sections describe the current progress in primary and secondary targeting.

Particle size, surface charge, mechanical properties and chemistry, as well as the route of administration play major roles in the localization of nanoparticles to specific organs (Table 1). Although it is difficult to independently control a single aspect of a nanoparticle, multiple studies have provided informative trends in nanoparticle biodistribution and targeting. For example, only particles of a limited size will be able to exit or enter fenestrated vessels in the liver endothelium or lung capillary beds. Particle surface charge can cause arrest in certain tissues, and material composition can also change the fate of nanoparticles, such as lipid complexes, which accumulate in the liver. Ultimately, life-threatening metastases occur most often in the brain, lungs, liver, lymph and bone; we will therefore focus on targeting these organs.

The brain is considered the most challenging organ to target with intravenously administered nanoparticles[47]. Protected by a lining of endothelial cells that are tightly bound to one another, the blood–brain barrier (BBB) permits only select materials to cross from the circulation into the cerebrospinal fluid. In general, gases (such as CO_2 and O_2), metabolic products (such as glucose) and hormones, as well as small, electrically neutral lipid-soluble molecules are exchanged across the BBB[48]. However, diseases of the central nervous system, including brain tumors and metastases, can disrupt the integrity of the BBB,[3] thereby altering the ability to access the brain with therapeutics[49-52].

When constructing nanoparticles for brain targeting, one must take into account restrictions posed by the BBB. Unlike other organs that permit uptake of materials in the higher nanoscale range, it has been reported that transport of particles across the BBB requires a size under 15 nm[52,53]. Particles in the range of 15–100 nm may also penetrate the brain, but with uptake efficiency that decreases exponentially with size[53,54]. Modifying the particle surface with lipophilic moieties and reducing surface charge may contribute to BBB passage;[54-57] such nanoparticles bind apolipoprotein E (ApoE) following systemic administration[58,59]. These ApoE-decorated particles have been reported to mediate BBB delivery[60,61]. Interestingly, ApoE also facilitates the trafficking of siRNA-loaded lipid nanoplexes to liver hepatocytes[59,62,63]. Conjugating monoclonal antibodies that target BBB receptors to the surface of nanoparticles has also been reported to increase uptake into the brain parenchyma[64].

Nanoparticles can also be trafficked to the brain after being taken up by cells in circulation. For example, sugar coated nanoparticles can be phagocytosed by leukocytes and macrophages[52,65]. Such cells accumulate at sites of BBB degradation associated with disease, and have the capacity to infiltrate the brain[66-68]. By targeting these cells in circulation, nanoparticles may be trafficked into the brain, where they can ultimately be released[65,69]. The ability of cells to infiltrate deep tissue, cross biological membranes, and target disease sites has made them attractive carriers of nanoparticles[70,71].

Lymph nodes, which are linked by lymphatic vessels, are distributed throughout the body and play an integral role in the immune response. Dissemination of cancer cells through the lymph network is thought to be an important route for metastatic spread. Tumor proximal lymph nodes are often the first site of metastases, and the presence of lymph node metastases portends

further metastatic spread and poor patient survival[72]. As such, lymph nodes have been targeted using cell-based nanotechnologies.

Certain characteristics are associated with preferential (but not exclusive) nanoparticle trafficking to lymph nodes following intravenous administration[73-76]. Targeting is usually an indirect process as receptors on the surface of leukocytes bind nanoparticles and transfer them to lymph nodes as part of a normal immune response. Several strategies have been used to enhance nanoparticle uptake by leukocytes in circulation. Coating iron-oxide nanoparticles with carbohydrates, such as dextran, results in increased accumulation of these nanoparticles in lymph nodes[75-77]. Conjugating peptides and antibodies, such as immunoglobulin G (IgG), to the particle surface also increases accumulation in the lymphatic network[78]. In general, negatively-charged particles are taken up at faster rates than positively-, or un-charged ones[73,74]. Conversely, 'stealth' polymers, such as polyethylene glycol (PEG), on the surface of nanoparticles, can inhibit uptake by leukocytes[79-81].

Tsuda and co-workers[82] reported that non-cationic particles with a size range of 6–34 nm, introduced to the lungs (intrapulmonary administration) are trafficked rapidly (<1 hr) to local lymph nodes. Administering <80 nm particles subcutaneously also results in trafficking to lymph nodes[83,84]. Interestingly, non-PEGylated particles exhibit enhanced accumulation in the lymphatics and PEGylated particles tended to appear in circulation several hours after administration[83].

The liver is a frequent site of metastasis. This well-vascularized tissue, with low shear rates and accessible capillaries, provides a 'friendly soil' for cancer cells. Many researchers think that targeting the liver is a simple task because a variety of injected agents can accumulate in this organ. However, recent studies aiming to deliver siRNA to liver hepatocytes show that precise particle engineering is required to pass through the fenestrae present in the liver endothelium[85]. In general, intravenously administered nanoparticles accumulate in activated Kupffer cells that reside within and near the liver vasculature, and do not reach the hepatocytes[86]. Active targeting through endothelial fenestrations to hepatocytes has been facilitated after ApoE adheres to the particle surface while in circulation, or by conjugating carbohydrates, such as GalNAc, to the surface of the particle[87]. This is an example of how organ and cell targeting are often inter-connected. An ongoing clinical trial is using lipid nanoparticles as siRNA carriers for treating liver cancer and metastases[88].

Like the liver, tumor vasculature can have fenestrae, however these spaces are even larger—up to 600 nm in the tumor compared to <200 nm in the liver[89-92]. Furthermore, tumor-associated lymphatic drainage is often hampered[90]. Consequently, some solid tumors will exhibit the "enhanced permeation and retention (EPR) effect" whereby nanomaterials may accumulate in the tumor and be retained (Fig. 4)[89,90,93]. The effect is often used to direct macromolecule-based therapies to a tumor site,[89,93] but it has limitations; it is present in tumors over approximately 100 mm^3 in volume, hindering its use for targeting small or un-vascularized metastases[94].

The lungs can be accessed directly through inhalation or indirectly following intravenous administration. Aerosolized, low density (<0.4 g/cm^3) micron-sized particles (>5 μm) can be engineered so that they are retained in the lungs for prolonged periods of time[95]. Alternatively, targeting the lungs by intravenous administration has been reported to be more effective using particles larger than 300 nm in diameter[96]. Smaller particles tend to reside in the lungs during the first 1-2 hr post administration and are thereafter detected in other organs[97]. This is explained by larger particles being physically trapped in the intricate capillary beds of the alveoli[98]. For both intravenous and intratracheal routes of administration, cationic nanoparticles tend to accumulate at higher levels and have longer residence times in the lungs, in comparison to negatively-charged or neutral nanoparticles[99-102]. It has been hypothesized that positively charged particles bind to erythrocytes and serum proteins, resulting in their inability to exit the lung due to the large size of the complex[103,104]. Recently, Cohen and coworkers used intravenously administered 300 nm particles to target laminin receptors over-expressed in melanoma metastasis residing in the lungs of mice[105].

The sinusoidal vasculature of bone marrow facilitates migration of hematopoietic progenitor cells and circulating cancer cells. Ninety percent of clinically detectable prostate metastases are present in the bone and about half of breast cancers metastasize to the bone, suggesting that the bone has an active role in cancer cell recruitment, survival or outgrowth[106]. Bone metastases which often occur in high multiplicity can result in bone degradation and complications such as fractures, hypercalcemia and nerve compression[107,108]. Targeting nanoparticles to bone is still in its infancy[108] and current investigative agents include small-molecules and proteins targeted to hydroxyapatite, the calcium-containing mineral which composes up to 50% of bone. Compounds such as bisphosphonate, which have been used to treat osteoporosis and bone metastases, have been shown to increase the accumulation of nanoparticles in the bone[109]. Nanoparticles targeting the bone-marrow could also make use of the sinusoidal endothelium to increase delivery of agents that target cancer cells directly[110].

Once at the target organ, steering nanoparticles towards the malignant cells poses an additional challenge. This has been addressed using several approaches. The first is by using external driving forces, such as magnetic fields to concentrate iron oxide nanoparticles,[111,112] or acoustic waves to trigger micro-bubble localization[113]. Recently, an active nano signaling system was developed, in which one targeted nanomaterial triggers a local biological cascade that, in turn, recruits other therapeutic nanoparticles to the disease site[114]. This ability to amplify a local signal may be especially important for locating and treating metastases. Another mechanism for steering nanomaterials to a disease site is by using self-propelled nanoparticles[115,116]. While this approach is still in its infancy, it represents the evolution of passive nanomaterials into autonomous self-activated systems.

Chapter 5.4 Targeting Metastasis – secondary targeting

Targeting a metastatic cancer cell, either in transit from the primary tumor or buried within a population of non-cancerous cells, presents a unique challenge. In contrast to primary targeting,

secondary targeting is the precise homing of a particle or drug to a specific cell type (Fig. 3). It can require a chemical specificity that enables the nanoparticle to bind to unique moieties presented by the cancer cell. Cancer cells, whether metastatic or part of the primary tumor, can up-regulate certain cell surface molecules and secreted factors, and may even express proteins that are usually only expressed during embryonic development[117]. The cell will also express endogenous surface proteins from its site of origin, which will differ from its site of implantation. For example, a metastatic pancreatic cancer cell will be distinct from cells within the liver strictly by virtue of its pancreatic origin. These characteristics provide investigators with handles to target cancer cells. They may also limit the potential side effects of targeting proteins expressed by a given cell type that are not exclusive to the cancer cell.

Strategies needed for targeting specific cells (secondary targeting) may differ from those used for targeting the organ (primary targeting). The researcher must take into account binding affinity to the molecules of interest, as well as binding specificity and immunological effects. Antibody conjugates—drug, polymer, or radioisotope-labeled antibodies, are currently in the clinic for targeting cancer. For instance ^{131}I-tositumomab (Bexxar®) is a combination therapy, which involves a radiolabeled anti-CD20 antibody for targeting follicular B-cell lymphoma[118]. Antibody-based targeting ligands have been used on various nano-delivery systems[119-123]. Likewise, short peptides, including those with integrin-binding domains RGD and IKVAV, can be appended to nanoparticles and increase their binding to specific cell types within a tissue[105,124-126].

High-throughput methods, such as phage display, ribosome display, in vitro evolution, and in vitro selection are being used to discover new targeting ligands,[127] such as antibodies, peptides and nucleic acid-based ligands (aptamers)[128,129]. Pegaptanib, an anti angiogenic aptamer-based agent, is being used clinically for the treatment of macular degeneration,[130] however, aptamers have not yet been approved for cancer treatment. Peptide nucleic acids (PNAs) can bind with a high affinity to complimentary DNA strands and the peptide backbone allows for covalent modification with targeting ligands and fluorophores[131]. PNAs have been used to target pro-metastatic genes and inhibit their expression[132].

Small-molecule binding domains, such as the folate receptor which is overexpressed in human oral carcinoma, metastatic- breast, colorectal and other cancers, are also under investigation and demonstrate affinity to nanoparticles functionalized with folic acid[133-136]. Certain cells which routinely undergo phagocytosis, such as macrophages, can be targeted with materials such as dextran[75] which resemble lipopolysaccharides expressed on the surface of bacteria. Phagosomes tend to fuse with lysosomes, however, resulting in degradation of the contents; thus strategies must be employed to control the route of uptake[137].

The route through which nanoparticles enter a cell can also be engineered; affecting which cellular compartment a drug is released into. This is an emerging area and will likely evolve into a separate field of *tertiary targeting*,[138] because the intracellular fate of the particle can decide the resulting efficacy of the encapsulated drug[139]. Clathrin-dependent endocytosis, one of the most-well characterized pathways of cell uptake, primarily results in the lysosomal

pathway. This type of endocytosis can be triggered by the protein transferrin or ligands for glycosylated receptors[140]. Lysosomes sequester their contents from the cytosol and are rich in enzymes, which degrade their contents. Therefore, lysosomal components may also degrade nanoparticles and their cargo or otherwise inhibit drug function by preventing access to the cytoplasm and nucleus. To bypass the lysosome, a nanoparticle can be engineered to break out of endosomes or enter the cell via non-lysosomal pathways. One mechanism proposed of disrupting lysosomes is the "proton sponge effect," whereby nanoparticles with cationic surface groups induce osmotic lysis, it is hypothesized, upon endosome acidification[141]. Uptake via caveolin-dependent endocytosis, which can bypass the lysosome, can be mediated by nanoparticles coated with folic acid, cholesterol or albumin[140]. Micropinocytosis, a less-understood process that results in vacuoles that are larger and distinct from clathrin and caveolin-coated vesicles[142], can be initiated by certain cell-penetrating peptides and lipid-like materials[143,144].

Chapter 5.5 Therapeutic Nanocarriers

Nanoscale vehicles have been derived from biological, organic and inorganic origins to address a wide variety of biological mechanisms and targets (Table 2). Lipid-based and polymeric materials constitute the majority of nano-vehicles used to date owing to their properties that enable the addition of targeting moieties, such as antibodies, their ability to degrade under specific conditions, and their capacity to carry a large amount of drug. A variety of new materials with potential as delivery agents include DNA origami cages,[145] macrophage specific nanoparticles,[146] targeted magnetic nanoparticles,[147,148] gold nano-materials,[149] functionalized carbon nanotubes,[150] worm-like filomicelles, silica particles,[151,152] modified plant viruses,[153,154] nano diamonds,[155] and others. This abundance of options, in fact, creates a new challenge for engineers who need to identify the appropriate combination of materials that will produce the most effective therapies. From liposomes and polymeric formulations to iron oxide particles and modified plant viruses, various materials and methods have been finding their niche in targeting metastasis.

Polymeric materials make up the largest category of vehicles for carrying drug payloads. Several sub-types include core-shell particles which often involve a material that surrounds a drug payload using non-covalent forces[156]. A noteworthy example is poly(lactic-*co*-glycolic acid) (PLGA)-based biodegradable nanoparticles, made from Food and Drug Administration (FDA)-approved materials that incorporate hydrophobic drugs[157]. Polymeric micelles are non-crosslinked particles involving block copolymers, a single polymer chain which incorporates more than one block of identical molecules. A simple polymeric micelle will contain many amphipathic polymers, which mimic the tail and head portions of the micelle. These spontaneously form micelles around hydrophobic drugs. Polymeric nanoparticles with controlled sizes and shapes have been fashioned to permit cell attachment but prevent internalization, allowing a cell to carry a drug payload to a second site for delivery, in effect creating a 'cell backpack'[70]. Polymers with long circulating time times may be used for

targeting circulating tumor cells (Fig. 2). Hydrogel nanoparticles, also known as nanogels, are cross-linked, hydrophilic polymer networks which swell with water in aqueous environments.[158] Nanogels can be engineered to covalently or non-covalently bind drugs or targeting ligands. They can also swell or shrink in response to factors such as pH or temperature.

Lipids are amphiphilic small molecules that can self-organize into vesicles (lipid bilayers/liposomes), micelles, or lipoplexes (amorphous particles). These nanoparticles have been synthesized for over half a century and can often be assembled with readily-available materials and off-the-shelf equipment[159]. These vehicles can be modified for targeted delivery of both water-soluble and insoluble therapeutics[160]. Coupled with appropriate targeting ligands, such as integrin binding peptides, liposomes can accumulate in tumor vasculature during angiogenesis[161] and deliver a therapeutic payload. Properties of liposomes such as size, carrying capacity, and targeting capabilities can be modified by varying the targeting ligands attached to the surface. pH-sensitive and temperature-sensitive formulations have been developed to control the release of the payload[162,163]. Synthetic, lipid-like materials that form lipoplexes have been produced by combinatorial techniques for applications such as siRNA delivery[85,144].

Gold nanoparticles have been employed for thermoablative therapies[39]. Gold shells, spheres and rods respond to near infra-red light by releasing energy in the form of heat that induces coagulation of the tumor vasculature and can cooperatively increase the therapeutic effect of other targeted therapies[164]. Gold nanoparticles can also be used as scaffolds to which multiple ligands are attached[165]. Other nanomaterial classes, such as iron nanoparticles and carbon nanotubes or spheres (buckyballs), have been used to deliver therapies, often by binding the drug to the outer surface or filling the interior where applicable[166].

Different types of materials exhibit varying bio-distribution, compatibility, degradation, and circulation properties. No single parameter can be denoted as the most important prerequisite for effective cancer therapy. Recent studies have identified cytokines that are up regulated after the administration of positively charged nanoparticles[102,167]. Compliment activation has been associated with nanoparticle administration. Particles with positive surface charge activate the classical compliment pathway, while negatively charged particles activate the alternative pathway[168,169]. Interestingly, it has been shown that different degrees of PEG on the surface of nanoparticles affect the complement activation pathways; lower levels of PEG are associated with the classical pathway, while higher degrees of PEG are associated with a less intense lectin-pathway activation[170]. Particle size also plays a role in this process, the larger the nanoparticle the higher the extent of opsonization[171].

In many cases adverse biological responses to nanoparticle administration, such as inflammation or compliment activation, can be treated with pre- or post-therapy medication[172]. In an attempt to improve the biocompatibility of nanoparticles *in vivo*, a hybrid biomimetic approach has been undertaken. Nanoparticles were disguised by coating them with a naturally derived erythrocyte membrane (also known as 'red-blood-cell ghosts')[173-177] or by physically loading the particles into stem cells, thereby evading reticuloendothelial-system (RES) clearance and utilizing natural pathways to target cancer[175,178,179]. A different approach uses cell

membranes as scaffolds for constructing nanoparticles, utilizing targeting moieties that are naturally present on the cell surface and of the biocompatibility of biologically-derived materials[180]. Taking advantage of the body's natural trafficking modalities (i.e., cells and complex proteins) is a new and extremely promising approach for delivering nanoparticles to specific tissue compartments.

The toxicity of nanomaterials is under investigation; a meta-analysis illustrates that their effect on tissues depends on the physicochemical properties of the materials used, including size, charge, and coating ligands[181]. For instance, the semiconductor cores of quantum dots can be cytotoxic, but certain polymer coatings have reduced toxic effects in vivo[181]. Nanoscale gold particles exhibit minimal toxicity on mammalian tissues, but they do not naturally degrade in vivo and can accumulate in organs unless their surface is decorated with "stealth" materials such as PEG[182]. Careful engineering of drug carriers can potentially reduce the amount of foreign material, both drug and nanoparticle, administered to the patient[144,183].

Chapter 5.6 Diagnostic nanomaterials

The treatment of metastatic disease increasingly depends on imaging and diagnostics (Fig. 1, Table 2). Some tools, such as directed radiotherapy, require precise tumor localization, and treatment decisions are based on understanding the extent of disease spread. Diagnostics, such as contrast agents for radioimaging, visualization aids for surgeons, and molecularly activated sensors, comprise an active area of investigation for materials engineers working at the nanoscale. Much of the excitement in this area stems from unique material properties that appear at this scale. For example, the fluorescent properties of highly-photostable tunable imaging agents, such as quantum dots, only appear when semiconductor crystals are synthesized with nanometer dimensions. For patients with metastatic cancer, the work in this field has the potential to reduce the toxicity while increasing the specificity and signal strength of imaging agents, enable visualization of metastases during surgery, and provide molecular sensors to aid in many areas, from the dosing of chemotherapy to defining the onset of malignancy.

For magnetic resonance imaging (MRI), superparamagnetic nanoparticles consisting of iron oxide (SPIONs) can yield higher contrast at low concentrations than Gd^{3+}, a common MRI contrast agent. Such particles decorated with dextran, which results in localization within lymph nodes, have been studied for nodal tumor detection in prostate cancer patients[77]. Targeted SPIONs, functionalized with RGD peptide, have been investigated in vivo to image integrin avb3–positive tumor neovasculature[184]. Nanoparticles have been explored for targeting gadolinium-based contrast agents. For instance, Gd encapsulated carbon fullerenes and Gd-DOTA-decorated liposomes can change the pharmacokinetics and localization of gadolinium[185,186].

Recently, silica nanoparticles have been approved for clinical trials for detecting lymph node metastases in melanoma patients using positron emission tomography (PET)[187]. Dual-modality nanoparticles, which combine two imaging methods into a single entity can provide the advantages of two different techniques, such as the important anatomical information gained from the soft-tissue contrast of MRI with the high sensitivity and/or functional information of

PET[188]. Examples include radiolabeled iron oxide nanoparticles for both PET and MRI imaging[189,190].

CT contrast agents often involve small molecules with short half-lives in the body[191]. Encapsulating the agents in nanoparticles can prolong the residence time, thereby reducing the required dose and allowing more logistical flexibility in the clinical setting[191]. Low-sensitivity techniques such as SPECT can be improved by nanoparticle administration of higher contrast-agent doses, such as with ^{111}In-labeled perfluorocarbon nanoparticles[192]. Nanoparticles are also being used to image tissue microstructure and delineate tumor margins by techniques such as optical coherence tomography (OCT)[193,194].

In addition to the use in diagnosis, diverse classes of nanomaterials have been used to aid surgical resection, identify cancer cells in the blood, and detect unique tumor sub-regions[195]. Optical nanomaterials synthesized to emit visible to near-infrared light and conjugated to targeting ligands, have been developed for *in vivo* diagnostic applications. Quantum dots have been used efficaciously to track metastatic cells[196] and to differentiate between cells in heterogeneous tumor subpopulations *in vivo*[197].

Nanoscale sensors promise to aid early detection of cancer and metastasis to improve patient prognosis by lowering the detection limit and specificity of biomarker recognition. Sensitivity down to the single molecule has been reached using nanomaterials with unique electronic and optical properties. For instance, single-walled carbon nanotubes have been used to measure single molecules of specific reactive oxygen species (ROS) and chemotherapeutic drug concentrations in real-time[198]. Localized surface plasmon resonance (LSPR) nanoparticles[199] and nanowires[200] detect cancer markers and other proteins with extremely high sensitivity via modulation of surface electrons. Schemes have been developed using nanoparticles to quench a fluorophore, such as a fluorescent polymer, until a specific protein binds[201]. Biologists are currently discovering important disease biomarkers in several molecular classes; for instance, microRNA-141 and carcinoembryonic antigen were discovered to be prognostic markers for metastatic colorectal cancer,[202] while the small molecule metabolite sarcosine portends metastatic prostate cancer[203]. Coupled with microfluidic device technologies which allow multiplexed biomarker assays using nanoliter volumes of whole blood,[204] nanoengineered materials will be instrumental for developing minimally invasive methods for detecting both cancer and metastatic disease at an early stage.

Chapter 5.7 Unmet needs in metastatic therapies

New strategies are needed to treat the complex problem of metastatic cancer, which is considered today to be largely incurable. Nanomaterials present tools with many potential benefits that are only starting to be realized in the clinic. To date, most nanotechnology cancer therapies have focused on the treatment of primary tumors but it is important to leverage the potential of nanotechnology to combat cancer spread at each stage of the metastatic process.

The biological mechanisms that specifically drive each step of metastasis: angiogenesis, intravasation, tumor cell circulation, extravasation, and growth in secondary sites can be co-

opted by nanoparticle therapies. The characteristics that make an environment susceptible to metastasis should also make specific and targeted therapeutic intervention possible. There is space for more inventive approaches for therapeutic interventions; more work should be focused on targeting the bone and the brain, targeting the tumor microenvironment, taking advantage of the payload-protective nature of nanoparticles, and combining novel nanoparticles for primary and secondary targeting with preclinical *in vivo* models of metastatic cancer.

As our knowledge of cancer biology becomes more complete, it is increasingly important for clinicians, biologists, and engineers to discuss ideas for diagnostics and treatments of metastatic cancer[2]. Developing nanoparticle therapies, which are aimed in the right directions with the right therapies, will improve the outcome for patients with metastatic cancer.

Chapter 5.8 Figures

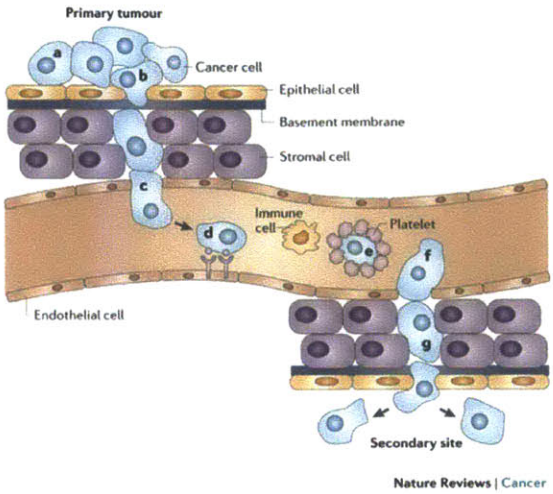

Figure 5.1. Metastasis requires several steps, each of which presents an opportunity for new therapies. First, metastatic cells must break free from the primary tumor. Cancer cells (a) reduce adhesion to neighboring cells and (b) clear a path for migration into the vasculature=rich stroma. Once at the vasculature, cells can freely enter the bloodstream if the vasculature is discontinuous, such as in certain regions of the liver, bone marrow, and kidneys. Intravasation (c) is required if the vasculature is continuous; cells either cause endothelial cell retraction by releasing compounds such as vascular endothelial growth factor (VEGF), or endothelial cell death by releasing reactive oxygen species and factors including matrix metalloproteinases (MMPs). In the bloodstream, cancer cell distribution is determined by blood flow and interactions between cancer cells and the secondary organs they colonize.

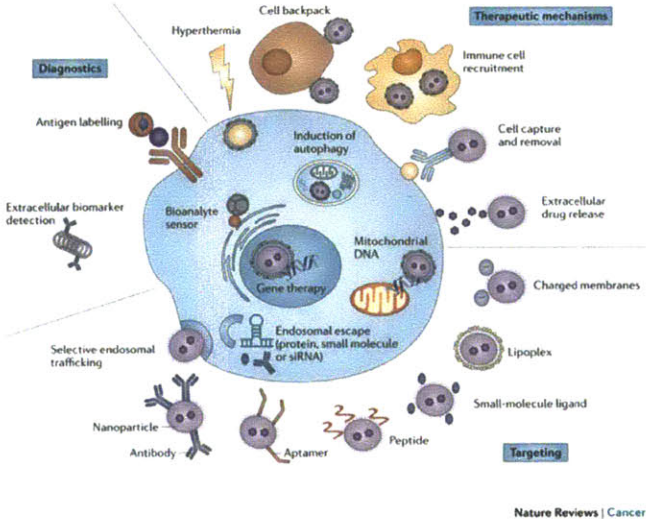

Figure 5.2. The ability to target nanoparticles to cancer cells (secondary targeting) and to influence their uptake into specific cellular compartments (tertiary targeting) is now feasible. This figure summarizes unique targeting, diagnostic and therapeutic mechanisms as they relate to the cancer cell. siRNA, small interfering RNA.

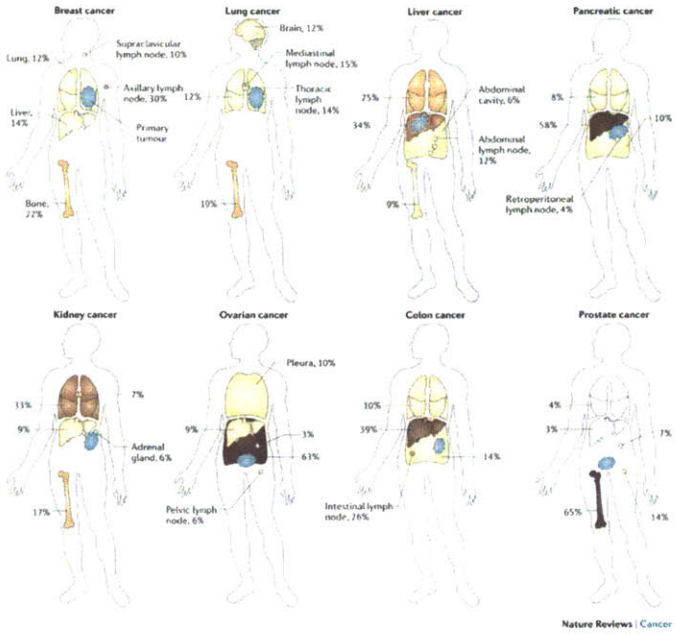

Figure 5.3. Blood flow patterns can predict the specific regions of metastases in approximately two-thirds of cancers[108]. For example, blood from the gastrointestinal tract flows through the hepatic-portal vein to the liver, where metabolic and detoxification processes are carried out. Following this pattern, the vast majority of metastatic colorectal tumours and the majority of metastatic pancreatic tumours spread to the liver108. In such a manner, magnetic nanoparticles, which are bound to an affinity ligand, can be used to remove circulating cancer cells[151,152]. Polymeric nanomaterials can scavenge cancer cell debris from circulation[22], and certain non-spherical, worm-like polymeric micelles (known as filomicelles), which have been reported to have long circulation times in the blood, may also be used for such applications[155,226]. Percentages refer to the relative incidence of metastatic spread to a specific organ for a specified cancer type.

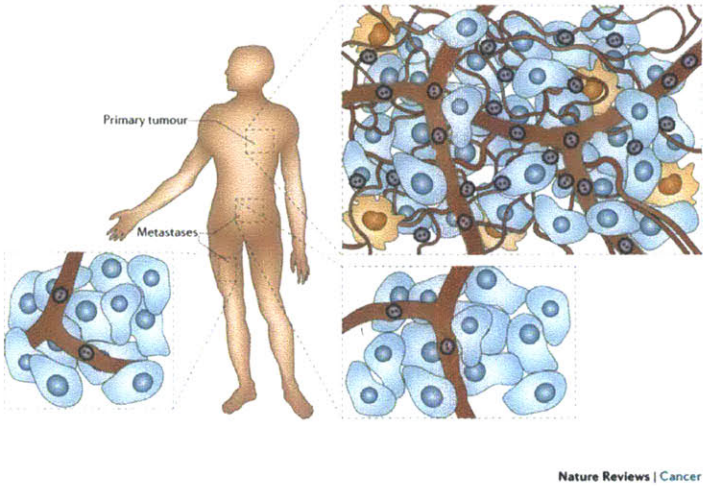

Figure 5.4. The EPR effect enables nanomaterials to accumulate and be retained by a tumour. A large primary tumour and its secondary metastasis are shown. Nanoparticles circulating in the blood can accumulate in a large and well-vascularized tumour by extravasating through leaky blood vessels at the tumour site. The particles are retained at the tumour site owing to poorly functioning lymphatic drainage. Small metastases (<100 mm^3 in size) are poorly vascularized and are not well accessed by nanoparticles via the EPR effect; therefore, alternative targeting methods are necessary.

Target organ	Particle size	Surface property	Comments
Brain	5–100 nm: uptake efficiency decreases exponentially with size	Lipophilic moieties and neutral charge enhance brain uptake	Leukocytes can take up nanoparticles in circulation and then carry them to disease sites in the brain
Lung	>200 nm: particles are trapped in lung capillaries	Positive surface charge	Inhaled particles with low density (<0.4 g per cm^3) and of large size (>5 mm) are also retained in the lung
Liver	<100 nm, to cross liver fenestrae and target hepatocytes. >100 nm particles will be taken up by Kupffer cells	No specificity needed	Lipid and lipid-like materials tend to accumulate in the liver
Lymph nodes	6–34 nm: intra-tracheal administration. 80 nm: subcutaneous administration	Non-cationic, non-pegylated and sugar-based particles	200 nm particles in circulation can be taken up by leukocytes and trafficked to lymph nodes
Bone	Unknown	Compounds such as alendronate and aspartic acid adhere to bone and have been used for bone targeting	Despite great importance, bone targeting is under-researched

Table 1. Primary targeting — general considerations for nanoparticle delivery to specific organs.

Building block	Vehicle	Uses
Polymers	Core-shell nanoparticles, nanogels and polymer micelles	Well-characterized, biocompatible and modular delivery vehicles
Lipids	Liposomes, lipoplexes, micelles and filomicelles	Delivers water-soluble and -insoluble drugs effectively
Metals	Gold nanorods, gold nanoparticles, iron oxide nanoparticles and quantum dots	Imaging agents for diagnosis. Thermoablative therapies
Carbon	Carbon nanotubes, nanodiamonds and graphene	Near-infrared emissions allow for tissue-transparent imaging for diagnosis and tracking. Therapies to potentially sidestep MDR in some leukaemias
Biologicals	Viruses, nucleic acid nanoparticles, DNA origami and protein nanoparticles	Viruses deliver a non-covalently bound payload without loss from passive diffusion

MDR, multi-drug resistance.

Table 2. Nanoparticulate building blocks and their uses.

Chapter 5.9 References

1. Howlader, N., *et al.* SEER Cancer Statistics Review, 1975-2008. (National Cancer Institute, Bethesda, MD, 2011).
2. Sharp, P.A. & Langer, R. Research agenda. Promoting convergence in biomedical science. *Science* 333, 527 (2011).
3. Safra, T., *et al.* Pegylated liposomal doxorubicin (doxil): reduced clinical cardiotoxicity in patients reaching or exceeding cumulative doses of 500 mg/m2. *Ann Oncol* 11, 1029-1033 (2000).
4. Tomao, S., Miele, E., Spinelli, G.P., Miele, E. & Tomao, F. Albumin-bound formulation of paclitaxel (Abraxane (R) ABI-007) in the treatment of breast cancer. *International Journal of Nanomedicine* 4, 99-105 (2009).
5. Harisinghani, M.G., *et al.* A pilot study of lymphotrophic nanoparticle-enhanced magnetic resonance imaging technique in early stage testicular cancer: a new method for noninvasive lymph node evaluation. *Urology* 66, 1066-1071 (2005).
6. Shih, H.A., *et al.* Mapping of nodal disease in locally advanced prostate cancer: rethinking the clinical target volume for pelvic nodal irradiation based on vascular rather than bony anatomy. *Int J Radiat Oncol Biol Phys* 63, 1262-1269 (2005).
7. Wang, J., Tian, S., Petros, R.A., Napier, M.E. & Desimone, J.M. The complex role of multivalency in nanoparticles targeting the transferrin receptor for cancer therapies. *J Am Chem Soc* 132, 11306-11313 (2010).
8. Li, Z., *et al.* Nanoparticle delivery of anti-metastatic NM23-H1 gene improves chemotherapy in a mouse tumor model. *Cancer Gene Ther* 16, 423-429 (2009).
9. Davis, M.E., *et al.* Evidence of RNAi in humans from systemically administered siRNA via targeted nanoparticles. *Nature* 464, 1067-1070 (2010).
10. Li, S.D., Chono, S. & Huang, L. Efficient oncogene silencing and metastasis inhibition via systemic delivery of siRNA. *Mol Ther* 16, 942-946 (2008).
11. Ma, L., *et al.* miR-9, a MYC/MYCN-activated microRNA, regulates E-cadherin and cancer metastasis. *Nat Cell Biol* 12, 247-256 (2010).
12. Ma, L., Teruya-Feldstein, J. & Weinberg, R.A. Tumour invasion and metastasis initiated by microRNA-10b in breast cancer. *Nature* 449, 682-688 (2007).
13. Ma, L., *et al.* Therapeutic silencing of miR-10b inhibits metastasis in a mouse mammary tumor model. *Nat Biotechnol* 28, 341-347 (2010).
14. Gupta, R.A., *et al.* Long non-coding RNA HOTAIR reprograms chromatin state to promote cancer metastasis. *Nature* 464, 1071-1076 (2010).
15. Pecot, C.V., Calin, G.A., Coleman, R.L., Lopez-Berestein, G. & Sood, A.K. RNA interference in the clinic: challenges and future directions. *Nat Rev Cancer* 11, 59-67 (2011).

16. Zamora-Avila, D.E., *et al.* WT1 gene silencing by aerosol delivery of PEI-RNAi complexes inhibits B16-F10 lung metastases growth. *Cancer Gene Ther* 16, 892-899 (2009).
17. Park, J.H., *et al.* Cooperative nanoparticles for tumor detection and photothermally triggered drug delivery. *Adv Mater* 22, 880-885 (2010).
18. von Maltzahn, G., *et al.* SERS-Coded Gold Nanorods as a Multifunctional Platform for Densely Multiplexed Near-Infrared Imaging and Photothermal Heating. *Adv Mater* 21, 3175-3180 (2009).
19. Gabizon, A., Shmeeda, H. & Barenholz, Y. Pharmacokinetics of pegylated liposomal Doxorubicin: review of animal and human studies. *Clin Pharmacokinet* 42, 419-436 (2003).
20. Lee, J., *et al.* Nucleic acid-binding polymers as anti-inflammatory agents. *Proc Natl Acad Sci U S A* 108, 14055-14060 (2011).
21. Hood, J.D., *et al.* Tumor regression by targeted gene delivery to the neovasculature. *Science* 296, 2404-2407 (2002).
22. Murphy, E.A., *et al.* Nanoparticle-mediated drug delivery to tumor vasculature suppresses metastasis. *Proc Natl Acad Sci U S A* 105, 9343-9348 (2008).
23. Gupta, P.B., *et al.* Identification of selective inhibitors of cancer stem cells by high-throughput screening. *Cell* 138, 645-659 (2009).
24. Aboody, K.S., *et al.* Development of a tumor-selective approach to treat metastatic cancer. *PLoS One* 1, e23 (2006).
25. Muller, A., *et al.* Involvement of chemokine receptors in breast cancer metastasis. *Nature* 410, 50-56 (2001).
26. Peer, D. & Margalit, R. Loading mitomycin C inside long circulating hyaluronan targeted nano-liposomes increases its antitumor activity in three mice tumor models. *International Journal of Cancer* 108, 780-789 (2004).
27. Poon, Z., *et al.* Ligand-clustered "patchy" nanoparticles for modulated cellular uptake and in vivo tumor targeting. *Angew Chem Int Ed Engl* 49, 7266-7270 (2010).
28. Ali, O.A., Emerich, D., Dranoff, G. & Mooney, D.J. In situ regulation of DC Subsets and T cells mediates tumor regression in mice. *SCIENCE Translational Med* 1, 8-19 (2009).
29. Timko, B.P., Dvir, T. & Kohane, D.S. Remotely triggerable drug delivery systems. *Adv Mater* 22, 4925-4943 (2010).
30. Fischel-Ghodsian, F., Brown, L., Mathiowitz, E., Brandenburg, D. & Langer, R. Enzymatically controlled drug delivery. *Proc Natl Acad Sci U S A* 85, 2403-2406 (1988).
31. Schroeder, A., *et al.* Controlling liposomal drug release with low frequency ultrasound: mechanism and feasibility *Langmuir* 23, 4019-4025 (2007).
32. Dromi, S., *et al.* Pulsed-high intensity focused ultrasound and low temperature sensitive liposomes for enhanced targeted drug delivery and antitumor effect. *Clin. Cancer Res.* 13, 2722-2727 (2007).

33. Burks, S.R., *et al.* Investigation of cellular and molecular responses to pulsed focused ultrasound in a mouse model. *PLoS One* 6, e24730 (2011).
34. Lu, J., Choi, E., Tamanoi, F. & Zink, J.I. Light-activated nanoimpeller-controlled drug release in cancer cells. *Small* 4, 421-426 (2008).
35. Kuruppuarachchi, M., Savoie, H., Lowry, A., Alonso, C. & Boyle, R.W. Polyacrylamide nanoparticles as a delivery system in photodynamic therapy. *Mol Pharm* 8, 920-931 (2011).
36. Wu, G., *et al.* Remotely triggered liposome release by near-infrared light absorption via hollow gold nanoshells. *J Am Chem Soc* 130, 8175-8177 (2008).
37. Derfus, A.M., *et al.* Remotely triggered release from magnetic nanoparticles. *Advanced Materials* 19, 3932-+ (2007).
38. Hoare, T., *et al.* Magnetically Triggered Nanocomposite Membranes: A Versatile Platform for Triggered Drug Release. *Nano Lett* (2011).
39. Lal, S., Clare, S.E. & Halas, N.J. Nanoshell-Enabled Photothermal Cancer Therapy: Impending Clinical Impact. *Accounts of Chemical Research* 41, 1842-1851 (2008).
40. Yang, W., *et al.* Do liposomal apoptotic enhancers increase tumor coagulation and end-point survival in percutaneous radiofrequency ablation of tumors in a rat tumor model? *Radiology* 257, 685-696 (2010).
41. Baker, I., Zeng, Q., Li, W.D. & Sullivan, C.R. Heat deposition in iron oxide and iron nanoparticles for localized hyperthermia. *Journal of Applied Physics* 99(2006).
42. Ivkov, R., *et al.* Application of high amplitude alternating magnetic fields for heat induction of nanoparticles localized in cancer. *Clin Cancer Res* 11, 7093s-7103s (2005).
43. Young, J.H., Wang, M.T. & Brezovich, I.A. Frequency-Depth-Penetration Considerations in Hyperthermia by Magnetically Induced Currents. *Electronics Letters* 16, 358-359 (1980).
44. Kennedy, J.E. High-intensity focused ultrasound in the treatment of solid tumours. *Nat Rev Cancer* 5, 321-327 (2005).
45. Ziegelberger, G. ICNIRP statement on far infrared radiation exposure. *Health Phys* 91, 630-645 (2006).
46. Curley, S.A., *et al.* Noninvasive radiofrequency field-induced hyperthermic cytotoxicity in human cancer cells using cetuximab-targeted gold nanoparticles. *J Exp Ther Oncol* 7, 313-326 (2008).
47. Eichler, A.F., *et al.* The biology of brain metastases-translation to new therapies. *Nat Rev Clin Oncol* 8, 344-356 (2011).
48. Lesniak, M.S. & Brem, H. Targeted therapy for brain tumours. *Nature Reviews Drug Discovery* 3, 499-508 (2004).
49. Minagar, A. & Alexander, J.S. Blood-brain barrier disruption in multiple sclerosis. *Multiple Sclerosis* 9, 540-549 (2003).

50. Kizelsztein, P., Ovadia, H., Garbuzenko, O., Sigal, A. & Barenholz, Y. Pegylated nanoliposomes remote-loaded with the antioxidant tempamine ameliorate experimental autoimmune encephalomyelitis. *J Neuroimmunol* 213, 20-25 (2009).
51. Jain, R.K. Physiological Barriers to Delivery of Monoclonal-Antibodies and Other Macromolecules in Tumors. *Cancer Research* 50, S814-S819 (1990).
52. Enochs, W.S., Harsh, G., Hochberg, F. & Weissleder, R. Improved delineation of human brain tumors on MR images using a long-circulating, superparamagnetic iron oxide agent. *Jmri-Journal of Magnetic Resonance Imaging* 9, 228-232 (1999).
53. Veiseh, O., *et al.* Specific Targeting of Brain Tumors with an Optical/Magnetic Resonance Imaging Nanoprobe across the Blood-Brain Barrier. *Cancer Research* 69, 6200-6207 (2009).
54. Calvo, P., *et al.* Long-circulating PEGylated polycyanoacrylate nanoparticles as new drug carrier for brain delivery. *Pharmaceutical Research* 18, 1157-1166 (2001).
55. Kreuter, J., Alyautdin, R.N., Kharkevich, D.A. & Ivanov, A.A. Passage of Peptides through the Blood-Brain-Barrier with Colloidal Polymer Particles (Nanoparticles). *Brain Research* 674, 171-174 (1995).
56. Lockman, P.R., Koziara, J.M., Mumper, R.J. & Allen, D.D. Nanoparticle surface charges alter blood-brain barrier integrity and permeability. *J Drug Target* 12, 635-641 (2004).
57. Rousselle, C., *et al.* New advances in the transport of doxorubicin through the blood-brain barrier by a peptide vector-mediated strategy. *Molecular Pharmacology* 57, 679-686 (2000).
58. Bisgaier, C.L., Siebenkas, M.V. & Williams, K.J. Effects of apolipoproteins A-IV and A-I on the uptake of phospholipid liposomes by hepatocytes. *J Biol Chem* 264, 862-866 (1989).
59. Akinc, A., *et al.* Targeted delivery of RNAi therapeutics with endogenous and exogenous ligand-based mechanisms. *Molecular Therapy* 18, 1357-1364 (2010).
60. Kreuter, J., *et al.* Apolipoprotein-mediated transport of nanoparticle-bound drugs across the blood-brain barrier. *Journal of Drug Targeting* 10, 317-325 (2002).
61. Michaelis, K., *et al.* Covalent linkage of apolipoprotein E to albumin nanoparticles strongly enhances drug transport into the brain. *Journal of Pharmacology and Experimental Therapeutics* 317, 1246-1253 (2006).
62. Mahley, R.W. Apolipoprotein E: cholesterol transport protein with expanding role in cell biology. *Science* 240, 622-630 (1988).
63. Yan, X., *et al.* The role of apolipoprotein E in the elimination of liposomes from blood by hepatocytes in the mouse. *Biochem Biophys Res Commun* 328, 57-62 (2005).
64. Huwyler, J., Wu, D.F. & Pardridge, W.M. Brain drug delivery of small molecules using immunoliposomes. *Proceedings of the National Academy of Sciences of the United States of America* 93, 14164-14169 (1996).

65. van Kasteren, S.I., *et al.* Glyconanoparticles allow pre-symptomatic in vivo imaging of brain disease. *Proceedings of the National Academy of Sciences of the United States of America* 106, 18-23 (2009).
66. Pollard, J.W. Macrophages define the invasive microenvironment in breast cancer. *Journal of Leukocyte Biology* 84, 623-630 (2008).
67. DeNardo, D.G., Johansson, M. & Coussens, L.M. Immune cells as mediators of solid tumor metastasis. *Cancer and Metastasis Reviews* 27, 11-18 (2008).
68. Afergan, E., *et al.* Delivery of serotonin to the brain by monocytes following phagocytosis of liposomes. *Journal of Controlled Release* 132, 84-90 (2008).
69. Wu, Y.J., *et al.* In vivo leukocyte labeling with intravenous ferumoxides/protamine sulfate complex and in vitro characterization for cellular magnetic resonance imaging. *American Journal of Physiology-Cell Physiology* 293, C1698-C1708 (2007).
70. Cheng, H., *et al.* Nanoparticulate Cellular Patches for Cell-Mediated Tumoritropic Delivery. *Acs Nano* 4, 625-631 (2010).
71. Stephan, M.T., Moon, J.J., Um, S.H., Bershteyn, A. & Irvine, D.J. Therapeutic cell engineering with surface-conjugated synthetic nanoparticles. *Nature Medicine* 16, 1035-U1135 (2010).
72. Moore, A., Sergeyev, N., Bredow, S. & Weissleder, R. A model system to quantitate tumor burden in locoregional lymph nodes during cancer spread. *Invasion Metastasis* 18, 192-197 (1998).
73. Raz, A., Bucana, C., Fogler, W.E., Poste, G. & Fidler, I.J. Biochemical, morphological, and ultrastructural studies on the uptake of liposomes by murine macrophages. *Cancer Res* 41, 487-494 (1981).
74. Hsu, M.J. & Juliano, R.L. Interactions of liposomes with the reticuloendothelial system. II: Nonspecific and receptor-mediated uptake of liposomes by mouse peritoneal macrophages. *Biochim Biophys Acta* 720, 411-419 (1982).
75. Tassa, C., Shaw, S.Y. & Weissleder, R. Dextran-Coated Iron Oxide Nanoparticles: A Versatile Platform for Targeted Molecular Imaging, Molecular Diagnostics, and Therapy. *Acc Chem Res* (2011).
76. Nahrendorf, M., *et al.* Detection of macrophages in aortic aneurysms by nanoparticle positron emission tomography-computed tomography. *Arterioscler Thromb Vasc Biol* 31, 750-757 (2011).
77. Harisinghani, M.G., *et al.* Noninvasive detection of clinically occult lymph-node metastases in prostate cancer. *N Engl J Med* 348, 2491-2499 (2003).
78. Finkelstein, M.C., Kuhn, S.H., Schieren, H., Weissmann, G. & Hoffstein, S. Liposome Uptake by Human-Leukocytes - Enhancement of Entry Mediated by Human-Serum and Aggregated Immunoglobulins. *Biochimica Et Biophysica Acta* 673, 286-302 (1981).
79. Torchilin, V.P. & Papisov, M.I. Why do polyethylene glycol-coated liposomes circulate so long? *J. Liposome Res.* 4, 725-739 (1994).

80. Gref, R., *et al.* Biodegradable long-circulating polymeric nanospheres. *Science* 263, 1600-1603 (1994).
81. Gabizon, A.A. Stealth liposomes and tumor targeting: One step further in the quest for the magic bullet. *Clinical Cancer Research* 7, 223-225 (2001).
82. Choi, H.S., *et al.* Rapid translocation of nanoparticles from the lung airspaces to the body. *Nat Biotechnol* 28, 1300-1303 (2010).
83. Allen, T.M., Hansen, C.B. & Guo, L.S. Subcutaneous administration of liposomes: a comparison with the intravenous and intraperitoneal routes of injection. *Biochim Biophys Acta* 1150, 9-16 (1993).
84. Reddy, S.T., *et al.* Exploiting lymphatic transport and complement activation in nanoparticle vaccines. *Nat Biotechnol* 25, 1159-1164 (2007).
85. Akinc, A., *et al.* A combinatorial library of lipid-like materials for delivery of RNAi therapeutics. *Nat Biotechnol* 26, 561-569 (2008).
86. Sadauskas, E., *et al.* Kupffer cells are central in the removal of nanoparticles from the organism. *Part Fibre Toxicol* 4, 10 (2007).
87. Baenziger, J.U. & Fiete, D. Galactose and N-acetylgalactosamine-specific endocytosis of glycopeptides by isolated rat hepatocytes. *Cell* 22, 611-620 (1980).
88. Cervantes, A., *et al.* Phase I dose-escalation study of ALN-VSP02, a novel RNAi therapeutic for solid tumors with liver involvement. in *2011 ASCO Annual Meeting* (2011).
89. Maeda, H. & Matsumura, Y. EPR effect based drug design and clinical outlook for enhanced cancer chemotherapy Preface. *Advanced Drug Delivery Reviews* 63, 129-130 (2011).
90. Carmeliet, P. & Jain, R.K. Angiogenesis in cancer and other diseases. *Nature* 407, 249-257 (2000).
91. Yuan, F., *et al.* Vascular-Permeability in a Human Tumor Xenograft - Molecular-Size Dependence and Cutoff Size. *Cancer Research* 55, 3752-3756 (1995).
92. Braet, F. & Wisse, E. Structural and functional aspects of liver sinusoidal endothelial cell fenestrae: a review. *Comp Hepatol* 1, 1 (2002).
93. Torchilin, V. Tumor delivery of macromolecular drugs based on the EPR effect. *Advanced Drug Delivery Reviews* 63, 131-135 (2011).
94. Adiseshaiah, P.P., Hall, J.B. & McNeil, S.E. Nanomaterial standards for efficacy and toxicity assessment. *Wiley Interdisciplinary Reviews-Nanomedicine and Nanobiotechnology* 2, 99-112 (2010).
95. Edwards, D.A., *et al.* Large porous particles for pulmonary drug delivery. *Science* 276, 1868-1871 (1997).
96. Azarmi, S., Roa, W.H. & Lobenberg, R. Targeted delivery of nanoparticles for the treatment of lung diseases. *Adv Drug Deliv Rev* 60, 863-875 (2008).

97. Ilium, L., *et al.* Blood clearance and organ deposition of intravenously administered colloidal particles. The effects of particle size, nature and shape. *International Journal of Pharmaceutics* 12, 135-146 (1982).
98. Pinkerton, N.M., *et al.* Lung targeting with triggered release using gel microparticles with encapsulated nanoparticles in *AICHE* 233860 (Minneapolis, MN, 2011).
99. Choi, H.S., *et al.* Rapid translocation of nanoparticles from the lung airspaces to the body. *Nature Biotechnology* 28, 1300-U1113 (2010).
100. Ekrami, H., Kennedy, A.R. & Shen, W.C. Disposition of Positively Charged Bowman-Birk Protease Inhibitor Conjugates in Mice - Influence of Protein Conjugate Charge-Density and Size on Lung Targeting. *Journal of Pharmaceutical Sciences* 84, 456-461 (1995).
101. Ma, Z., *et al.* Redirecting adenovirus to pulmonary endothelium by cationic liposomes. *Gene Therapy* 9, 176-182 (2002).
102. Polach, K.J., *et al.* Delivery of siRNA to the Mouse Lung via a Functionalized Lipopolyamine. *Mol Ther* (2011).
103. Sakurai, F., Nishioka, T., Yamashita, F., Takakura, Y. & Hashida, M. Effects of erythrocytes and serum proteins on lung accumulation of lipoplexes containing cholesterol or DOPE as a helper lipid in the single-pass rat lung perfusion system. *Eur J Pharm Biopharm* 52, 165-172 (2001).
104. Senior, J.H., Trimble, K.R. & Maskiewicz, R. Interaction of positively-charged liposomes with blood: implications for their application in vivo. *Biochim Biophys Acta* 1070, 173-179 (1991).
105. Sarfati, G., Dvir, T., Elkabets, M., Apte, R.N. & Cohen, S. Targeting of polymeric nanoparticles to lung metastases by surface-attachment of YIGSR peptide from laminin. *Biomaterials* 32, 152-161 (2010).
106. Hess, K.R., *et al.* Metastatic patterns in adenocarcinoma. *Cancer* 106, 1624-1633 (2006).
107. Roodman, G.D. Mechanisms of bone metastasis. *N Engl J Med* 350, 1655-1664 (2004).
108. Wang, D., Miller, S.C., Kopeckova, P. & Kopecek, J. Bone-targeting macromolecular therapeutics. *Adv Drug Deliv Rev* 57, 1049-1076 (2005).
109. Hengst, V., Oussoren, C., Kissel, T. & Storm, G. Bone targeting potential of bisphosphonate-targeted liposomes. Preparation, characterization and hydroxyapatite binding in vitro. *Int J Pharm* 331, 224-227 (2007).
110. Steeg, P.S. Metastasis suppressors alter the signal transduction of cancer cells. *Nat Rev Cancer* 3, 55-63 (2003).
111. Chertok, B., David, A.E. & Yang, V.C. Brain tumor targeting of magnetic nanoparticles for potential drug delivery: Effect of administration route and magnetic field topography. *J Control Release* 155, 393-399 (2011).
112. Chertok, B., David, A.E., Huang, Y. & Yang, V.C. Glioma selectivity of magnetically targeted nanoparticles: a role of abnormal tumor hydrodynamics. *J Control Release* 122, 315-323 (2007).

113. Lum, A.F., *et al.* Ultrasound radiation force enables targeted deposition of model drug carriers loaded on microbubbles. *J Control Release* 111, 128-134 (2006).
114. von Maltzahn G Fau - Park, J.-H., *et al.* Nanoparticles that communicate in vivo to amplify tumour targeting. *Nature Materials* 10, 545-552 (2011).
115. Ebbens, S.J. & Howse, J.R. In pursuit of propulsion at the nanoscale. *Soft Matter* 6, 726-738 (2010).
116. Mallouk, T.E. & Sen, A. Powering nanorobots. *Sci Am* 300, 72-77 (2009).
117. Balzar, M., Winter, M.J., de Boer, C.J. & Litvinov, S.V. The biology of the 17-1A antigen (Ep-CAM). *J Mol Med-Jmm* 77, 699-712 (1999).
118. Kaminski, M.S., *et al.* I-131-tositumomab therapy as initial treatment for follicular lymphoma. *New England Journal of Medicine* 352, 441-449 (2005).
119. Cheever, M.A., *et al.* The prioritization of cancer antigens: a national cancer institute pilot project for the acceleration of translational research. *Clin Cancer Res* 15, 5323-5337 (2009).
120. Jain, R.K., *et al.* Phase I oncology studies: evidence that in the era of targeted therapies patients on lower doses do not fare worse. *Clin Cancer Res* 16, 1289-1297 (2010).
121. Torchilin, V.P., Lukyanov, A.N., Gao, Z. & Papahadjopoulos-Sternberg, B. Immunomicelles: targeted pharmaceutical carriers for poorly soluble drugs. *Proc Natl Acad Sci U S A* 100, 6039-6044 (2003).
122. Brannon-Peppas, L. & Blanchette, J.O. Nanoparticle and targeted systems for cancer therapy. *Adv Drug Deliv Rev* 56, 1649-1659 (2004).
123. Kirpotin, D.B., *et al.* Antibody targeting of long-circulating lipidic nanoparticles does not increase tumor localization but does increase internalization in animal models. *Cancer Res* 66, 6732-6740 (2006).
124. Yang, W., *et al.* TMTP1, a novel tumor-homing peptide specifically targeting metastasis. *Clin Cancer Res* 14, 5494-5502 (2008).
125. Chen, K., *et al.* Triblock copolymer coated iron oxide nanoparticle conjugate for tumor integrin targeting. *Biomaterials* 30, 6912-6919 (2009).
126. Desgrosellier, J.S. & Cheresh, D.A. Integrins in cancer: biological implications and therapeutic opportunities. *Nat Rev Cancer* 10, 9-22 (2010).
127. Hanes, J., Jermutus, L. & Pluckthun, A. Selecting and evolving functional proteins in vitro by ribosome display. *Applications of Chimeric Genes and Hybrid Proteins, Pt C* 328, 404-430 (2000).
128. Farokhzad, O.C., *et al.* Nanopartide-aptamer bioconjugates: A new approach for targeting prostate cancer cells. *Cancer Research* 64, 7668-7672 (2004).
129. Shigdar, S., *et al.* RNA aptamer against a cancer stem cell marker epithelial cell adhesion molecule. *Cancer Science* 102, 991-998 (2011).
130. Gragoudas, E.S., Adamis, A.P., Cunningham, E.T., Jr., Feinsod, M. & Guyer, D.R. Pegaptanib for neovascular age-related macular degeneration. *N Engl J Med* 351, 2805-2816 (2004).

131. Hanvey, J.C., *et al.* Antisense and Antigene Properties of Peptide Nucleic-Acids. *Science* 258, 1481-1485 (1992).
132. Zannetti, A., *et al.* Inhibition of Sp1 activity by a decoy PNA-DNA chimera prevents urokinase receptor expression and migration of breast cancer cells. *Biochemical Pharmacology* 70, 1277-1287 (2005).
133. Yamada, A., *et al.* Design of Folate-Linked Liposomal Doxorubicin to its Antitumor Effect in Mice. *Clinical Cancer Research* 14, 8161-8168 (2008).
134. Hartmann, L.C., *et al.* Folate receptor overexpression is associated with poor outcome in breast cancer. *Int J Cancer* 121, 938-942 (2007).
135. Wang, X., *et al.* A Folate Receptor-Targeting Nanoparticle Minimizes Drug Resistance in a Human Cancer Model. *ACS Nano* (2011).
136. D'Angelica, M., *et al.* Folate receptor-alpha expression in resectable hepatic colorectal cancer metastases: patterns and significance. *Mod Pathol* (2011).
137. Garin, J., *et al.* The phagosome proteome: insight into phagosome functions. *J Cell Biol* 152, 165-180 (2001).
138. Rajendran, L., Knolker, H.J. & Simons, K. Subcellular targeting strategies for drug design and delivery. *Nat Rev Drug Discov* 9, 29-42 (2010).
139. Verma, A., *et al.* Surface-structure-regulated cell-membrane penetration by monolayer-protected nanoparticles. *Nat Mater* 7, 588-595 (2008).
140. Bareford, L.A. & Swaan, P.W. Endocytic mechanisms for targeted drug delivery. *Advanced Drug Delivery Reviews* 59, 748-758 (2007).
141. Schroeder, A., Levins, C.G., Cortez, C., Langer, R. & Anderson, D.G. Lipid-based nanotherapeutics for siRNA delivery. *Journal of Internal Medicine* 267, 9-21 (2010).
142. Kabanov, A.V., Sahay, G. & Alakhova, D.Y. Endocytosis of nanomedicines. *Journal of Controlled Release* 145, 182-195 (2010).
143. Torchilin, V.P. Cell penetrating peptide-modified pharmaceutical nanocarriers for intracellular drug and gene delivery. *Biopolymers* 90, 604-610 (2008).
144. Love, K.T., *et al.* Lipid-like materials for low-dose, in vivo gene silencing. *Proc Natl Acad Sci U S A* 107, 1864-1869 (2010).
145. Andersen, E.S., *et al.* Self-assembly of a nanoscale DNA box with a controllable lid. *Nature* 459, 73-76 (2009).
146. Zhang, W., *et al.* Depletion of tumor-associated macrophages enhances the effect of sorafenib in metastatic liver cancer models by antimetastatic and antiangiogenic effects. *Clin Cancer Res* 16, 3420-3430 (2010).
147. Scarberry, K.E., Dickerson, E.B., Zhang, Z.J., Benigno, B.B. & McDonald, J.F. Selective removal of ovarian cancer cells from human ascites fluid using magnetic nanoparticles. *Nanomedicine* 6, 399-408 (2010).
148. Galanzha, E.I., *et al.* In vivo magnetic enrichment and multiplex photoacoustic detection of circulating tumour cells. *Nat Nanotechnol* 4, 855-860 (2009).

149. Coffey, D.S., Getzenberg, R.H. & DeWeese, T.L. Hyperthermic biology and cancer therapies: a hypothesis for the "Lance Armstrong effect". *JAMA* 296, 445-448 (2006).
150. Ruggiero, A., *et al.* Paradoxical glomerular filtration of carbon nanotubes. *Proceedings of the National Academy of Sciences of the United States of America* 107, 12369-12374 (2010).
151. Slowing, II, Trewyn, B.G. & Lin, V.S. Mesoporous silica nanoparticles for intracellular delivery of membrane-impermeable proteins. *J Am Chem Soc* 129, 8845-8849 (2007).
152. Gratton, S.E., *et al.* The effect of particle design on cellular internalization pathways. *Proc Natl Acad Sci U S A* 105, 11613-11618 (2008).
153. Wiltschke, C., *et al.* A phase I study to evaluate safety, immunogenicity and antitumor activity of a HER2 multi-peptide virosome vaccine in patients with metastatic breast cancer. *J Clin Oncol* 26, 3055 (2008).
154. Brunel, F.M., *et al.* Hydrazone Ligation Strategy to Assemble Multifunctional Viral Nanoparticles for Cell Imaging and Tumor Targeting. *Nano Letters* 10, 1093-1097 (2010).
155. Chow, E.K., *et al.* Nanodiamond therapeutic delivery agents mediate enhanced chemoresistant tumor treatment. *Sci Transl Med* 3, 73ra21 (2011).
156. Alexis, F., Pridgen, E., Molnar, L.K. & Farokhzad, O.C. Factors affecting the clearance and biodistribution of polymeric nanoparticles. *Mol Pharm* 5, 505-515 (2008).
157. Astete, C.E. & Sabliov, C.M. Synthesis and characterization of PLGA nanoparticles. *Journal of Biomaterials Science-Polymer Edition* 17, 247-289 (2006).
158. Murphy, E.A., *et al.* Targeted nanogels: a versatile platform for drug delivery to tumors. *Mol Cancer Ther* 10, 972-982 (2011).
159. Schroeder, A., Kost, J. & Barenholz, Y. Ultrasound, liposomes, and drug delivery: principles for using ultrasound to control the release of drugs from liposomes. *Chem Phys Lipids* 162, 1-16 (2009).
160. Murphy, E.A., *et al.* Nanoparticle-mediated drug delivery to tumor vasculature suppresses metastasis. *Proceedings of the National Academy of Sciences of the United States of America* 105, 9343-9348 (2008).
161. Liu, X.Q., Song, W.J., Sun, T.M., Zhang, P.Z. & Wang, J. Targeted Delivery of Antisense Inhibitor of miRNA for Antiangiogenesis Therapy Using cRGD-Functionalized Nanoparticles. *Molecular Pharmaceutics* 8, 250-259 (2011).
162. Tannock, I.F. & Rotin, D. Acid pH in tumors and its potential for therapeutic exploitation. *Cancer Res* 49, 4373-4384 (1989).
163. Lee, E.S., Gao, Z. & Bae, Y.H. Recent progress in tumor pH targeting nanotechnology. *J Control Release* 132, 164-170 (2008).
164. Park, J.H., *et al.* Cooperative nanomaterial system to sensitize, target, and treat tumors. *Proceedings of the National Academy of Sciences of the United States of America* 107, 981-986 (2010).
165. Libutti, S.K., *et al.* Phase I and pharmacokinetic studies of CYT-6091, a novel PEGylated colloidal gold-rhTNF nanomedicine. *Clin Cancer Res* 16, 6139-6149 (2010).

166. Dai, H.J., Kam, N.W.S. & Liu, Z. Functionalization of carbon nanotubes via cleavable disulfide bonds for efficient intracellular delivery of siRNA and potent gene silencing. *Journal of the American Chemical Society* 127, 12492-12493 (2005).
167. Kedmi, R., Ben-Arie, N. & Peer, D. The systemic toxicity of positively charged lipid nanoparticles and the role of Toll-like receptor 4 in immune activation. *Biomaterials* 26, 6867-6875 (2010).
168. Chonn, A., Cullis, P.R. & Devine, D.V. The role of surface charge in the activation of the classical and alternative pathways of complement by liposomes. *J Immunol* 146, 4234-4241 (1991).
169. Reddy, J.A., *et al.* Preclinical evaluation of EC145, a folate-vinca alkaloid conjugate. *Cancer Res* 67, 4434-4442 (2007).
170. Hamad, I., *et al.* Distinct polymer architecture mediates switching of complement activation pathways at the nanosphere-serum interface: implications for stealth nanoparticle engineering. *ACS Nano* 4, 6629-6638 (2010).
171. Harashima, H., Sakata, K., Funato, K. & Kiwada, H. Enhanced hepatic uptake of liposomes through complement activation depending on the size of liposomes. *Pharm Res* 11, 402-406 (1994).
172. Chanan-Khan, A., *et al.* Complement activation following first exposure to pegylated liposomal doxorubicin (Doxil): possible role in hypersensitivity reactions. *Annals of Oncology* 14, 1430-1437 (2003).
173. Grimaldi, S., Lisi, A., Pozzi, D. & Santoro, N. Attempts to use liposomes and RBC ghosts as vectors in drug and antisense therapy of virus infection. *Res Virol* 148, 177-180 (1997).
174. Pierige, F., Serafini, S., Rossi, L. & Magnani, M. Cell-based drug delivery. *Adv Drug Deliv Rev* 60, 286-295 (2008).
175. Hu, C.M., Zhang, L., Aryal, S., Cheung, C. & Fang, R.H. Erythrocyte membrane-camouflaged polymeric nanoparticles as a biomimetic delivery platform. *Proc Natl Acad Sci U S A* (2011).
176. Updike, S.J., Wakamiya, R.T. & Lightfoot, E.N., Jr. Asparaginase entrapped in red blood cells: action and survival. *Science* 193, 681-683 (1976).
177. Kruse, C.A., Tin, G.W. & Baldeschwieler, J.D. Stability of erythrocyte ghosts: a gamma-ray perturbed angular correlation study. *Proc Natl Acad Sci U S A* 80, 1212-1216 (1983).
178. Yang, F., *et al.* Genetic engineering of human stem cells for enhanced angiogenesis using biodegradable polymeric nanoparticles. *Proc Natl Acad Sci U S A* 107, 3317-3322 (2010).
179. Rachakatla, R.S., *et al.* Attenuation of mouse melanoma by A/C magnetic field after delivery of bi-magnetic nanoparticles by neural progenitor cells. *ACS Nano* 4, 7093-7104 (2010).
180. Bronshtein, T., Toledano, N., Danino, D., Pollack, S. & Machluf, M. Cell derived liposomes expressing CCR5 as a new targeted drug-delivery system for HIV infected cells. *J Control Release* 151, 139-148 (2011).

181. Hardman, R. A toxicologic review of quantum dots: Toxicity depends on physicochemical and environmental factors. *Environmental Health Perspectives* 114, 165-172 (2006).
182. Lytton-Jean, A.K.R., Langer, R. & Anderson, D.G. Five Years of siRNA Delivery: Spotlight on Gold Nanoparticles. *Small* 7, 1932-1937 (2011).
183. Duncan, R. & Gaspar, R. Nanomedicine(s) under the Microscope. Vol. 2011 (2011).
184. Zhang, C., *et al.* Specific targeting of tumor angiogenesis by RGD-conjugated ultrasmall superparamagnetic iron oxide particles using a clinical 1.5-T magnetic resonance scanner. *Cancer Res* 67, 1555-1562 (2007).
185. Bolskar, R.D., *et al.* First soluble M@C-60 derivatives provide enhanced access to metallofullerenes and permit in vivo evaluation of Gd@C-60[C(COOH)(2)](10) as a MRI contrast agent. *Journal of the American Chemical Society* 125, 5471-5478 (2003).
186. Yu, X., *et al.* High-resolution MRI characterization of human thrombus using a novel fibrin-targeted paramagnetic nanoparticle contrast agent. *Magnetic Resonance in Medicine* 44, 867-872 (2000).
187. Benezra, M., *et al.* Multimodal silica nanoparticles are effective cancer-targeted probes in a model of human melanoma. *J Clin Invest.*
188. Jennings, L.E. & Long, N.J. 'Two is better than one'-probes for dual-modality molecular imaging. *Chemical Communications*, 3511-3524 (2009).
189. Lee, H.Y., *et al.* PET/MRI dual-modality tumor imaging using arginine-glycine-aspartic (RGD) - Conjugated radiolabeled iron oxide nanoparticles. *Journal of Nuclear Medicine* 49, 1371-1379 (2008).
190. Lewin, M., *et al.* Tat peptide-derivatized magnetic nanoparticles allow in vivo tracking and recovery of progenitor cells. *Nat Biotechnol* 18, 410-414 (2000).
191. Rabin, O., Perez, J.M., Grimm, J., Wojtkiewicz, G. & Weissleder, R. An X-ray computed tomography imaging agent based on long-circulating bismuth sulphide nanoparticles. *Nature Materials* 5, 118-122 (2006).
192. Hu, G., *et al.* Imaging of Vx-2 rabbit tumors with alpha(nu)beta3-integrin-targeted 111In nanoparticles. *Int J Cancer* 120, 1951-1957 (2007).
193. Choi, J.H., *et al.* Multimodal biomedical imaging with asymmetric single-walled carbon nanotube/iron oxide nanoparticle complexes. *Nano Letters* 7, 861-867 (2007).
194. Kim, C.S., *et al.* Enhanced detection of early-stage oral cancer in vivo by optical coherence tomography using multimodal delivery of gold nanoparticles. *J Biomed Opt* 14, 034008 (2009).
195. Nguyen, Q.T., *et al.* Surgery with molecular fluorescence imaging using activatable cell-penetrating peptides decreases residual cancer and improves survival. *Proceedings of the National Academy of Sciences of the United States of America* 107, 4317-4322 (2010).
196. Voura, E.B., Jaiswal, J.K., Mattoussi, H. & Simon, S.M. Tracking metastatic tumor cell extravasation with quantum dot nanocrystals and fluorescence emission-scanning microscopy. *Nature Medicine* 10, 993-998 (2004).

197. Stroh, M., *et al.* Quantum dots spectrally distinguish multiple species within the tumor milieu in vivo. *Nat Med* 11, 678-682 (2005).
198. Heller, D.A., *et al.* Multimodal optical sensing and analyte specificity using single-walled carbon nanotubes. *Nature Nanotechnology* 4, 114-120 (2009).
199. Haes, A.J. & Van Duyne, R.P. A nanoscale optical blosensor: Sensitivity and selectivity of an approach based on the localized surface plasmon resonance spectroscopy of triangular silver nanoparticles. *Journal of the American Chemical Society* 124, 10596-10604 (2002).
200. Zheng, G.F., Patolsky, F., Cui, Y., Wang, W.U. & Lieber, C.M. Multiplexed electrical detection of cancer markers with nanowire sensor arrays. *Nature Biotechnology* 23, 1294-1301 (2005).
201. Bajaj, A., *et al.* Detection and differentiation of normal, cancerous, and metastatic cells using nanoparticle-polymer sensor arrays. *Proceedings of the National Academy of Sciences of the United States of America* 106, 10912-10916 (2009).
202. Cheng, H.Y., *et al.* Circulating Plasma MiR-141 Is a Novel Biomarker for Metastatic Colon Cancer and Predicts Poor Prognosis. *PLoS One* 6(2011).
203. Chinnaiyan, A.M., *et al.* Metabolomic profiles delineate potential role for sarcosine in prostate cancer progression. *Nature* 457, 910-914 (2009).
204. Heath, J.R., *et al.* Integrated barcode chips for rapid, multiplexed analysis of proteins in microliter quantities of blood. *Nature Biotechnology* 26, 1373-1378 (2008).

Chapter 6. Future work – Improved RNA delivery vehicles

Delivery systems that have been designed over the past ten years have significantly improved the likelihood successful siRNA therapies will be approved for clinical use. Many of the most clinically advanced delivery systems target hepatocytes. As a result, patients with a myriad of liver diseases stand to benefit from RNAi therapies. These advances are particularly exciting given the number of severe genetic liver diseases driven by a small number of genes that significantly diminish the quality of life (e.g. TTR amyloidosis, hemophilia, and porphyria). Successful long-term inhibition of these genes may effectively cure these diseases. Because the biodistribution, pharmacokinetics, and safety profile of the administered drugs will not vary significantly siRNA sequence, the same delivery vehicles may be used to treat liver diseases that are driven by a specific collection of genes with RNA combination therapies. Finally, as delivery systems that are administered subcutaneously continue to improve, siRNA therapies may also be used to treat more common diseases like hypercholesterolemia. For instance, inactive forms of ApoC3 or PCSK9 may significantly reduce serum cholesterol concentrations, and resultant cardiovascular disease. Pharmaceutical companies are developing antibody therapies that block the extracellular component of these targets. However, if subcutaneous conjugate delivery systems are shown to be safe and effective, these blockbuster antibodies may need to compete with siRNA therapies that "delete" both the extracellular and intracellular components of the protein target.

As RNA therapies become more commonplace in the clinic, they may be used in concert with traditional drugs. This effect is most easily illustrated in cancer: tumors undergo a number of genetic changes that decrease the efficacy of administered drugs. siRNA therapies targeting these resistance pathways can be designed to improve outcomes, for example, by knocking out efflux proteins that pump chemotherapeutics out of the cell. Similarly, cancer cells that are affected by a small molecule inhibiting one pathway survive by reverting to another distinct pathway. Rational combination therapies could use siRNAs that knockdown the second pathway, and increase the likelihood the cancer cell will undergo apoptosis.

While a majority of the most advanced siRNA delivery systems currently target the liver, there are innumerable patients that would benefit from efficient delivery to non-liver tissues. It is likely that significant advances in delivery vehicles targeting almost every other tissue in the body will be required before the same clinical success is observed outside the liver. For example, there are already many well-known genetic diseases that affect the function of skeletal muscle (muscular dystrophies), cardiomyocytes (cardiomyopathies), and neurons (Huntington's disease). Many patients afflicted with these disorders would likely experience a dramatic improvement in their quality of life if appropriate delivery vehicles are discovered. However, testing for effective *in vivo* delivery using traditional molecular biology techniques can be time-consuming, difficult, and expensive. As a result, new assays designed to easily measure non-liver delivery in a meaningful way will need to be developed to efficiently screen for lead candidates.

Non-liver delivery may be further improved by a more complete understanding of the physiology that promotes disease. For instance, a number of neurological disorders are characterized by inflammatory signaling that results in dysfunctional and leaky vasculature. This pathological change may be used to differentially deliver siRNA to regions affected by disease. In the same way, diseases that result in differential metabolism and subsequent changes in lipid uptake may be targeted by conjugating siRNA to the lipids that are taken up by diseased cells. Although not all diseases will result in physiological changes that promote delivery, many new strategies for specific passive targeting may be uncovered by understanding disease physiology more completely.

Techniques that helped dramatically improve the efficiency of liver-targeting LNPs may be applied to next-generation conjugates targeting non-liver tissues. Many of the most successful LNP formulations were discovered by screening large numbers of compounds that were synthesized using high-throughput chemistry. These chemical synthesis schemes were robust, and did not require purification steps. As a result, thousands of materials could be synthesized with relative ease. By contrast, the chemistry required to conjugate different materials directly to siRNA has remained slow, complicated, and expensive. New chemical synthetic schemes will need to be developed so that large material libraries of conjugates can be easily synthesized and tested.

Advances in nanoparticle- and conjugate-based delivery systems are sure to affect the future of RNA-based medicine. Because RNAs can bind to nearly every type of biomolecule in a cell, the number of diseases that can be impacted by their regulation is likely to increase rapidly. As a result, delivery systems which deliver siRNA may be exploited to deliver other small RNAs, while completely new systems may be required to deliver larger RNAs. In just over ten years, our understanding of RNAs has made it clear that they will continue to play an increasingly important role in medicine, as long as we can deliver them safely *in vivo*.